EXPERIMENTAL TESTS OF THE STRONG INTERACTION AND ITS ENERGY DEPENDENCE IN ELECTRON–POSITRON ANNIHILATION

O. BIEBEL

III. Physikalisches Institut A, RWTH Aachen, Physikzentrum, 52056 Aachen, Germany

ELSEVIER

AMSTERDAM – LONDON – NEW YORK – OXFORD – PARIS – SHANNON – TOKYO

ELSEVIER

Physics Reports 340 (2001) 165–289

PHYSICS REPORTS

www.elsevier.com/locate/physrep

Experimental tests of the strong interaction and its energy dependence in electron–positron annihilation

O. Biebel[1]

III. Physikalisches Institut A, RWTH Aachen, Physikzentrum, 52056 Aachen, Germany

Received April 2000; editor: J.V. Allaby

Contents

Abstract

e^+e^- an nihilation into quark–antiquark pairs is a valuable platform for the investigation of the strong interaction. The level of sophistication reached by theory and experiment allows one to verify predictions with significant precision for centre-of-mass energies ranging from the τ lepton mass up to about 200 GeV. This report summarizes studies of the dependence of the strong interaction on the energy scale. Determinations of α_s from total cross-sections, hadronic branching fractions of the τ lepton and of heavy quarkonia, jet rates, and event shape observables confirm the energy dependence of the strong coupling constant. Tests of the flavour independence of the strong interaction and mass effects are reviewed. Perturbation calculations of

[1] Now at: Max-Planck-Institut für Physik, Föhringer Ring 6, 80805 München, Germany.
E-mail address: otmar.biebel@cern.ch (O. Biebel).

PII: S0370-1573(00)00072-7

mass effects allow the determination of the bottom quark mass at high energies and, therefore, the scale dependence of quark masses predicted by QCD. Experimental studies of theoretical approaches to hadronization are presented. Besides fragmentation functions, scaling violations, and longitudinal cross-sections, successes of the modified leading-logarithmic approximation and local parton–hadron duality are exemplified. Power suppressed corrections, which are expected to be related to hadronization, are discussed for mean values and distributions of event shape observables. From the energy dependence of the strong interaction missing higher-order terms of the perturbation series can be determined. The scrutiny of the scale dependence of α_S showed no evidence for power corrections, light gluinos, or anomalous strong couplings. The results on α_S from e^+e^- annihilation are also very consistent with determinations of the strong coupling constant from other hard processes.

PACS: 06.20.Tr; 12.38. − t

Keywords: Fundamental constants; Quantum chromodynamics

1. Introduction

Over many decades nature has been probed by the scattering of elementary particles at higher and higher energies in order to reveal more and more the secrets of matter and forces. A fruitful connection of experimental and theoretical particle physics culminated in what is today called *standard model of the electroweak and strong interactions*. Based on quantum field theory, it is the foundation of the current understanding of all elementary particles, and it jointly describes all known forces but gravitation. Half-integer spin fermions act as the building blocks of matter with integer spin bosons acting as mediators of forces. Fermions appear in two species: leptons and quarks. These are, according to their respective quantum numbers, subject to the forces represented by the coupling and its strength. Each force has its bosons, namely the photon, the Z and the charged $W^{\pm}$ for the electroweak interaction, and the gluons for the strong interaction. All this is summarized in Table 1 which also lists the relevant quantum numbers.

An enormous effort of both experimental and theoretical physics has brought knowledge about the constituents of matter and the forces. On the experimental side this has been achieved predominantly by scattering particles off each other, observing the outcome, and analysing and understanding it in terms of basic and elementary processes between the particles. This would have been impossible without the theoretical advances. Calculations largely based on perturbation theory are the key to understanding the results of the measurements. More precise measurements required more precise calculations and vice versa, thus driving each other.

Table 1
Elementary fermions and bosons, that are known in the standard model of the electroweak and strong interactions, and the relevant quantum numbers assigned. Antifermions which are not listed have the signs of the charge, weak isospin, and colour charge quantum numbers inverted

Fermions	Generations			Charge Q_f	Weak isospin T_f^3	Colour charge	Spin
	1st	2nd	3rd				
Leptons	ν_e	ν_μ	ν_τ	0	$+\frac{1}{2}$	0	$\frac{1}{2}$
	e^-	μ^-	τ^-	-1	$-\frac{1}{2}$	0	$\frac{1}{2}$
Quarks	u	c	t	$+\frac{2}{3}$	$+\frac{1}{2}$	r, g, or b	$\frac{1}{2}$
	d	s	b	$-\frac{1}{3}$	$-\frac{1}{2}$	r, g or b	$\frac{1}{2}$
Bosons	**Coupling**			**Charge Q_f**	**Weak isospin T_f^3**	**Colour charge**	**Spin**
Photon	Electromagn.		γ	0	0	0	1
Weakons	Weak		W^+	$+1$	$+1$	0	1
			Z	0	0	0	1
			W^-	-1	-1	0	1
Gluons	Strong		G	0	0	1 colour + 1 anticolour	1

During the last 15 yr significant contributions came from high-energy electron–positron scattering, in particular annihilation. Large particle accelerators such as PEP, SLC, PETRA, TRISTAN, LEP and others have been built to collide electrons and positrons at very high energy. Particle detectors have been installed to register and measure the outgoing particles of the scattering processes. Thus many valuable results on the standard model have been obtained for both the electroweak and the strong interaction.

The LEP accelerator [1] which is still in operation has achieved a collision energy of electrons and positrons never reached before. Since the start of the PEP and PETRA colliders [2,3] which are no longer employed, the energy examined by LEP has almost increased twenty-fold. Results of very many investigations using the particle detectors installed at LEP have consolidated in particular the standard model of the electroweak interaction at an unprecedented level of precision [4–7].

This report will focus on results about the standard model of the strong interaction. After introducing the basic concepts in Section 2, Section 3 will explain how the strong interaction is scrutinized in electron–positron annihilation. This report will only touch on some topics of the inconceivably huge variety of investigations of the strong interaction done during the phase I operation of the LEP collider when it was tuned to produce Z bosons. More detailed reports on the LEP phase I results on the strong interaction can be found in [8–11] and also in textbooks [7,12]. The main topic of this report will be the combination of results from electron–positron collisions at various energies, thus taking advantage of the large energy range available. Naturally, the energy dependence of the strong interaction will be of particular interest. This will be addressed in Section 4 while Section 5 is dedicated to some recent theoretical developments which could allow even more precise tests of the standard model of the strong interaction. Before completing the report with a summary, concluding remarks, and a brief flash on future examinations of the theory, Section 6 will show some investigations concerning extensions of and deviations from the standard model of the strong interaction.

2. QCD – a theory of the strong interaction

The key to the understanding of strong interaction processes observed in the scattering of elementary particles is *Quantum Chromodynamics* (QCD) which was developed about 30 yr ago. It is a quantum field theory describing interactions between quarks and gluons based on the concept of a new charge, similar to but different from electric charge. This new charge appears in three variations which are usually associated with colours. Quarks are, besides their one third integer electric charge, carriers of one unit of this colour charge. Thus quarks exist three times each with a different colour charge.

In QCD hadrons are composed of quarks and are colourless. The concept of colour charge is supported experimentally for example by the observation of hadrons like Ω^- and Δ^{++} which are made of three quarks with identical quantum numbers. Pauli's principle is recuperated due to the three different colour charges of the constituent quarks. Other evidence for colour stems from the decay rate of $\pi^0 \to \gamma\gamma$. Without a colour factor of three the theoretical estimate for the decay rate would not agree with the experimentally measured value (for details see, e.g. Ref. [12]). Also in electron–positron scattering evidence has been found for the existence of colour. The virtual photon into which an electron and positron annihilate excites from the vacuum all electrically

charged pairs of particle and antiparticle, in particular quark and antiquark. As quarks may carry one out of three colours the total excitement of quark–antiquark pairs is enhanced by a colour factor of three (see, e.g. Ref. [6]).

In this section we will outline the structure of QCD. The focus will be on the origin of the energy dependence of the strong interaction.

2.1. Group structure of QCD

QCD is a non-Abelian Yang-Mills type theory. The features of QCD are determined through the $SU(3)$ group structure of colour. These features are reflected in the Lagrangian density which describes the interaction of half-integer spin quarks of mass m_q and massless spin-1 gluons. Suppressing a gauge and a ghost field term[2] the Lagrangian density of QCD is given by [12–14]

$$\mathscr{L}_{\mathrm{QCD}} = -\frac{1}{4}G^A_{\mu\nu}G^{\mu\nu}_A + \sum_{\text{quarks}} \bar{q}_a(\mathrm{i}\gamma^\mu D_\mu - m_q)_{ab}q_b \tag{1}$$

where the sum is over all quark flavours. Furthermore, repeated indices indicate a sum. In Eq. (1) D_μ is the covariant derivative and γ^μ are the four gamma matrices. The indices a, b of the quark spinors q are the quark colour indices running from 1 to the number of colours, i.e. 3. Thus quarks appear as colour triplets. In addition, the quark spinors and also the gamma matrix γ^μ have spinor indices that are suppressed for clarity. The field strength tensor $G^A_{\mu\nu}$ depends on the gluon fields G^A_μ. It is given by the relation

$$G^A_{\mu\nu} = \partial_\mu G^A_\nu - \partial_\nu G^A_\mu - g_S f^{ABC} G^B_\mu G^C_\nu \tag{2}$$

where the indices A, B, C denote the eight elements of the gluon field octet of QCD. The last term in Eq. (2) allows for interactions between gluon fields as will be demonstrated more clearly below. It contains the structure constants f^{ABC} of $SU(3)$ which determine the properties of QCD. Thus the last term is responsible for many peculiar features of QCD, in the first place that gluons, carrying two units of colour charge, may interact with each other. The constant g_S determines the strength of the colour interaction. It is related to the strong coupling constant

$$\alpha_{\mathrm{S}} = g_S^2/4\pi \tag{3}$$

which is the analogue to the fine structure constant α_{em} of Quantum Electrodynamics (QED). Thus g_S can be regarded as the colour charge.

The covariant derivative D_μ in Eq. (1) is given by the expression

$$(D_\mu)_{ab} = \partial_\mu \delta_{ab} + \mathrm{i}g_S(t^A G^A_\mu)_{ab}\,. \tag{4}$$

It depends on the coupling strength g_S and on the generators t^A of $SU(3)$. With three colour charges forming the fundamental representation of $SU(3)$, the generators are 3×3 matrices. The traditional

[2] A gauge has to be chosen to fix two of the four degrees of freedom for a massless gluon. This term explicitly breaks gauge invariance thus causing unphysical interaction terms which are compensated by introducing non-physical ghost terms. For details see, e.g. [12].

choice for these matrices is the Gell–Mann matrices λ^A, with $A = 1, \ldots, 8$. These are hermitian and traceless matrices that can be derived from the usual Pauli matrices. A full representation of the Gell–Mann matrices can be found in [12]. Using these matrices, the generators are defined as

$$t^A = \tfrac{1}{2}\lambda^A . \tag{5}$$

The relevant property that the generators inherit from the Gell–Mann matrices is the commutation relation which reads

$$[t^A, t^B] = \mathrm{i} f^{ABC} t^C \tag{6}$$

thus defining the structure constants f^{ABC}. Conventionally the normalization of the generators is chosen such that

$$\mathrm{Tr}\ t^A t^B = T_F \cdot \delta^{AB} \quad \text{with } T_F = \tfrac{1}{2}. \tag{7}$$

Two more colour factors can be derived using the generators and the structure constants. The sum over all colour indices A of the product of two generators defines the colour factor C_F of an $SU(N)$ theory

$$\sum_A (t^A)_{ab}(t^A)_{bc} = C_F \cdot \delta_{ac} \quad \text{with } C_F = \frac{N^2 - 1}{2N} \overset{N=3}{=} \frac{4}{3}. \tag{8}$$

Summing the product of two structure constants gives a defining relation for the C_A colour factor of $SU(N)$

$$\sum_{A,B} f^{ABC} f^{ABD} = C_A \cdot \delta^{CD} \quad \text{with } C_A = N \overset{N=3}{=} 3. \tag{9}$$

These colour factors play the dominant role in the coupling between quarks and gluons. All features of QCD are related to the colour factors T_F, C_F and C_A. This will become more obvious in a moment.

The Lagrangian of Eq. (1), even though lacking gauge fixing and ghost terms, is rather involved. In order to make the physical implications of the Lagrangian visible, we plug in the covariant derivative Eq. (4). If, furthermore, colour indices of the quark fields q and the sum over the quark flavours are suppressed one obtains

$$\mathscr{L}_{\mathrm{QCD}} = \bar{q}(\mathrm{i}\gamma_\mu \partial^\mu - m_q)q + \mathrm{i} g_S (\bar{q}\gamma^\mu t^A q) G^A_\mu - \tfrac{1}{4} G^A_{\mu\nu} G^{\mu\nu}_A . \tag{10}$$

Inserting the gluon field strength tensor $G_{\mu\nu}$ defined in Eq. (2) and recalling that q and G refer to quark and gluon fields, respectively, the Lagrangian can be written in a symbolic form which separates the different interaction terms specific to QCD. Each of these terms can be associated to

a Feynman graph characterizing the interacting particles and the kind of the interaction

$$\mathscr{L}_{\mathrm{QCD}} = \text{“}\bar{q}\,q\text{”} + \text{“}G^2\text{”} + g_S \cdot t\text{“}\bar{q}\,qG\text{”} + g_S \cdot f\text{“}G^3\text{”} + g_S^2 \cdot f^2\text{“}G^4\text{”} \quad . \tag{11}$$

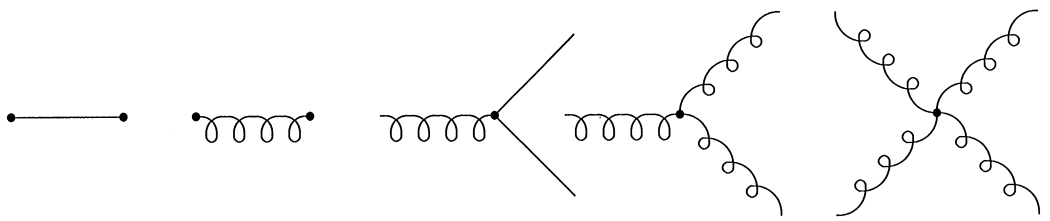

The first three terms are well known from their QED analogues. Terms one and two describe the propagation of a quark and a gluon, respectively. The third term contains the coupling between quarks and gluons. It can be interpreted as the decay of a gluon into a quark–antiquark pair (as shown above) and also as gluon radiation off a quark (antiquark) by crossing the antiquark (quark) and gluon lines in the picture. The two processes have different colour flows which result in different couplings as will be illustrated below. What distinguishes QCD from QED are the last two graphs which introduce gluon–gluon coupling in the form of a triple and a quartic gluon vertex, respectively.

The symbolic representation of the QCD Lagrangian in Eq. (11) includes also the parameters that determine the strength of the couplings. In the case of the quark–gluon coupling, represented by the third term, the coupling depends on g_S and on the generators t. Also the details of the colour flow determined by the colour indices are involved. Considering the gluon splitting into a quark–antiquark pair the coupling is

$$\left|\;\right|^2 \sim \alpha_S \cdot T_F \cdot n_f \quad . \tag{12}$$

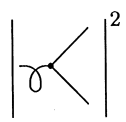

The additional factor n_f is due to the n_f different quark flavours that the gluon may split into. For the radiation of a gluon from a quark one finds a coupling of

$$\left|\;\right|^2 \sim \alpha_S \cdot C_F \quad . \tag{13}$$

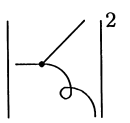

In the triple gluon case the coupling is

$$\left|\;\right|^2 \sim \alpha_S \cdot C_A \quad , \tag{14}$$

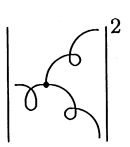

and for a quartic vertex it is

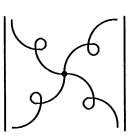

$$\sim \alpha_S^2 \cdot C_A^2 \quad . \tag{15}$$

These are the elementary graphs of QCD. Every interaction between strongly interacting particles can be described perturbatively using these basic exchange graphs and the colour factors. Any experimental verification of QCD as *the* theory of strong interaction, therefore, does not only require the discovery of colour, of quarks and gluons and their properties, but also requires the measurement of the colour factors and the observation of the consequences of the renormalization of QCD which we will address next.

2.2. Renormalization of QCD

One of the bizarre features of quantum field theory is that it involves divergences when calculating, e.g. the self-interaction of a particle. Such divergences would render every calculation of quantum field theory unusable. Thus one has to eliminate these poles by renormalizing the terms containing the poles. A very complete description of renormalization can be found in Ref. [15]. In brief, renormalization is a prescription to introduce counterterms which absorb infinities into physical quantities such as charge or mass of a particle. This concept seems to be rather artificial at first. However, an electron moving in a solid interacts with the atoms in the lattice such that its effective mass is different from the nominal mass value. This is analogous to renormalization in quantum electrodynamics where the electron interacts with the vacuum. The difference is that one can remove the atoms of the solid to measure the mass of a free electron, but one cannot remove the vacuum. Following the lines of renormalization to absorb infinities into physical mass or charge, a price has to be paid. It is that the renormalized theory acquires new properties.

Only in 1971 was the renormalizability of non-abelian field theories such as QCD shown [16]. Today, dimensional regularization (see references in [15], particularly Ref. [17]) is frequently applied in QCD calculations. It uses the space–time dimension, d, as a regulator treating $d = 4 - 2\varepsilon$ as a continuous variable. The renormalization prescription, in which counter-terms are pure $1/\varepsilon$ poles at the physical value of $d = 4$, is called the minimal subtraction renormalization scheme (MS) [18]. A modification of this scheme is the $\overline{\text{MS}}$ scheme [19] which is used throughout this report. It differs from the MS scheme in that it also subtracts $\ln(4\pi) - \gamma_E$ terms, responsible for large coefficients in the perturbation expansion, where $\gamma_E \approx 0.5772$ is Euler's constant. The MS and especially the $\overline{\text{MS}}$ scheme are now widely used owing to their advantages. Both schemes automatically preserve many complicated symmetries except chiral symmetry. They have no problems with massless QCD theory. The calculations are convenient and the computation of the divergent part is not too difficult. However, the MS and $\overline{\text{MS}}$ schemes are both unphysical because there is no physical reason for the introduction of the counter-terms.

Another complication of minimal subtraction is that it is in effect a whole family of renormalization prescriptions with a single parameter μ. This parameter represents an entirely arbitrary mass scale. It is introduced in the dimensional regularization process because from Eq. (2) it can be seen

that the bare coupling g_S acquires a dimension if $d \neq 4$. As a consequence every physical quantity R depends not only on the coupling g_S and masses m but also on this scale μ. In general, g_S and m will also depend on μ. Since the scale is entirely arbitrary, it cannot be related to any physical observable and, hence, physical observables should be invariant under the change of variables $(\mu, g_S(\mu), m(\mu)) \to (\mu', g_S(\mu'), m(\mu'))$. This invariance can be expressed by

$$\mu^2 \frac{\mathrm{d}R}{\mathrm{d}\mu^2} = 0\,. \tag{16}$$

Replacing g_S by α_s with the help of Eq. (3) the total derivative with respect to μ can be written as

$$\begin{aligned}\mu^2 \frac{\mathrm{d}}{\mathrm{d}\mu^2} &= \mu^2 \frac{\partial}{\partial \mu^2} + \mu^2 \frac{\partial \alpha_s}{\partial \mu^2} \frac{\partial}{\partial \alpha_s} + \mu^2 \frac{\partial m}{\partial \mu^2} \frac{\partial}{\partial m} \\ &= \mu^2 \frac{\partial}{\partial \mu^2} + \beta(\mu^2) \frac{\partial}{\partial \alpha_s} - \gamma_m(\mu^2) m \frac{\partial}{\partial m}\end{aligned} \tag{17}$$

which defines two renormalization group coefficients β and γ_m which are usually called the β function and the mass anomalous dimension, respectively. From Eq. (17) both coefficients can be read off respecting the usual sign convention for the mass anomalous dimension [20]

$$\beta(\mu^2) = \mu^2 \frac{\partial \alpha_s}{\partial \mu^2}\,, \tag{18}$$

$$\gamma_m(\mu^2) = -\mu^2 \frac{1}{m} \frac{\partial m}{\partial \mu^2}\,. \tag{19}$$

The solutions of these two differential equations reveal two fundamental properties of QCD and, hence, the strong interaction – *running coupling*, $\alpha_s(Q^2)$, and *running masses*, $m(Q^2)$.

2.2.1. *The running coupling constant* $\alpha_s(Q^2)$

The value of the coupling α_s changes with the energy scale of the process under consideration. This can easily be seen from the renormalization group equation (RGE)

$$Q^2 \frac{\partial \alpha_s(Q^2)}{\partial Q^2} = \beta(\alpha_s) \tag{20}$$

which is obtained from Eq. (18) after separation of variables, integration and derivation with respect to the squared energy scale of the process, Q^2. It still is a differential equation but we will obtain an explicit expression for $\alpha_s(Q^2)$ using the β function. It has been calculated by perturbation expansion considering counter-terms to the divergent self-energy contributions involving Feynman diagrams with up to four loops. Joining the results of all calculations [21,22] leads to the expansion

$$\beta(\alpha_s) = Q^2 \frac{\partial \alpha_s}{\partial Q^2} = -\beta_0 \alpha_s^2 - \beta_1 \alpha_s^3 - \beta_2 \alpha_s^4 - \beta_3 \alpha_s^5 + \mathcal{O}(\alpha_s^6) \tag{21}$$

with[3]

$$\beta_0 = \frac{1}{12\pi}(33 - 2n_f),$$

$$\beta_1 = \frac{1}{24\pi^2}(153 - 19n_f),$$

$$\beta_2 \approx \frac{1}{\pi^3}(22.320 - 4.3689n_f + 0.09404n_f^2),$$

$$\beta_3 \approx \frac{1}{\pi^4}(114.23 - 27.134n_f + 1.5824n_f^2 + 0.00586n_f^3).$$

A very important property of QCD is to be noted from β_0. This coefficient is positive as long as $n_f < 17$ causing α_S to decrease with increasing Q^2. Therefore, in contrast to QED, QCD obeys asymptotic freedom meaning that quarks and gluons behave at very short distances like free particles. Turning to very low-energy scales, the strong coupling constant grows, thus suggesting that coloured objects will eventually be confined in colourless compounds. These compounds are the usual mesons and baryons which one can find in the final state of scattering processes.

An explicit expression for the running coupling $\alpha_S(Q^2)$ can be obtained by solving the renormalization group equation (20) either numerically or by integration. In [23] the integration has been done using the 4-loop expression for the β function in the $\overline{\text{MS}}$ renormalization scheme. The result for the running coupling

$$\begin{aligned}\alpha_S(Q^2) = {} & \frac{1}{\beta_0 L} - \frac{\beta_1 \ln L}{\beta_0^3 L^2} + \frac{1}{\beta_0^3 L^3}\left[\frac{\beta_1^2}{\beta_0^2}(\ln^2 L - \ln L - 1) + \frac{\beta_2}{\beta_0}\right] \\ & + \frac{1}{\beta_0^4 L^4}\left[\frac{\beta_1^3}{\beta_0^3}\left(-\ln^3 L + \frac{5}{2}\ln^2 L + 2\ln L - \frac{1}{2}\right) - 3\frac{\beta_1\beta_2}{\beta_0^2}\ln L + \frac{\beta_3}{2\beta_0}\right] \\ & + \mathcal{O}\left(\frac{1}{L^5}\right)\end{aligned} \tag{22}$$

is expressed in inverse powers of $L = \ln(Q^2/\Lambda^2_{\overline{\text{MS}}})$ where $\Lambda_{\overline{\text{MS}}}$ is the constant of integration which depends in general on the renormalization scheme. One notes that the explicit expression for α_S reveals a pole at $Q^2 = \Lambda^2_{\overline{\text{MS}}}$. This is an unphysical Landau pole [24] indicating that the perturbation expansion cannot be applied at very small scales. Non-perturbative effects become important at such scales. These will be discussed in Section 5. The running of the coupling $\alpha_S(Q^2)$ is exemplified in Fig. 1 using the explicit expression Eq. (22) for various values of $\Lambda_{\overline{\text{MS}}}$.

[3] The coefficients β_i are known exactly for $i = 0, \ldots, 3$ (see, e.g. [22]). Here we quote for simplicity only approximate expressions for β_2 and β_3.

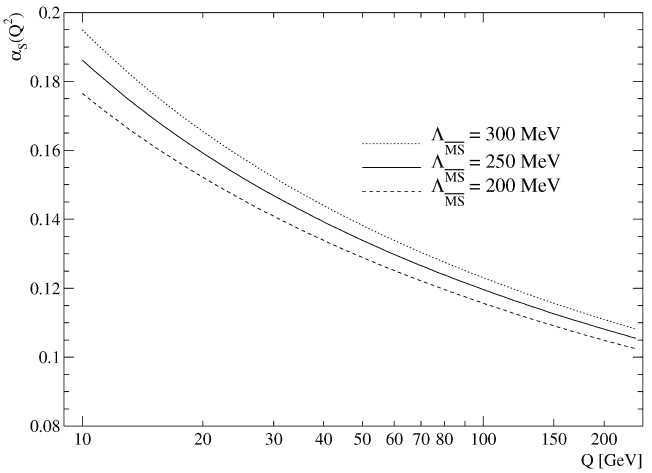

Fig. 1. Running coupling constant $\alpha_S(Q^2)$ using the 4-loop expression Eq. (22) and different values for $\Lambda^{\overline{MS}}$.

2.2.2. *The running masses $m(Q^2)$*

The defining equation (19) for the mass anomalous dimension γ_m describes the running of quark masses. Solving this equation by separation of variables and integration one finds an expression for the running mass:

$$m(Q^2) = m(\mu^2)\exp\left\{-\int_{\mu^2}^{Q^2}\gamma_m(\mu^2)\frac{d\mu^2}{\mu^2}\right\}$$
$$= m(\mu^2)\exp\left\{-\int_{\alpha_S(\mu^2)}^{\alpha_S(Q^2)}\gamma_m(\alpha_S)\frac{d\alpha_S}{\beta(\alpha_S)}\right\} \tag{23}$$

when substituting with Eq. (18). One notes that the β function determines, together with γ_m, also the running of the masses.

As for the β function, a perturbation expression for the mass anomalous dimension γ_m has been derived [25–27]:

$$-\gamma_m(\alpha_S) = \frac{1}{m}Q^2\frac{\partial m}{\partial Q^2} = -\gamma_{m,0}\alpha_S - \gamma_{m,1}\alpha_S^2 - \gamma_{m,2}\alpha_S^3 - \gamma_{m,3}\alpha_S^4 + \mathcal{O}(\alpha_S^5) \tag{24}$$

with[4]

$$\gamma_{m,0} = \frac{1}{\pi},$$

$$\gamma_{m,1} = \frac{1}{72\pi^2}(303 - 10n_f),$$

[4] The coefficients $\gamma_{m,i}$ are known exactly for $i = 0, \ldots, 3$ (see, e.g. [27]). For simplicity only approximate expressions for $\gamma_{m,2}$ and $\gamma_{m,3}$ are quoted.

$$\gamma_{m,2} \approx \frac{1}{\pi^3}(19.516 - 2.2841 n_f - 0.027006 n_f^2),$$

$$\gamma_{m,3} \approx \frac{1}{\pi^4}(98.943 - 19.1075 n_f + 0.27616 n_f^2 + 0.005793 n_f^3).$$

The expansions of the mass anomalous dimension γ_m and of the beta function Eq. (21) can now be inserted into the evolution equation for the quark masses Eq. (23). A 4-loop expansion for the running of the quark masses $m(Q^2)$ in the $\overline{\text{MS}}$ scheme is given in [27]. For the charm ($n_f = 4$) and the bottom quark ($n_f = 5$) these expansions read

$$\bar{m}_c(Q^2) = \bar{m}_c(Q_0^2)\left(\frac{\alpha_s(Q^2)}{\alpha_s(Q_0^2)}\right)^{12/25} \times \frac{1 + 1.0141(\alpha_s(Q^2)/\pi) + 1.389(\alpha_s(Q^2)/\pi)^2 + 1.09(\alpha_s(Q^2)/\pi)^3}{1 + 1.0141(\alpha_s(Q_0^2)/\pi) + 1.389(\alpha_s(Q_0^2)/\pi)^2 + 1.09(\alpha_s(Q_0^2)/\pi)^3} \tag{25}$$

$$\bar{m}_b(Q^2) = \bar{m}_b(Q_0^2)\left(\frac{\alpha_s(Q^2)}{\alpha_s(Q_0^2)}\right)^{12/23} \times \frac{1 + 1.1755(\alpha_s(Q^2)/\pi) + 1.501(\alpha_s(Q^2)/\pi)^2 + 0.17(\alpha_s(Q^2)/\pi)^3}{1 + 1.1755(\alpha_s(Q_0^2)/\pi) + 1.501(\alpha_s(Q_0^2)/\pi)^2 + 0.17(\alpha_s(Q_0^2)/\pi)^3} \tag{26}$$

where $\overline{\text{MS}}$ masses are denoted $\bar{m}$ and a reference scale Q_0^2 is introduced. Fig. 2 shows the running of the bottom quark mass in the $\overline{\text{MS}}$ renormalization scheme for $n_f = 5$. The reference scale is chosen such that $\bar{m}_b(Q_0^2 = (4.25\,\text{GeV})^2) = 4.25\,\text{GeV}$. This mass value is the central value derived from the compilation of the Particle Data Group [28].

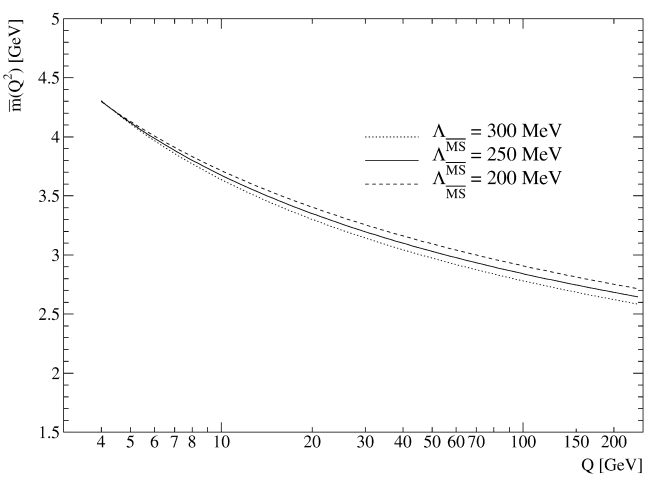

Fig. 2. Running of bottom quark mass with 4-loop precision in the $\overline{\text{MS}}$ renormalization scheme for 5 flavours.

Recalling Eq. (20) and Eq. (21) it should be pointed out that the β function and consequently also $\alpha_S(Q^2)$ explicitly depend on the number of flavours n_f. This is of practical importance due to the very different quark masses (see Ref. [28]). The dependence of α_S on the energy scale means that one has to carefully consider how many quark flavours n_f actively contribute to the running of α_S. In particular, crossing the production threshold of a further quark flavour means a change of n_f and, hence, of α_S and m. This has to be taken into account when solving the renormalization group equations (21) and (24). For practical reasons, one usually evolves α_S using Eq. (22) for $n_f - 1$ flavours to the mass scale of the heavy quark flavour n_f. From a matching condition at this scale, $\alpha_S^{(n_f)}$ is calculated from $\alpha_S^{(n_f-1)}$, and $\alpha_S^{(n_f)}$ is evolved for n_f active flavours using Eq. (22) again. In [23,29] the matching conditions for α_S and for quark masses m have been calculated allowing an arbitrary matching scale Q^2. The matching relation can be significantly simplified when choosing the $\overline{\text{MS}}$ mass for that scale, that is $Q^2 = \bar{m}^2 = \bar{m}^2(\bar{m}^2)$, where α_S is matched for $n_f - 1$ and n_f active flavours. Then the ratio becomes [23]

$$\frac{\alpha_S^{(n_f-1)}(\bar{m}^2)}{\alpha_S^{(n_f)}(\bar{m}^2)} = 1 + \frac{(\alpha_S^{(n_f)}(\bar{m}^2))^2}{\pi^2}\left(\frac{11}{72}\right) + \frac{(\alpha_S^{(n_f)}(\bar{m}^2))^3}{\pi^3}(1.057 - 0.085 n_f). \tag{27}$$

It should be observed that the ratio is greater than unity at this matching point. Thus $\alpha_S(Q^2)$ is reduced when increasing the number of active flavours.

In summary it should be kept in mind that renormalizing QCD introduces rather peculiar properties – energy dependent coupling and mass. The coupling reveals that QCD is an asymptotic free theory. At very short distances or, equivalently, at very high energies quarks and gluons behave like free particles. On the other hand, we observe the confinement of coloured objects in colourless hadrons, an experimental fact which still has to be proven as a result of the equations of QCD.

2.2.3. Choice of renormalization scale

Up to now all details concerning renormalization have been neglected. In particular, the relation between the arbitrary renormalization scale μ and the scale of a physical process Q has to be considered. Choosing $Q \sim \mu$ would be natural. All calculations, however, will be done in some limited order of perturbation theory, in which $Q \sim \mu$ is not conclusive. This can be readily seen from an explicit solution of the two-loop approximation of Eq. (20), yielding

$$\alpha_S(Q^2) = \alpha_S(\mu^2)\left[1 - \alpha_S(\mu^2)X + \alpha_S^2(\mu^2)\left(X^2 - X\frac{\beta_1}{\beta_0}\right) + \mathcal{O}(\alpha_S^3)\right], \tag{28}$$

with $X = \beta_0 \ln(Q^2/\mu^2)$. This equation reveals the relation between the renormalized coupling $\alpha_S(\mu^2)$ and the size of the coupling which is relevant for the physical process under consideration, that is $\alpha_S(Q^2)$.

Each physical process must be independent of the renormalization scale μ, as has been stated in Eq. (16). When calculating the physical observable R as a power series in $\alpha_S(\mu^2)$

$$R(Q^2) = R_0 + R_1\alpha_S(\mu^2) + R_2\alpha_S^2(\mu^2) + R_3\alpha_S^3(\mu^2) + \mathcal{O}(\alpha_S^4), \tag{29}$$

applying the derivative (17) and, for simplicity, neglecting mass terms, one finds from this independence that

$$0 = \mu^2 \frac{\mathrm{d}R(Q^2)}{\mathrm{d}\mu^2} = \mu^2 \frac{\partial R}{\partial \mu^2} + \beta(\mu^2) \frac{\partial R}{\partial \alpha_\mathrm{S}}$$
$$= \frac{\partial R_0}{\partial \ln \mu^2} + \alpha_\mathrm{S} \frac{\partial R_1}{\partial \ln \mu^2} + \alpha_\mathrm{S}^2 \left[\frac{\partial R_2}{\partial \ln \mu^2} - \beta_0 R_1 \right] + \alpha_\mathrm{S}^3 \left[\frac{\partial R_3}{\partial \ln \mu^2} - (2\beta_0 R_2 + \beta_1 R_1) \right] + \mathcal{O}(\alpha_\mathrm{S}^4). \tag{30}$$

In the calculation we have used $\alpha_\mathrm{S} = \alpha_\mathrm{S}(\mu^2)$ and Eq. (21) for $\beta(\alpha_\mathrm{S})$. In order to ensure the independence from the renormalization scale order by order in α_S, the coefficients R_n with $n \geq 2$ of the perturbation series of R must depend on μ. For example, the next-to-leading order coefficient R_2 needs to be

$$R_2\left(\frac{Q^2}{\mu^2}\right) = R_2(1) - \beta_0 R_1 \ln \frac{Q^2}{\mu^2}. \tag{31}$$

Only the constant R_0 and the leading order (LO) coefficient, R_1, are independent of the scale.

Substituting Eq. (28) in Eq. (29) and comparing with Eq. (30), one finds that the μ scale dependence of the coefficients exactly compensates the change in the coupling $\alpha_\mathrm{S}(\mu^2)$, thus yielding a μ-independent result for the full series. If, however, the series is truncated, the μ-independence breaks down.

The scale dependence entails an uncertainty due to the choice of the scale. This needs to be considered in each perturbation calculation of observable physical quantities. The uncertainty due to a change of the scale is one order higher than the order of the perturbative calculation. Thus it is $\mathcal{O}(\alpha_\mathrm{S}^4)$ only for a next-to-next-to-leading order (NNLO) calculation, while for next-to-leading order (NLO) it is $\mathcal{O}(\alpha_\mathrm{S}^3)$ and, hence, more pronounced. Such uncertainties will pop up in each experimental determination of the strong coupling constant as will be seen in Section 4.

3. The strong interaction in e^+e^- annihilation

Strong interaction phenomena have been observed in the scattering of various particles, in particular protons, antiprotons, electrons and positrons. Among these, the collision and annihilation of electron and positron has several appealing features due to the well-defined initial state. Total centre-of-mass energy and momentum are precisely known as is the colour state. This rendered the electron–positron annihilation experiments at the colliders PEP, PETRA, TRISTAN, SLC, and LEP a valuable testing ground for the investigation of the strong interaction and for the scrutiny of QCD. This section addresses the question of how QCD can be examined in electron–positron annihilation processes. Broadly speaking, the process can in principle be subdivided into four steps as is illustrated in Fig. 3:

- the actual annihilation possibly involving initial state photon radiation and the decay of the intermediate boson into a quark–antiquark pair,

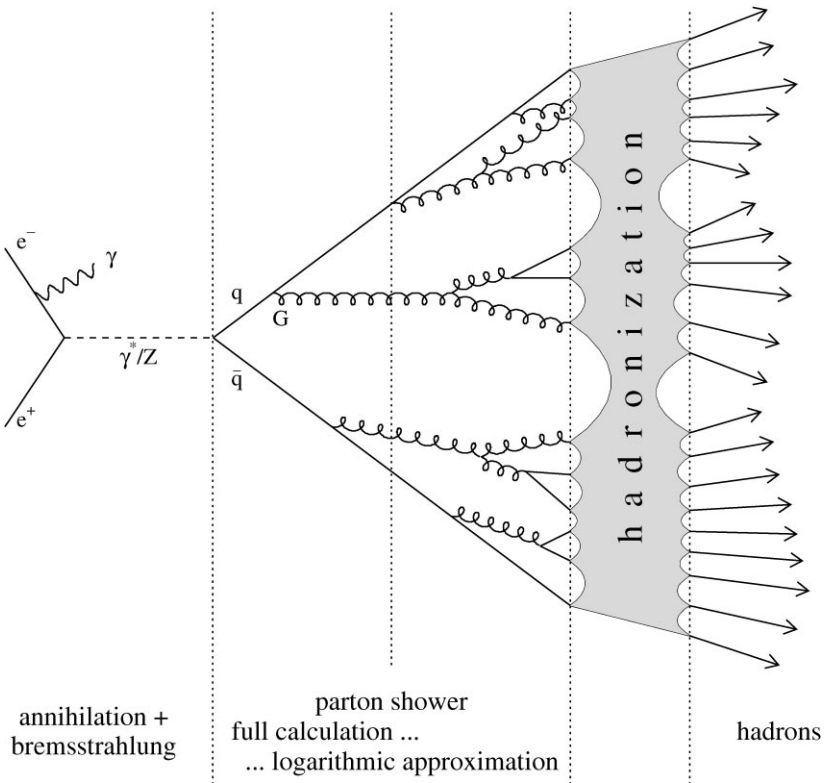

Fig. 3. Schematic representation of an e^+e^- annihilation process into hadrons.

- the radiation of gluons and the gluon-splitting into quark–antiquark pairs leading to a parton[5] shower,
- the process of hadronization which summarizes the transition of quarks and gluons into hadrons,
- and finally the hadrons and their potential decays.

The very first of these steps is well understood from electroweak theory. Details of this step can be found in many reports and textbooks, for example [4–7]. In this section the two middle steps will be considered in more detail.

3.1. QCD and e^+e^- annihilation

3.1.1. e^+e^- annihilation into quark–antiquark pairs

In the collision of an electron and a positron an annihilation of the two into a virtual photon or a Z boson can occur. Both the virtual photon and the Z decay into pairs of a fermion and an antifermion, in particular a quark and an antiquark. This is depicted in the language of Feynman

[5] The word parton is used as a generic notation for quark, antiquark and gluon.

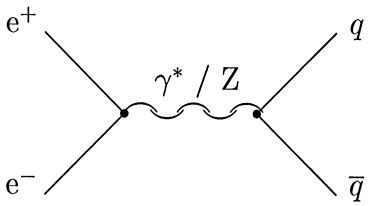

Fig. 4. Lowest order Feynman graph for the annihilation of an electron–positron pair into a virtual photon γ^* or a Z boson and its decay into a quark–antiquark pair.

graphs in Fig. 4. Relevant for a study of the strong interaction is the fraction of annihilation events that generate a quark–antiquark final state and the amounts of the various quark flavours. Both quantities are related to the coupling of the virtual photon or the Z to the quark–antiquark pair. Instead of the absolute production cross-section for quark–antiquark pairs, its ratio to the lowest-order muon pair production cross-section is usually considered. At energies far below the mass of the Z this ratio is simply given by the electromagnetic coupling of the photon to the charge of the quarks Q_q [13]

$$R_\gamma = \frac{\sum_q \sigma(e^+e^- \to q\bar{q})}{\sigma(e^+e^- \to \mu^+\mu^-)} = 3\sum_q Q_q^2 . \tag{32}$$

The sum is over all quark flavours that can be created in the annihilation process. Additionally a factor of three enters the relation from the sum over quark colours.

At energies close to the mass of the Z a pole occurs in the cross-section. It is due to the resonance production of the Z which dominates over the virtual photon exchange. In the vicinity of the pole the R ratio is expressed using the partial decay width of the Z into quark and muon pairs, respectively, [12]

$$R_Z = \frac{\sum_q \Gamma(Z \to q\bar{q})}{\Gamma(Z \to \mu^+\mu^-)} = \frac{3\sum_q (A_q^2 + V_q^2)}{A_\mu^2 + V_\mu^2} . \tag{33}$$

It depends on the axial, A, and vector, V, couplings of the fermions to the Z. These are related to the third component of the weak isospin T^3 and the charge Q of a fermion f, and also to the weak mixing angle θ_W according to

$$V_f = T_f^3 - 2Q_f \sin^2\theta_W, \quad A_f = T_f^3 . \tag{34}$$

The fermions known in the standard model of the strong and electroweak interactions are assigned the following values for the weak isospin and electric charge (see Table 1): Neutrinos and the up-type quarks (u, c, t) have $T_f^3 = +1/2$ while electron, muon, tau, and the down-type quarks (d, s, b) have $T_f^3 = -1/2$. In units of the elementary charge the up-type quarks have electric charge $+2/3$, the down-type quarks $-1/3$, neutrinos are neutral and electron, muon, tau have each -1. These values change sign when considering the respective antiparticles.

Eqs. (32) and (33) are approximations for restricted energy regions. The complete R ratio is shown[6] (dotted line) in Fig. 5(a) for a large region of centre-of-mass energies, $\sqrt{s}$, ranging from

[6] Contributions due to W and Z pair production are not included.

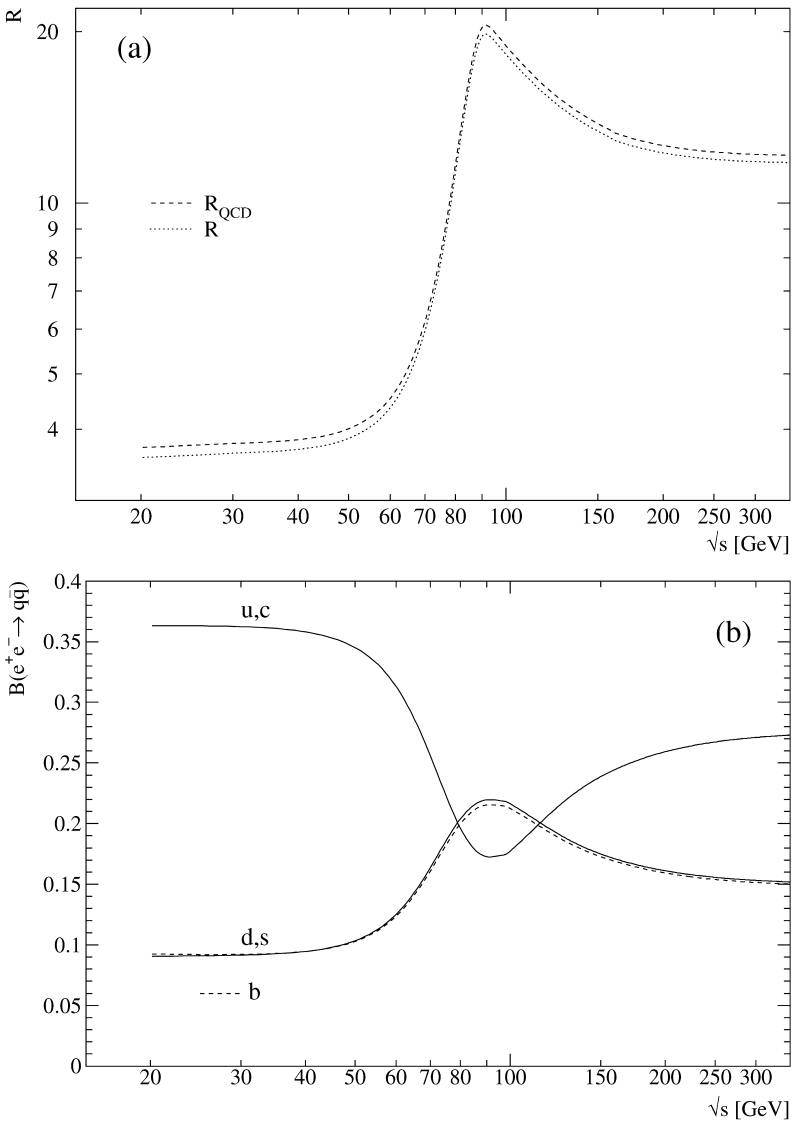

Fig. 5. (a) The ratio of the hadronic and the muonic cross-section R in e^+e^- annihilation is shown with all but QCD corrections (dotted line). The dashed line represents R_{QCD} which includes QCD corrections according to Eq. (37). (b) The branching ratio B of e^+e^- annihilation into quarks is shown separately for up-type, down-type, and bottom quarks. Bottom quarks (dashed) deviate from the down-type behaviour due to their large mass and due to vertex corrections involving the top quark, and the W and Higgs bosons. The curves were produced by the ZFITTER program [30] considering initial state photon radiation. Pair production of W and Z bosons is not included.

close to the pair production threshold of bottom quarks at about $\sqrt{s} = 10\,\text{GeV}$ to just below the threshold for top quark pairs at roughly 350 GeV. It has been calculated with the ZFITTER program[7] [30]. At a centre-of-mass energy of $\sqrt{s} = M_Z$ the R_Z ratio dominates while for energies much

[7] Version 5.0 has been used.

below the Z pole R_γ is significant. Above the Z pole the R ratio is given by a combination of contributions from Z and γ exchange.

Due to the different coupling of Z and γ to the quarks, also the proportions of the individual quark flavours change with the centre-of-mass energy. This is shown in Fig. 5(b) for the five light quark flavours. At very low energies, up-type quarks are most frequently produced because of the dominance of the γ exchange which yields a coupling proportional to the square of the quark charge (cf. Eq. (32)). Around the Z pole, down-type quarks dominate due to the Z boson exchange (cf. Eq. (33)), whereas at very high energies, the interference of γ and Z entails again the domination of up-type quarks. Bottom quarks follow the trend of the down-type quarks but deviate a little due to mass effects and corrections which involve virtual top quarks, W and Higgs bosons.

3.1.2. Gluon radiation from quarks – full calculation

The strong interaction comes into play with the radiation of gluons off the quarks. It involves two contributions: the radiation of virtual and real gluons. These two are exemplified in Fig. 6. Only in the case of real gluon radiation is a gluon left over in the final state, together with the quark and the antiquark. The probability of real gluon emission as shown in Fig. 6 depends on the coupling strength. Applying Feynman rules (see for example [13]) the differential cross-section for this particular process, $e^+e^- \to q\bar{q}G$, has been calculated. The result is [31]

$$\frac{1}{\sigma_0}\frac{d^2\sigma}{dx_q dx_{\bar{q}}} = C_F\frac{\alpha_S}{2\pi}\frac{x_q^2 + x_{\bar{q}}^2}{(1-x_q)(1-x_{\bar{q}})}, \tag{35}$$

where $x_i = 2E_i/\sqrt{s}$, $i = q, \bar{q}$, are the centre-of-mass energy fractions of the massless final state quark and antiquark, respectively, and σ_0 is the total cross-section in absence of QCD radiation which is usually denoted Born or tree level cross-section. The differential cross-section is directly proportional to the coupling strength α_S as is obvious from Eq. (35).

A complication for this differential cross-section is due to infrared and collinear divergences for real gluon emission. Such divergences occur if the gluon is either very low in energy or if it is emitted collinearly to the quark. In fact, the collinear divergence is due to neglecting masses in these calculations. These two fundamental divergences can be made evident in Eq. (35) using four-momentum conservation for the exchange boson, $\mathbf{p}_\gamma = (\mathbf{p}_q + \mathbf{p}_{\bar{q}} + \mathbf{p}_G)$ and $s = \mathbf{p}_\gamma^2$. One finds for the

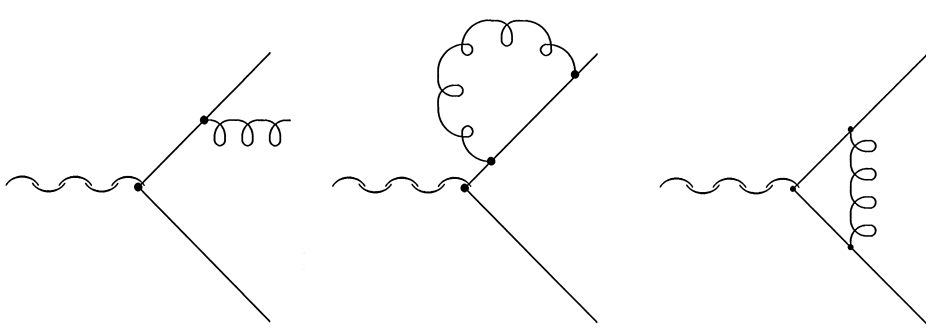

Fig. 6. Lowest-order Feynman graphs for real (left) and virtual radiation (middle and right) of a gluon off a quark or an antiquark. Analogous graphs exist for the radiation from the other final state quark.

case of a gluon emitted by the antiquark

$$
\begin{aligned}
(\mathbf{p}_{\bar{q}} + \mathbf{p}_{\mathrm{G}})^2 &= \mathbf{p}_{\gamma}^2 - 2\mathbf{p}_q \cdot (\mathbf{p}_{\bar{q}} + \mathbf{p}_{\mathrm{G}}) = \mathbf{p}_{\gamma}^2 - 2\mathbf{p}_q \cdot \mathbf{p}_{\gamma} = s(1 - x_q) \\
&= 2\mathbf{p}_{\bar{q}} \cdot \mathbf{p}_{\mathrm{G}} = 2E_{\bar{q}} E_{\mathrm{G}}(1 - \cos\theta_{\bar{q},\mathrm{G}}) \\
\Rightarrow 1 - x_q &= \frac{2E_{\bar{q}} E_{\mathrm{G}}(1 - \cos\theta_{\bar{q},G})}{s}
\end{aligned}
\tag{36}
$$

where quarks and gluons are treated as massless which means $\mathbf{p}_i^2 = 0$ for $i = q, \bar{q}, \mathrm{G}$. An infrared gluon whose energy, E_{G}, is small with respect to the centre-of-mass energy, $\sqrt{s}$, leaves the corresponding energy fractions x_q of the quark close to unity. Hence, the differential cross-section is divergent (Eq. (35)). For the case of collinear gluon emission the angle between antiquark and gluon, $\theta_{\bar{q},\mathrm{G}}$, is small and, again, $1 - x_q$ is close to zero such that the differential cross-section diverges.

In order to obtain the total cross-section, the differential cross-section Eq. (35) is to be integrated over the phase-space $x_q, x_{\bar{q}} = 0 \ldots 1$ and $x_{\mathrm{G}} = 2 - x_q - x_{\bar{q}}$. In addition to this integration which includes the regions of the divergences, the Feynman graphs involving virtual gluon lines shown in Fig. 6 have to be added. It can be shown that, for instance, in the total cross-section the divergences of the differential cross-section are cancelled by identical divergences with opposite sign from the virtual gluon graphs [12]. Thus, the total cross-section is finite.

Adding the contributions from real and virtual gluon radiation increases the total cross-section for the annihilation of electron and positron into a final state of partons. The increase can be expressed by a simple α_{S} dependent factor. This correction factor to the R ratio is known up to third order in α_{S} [28]. In leading order the corrected R ratio[8] is

$$
R_{\mathrm{QCD}} = R\left(1 + \frac{\alpha_{\mathrm{S}}}{\pi} + \mathcal{O}(\alpha_{\mathrm{S}}^2)\right). \tag{37}
$$

In Fig. 5(a) the R_{QCD} ratio is shown as a dashed line versus the centre-of-mass energy $\sqrt{s}$. The size of the correction can be seen from the difference to the dotted line in this figure which represents the R ratio without the QCD correction from Eq. (37). The α_{S} dependence entering the R ratio through this correction allows a measurement of the strong coupling from total cross-sections alone. It is a fully inclusive measurement in the sense that nothing needs to be known about the details of the final state except that it has quarks. Experimentally the measurement is hampered because the correction is a rather small effect on a large R value, as can be seen from Fig. 5(a). This is in particular the case at higher energies where α_{S} assumes a small value.

To determine the coupling strength α_{S}, one can also investigate the details of the final state itself. It is the differential cross-section from Eq. (35) which determines the final state of quark, antiquark and gluon depending on the coupling strength α_{S}. Common to all approaches is the measurement of the probability of gluon radiation off the quark or antiquark. A very direct method would be to

[8] Further corrections, in particular charm, bottom and top quark mass effects and the non-universality of the Z coupling to the quarks have to be taken into account. These modify the coefficient but maintain the principle structure. See Section 4.1.1.

detect quark, antiquark and gluon, to measure their energy fractions x_i, and to determine the differential cross-section from counting rates.

Other approaches consider the spatial distribution of quark, antiquark and gluon in the final state. At large centre-of-mass energy a quark–antiquark final state without a gluon is pencil-like in its rest frame, with a gluon it is planar, and with many partons the final state might look spherical. Such methods are measurements of the shape of the final state. The quantities, commonly called event shape observables, are calculated from the energies and momenta of the particles in the final state. Again a differential cross-section is given for each observable $\mathscr{F}$. It results in leading order perturbation theory from the integration of the differential cross-section for real gluon emission Eq. (35) over the whole phase-space

$$\frac{1}{\sigma_0}\frac{\mathrm{d}\sigma}{\mathrm{d}\mathscr{F}} = \iint \mathrm{d}x_q\,\mathrm{d}x_{\bar{q}}\,C_F\frac{\alpha_S}{2\pi}\frac{x_q^2+x_{\bar{q}}^2}{(1-x_q)(1-x_{\bar{q}})}\delta(\mathscr{F}-f_{\mathscr{F}}(x_q,x_{\bar{q}},x_G)) + \mathscr{O}(\alpha_S^2)$$

$$= \mathscr{A}(\mathscr{F})\cdot\frac{\alpha_S}{2\pi} + \mathscr{O}(\alpha_S^2) \tag{38}$$

where the function $f_{\mathscr{F}}$ represents the value of the event shape observable $\mathscr{F}$ for the particular values of the energy fractions x_i of quark, antiquark and gluon. The result of the integral is given by the function $\mathscr{A}(\mathscr{F})$ which can be obtained by either analytical or numerical integration. Measuring this differential cross-section for an event shape observable $\mathscr{F}$ thus allows a determination of the coupling constant α_S.

An example is the *thrust* observable T. It is determined from the fractional energies of quark, antiquark and gluon according to

$$T \equiv f_T(x_q,x_{\bar{q}},x_G) = \max(x_q,x_{\bar{q}},x_G). \tag{39}$$

Thrust acquires unity for final states without gluons whereas its value is $\geq 2/3$ when gluon emission is present in the final state. Thus being sensitive to gluon radiation, α_S can be determined from a measurement of T. Further explicit examples of event shape observables will be presented in Section 4.1.2.

Experimentally it turns out, however, that all such determinations of the strong coupling from the final state of the partons are hampered since hadrons rather than quarks and gluons are observed by a particle detector. This problem will be addressed in more detail in Section 3.2.

A theoretical complication is due to the aforementioned infrared and collinear divergences of the differential cross-section for the real gluon emission. In the case of the event shape observables the divergences are present in the function $\mathscr{A}(\mathscr{F})$ of Eq. (38). As a consequence the perturbative calculation of any differential cross-section is only applicable in a region of the phase-space not too close to the kinematical boundaries $x_q, x_{\bar{q}} = 1$, or $x_q + x_{\bar{q}} = 1$, that is $x_G = 0$, where the differential cross-section becomes divergent. Interpreted with the help of Eq. (36) this requirement translates into cut-offs, namely that the gluon must be sufficiently energetic and not too close to either to the quark or antiquark. If a gluon in an event fails these requirements the corresponding three-parton configuration is experimentally indistinguishable from the back-to-back parton configuration in a two-parton final state. In other words, one has to require a *resolvable* gluon in the final state. In consequence, only within this phase-space region is a determination of the strong coupling possible using perturbative calculations as described above.

One could improve on this situation. Since the physical cross-section is finite, the theoretically calculated one has to be finite too. This, however, would be the case for a perturbation series for the differential cross-section in Eq. (35) which includes all powers in α_S. Currently the differential cross-section of three parton final states is known to second order $\mathcal{O}(\alpha_S^2)$ [32,33] only. At this order final states with up to four partons are possible, for example $q\bar{q}q'\bar{q}'$ and $q\bar{q}$GG. The differential cross-section for these final states were calculated in leading order $\mathcal{O}(\alpha_S^2)$ by several groups [32,34] and also in next-to-leading order ($\mathcal{O}(\alpha_S^3)$) for some event shape observables [35]. Furthermore there are computations of the five-parton final state in leading order, i.e. $\mathcal{O}(\alpha_S^3)$ [36], and also the six-parton final state was calculated in leading order [37].

3.1.3. Logarithmic approximation of gluon radiation

Although $\mathcal{O}(\alpha_S^2)$ calculations constitute a significant improvement over the $\mathcal{O}(\alpha_S)$ formulae, the differential cross-sections obtained from the calculations still suffer divergences at the kinematical boundaries. The inclusion of even higher orders is progressing slowly. In particular the computation of virtual correction terms of such higher orders to the three-parton differential cross-section is very cumbersome. To obtain improved calculations different methods have been developed which resum to all orders in α_S contributions to the differential cross-section that become large close to the kinematic limit.

The basic idea is to consider the probability of gluon emission in certain regions of phase-space. This probability becomes divergent close to the kinematical boundaries where the energy of the gluon becomes small, or the gluon is collinear with the parton emitting it. In such regions the simple perturbation expansion in powers of α_S is not reliable as the differential cross-section Eq. (35) is logarithmically divergent. This can be seen if one considers a region of the phase-space where, for instance, the gluon is emitted by the antiquark and x_q is close to unity. Choosing the nomenclature of Eq. (36), we have a kinematical invariant $m^2 = (\boldsymbol{p}_{\bar{q}} + \boldsymbol{p}_G)^2 = s(1 - x_q)$. With this invariant, one can change variables in Eq. (35) from x_q to m^2, yielding to the limit $x_q \approx 1$

$$\frac{1}{\sigma_0}\frac{d^2\sigma}{dz\,dm^2} \approx \frac{\alpha_S}{2\pi}\frac{1}{-m^2}C_F\left[\frac{1+z^2}{1-z}\right], \tag{40}$$

where $z = x_{\bar{q}}/(x_{\bar{q}} + x_G)$ is the fraction of energy of the antiquark. What has been achieved is, in fact, a factorization of the differential cross-section into the product of the subprocesses, namely the mass of the antiquark–gluon system, m, and the energy fraction of the antiquark, z.

Integrating over m^2 or z while keeping the other variable fixed yields in both cases logarithms in the integration variable, for example

$$\int dm^2 \frac{d^2\sigma}{dz\,dm^2} = \frac{d\sigma}{dz} \sim \ln(m^2)\frac{\alpha_S}{2\pi}C_F\left[\frac{1+z^2}{1-z}\right], \tag{41}$$

which become large as the integration approaches the kinematic limit at $m^2 = 0$ and $z = 1$, respectively. These large logarithmic terms will dominate the cross-section in such regions of phase-space whereas contributions due to gluon emission at high energy and large angle are only important outside. In the framework of the leading-logarithmic approximation (LLA) only these logarithms in the perturbative expansion are kept and resummed to all orders in α_S. Different schemes have been devised such as the *double leading-log approximation* (DLLA) [38],

the *next-to-leading-log approximation* (NLLA) [39], or the *modified leading-log approximation* (MLLA) [40,41] in order to take into account some subleading corrections, which are suppressed by additional logarithmic factors. The leading-log approximation and its refinements rely on simplifications in kinematic variables. Its predictive power for hard, wide angle parton emission remains limited. Such cases still have to be treated using the full calculation of the matrix element as in Eq. (35).

What makes LLA a success is that it is possible to understand it together with the resummation in a probabilistic picture, which allows an implementation in Monte Carlo generators of multi-parton final states (see below). To reveal this picture, the $\ln(t) = \ln(Q^2/\Lambda^2_{\mathrm{LLA}})$ derivative of Eq. (41), with m^2 replaced by Q^2, is integrated over z yielding

$$\frac{\mathrm{d}\mathscr{P}_{q\to qG}}{\mathrm{d}\ln(t)} \sim \int \mathrm{d}z \frac{\alpha_S(Q^2)}{2\pi} C_F \left[\frac{1+z^2}{1-z}\right]. \tag{42}$$

This equation can be interpreted as the leading order probability $\mathscr{P}$ of a quark splitting,[9] $q \to qG$, into a quark of fractional energy z and a gluon. The term in square brackets of Eq. (42) determines this probability. Similar expressions, known as Altarelli-Parisi splitting functions [42], are derived for all basic branchings, yielding in leading order

$$\begin{aligned} P_{q\to qG}(z) &= C_F\left[\frac{1+z^2}{1-z}\right], \\ P_{G\to GG}(z) &= 2C_A\frac{[1-z(1-z)]^2}{z(1-z)}, \\ P_{G\to q\bar{q}}(z) &= T_F[z^2+(1-z)^2], \end{aligned} \tag{43}$$

where as an additional requirement flavour and energy conservation have to be maintained. First-order corrections, $\mathcal{O}(\alpha_S)$, to these functions are also known [43,44].

Cascading these branchings according to the probabilities $\mathscr{P}$ of Eq. (43), allows the creation of a multi-parton final state. An example is sketched in Fig. 3. A definite course of the cascading requires that $t = Q^2/\Lambda^2_{\mathrm{LLA}}$ of Eq. (42) be regarded as a dimensionless *evolution* or *ordering* parameter. One of many possible choices for Q^2 would be the square of the virtual mass, m^2, of the branching parton as was chosen for the derivation above. Repeated branchings which occur at subsequent steps in t of the evolution lead to a parton shower which, at the end, consists of many partons, mainly gluons due to the larger colour factor C_A in the gluon–gluon coupling. The variable Λ^2_{LLA} is related to the constant of integration of the renormalization group equation, see Eq. (22). It signals that perturbative QCD is applicable only for $Q \gg \Lambda_{\mathrm{LLA}}$. To account for this and, furthermore, to avoid excessive production of very soft gluons close to the singular region of the z integration, one has to limit the evolution of the parton shower. This can be achieved by introducing a cut-off, Q_0, on the virtuality of the partons in the shower.

The concept of parton showers, because of its probabilistic nature, can be easily implemented into Monte Carlo generator programs. Several such programs are available which mainly differ in the interpretation of t, Q^2 and z, and some also include subleading logarithmic approximations. See Ref. [45,46] for details on the implementation of the parton shower approach in these programs.

[9] Likewise antiquark.

Predictions of the programs are compared with measurements quite extensively as will be indicated in the following sections.

In summary, a parton shower calculation is complementary to an order-by-order calculation in the sense that the former may give a good description of the structure of partons which are close together. The parton shower approach, however, is not expected to cover the full information content available in the matrix-element expression, in particular when the partons are well separated. Nevertheless, patching up the parton shower Monte Carlo generators allows a reasonable description of hard gluon emission to be retrieved.

3.2. Phenomenology of QCD in e^+e^- experiments

In the preceding section final states were considered which consisted of partons only. What remains detectable from an annihilation into quarks and gluons, however, are hadrons built up from quarks and antiquarks. Fig. 7 shows two examples of e^+e^- annihilation into a quark–antiquark pair developing a hadronic final state. It should be noticed that the plots in the figure show two and three bundles of detected particles, respectively. Such bundles, usually called *jets*, reflect the processes at the level of the partons. Therefore the right plot of Fig. 7 shows a jet of a well separated gluon high in energy in addition to the jets of quark and antiquark.

So obvious as the connection between the observed jets and the underlying parton process might be, it is impossible to calculate the *hadronization* which is the transition of partons into hadrons in the framework of perturbative QCD. This is due to the very low energy scale Q involved in this transition which renders α_S too large for a useful perturbation expansion. The effects of hadronization, however, which blur the view of the partons, have to be taken into account when deducing

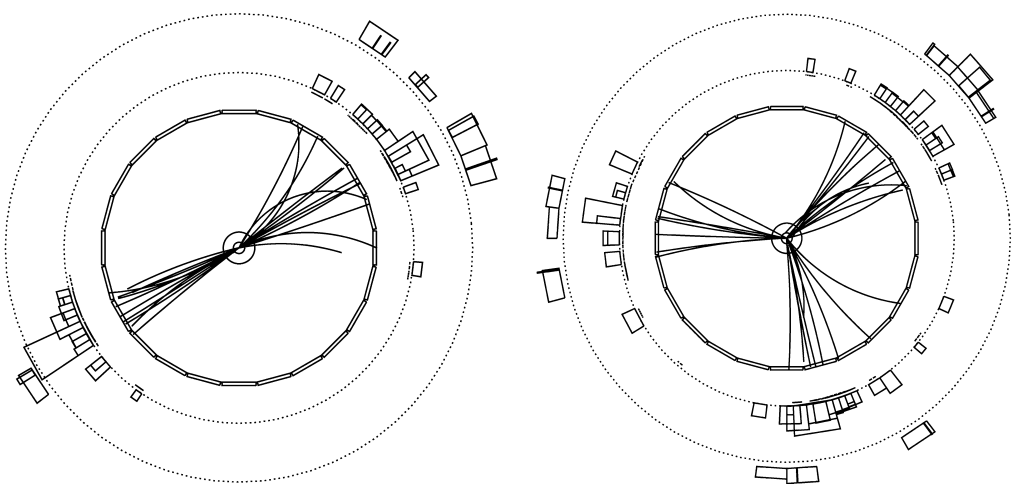

Fig. 7. Two examples of hadronic final states in e^+e^- annihilation recorded in a particle detector. The final state on the right results from an additional well separated gluon radiated by the quark–antiquark pair. The measured particles are shown in the plane perpendicular to the direction of e^+ and e^- which annihilated in the centre of each plot. Charged particles, bent by a solenoidal magnetic field, are shown as curves. The boxes represent the energy deposit of neutral and charged particles in outer components of the particle detector.

information on the partons from the hadronic final state. Therefore many models have been devised which describe the hadronization of partons at the end of the parton shower development on a phenomenological basis. A detailed overview can be found in Refs. [45,46] and in Ref. [11] which also summarizes experimental results on hadronization effects.

All existing models implement hadronization as a probabilistic and iterative procedure, usually named fragmentation, which applies one or more types of simple branchings:

(IF) jet → hadron + remainder-jet,
(SF) string → hadron + remainder-string,
(CF) cluster → hadron + hadron, or cluster → cluster + cluster.

Probabilistic rules prescribe at each branching the production of new flavours and the sharing of energy and momentum between the fragments. In practice, these fragmentation rules depend on parameters which cannot be calculated from first principles but have to be adjusted to obtain a useful description of measured data. In the following a brief description of the main types of models and some relevant parameters is given.

3.2.1. Independent fragmentation

The name of this hadronization model [47] suggests that each quark is hadronized independently. Fig. 8 illustrates the principle of the iterative fragmentation procedure. The quark jet q is split into a hadron consisting of $q\bar{q}_1$ and a remainder-jet q_1. The hadron takes a fraction z of the available energy and momentum according to a probability function $f(z)$, leaving $1-z$ for the remainder-jet. Usually, z is the light-cone energy-momentum fraction defined as

$$z = \frac{(E + p_{\parallel})_{\text{hadron}}}{(E + p)_q}, \tag{44}$$

where $p_{\parallel}$ is the longitudinal momentum along the jet axis. The fragmentation function $f(z)$ which is used in the independent fragmentation model is assumed to be energy independent, thus being the same at each fragmentation step.

The independent fragmentation model has a number of drawbacks. To start with it is not Lorentz invariant and does not exactly conserve energy, momentum and flavour which all have to be patched up at the end. On top of that independent fragmentation does not intrinsically contain

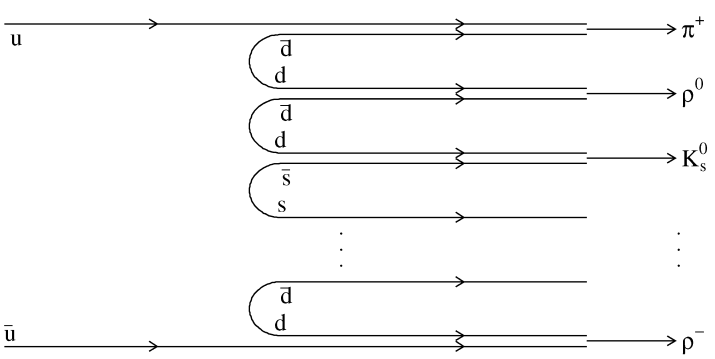

Fig. 8. Schematic representation of the independent fragmentation procedure (adapted from Ref. [45]).

gluon interference effects which are expected from MLLA calculations [41,48] and were observed by the PETRA and the LEP experiments [49–53]. The independent fragmentation model is, therefore, now largely disfavoured. A Monte Carlo generator based on this model which is routinely used in comparisons with data is COJETS [54].

Irrespective of the principal deficiencies of the independent fragmentation model, the concept is still commonly used when fragmenting the heavy charm and bottom quarks into hadrons containing these quarks. In particular, the Peterson et al. fragmentation function [55] is experimentally preferred (see [11]) because of its energy-momentum spectrum which is peaked at large values of z (see Fig. 9). The function is of the form

$$f(z) \sim \frac{1}{z}\left(1 - \frac{1}{z} - \frac{\varepsilon_Q}{1-z}\right)^{-2}. \tag{45}$$

It is controlled by a single free parameter, ε_Q, which is expected to scale between flavours as $\varepsilon_Q \sim 1/m_Q^2$. Fig. 9(a) shows this fragmentation function, respectively, for charm and bottom quarks, assuming $\varepsilon_c = 0.031$, $\varepsilon_b = 0.0038$ as given in Ref. [56].

3.2.2. String fragmentation

The string fragmentation scheme, which was first proposed in Ref. [57] and later elaborated by the Lund group [58], considers the colour field between the partons. As a quark–antiquark pair of complementary colour moves apart the colour field between them collapses due to the gluon self-interaction into a uniform colour flux tube, which is called a string. It has a transverse dimension of typical hadronic sizes (1 fm) and a constant tension $\kappa \approx 1\,\mathrm{GeV/fm}$. Energetic gluon emission can be regarded as energy-momentum carrying "kinks" of the string [59]. Hence, a complicated string moving in space–time is associated with a multiparton state.

The fragmentation into hadrons occurs, if the potential energy stored in the string is sufficient to create a $q'\bar{q}'$ pair from the vacuum, by breaking the string up into colour singlet systems as long as the invariant mass of the string pieces is larger than the on-shell mass of a hadron. Thus, at the end of the fragmentation each hadron corresponds to a small piece of string. This is illustrated in Fig. 10.

The creation of the string breaking quark–antiquark pairs is governed by a quantum mechanical tunneling probability which depends on the hadron transverse mass $m_\perp$ and the string tension κ.

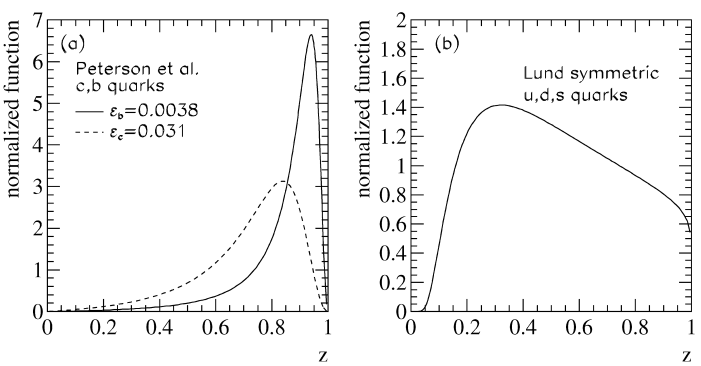

Fig. 9. (a) Peterson et al. [55] and (b) Lund symmetric [58] fragmentation function with parameters taken from Ref. [56].

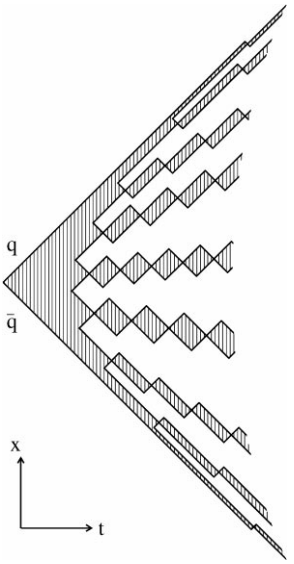

Fig. 10. Schematic representation of the string fragmentation procedure (adapted from Ref. [45]). A string stretched between q and $\bar{q}$ in two-dimensional space–time is repeatedly broken up by quark–antiquark pairs until on-mass-shell hadrons remain.

The probability is proportional to

$$\exp\left(-\frac{\pi m_\perp^2}{\kappa}\right) = \exp\left(-\frac{\pi m^2}{\kappa}\right)\exp\left(-\frac{\pi p_\perp^2}{\kappa}\right), \tag{46}$$

where the transverse momentum $p_\perp$ is locally compensated between quark and antiquark. As a consequence the dependence on the hadron mass, m, results in a suppression of strange and, especially, charm and bottom quark production at this step of the fragmentation process.

Finally, energy and momentum have to be shared between the string pieces such that the symmetry between the two ends of the string is maintained. The symmetry requirement restricts the choice of the fragmentation function which takes the simplified form

$$f(z) \sim \frac{1}{z}(1-z)^a \exp\left(-\frac{bm_\perp^2}{z}\right), \tag{47}$$

with two free parameters, a and b. These need to be adjusted so that the fragmentation is in accordance with measured data. The shape of this function is shown in Fig. 9(b) for $a = 0.11$, $b = 0.52\,\mathrm{GeV}^{-2}$, $m = 0.7\,\mathrm{GeV}$, and $p_\perp = 0.4\,\mathrm{GeV}$ as given in Ref. [56].

The concept of string fragmentation is implemented in several Monte Carlo generator programs, for example JETSET [60] and ARIADNE [61].

3.2.3. Cluster fragmentation

The cluster fragmentation scheme, which is implemented in the HERWIG [62] Monte Carlo generator, assumes a local compensation of colour based on the *pre-confinement* property of

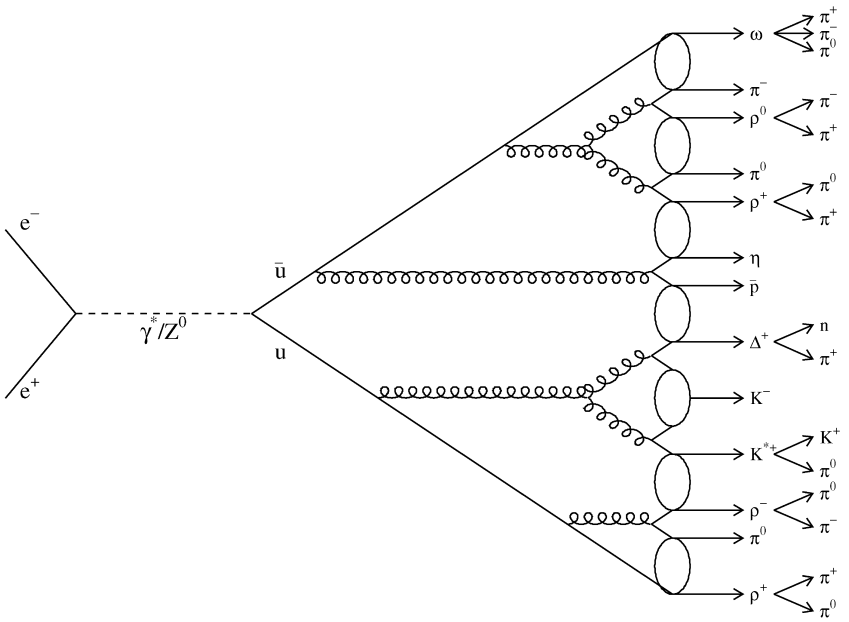

Fig. 11. Schematic representation of the cluster fragmentation procedure (adapted from [45]).

perturbative QCD [63]. The whole process of cluster fragmentation is illustrated in Fig. 11. This scheme keeps track of the colour flow during the parton shower evolution. To locally compensate colour at the end of the parton shower the remaining gluons are split into quark–antiquark pairs. A quark from such a splitting may form a colour singlet cluster with the antiquark from an adjacent splitting. Thus clusters are formed which have a typical mass of a couple of GeV.

Finally, to obtain hadrons, a cluster is assumed to decay into two hadrons unless it is either too heavy, in which case it will decay into two clusters, or too light, in which case the cluster decays into a single hadron, requiring a rearrangement of energy and momentum with neighbouring clusters. For the decay into two hadrons, which is assumed to be isotropic in the rest frame of the cluster except if the primary quark is involved, a decay channel is chosen based on the phase-space probability only. It involves the density of states, in particular the spin degeneracy of the hadrons. Due to the phase-space dominance in the hadron formation, the cluster fragmentation has a compact description with few parameters.

3.2.4. Theoretical approaches to hadronization

Apart from the many phenomenological fragmentation schemes that were proposed (see surveys in Refs. [45,46]), two approaches will be presented which are characterized by a simple but experimentally successful concept. Section 5 is devoted to the application of these two approaches to experimental data.

One is the concept of *local parton–hadron duality* (LPHD) [41,64]. It assumes an immediate relation between the properties of the final state at the parton and at the hadron level based on the conjecture that the transition from partons to hadrons is local in phase space, blanching and hadronization of the coloured partons. The idea arose from the *preconfinement* property of

perturbative QCD [63]. There is not an explicit formation of hadrons from the partons in the LPHD approach and, therefore, it does not involve dedicated fragmentation functions. The energy and momentum distributions at the hadron level are derived from the parton level distributions by employing a normalization factor.

The other concept, which is now intensively investigated, considers non-perturbative corrections [65–74] to the perturbatively calculated standard cross-section. Non-perturbative corrections, which cannot be obtained from an expansion of the differential cross-section in powers of α_S, are expected to become significant because of hadronization.

The effect of hadronization can be qualitatively estimated using the simple longitudinal phase-space or 'tube' model [75] (see also [76]). In this model a parton produces a jet of light hadrons, each of them characterized by the rapidity y and the momentum p_t transverse to the direction of the initial parton. The rapidity is defined as $y = 0.5 \ln[(E + p_z)/(E - p_z)]$ where E is the energy and p_z is the momentum along the direction of the parton. The hadrons jointly occupy a tube in (y, p_t)-space as is illustrated in Fig. 12. The transverse momentum of the hadrons in the tube is due to the hadronization. Thus, from a hadron density $\rho(p_t)$ in the tube, one finds its hadronization scale $\lambda = \int d^2 p_t \, \rho(p_t) p_t$. Noting that $\cosh y = E_{\text{hadron}}/m_{\text{hadron}}$ and $\sinh y = p_{\text{hadron}}/m_{\text{hadron}}$ one can calculate the energy and momentum of a tube of rapidity length Y for $m_{\text{hadron}} \approx \lambda$, yielding

$$E = \int_0^Y dy \, \lambda \cosh y = \lambda \sinh Y ,$$

$$P = \int_0^Y dy \, \lambda \sinh y = \lambda(\cosh Y - 1) . \tag{48}$$

For $Y \gg 1$ one obtains approximately $P \approx E - \lambda$.

In order to find in this model the effects of hadronization on observables like thrust, a two-jet configuration should be considered. The full energy of this system is Q. Thus each massless parton

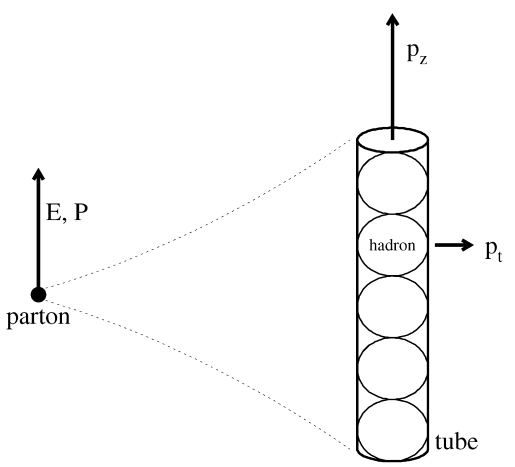

Fig. 12. Schematic representation of the simple tube hadronization model in which hadrons occupy a tube in rapidity and transverse momentum. It can be deduced from this model that hadronization effects cause power corrections to observables.

has $E = Q/2$ and, hence, $x \equiv E/(Q/2) = 1$ whereas for the tube $x_{\text{tube}} = 2P/Q \approx 2(E - \lambda)/Q$. Recalling the definition of thrust from Eq. (39) one finds for the tube

$$T = \max(x_{\text{tube}}) \approx 1 - 2\lambda/Q\,. \tag{49}$$

This exemplifies the impact of hadronization on thrust. Similar conclusions can be drawn for other observables such that hadronization effects are generally expected to be suppressed by one or more powers of $1/Q$.

3.2.5. Treatment of hadronization in measurements

Calculations of observables like thrust rely on perturbation theory, yielding power series in α_S as shown in Eq. (38). When performed only up to a certain finite order in α_S, the result of the calculations is applicable to a final state with a small number of partons. However, observables are measured from the particles (hadrons) emerging from the hadronization of the partons which is still not calculable from basic QCD principles. Effects due to hadronization are usually not negligible as one may deduce from the fact that at most four partons are described by an $\mathcal{O}(\alpha_S^2)$ calculation whereas about 40 charged and neutral particles are observed in the detector (see Fig. 7).

The phenomenological models of hadronization, which are implemented in Monte Carlo programs and some of which have been described in this section, have to be invoked to bridge the gap between hadrons and partons. Broadly speaking, a measured distribution is numerically deconvolved for hadronization distortions using events simulated by Monte Carlo event generators. Given that the differential cross-section for an observable is measured as a histogram, two principal approaches are commonly pursued for the deconvolution: (i) bin-by-bin correction factors, and (ii) a correction matrix.

In most studies correction factors are well-suited to account for hadronization so long as the differential cross-section varies only slightly with the value of the observable and if the width of the bins is sufficiently large. Otherwise hadronization may lead to significant distortions due to bin migration effects which need to be corrected using a correction matrix. Such a matrix relates the values the observable assumes for a partonic final state with those of the associated hadronic final state. To apply a correction matrix to a measured distribution, it needs to be inverted. Doing this analytically usually yields unstable results due to statistical fluctuations. A variety of recipes are on the market like iterative inversion, singular value decomposition (SVD), Bayesian method and regularization, which will not be detailed in this report (for details see [77,78]).

Since all these prescriptions rely heavily on the phenomenological hadronization models and their many non-calculable parameters, one naturally attempts to find observables which do not suffer significant hadronization distortions. Moreover, the determination of the strong coupling constant, α_s, is usually restricted to regions with small hadronization effects. Examples of such observables will be described in the following section.

4. Studies of the energy dependence of QCD

To obtain a finite result for the calculation of cross-sections, renormalization of colour charge and quark mass has to be invoked. As a consequence both the renormalized charge and mass depend on the renormalization scale μ. However, cross-sections of physical processes must not

depend on it. This requirement leads to a scale dependence of the strong coupling constant (Eq. (22)) and the quark masses (Eq. (23)). The scale dependence due to renormalization is a fundamental prediction of QCD which has to be verified by experiment.

This section presents determinations of the strong coupling at various energy scales using different methods, thus reducing potential biases of the energy dependence due to the method of determination. The review of results will be mostly limited to energy scales above the threshold for bottom quark pairs, that is $\approx 10\,\mathrm{GeV}$, where perturbative calculations are assumed to be very reliable. At the end of the section the running of the quark masses will be considered. Experimental effects due to non-vanishing quark masses were looked for in studies of the flavour independence of α_S. Direct determinations of the scale dependence of quark masses are becoming available now since the $\mathcal{O}(\alpha_S^2)$ matrix elements including quark masses have been calculated.

4.1. Determination of the running of α_S

Many different approaches to determine the strong coupling constant α_S in e^+e^- annihilation exist. Recalling the collinear and infrared singularities associated with the perturbative calculation of cross-sections, one may distinguish two different classes of α_S determinations depending on the inclusiveness of the measured quantity. Fully inclusive quantities have real and virtual contributions added such that infrared singularities cancel while remaining collinear divergences are factorizable and can be absorbed into process-independent parton distributions and fragmentation functions. Although inclusive quantities like event shape observables and jet rates consider the full final state, collinear and, in particular, infrared singularities affect the measurement through the sensitivity of the observables to the details of the final state.

Another argument in favour of the fully inclusive and inclusive quantities concerns the renormalization scale dependence which has been explained in Section 2.2.3. Many fully inclusive quantities are calculated in α_S to orders higher than next-to-leading (NLO), mainly next-to-next-to-leading (NNLO). While NLO predictions still significantly depend on the choice of the renormalization scale μ, the dependence at NNLO is greatly reduced because it is suppressed by a factor α_S^4, that is one power more than for NLO. In general, the more terms of the perturbation series are added, the more stable is the prediction against arbitrary scale choices. Therefore, higher-order perturbation calculations are expected to yield results less sensitive to an arbitrary choice of the scale.

4.1.1. Fully inclusive quantities: cross-sections and hadronic branching fractions

The total hadronic cross-section, σ_{had}, is obviously a fully inclusive observable. In particular at the Z pole high statistics measurements of cross-sections were done in order to precisely survey the Z resonance. With the use of dedicated subdetectors installed in each of the LEP experiments the luminosity, which is needed in the determination of cross-sections, is measured to an accuracy of better than 0.1% (see for example [5]). At such high precision, the strong coupling constant α_S can be determined from the QCD corrections that have to be applied to the hadronic cross-section. Away from the Z pole, i.e. at higher energies at LEP II, at lower energies at TRISTAN, PETRA, PEP, and even near the bottom quark production threshold at about 10 GeV at CESR, measurements of the hadronic cross-section can be used to determine the strong coupling constant.

Inclusive branching fractions of particle decays into hadrons are also fully inclusive quantities since they do not rely on any details of the final state. Precise measurements and perturbative

predictions exist for the τ lepton, the $J/\psi(1S)$ and the Υ resonances. These have been used to determine the strong coupling constant at very low scales in the range of 1.8–10 GeV. Since α_S is rather large at these scales, non-perturbative and mass effects are not negligible. Some of the corrections are even not calculable and, hence, have to be determined from the measured data. Nevertheless, determinations of α_S from these particles provide valuable input to test the running of the strong coupling.

4.1.1.1. Hadronic cross-sections. The total hadronic cross-section, σ_{had}, for e^+e^- annihilation has been calculated to third order in α_S (NNLO) [79], yielding

$$\sigma_{had} = \sigma_0\left[1 + \frac{\alpha_S}{\pi} + 1.409\left(\frac{\alpha_S}{\pi}\right)^2 - 12.808\left(\frac{\alpha_S}{\pi}\right)^3 + \mathcal{O}(\alpha_S^4)\right], \tag{50}$$

where σ_0 is the Born level cross-section without QCD corrections. This formula receives further corrections due to the finite masses of the quarks. One also has to consider the differences between vector and axial contributions due to the Z weak coupling even for massless final state quarks. In Ref. [80] a parameterization applicable at the Z pole is obtained which includes these effects. It approximates the R_{QCD} ratio which has been introduced in Section 3.1.1 at a precision of $\Delta R = 0.0005$. For a top quark mass of $m_{top} = 173.8$ GeV [81] and a Higgs boson mass of $m_{Higgs} = 300$ GeV the parameterization is [80]

$$R_{QCD} = \frac{\sigma_{had}(m_Z)}{\sigma_0(m_Z)} \approx R_0\left[1 + 1.060\frac{\alpha_S}{\pi} + 0.852\left(\frac{\alpha_S}{\pi}\right)^2 - 15\left(\frac{\alpha_S}{\pi}\right)^3\right]. \tag{51}$$

Electroweak radiative corrections and the Higgs mass dependence are all absorbed into the factor R_0 which assumes a value of 19.938 for the aforementioned top quark and Higgs boson masses.

The R_{QCD} ratio has been inferred very precisely at the LEP collider from a measurement of the hadronic and leptonic decay widths, Γ_{had} and Γ_{lept}, of the Z boson. A value of $R_{QCD} = 20.765 \pm 0.026$ was determined in Ref. [4]. Solving Eq. (51) for $\alpha_S(m_Z^2)$ one obtains

$$\begin{aligned}\alpha_S(m_Z^2) &= 0.1217 \pm 0.0039\ (\text{exp.}) \ \pm 0.0040\ (\text{theor.})\\ &= 0.1217 \pm 0.0056\,,\end{aligned} \tag{52}$$

where the first error is due to the uncertainty of R_{QCD}.[10] The second error is the quadratic sum of the contributions from the uncertainties of the electroweak calculations, from missing higher-order QCD corrections, and from the variation of the unknown Higgs boson mass between 60 and 1000 GeV. This result for the strong coupling, however, is based on the assumption that electroweak interactions (see Ref. [83]) are accurately described by the electroweak standard model, in particular Γ_{had}. One can reduce this sensitivity when in addition to R_{QCD} also the full decay width, Γ_Z, and the hadronic pole cross-section of Z exchange are considered in a simultaneous fit of m_{top}, α_S and m_{Higgs}. Such a fit has been performed in Ref. [4]. Considering all available electroweak

[10] Meanwhile a new parameterization based on the improved version of the ZFITTER program became available in Ref. [82], which slightly increases the central value of $\alpha_S(m_Z^2)$ in Eq. (52) by 0.0020.

data, including direct measurements of m_W and m_{top}, the fit yielded

$$\alpha_S(m_Z^2) = 0.119 \pm 0.003 \tag{53}$$

with $m_{top} = 171.1 \pm 4.9\,\text{GeV}$ and $m_{Higgs} = 76^{+85}_{-47}\,\text{GeV}$. It should be noted that the lower value of α_S from the simultaneous fit is due to the Higgs boson mass for which a value much lower than the assumed value of 300 GeV, is preferred by this fit.

The energy dependence of the strong coupling can be directly deduced from the cross-section measurements done by the experiments at the LEP collider above the Z pole at centre-of-mass energies of 130, 136, 161, 172, 183 and 189 GeV. The combination of these measurements [84–89], shown in Fig. 13 including measurements at lower centre-of-mass energies [90], is given in Table 2.

Although the weighted averages of the measurements at each energy have a total relative error of only about 1.5%, this uncertainty is still too large for a significant determination of α_S at each energy. Therefore, the results at the six different energies are combined in a fit in order to extract a value of the strong coupling at 161 GeV, which is just in the middle of the whole range of energies considered.

Since both Z and γ exchange contribute to the total hadronic cross-section above the pole, and due to the differences of the coupling of Z and γ to the quark flavours one cannot simply apply Eq. (50) to determine α_S. Moreover, a substantial fraction of the total cross-section at these high energies is due to very high energy initial state photon radiation, such that the effective centre-of-mass energy is close to the Z mass. In order to assess the value of the strong coupling the ZFITTER program [30] is employed to account for these details which are precisely known from perturbative

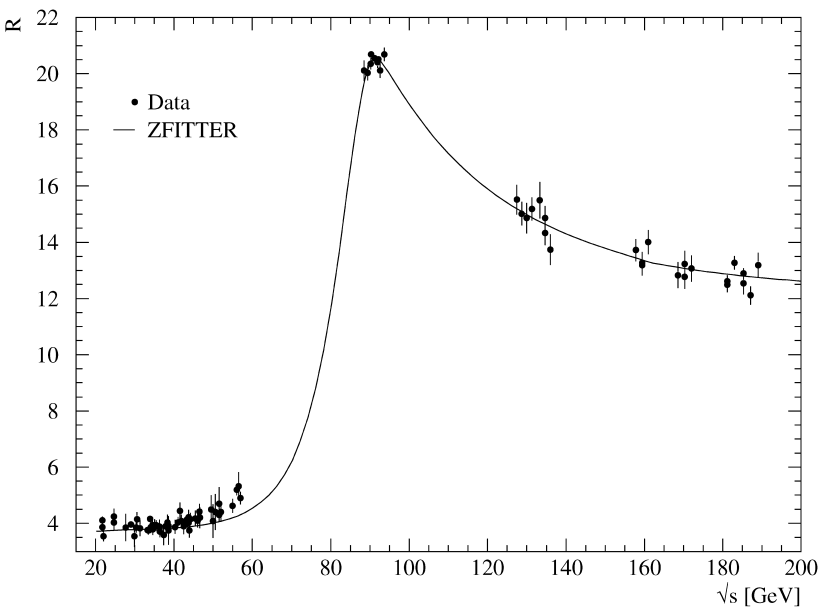

Fig. 13. The ratio of hadronic and muonic cross-section measured between 20 and 189 GeV is shown [84–90]. Measurements at identical energies are spread horizontally for clarity. For the same reason solely OPAL data are presented at the Z pole. The curve is calculated using the ZFITTER program [30]. It includes initial state photon radiation but not contributions from pair production of W and Z bosons.

Table 2
Total hadronic cross-sections measured at LEP above the Z pole [84–89]. The R_{QCD} ratios are obtained using the theoretical muon pair cross-sections calculated at the individual centre-of-mass energies by ZFITTER [30]

$\sqrt{s}$ (GeV)	hadr. cross-section (pb)	R_{QCD}
130	334.7 ± 5.0	15.15 ± 0.23
136	275.1 ± 4.6	14.56 ± 0.24
161	152.8 ± 2.3	13.52 ± 0.20
172	124.4 ± 2.2	12.96 ± 0.23
183	106.3 ± 1.2	12.79 ± 0.14
189	98.2 ± 1.1	12.72 ± 0.14

calculations. ZFITTER takes $\alpha_S(m_Z^2)$ as input, evolving it internally to the appropriate energy scale by means of the 3-loop β function. Applying the ZFITTER evolution, a χ^2 fit to the hadronic cross-section yielded for the coupling at 161 GeV

$$\alpha_S((161\,\mathrm{GeV})^2) = 0.128 \pm 0.033\ (\mathrm{exp.})^{+0.011}_{-0.007}\ (\mathrm{top, Higgs}), \tag{54}$$

where the first error is due to experimental uncertainties, whereas the second error stems from a variation of the top quark mass $m_t = 173.8 \pm 5.0$ GeV [81] and of the Higgs mass between 60 and 1000 GeV. The large error of the result underlines that, even if all LEP II results are combined, the precision of the measured cross-section limits the sensitivity to the size of the strong coupling because it contributes a small correction to the total hadronic cross-section only (cf. Eq. (50)). Even worse, the size of this correction decreases with increasing energies thus rendering this determination barely usable for a verification of the running of α_S at LEP II energies.

Since the expected energy dependence of the strong coupling is more pronounced towards lower scales, determinations of α_S from measurements of the total hadronic cross-section at lower centre-of-mass energies might yield a significant test of the running. In Ref. [91] measurements of the R_γ ratio at centre-of-mass energies below approximately 60 GeV were used to determine α_S. A correction to the erroneous third order coefficient of the theoretical calculation was applied to the original results in Ref. [9] which yielded

$$\alpha_S((31.6\,\mathrm{GeV})^2) = 0.163 \pm 0.022 \rightarrow \alpha_S(m_Z^2) = 0.133 \pm 0.015\,. \tag{55}$$

Eq. (22) has been applied to evolve to the m_Z scale. Within the large errors, which are due to the uncertainties of the cross-section measurements, this result agrees with the determinations (52) and (53) at the Z pole.

At around $\sqrt{s} = 10$ GeV many experiments precisely measured the R ratio for e^+e^- annihilation in the continuum [92,93]. A compilation can be found in Ref. [93]. The weighted average of these measurements is $R(\sqrt{s} \approx 10\,\mathrm{GeV}) = 3.53 \pm 0.05$. To determine α_S from it one has to consider the effects of quark masses and QED radiation. These were calculated in Ref. [94] to NNLO. The result is

$$R_{QCD}(\sqrt{s} = 10\,\mathrm{GeV}) \approx R_0\left[1 + 1.0179\frac{\alpha_S}{\pi} + 1.9345\left(\frac{\alpha_S}{\pi}\right)^2 - 10.7484\left(\frac{\alpha_S}{\pi}\right)^3\right], \tag{56}$$

which differs only marginally from the result for massless quarks (cf. Eq. (50)). Since the measurements of R were performed below the $\Upsilon(4S)$ resonance, $b\bar{b}$ production is kinematically forbidden. Thus only $n_f = 4$ quark flavours, namely u, d, s, c, need to be considered in the calculation of R_0 according to Eq. (32), yielding $R_0 = 10/3$. Solving Eq. (56) for α_S one obtains

$$\alpha_S^{(n_f=4)}((10\,\mathrm{GeV})^2) = 0.169 \pm 0.040\,. \tag{57}$$

With the help of Eq. (27) and using $m_b = 4.25 \pm 0.15\,\mathrm{GeV}$ [28] this result can be transformed to $\alpha_S((10\,\mathrm{GeV})^2) = 0.173 \pm 0.042$ for $n_f = 5$ active quark flavours, where the error includes a negligible uncertainty (± 0.0002) due to the error on the bottom quark mass m_b. Applying Eq. (22) the value of the strong coupling becomes

$$\alpha_S(m_Z^2) = 0.116^{+0.017}_{-0.020} \tag{58}$$

at the Z pole which is in agreement with the result obtained directly at the pole.

There also exist many measurements of the R ratio towards even lower energies (see compilation in Ref. [28]). These, however, do not allow a precise determination of the strong coupling constant. Measurements of the R ratio at energies in the range of 2–5 GeV have been completed by the BES collaboration [95]. Given an uncertainty of the order of a few per mill, a precise determination of α_S will become possible, thus testing its scale dependence at very low energies.

4.1.1.2. Hadronic branching fraction of the τ lepton. In the case of hadronic decays of the τ lepton, hadrons are formed from the $q\bar{q}'$ pair which stems from the virtual W boson of the weak decay. The hadronic branching fraction of the τ lepton, which is given by the ratio of the hadronic and electronic decay widths Γ_h and Γ_e, can be expressed as a power series up to third order in α_S [96] enhanced by additional correction terms [97]

$$\begin{aligned} R_\tau &= \frac{\Gamma_h}{\Gamma_e} = \frac{B_{\mathrm{hadrons}}}{B_e} = \frac{1 - B_e - B_\mu}{B_e} \\ &= 3.058\left[1 + \frac{\alpha_S(m_\tau^2)}{\pi} + 5.2023\frac{\alpha_S^2(m_\tau^2)}{\pi^2} + 26.366\frac{\alpha_S^3(m_\tau^2)}{\pi^3} + \delta_{ew} + \delta_m + \delta_{np}\right]. \end{aligned} \tag{59}$$

The electroweak correction $\delta_{ew} = 5\alpha_{em}(m_\tau^2)/(12\pi) \approx 0.001$ is small [98]. The relative sizes of the corrections owing to finite quark masses, $\delta_m \equiv (m_q/m_\tau)^2$, and owing to non-perturbative effects, δ_{np}, are estimated in Refs. [96,99,100] to be -0.014 ± 0.005 in total.

The ratio R_τ is derived in Ref. [28] from the measured branching fractions of the decays into electrons, B_e, and muons, B_μ, yielding $R_\tau = 3.642 \pm 0.024$. Furthermore, a value $R_\tau = 3.636 \pm 0.021$ is determined from lifetimes and masses of τ and μ, from which $B_e = (\tau_\tau/\tau_\mu)(m_\tau/m_\mu)^5$ is calculated assuming lepton universality. Averaging these, a value of $\alpha_S^{(n_f=3)}(m_\tau^2) = 0.35 \pm 0.03$ can be derived for the strong coupling constant, where the error is dominated by the estimated theoretical error from missing α_S^4 and higher-order terms in the power series, and from uncertainties of the non-perturbative contributions.

Instead of theoretically estimating the non-perturbative corrections they may be inferred from data by fitting to the invariant mass distribution of the hadronic τ decay. This way some theoretical uncertainties can be avoided. One has to consider moments of the mass distribution, since the

differential partial width $\mathrm{d}\Gamma_h/\mathrm{d}s$ in the integral

$$R_\tau(s_0) = \frac{1}{\Gamma_e}\int_0^{s_0} \mathrm{d}s\, \frac{\mathrm{d}\Gamma_h}{\mathrm{d}s} \tag{60}$$

is not yet directly accessible within existing theoretical skills. However, k,l-moments of the mass distribution, which are obtained by introducing a factor $(1-(s/m_\tau^2))^k(s/m_\tau^2)^l$ into the integrand, were calculated in Ref. [97]. Aside from a mere determination of α_S at the τ mass scale, that is $s_0 = m_\tau^2$, one may test the running of the coupling by restricting the moments to invariant mass squared of $s_0 < m_\tau^2$. This allows the size of the strong coupling at various values of s_0 to be determined.

Investigations of the invariant mass moments were performed by the ALEPH and OPAL collaborations at LEP, exploiting Z decays into τ pairs, and also by the CLEO collaboration [101–103]. Fig. 14 exemplifies the results on $\alpha_S(s_0)$ from fits of the restricted moments. The band represents the experimental error. Also shown is the expected running of α_S assuming 2 and 3 active flavours. Despite large correlations between the α_S values determined at adjacent s_0, a satisfactory agreement is found. Table 3 provides a compilation of the results on α_S obtained at $s_0 = m_\tau^2$. These were found from the application of the fixed order perturbation theory to the values of R_τ derived from the separately measured vector and axial-vector contributions to $\mathrm{d}\Gamma_h/\mathrm{d}s$. Due to the large value of α_S at the τ mass scale the power series in Eq. (59) does not converge well. To improve the convergence, attempts were made to obtain a resummation of some of the higher-order terms. Details can be found in Refs. [97,100,102]. In Ref. [102] variations in $\alpha_S^{(n_f=3)}(m_\tau^2)$ of up to $\pm$ 7%, that is $\pm$ 0.022, were found on average owing to modified perturbative descriptions.

The central result in Table 3 is obtained from a weighted average following the prescription of Ref. [104]. In brief, the value is calculated using the inverse squares of the total errors of the individual results as the weights. Ignoring tiny statistical correlations, but taking into account dominant systematic correlations, the error on the central result is determined by calculating a weighted average of the errors of the individual results using the same weights.

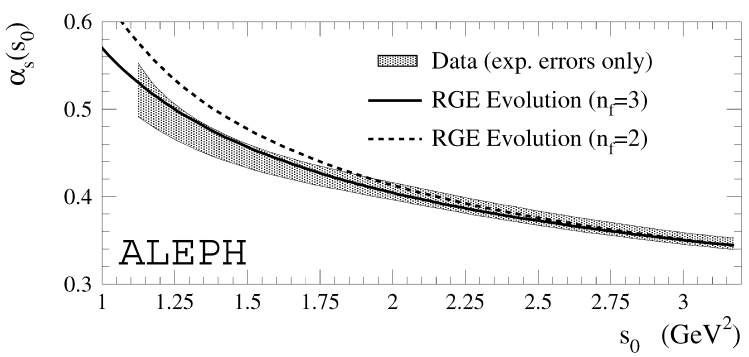

Fig. 14. The running of $\alpha_S(s_0)$ obtained in Ref. [101] from fits of an improved theoretical prediction to the invariant mass moments restricted to $s_0 < m_\tau^2$. A large correlation is present between the experimental values. The shaded band represents the experimental errors. Superimposed is the theoretical expectation of the scale dependence for 2 and 3 active flavours, respectively. Not shown is an overall uncertainty of about 7% due to the scatter from employing various improved theoretical predictions (see text and Refs. [101,102]).

Table 3
Compilation of $\alpha_S^{(n_f=3)}(m_\tau^2)$ determined from R_τ and from the measured vector and axial-vector decomposition of $d\Gamma_h/ds$ [101–103]. The results were obtained using fixed-order perturbation theory. An overall error of $\pm$ 7% has to be added to the results to account for changes due to missing higher-order terms of the perturbative series. The first error denotes the experimental uncertainties which include errors propagated from external branching ratios. The second error is the theoretical uncertainty. A weighted average is calculated taking into account the correlations of the individual values

Experiment	$\alpha_S^{(n_f=3)}(m_\tau^2)$
ALEPH93	$0.330 \pm 0.043 \pm 0.016$[a]
CLEO95	$0.306 \pm 0.017 \pm 0.017$
ALEPH98	$0.322 \pm 0.005 \pm 0.019$
OPAL98	$0.324 \pm 0.006 \pm 0.013$
Average	$0.321 \pm 0.009 \pm 0.015$

[a] Experimental and theoretical error are estimated from the total errors using the respective error contributions quoted for R_τ.

To evolve α_S from the τ mass scale to the Z pole Eq. (22) has to be applied. Since the number of active flavours at the m_τ scale is 3, the matching relations (27) have to be used at both the charm ($\bar{m}_c(\bar{m}_c) = (1.25 \pm 0.15)$ GeV [105]) and the bottom $\overline{\text{MS}}$ mass scale ($\bar{m}_b(\bar{m}_b) = (4.25 \pm 0.15)$ GeV [28]). Thus evolved to the Z scale, $\alpha_S^{(n_f=3)}(m_\tau^2)$ assumes a value of

$$\alpha_S(m_Z^2) = 0.1191 \pm 0.0011\ (\text{exp.}) \pm 0.0019\ (\text{theor.}) \pm 0.0029\ (\text{pert.}) \pm 0.0003\ (\text{evol.}), \tag{61}$$

where the first and second errors are experimental and theoretical, the third error is due to modified perturbation series, and the fourth error propagates from uncertainties of the evolution and matching equations [29]. This result is in excellent agreement with the value obtained from the determination of α_S from R_{had} at the Z pole and also from the fit to the electroweak data.

4.1.1.3. Hadronic decays of Υ resonances. Although the J/ψ meson has a mass of about 3.1 GeV it is sufficiently light that relativistic and non-perturbative effects are very significant. However, an α_S determination from hadronic decays of the Υ is possible. From its decay modes, two different R ratios can be defined for the Υ. Both are known in next-to-leading order NLO [106,107]

$$\begin{aligned} R_{GGG} &= \frac{\Gamma(\Upsilon \to GGG \to \text{hadrons})}{\Gamma(\Upsilon \to \mu^+\mu^-)} \\ &= \frac{10(\pi^2-9)}{9\pi}\frac{\alpha_S^3(\mu^2)}{\alpha_{em}^2}\left\{1 + \left[9.1 + 6.3\ln\left(\frac{\mu^2}{m_\Upsilon^2}\right)\right]\frac{\alpha_S(\mu^2)}{\pi}\right\}, \\ R_{\gamma GG} &= \frac{\Gamma(\Upsilon \to \gamma GG \to \gamma + \text{hadrons})}{\Gamma(\Upsilon \to \mu^+\mu^-)} \\ &= \frac{8(\pi^2-9)}{9\pi}\frac{\alpha_S^2(\mu^2)}{\alpha_{em}}\left\{1 + \left[3.7 + 4.2\ln\left(\frac{\mu^2}{m_\Upsilon^2}\right)\right]\frac{\alpha_S(\mu^2)}{\pi}\right\}. \end{aligned} \tag{62}$$

The fine structure constant α_{em} in this equation is to be evaluated at the Υ scale, that is $m_\Upsilon \approx 10\,\mathrm{GeV}$. In Ref. [107] a value of $\alpha_{em}^{-1}(m_\Upsilon) \approx 132.0$ was used in order to determine the strong coupling constant from measurements of the R_{GGG} ratio for the Υ and the J/ψ resonance states. At the Υ scale the result is [108]

$$\alpha_S^{(n_f=4)}(m_\Upsilon^2) = 0.167^{+0.015}_{-0.011} \rightarrow \alpha_S(m_Z^2) = 0.115^{+0.007}_{-0.005}\,, \tag{63}$$

where the value of the coupling at the Z pole is obtained from numerically solving Eq. (20).

The ratio $R_{\gamma GG}$ has been measured to high accuracy by the CLEO experiment [109], yielding

$$\alpha_S^{(n_f=4)}(m_\Upsilon^2) = 0.163 \pm 0.014 \rightarrow \alpha_S(m_Z^2) = 0.112^{+0.006}_{-0.007}\,, \tag{64}$$

where the error is dominated by theoretical uncertainties associated with the scale choice.

In Ref. [110] an investigation of moments of the $R(s)$ ratio for the first six Υ resonances was performed. From the perturbative series up to $\mathcal{O}(\alpha_S^2)$ (NLO) for these moments, which are calculated using measured masses and electronic decay widths of the Υ resonances, the $\overline{\mathrm{MS}}$ bottom quark mass $\bar{m}_b = (4.13 \pm 0.06)\,\mathrm{GeV}$ was obtained and the strong coupling constant was determined at this scale to be

$$\alpha_S^{(n_f=4)}((4.13\,\mathrm{GeV})^2) = 0.233^{+0.045}_{-0.030} \rightarrow \alpha_S(m_Z^2) = 0.120^{+0.010}_{-0.008}\,. \tag{65}$$

The dominant contribution to the error comes from uncertainties due to the choice of the renormalization scales for the bottom quark mass and α_S.

4.1.1.4. Summary of α_S determinations from fully inclusive quantities. In Table 4 the various α_S determinations presented in this section are listed. Motivated by the different dominance of theoretical, scale, and statistical uncertainties, the weighted average is calculated from the averages of each of the three groups of α_S determinations, viz. from R_τ, from quarkonia and from R_{QCD}, respectively. For the quarkonia the average α_S value and its error is determined using the total

Table 4
Listing of α_S determinations from fully inclusive quantities: the total hadronic cross-section and the hadronic branching fraction of the τ lepton and of the J/ψ and Υ mesons. The values at m_Z^2 were evolved from the values measured at $\sqrt{s}$ by numerically solving the 4-loop renormalization group equation (20) using $\bar{m}_c = 1.25 \pm 0.15\,\mathrm{GeV}$ [105] and $\bar{m}_b = 4.25 \pm 0.15\,\mathrm{GeV}$ [28]. The weighted average takes correlations into account

Observable quantity	$\sqrt{s}$(GeV)	n_f	$\alpha_S(s)$	$\alpha_S(m_Z^2)$	Theory
R_τ	1.777	3	0.321 ± 0.017	0.119 ± 0.004	NNLO
Υ [QCD moments]	4.13	4	$0.233^{+0.045}_{-0.030}$	$0.120^{+0.010}_{-0.008}$	NLO
$R_{GGG}(J/\psi,\Upsilon)$	10.0	4	$0.167^{+0.015}_{-0.011}$	$0.115^{+0.007}_{-0.005}$	NLO
$R_{\gamma GG}(\Upsilon)$	10.0	4	0.163 ± 0.014	$0.112^{+0.006}_{-0.007}$	NLO
R_{QCD}	10.0	4	0.169 ± 0.040	$0.115^{+0.017}_{-0.019}$	NNLO
R_{QCD}	31.6	5	0.163 ± 0.022	0.133 ± 0.015	NNLO
R_{QCD}	91.2	5	0.122 ± 0.006	0.122 ± 0.006	NNLO
R_{QCD}	161.0	5	0.130 ± 0.035	0.141 ± 0.044	NNLO
Weighted average	91.2	5		0.1195 ± 0.0025	

errors for the weights, while when averaging the R_{QCD} results no correlation is assumed due to the dominance of both the statistical uncertainties and the result at the Z pole. Also it has to be remembered that the α_S results obtained from the total hadronic cross-section are affected by tiny uncertainties only due to the choice of the scale. The uncertainty of the overall average is, therefore, calculated taking the full systematic error from the R_τ result as the sole common error for the α_S determinations from R_τ and the quarkonia decays.

One notes that the value of the coupling falls off significantly when the energy scale increases. This can be seen in Fig. 15 which shows these results together with the expectation of QCD for $\alpha_S(m_Z^2) = 0.119$. Comparing the α_S values evolved to the Z pole, one observes a good agreement between the various results. From this agreement, one may deduce that the energy dependence as predicted by the renormalization group equation (20), which is used to evolve the α_S from their respective to the m_Z scale, is very consistent with the data. The total error of the individual α_S determinations is still significant at the level of several percent.

4.1.2. Inclusive quantities: jet rates and event shapes

In order to determine α_S, one may directly investigate quarks and gluons in the final state of a hadronic event. Gluon emission by the quarks is connected with the coupling constant. This becomes immediately obvious from the differential cross-section shown in Eq. (35). Thus, to lowest order, the probability for a parton to radiate a gluon is directly proportional to α_S. Exploiting this property, one may pursue two approaches to assess the size of the coupling. One can either determine α_S by counting how often a gluon is emitted by a quark, that is by measuring the jet rates which requires the reconstruction of quarks and gluons from the jets of particles measured by the detector. Alternatively, one may take advantage of the fact that gluon radiation changes the spatial

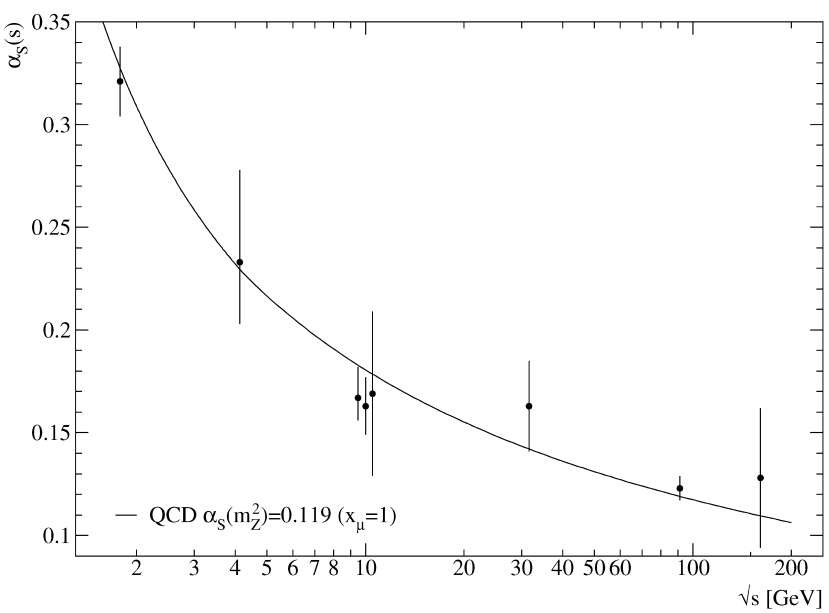

Fig. 15. The value of the strong coupling constant obtained from fully inclusive quantities at various centre-of-mass energies is shown. Superimposed on the data is the QCD expectation at 4-loop precision using $\alpha_S(m_Z^2) = 0.119$.

as well as the energy and momentum distributions of the particles in the detector, that is by performing a measurement of the shape of an event. Determinations of α_S based on both jet rates and event shapes will be presented in this section, starting with a theoretical description of the observables in each case.

4.1.2.1. Perturbative predictions for jet rates and event shapes. Although jet rates and event shapes are formally different in how they analyse an event, both are similarly described by perturbation theory. The general approach to the perturbative description of this kind of observable has already been presented in Eq. (38). Going beyond leading order (LO), analytical calculations become difficult due to the complicated phase space for multiparton final state configurations. Moreover, a special treatment of infrared and collinear singularities in real and virtual contributions to the differential cross-section of an observable is necessary.

Due to these difficulties full perturbation calculations of jet rates and event shapes are currently next-to-leading order (NLO) only. However, there exist improvements on these predictions using resummation of large logarithmic terms as will be detailed below. In NLO the distribution of an inclusive observable $\mathscr{F}$ is given by a series (cf. Eq. (38))

$$\frac{1}{\sigma_0}\frac{\mathrm{d}\sigma}{\mathrm{d}\mathscr{F}} = \frac{\alpha_S(\mu^2)}{2\pi}\mathscr{A}(\mathscr{F}) + \frac{\alpha_S^2(\mu^2)}{4\pi^4}(2\pi\beta_0\mathscr{A}(\mathscr{F})\ln x_\mu^2 + \mathscr{B}(\mathscr{F})) + \mathscr{O}(\alpha_S^3), \tag{66}$$

where $\mathscr{A}$ and $\mathscr{B}$ are perturbatively calculable coefficient functions of $\mathscr{F}$ which are tabulated in Ref. [111] for many event shape observables. The variable $x_\mu^2 = \mu^2/s$ is the renormalization scale factor, which relates the physical scale $\sqrt{s}$ to the renormalization scale μ. In contrast to fully inclusive quantities one must not neglect the arbitrariness of the choice of the scale μ at which α_S is renormalized.

Inclusive quantities are affected by infrared and collinear singularities since they are related to the differential cross-section for multiparton final states. As a consequence the perturbative prediction becomes unreliable for partons that are close together. This is in particular the case when approaching the 2-jet region with a back-to-back quark–antiquark final state, for which[11] $\mathscr{F} \to 0$. Due to large logarithmic contributions from $\ln(1/\mathscr{F})$ (see Section 3.1.3) perturbation calculations using α_S as expansion variable are not reliable in this region which occupies a significant fraction of the whole phase space (see for instance [12]). To overcome this deficiency of fixed-order perturbation theory, an expansion in $\alpha_S L$ is envisaged, where $L = \ln(1/\mathscr{F})$. For this purpose the normalized event shape cross-section is rewritten,

$$R(\mathscr{F}) = \int_0^{\mathscr{F}} \mathrm{d}\mathscr{F}' \frac{1}{\sigma_0}\frac{\mathrm{d}\sigma}{\mathrm{d}\mathscr{F}'} = C(\alpha_S)\exp\left[G\left(\alpha_S, \ln\frac{1}{\mathscr{F}}\right)\right] + D(\alpha_S, \mathscr{F}), \tag{67}$$

using a coefficient function $C(\alpha_S)$, an exponential of a function $G(\alpha_S, \ln(1/\mathscr{F}))$, and a remainder function $D(\alpha_S, \mathscr{F})$, which vanishes for $\mathscr{F} \to 0$ if $\mathscr{F}$ can be exponentiated this way. The functions

[11] Usually event shapes are normalized such that 0 corresponds to the 2-jet case.

C and G can be expanded in α_s and L

$$
\begin{aligned}
C(\alpha_s) &= 1 + \sum_{n=1}^{\infty} C_n \frac{\alpha_s^n}{(2\pi)^n} \\
G(\alpha_s, L) &= \sum_{n=1}^{\infty} \sum_{m=1}^{n+1} G_{nm} \frac{\alpha_s^n}{(2\pi)^n} L^m \\
&= L \sum_{n=1}^{\infty} G_{n,n+1} \frac{(\alpha_s L)^n}{(2\pi)^n} + \sum_{n=1}^{\infty} G_{n,n} \frac{(\alpha_s L)^n}{(2\pi)^n} \\
&\quad + \frac{\alpha_s}{2\pi} \sum_{n=2}^{\infty} G_{n,n-1} \frac{(\alpha_s L)^n}{(2\pi)^n} + \cdots \\
&\equiv L g_1(\alpha_s L) + g_2(\alpha_s L) + \alpha_s g_3(\alpha_s L) + \cdots .
\end{aligned}
\tag{68}
$$

The key point of the expansion of G is that some of the power series in $\alpha_s L$ could be summed to all orders for a number of event shape observables and jet rates [112–121], yielding specific functions g_i for $i = 1$ and 2. The function g_1 resums all *leading logarithmic* (LL) contributions, g_2 all *next-to-leading logarithms* (NLL). *Subleading* logarithms are contained in g_3, etc. Obviously g_1 becomes important if L is large, that is for $\mathscr{F}$ close to the 2-jet region. Provided g_3, $D(\alpha_s, \mathscr{F})$, etc. behave reasonably in this region, one may exploit g_1 and g_2 to predict the distribution of $\mathscr{F}$ down to $\alpha_s L \lesssim 1$, i.e. much lower than using a fixed-order perturbative expansion, which is applicable for $\alpha_s L^2 \ll 1$ only [12]. Thus the resummed expression complements the fixed order calculation towards the 2-jet region.

Before joining the two calculations, it has to be recalled that the logarithmic approximation (NLLA) presented above depends on the choice of the renormalization scale similarly to the fixed-order prediction ($\mathcal{O}(\alpha_s^2)$) in Eq. (66). While g_1 is invariant under changes of the scale $x_\mu^2 = \mu^2/s$, g_2 assumes an explicit scale dependence according to [112]

$$
g_2(\alpha_s(\mu^2)L) = g_2(\alpha_s(s)L) + (\alpha_s(s)L)^2 \beta_0 \ln x_\mu^2 \frac{\mathrm{d}g_1(\alpha_s(s)L)}{\mathrm{d}(\alpha_s(s)L)} . \tag{69}
$$

Since the resummation accounts for large logarithms to all orders, one expects, however, the scale dependence of α_s as determined using the NLLA calculations to be reduced. This is, in fact, the case as will be shown below.

In order to take advantage of the improved prediction in determinations of the strong coupling constant from event shapes and jet rates, the resummed and the full second-order calculations [32,111] should be combined. Several prescriptions to match the two calculations have been proposed [77,112], which differ in the treatment of subleading terms in third and higher-order of $\alpha_s L$. In general one considers, for both the NLL approximation and the $\mathcal{O}(\alpha_s^2)$ calculation, the normalized cross-section $R(\mathscr{F})$ given by Eq. (67) and by the integral $\int_0^{\mathscr{F}} \mathrm{d}\mathscr{F}'$ of Eq. (66), respectively. To combine the two, one determines the remainder function $D(\alpha_s, \mathscr{F})$. This can be done by relating the α_s expansions of the two $R(\mathscr{F})$ formulae, yielding the so-called *R-matching*. Alternatively one can do the same but for the logarithm, $\ln R(\mathscr{F})$, of the two formulae which is called $\ln R$*-matching*. A different treatment of higher-order terms which do not vanish for $\mathscr{F} \to 0$, or imposing constraints

at the kinematic limit $\mathscr{F} \to 1$ leads, respectively, to *modified R-* or *modified* ln *R-matching* prescriptions (see for instance the appendix of Ref. [122]).

The general formulae for these matching prescriptions can be found in Ref. [112]. Detailed formulae and tables of the coefficients G_{nm} and C_n for several event shapes are given in Refs. [77,116,119,120], which include tables of the coefficients G_{nm} and C_n for several event shape observables and jet rates.

4.1.2.2. Jet rates. The existence of jets of particles and the connection of a jet to a parton rely on the fact that the particles emerging from a parton receive during hadronization only a limited transverse momentum relative to the parton momentum. Thus the dominant direction of the particles is given by the parton.

Although the existence of jets might be obvious from looking at event displays (see for example Fig. 7), in practice one has to apply an algorithm to build up a jet from the particles measured in the detector. A large variety of algorithms has been proposed. Algorithms that reconstruct a fixed number of jets, for example three jets, were popular in the early time of the PETRA experiments, when the gluon was discovered (see examples in Ref. [123]).

A reconstruction prescription is widely used which was proposed by the JADE collaboration [124]. Starting with measured particles, the general principle is to determine a resolution parameter y_{ij} for pairs of resolvable jets (particles) i and j. Jet pairs whose y_{ij} exceeds a chosen threshold value y_{cut} are combined into a single jet. A difficulty arises from jets acquiring mass due to the recombination since the perturbative calculations are performed for massless partons. To resolve this potential problem, various algorithms were devised which differ in the resolution parameter definition and the recombination prescription. Some of the frequently employed algorithms are listed in Table 5. Further algorithms and more detailed descriptions may be found in Ref. [125].

The CAMBRIDGE C-algorithm, which is a modification of the D-algorithm, was proposed in Ref. [126]. Its aim is to reduce non-perturbative corrections and to provide a better resolution of the jet substructure. An implementation and results from an investigation using Monte Carlo generator events can be found in Ref. [127]. The algorithm applies a two-fold resolution criterion in order to 'freeze' soft resolved jets. It begins by looking for the pair of objects which are closest in angle θ_{ij}, that is, the pair with the smallest v_{ij} (see Table 5). The least energetic object is considered a jet if the resolution parameter y_{ij} exceeds a given y_{cut}, otherwise i and j are combined (see Ref. [126]).

To assess the size of the strong coupling constant from jets, one may recall that an event with three jets is due to the emission of a gluon carrying a significant fraction of the centre-of-mass energy at large angle. Thus the ratio of the number of observed 3-jet to 2-jet events is to leading order proportional to α_S, and a measurement of the rate of 3-jet events allows a determination of the coupling. The n-jet rate $R_n(y)$, which depends on the choice for $y = y_{\text{cut}}$, is defined in terms of the respective cross-sections for $n \geq 2$ jets

$$R_n(y,\sqrt{s}) \equiv \frac{\sigma_{n\text{-jet}}}{\sigma_{\text{had}}} = \sum_{j=n-2}^{\infty} C_{n,j}(y, x_\mu^2)\left(\frac{\alpha_S(\mu^2)}{2\pi}\right)^j$$

$$\to R_3(y,\sqrt{s}) \equiv \frac{\sigma_{3\text{-jet}}}{\sigma_{\text{had}}} = C_{3,1}(y)\left(\frac{\alpha_S(\mu^2)}{2\pi}\right) + C_{3,2}(y, x_\mu^2)\left(\frac{\alpha_S(\mu^2)}{2\pi}\right)^2 + \cdots \tag{70}$$

Table 5
Definition of the resolution parameters and recombination prescriptions for various frequently used jet algorithms. Energy and three-momentum of jets are indicated as E and $\boldsymbol{p}$, respectively, while upright boldface variables denote four-vectors. The centre-of-mass energy is $\sqrt{s}$, but often the total visible energy is used instead in experiments. For massless quarks the E0- and JADE-algorithms are identical in second-order perturbation theory. The C-algorithm has a two-stage resolution criterion which is described in the text

Algorithm	Resolution parameter	Recombination	Remarks	Theory
E	$y_{ij} = \frac{(\mathbf{p}_i + \mathbf{p}_j)^2}{s}$	$\mathbf{p}_k = \mathbf{p}_i + \mathbf{p}_j$	Lorentz invariant	NLO
E0	$y_{ij} = \frac{(\mathbf{p}_i + \mathbf{p}_j)^2}{s}$	$E_k = E_i + E_j$ $\boldsymbol{p}_k = E_k \cdot \frac{\boldsymbol{p}_i + \boldsymbol{p}_j}{\lvert\boldsymbol{p}_i + \boldsymbol{p}_j\rvert}$	Conserves $\sum E$, Violates $\sum \boldsymbol{p}$	NLO
JADE	$y_{ij} = \frac{2E_iE_j(1-\cos\theta_{ij})}{s}$	$E_k = E_i + E_j$ $\boldsymbol{p}_k = \boldsymbol{p}_i + \boldsymbol{p}_j$	Conserves $\sum E$, $\sum \boldsymbol{p}$	NLO
P	$y_{ij} = \frac{(\boldsymbol{p}_i + \boldsymbol{p}_j)^2}{s}$	$\boldsymbol{p}_k = \boldsymbol{p}_i + \boldsymbol{p}_j$ $E_k = \lvert\boldsymbol{p}_k\rvert$	Conserves $\sum \boldsymbol{p}$, Violates $\sum E$	NLO
P0	$y_{ij} = \frac{(\boldsymbol{p}_i + \boldsymbol{p}_j)^2}{s}$	$\boldsymbol{p}_k = \boldsymbol{p}_i + \boldsymbol{p}_j$ $E_k = \lvert\boldsymbol{p}_k\rvert$	As p-scheme, but $\sum E$ updated after each recombination	NLO
D, k_t	$y_{ij} = \frac{2\min(E_i^2, E_j^2)(1-\cos\theta_{ij})}{s}$	$E_k = E_i + E_j$ $\boldsymbol{p}_k = \boldsymbol{p}_i + \boldsymbol{p}_j$	Conserves $\sum E$, $\sum \boldsymbol{p}$; avoids exp. problems	NLO + NLLA
G	$y_{ij} = \frac{8E_iE_j(1-\cos\theta_{ij})}{9(E_i + E_j)^2}$	$\mathbf{p}_k = \mathbf{p}_i + \mathbf{p}_j$	Conserves $\sum E$, $\sum \boldsymbol{p}$; avoids exp. problems	NLO
C	$v_{ij} = 2(1-\cos\theta_{ij})$ $y_{ij} = \min(E_i^2, E_j^2)v_{ij}$	$E_k = E_i + E_j$ $\boldsymbol{p}_k = \boldsymbol{p}_i + \boldsymbol{p}_j$	Conserves $\sum E$, $\sum \boldsymbol{p}$; accounts for angular ordering	NLO + NLLA

such that $\sum_{n=2}^{\infty} R_n = 1$. In this definition the renormalization scale factor $x_\mu^2 = \mu^2/s$ is introduced. The coefficients $C_{n,j}$ of the perturbative expansion are known up to order $\mathcal{O}(\alpha_s^2)$, which implies $j \leq 2$. They were calculated by numeric integration of the full second-order matrix elements [32] and are tabulated in Ref. [111]. The jet rates R_n are thus predicted for up to $n = 4$ jets. Recently the 4-jet rate was calculated in next-to-leading (up to α_s^3 terms) and the 5- and 6-jet rates in leading order [35–37].

Considering the 3-jet rate obtained using the JADE jet algorithm at a fixed $y_{\text{cut}} = 0.08$, the scale dependence of the coupling can be made apparent. In this specific case the coefficients of the

Table 6
Measured 3-jet rates and total errors using the JADE jet algorithm at $y_{\rm cut} = 0.08$. Data are compiled from Refs. [122,129–132][a]

$\sqrt{s}$(GeV)	DELPHI	L3	OPAL
130–136	18.2 ± 2.4	19.4 ± 3.3	18.9 ± 2.6
161		19.0 ± 2.8[a]	14.5 ± 2.8
172		14.0 ± 4.7[a]	14.9 ± 3.8
183			15.5 ± 2.8
189			16.5 ± 1.6

[a]Calculated from $\langle n_{\rm jet} \rangle$ assuming a negligible $\geq$ 4-jet rate.

perturbative expansion (70) read [111]

$$C_{3,1} = 6.76 \pm 0.006 \quad \text{and} \quad C_{3,2} = 163.5 \pm 0.3\,, \tag{71}$$

thus allowing a determination of α_S from the 3-jet rate. Measurements of this rate at and below the Z pole are compiled in Ref. [128]. Comparable results for energies above the Z mass are summarized in Table 6. All the 3-jet rates are presented in Fig. 16 versus the centre-of-mass energy. Superimposed is the QCD expectation Eq. (70) with (71) for $\alpha_S(m_Z^2) = 0.121$.

Another source of uncertainty is assumed negligible, namely the effects due to hadronization. The perturbation calculation, Eqs. (70) and (71), applies only to a final state with a small number of partons. The jets, however, are constructed from the many particles (hadrons) that emerged from the hadronization of the partons. In order to keep uncertainties low an observable like R_3 should have a small hadronization correction. Earlier investigations (see, e.g. [108]) demonstrated that the JADE jet algorithm exhibits small hadronization corrections over a large centre-of-mass energy range as is shown in Fig. 17. Also shown in the figure is the DURHAM (D) jet algorithm [118] (see Table 5) which was devised after LEP came into operation to circumvent some deficiencies of the JADE algorithm, for example that leading and next-to-leading logarithms (NLLA) cannot be resummed [133]. As can be seen from the figure both the JADE and D-algorithm have fairly small hadronization corrections, those for D being smaller at higher centre-of-mass energies. For these reasons and owing to the resummation of leading and next-to-leading logarithms the DURHAM algorithm is now frequently used for determinations of α_S at LEP.

Not long ago the CAMBRIDGE or C-algorithm was proposed [126] (see Table 5) which takes into account coherence effects of the gluon radiation during the parton shower development implemented in the parton shower models as angular ordering of consecutive gluon emissions. Although very small hadronization corrections were found for the mean jet rate from the C-algorithm, detailed investigations of n-jet rates showed that the hadronization corrections are larger than for the D and JADE algorithms [127].

Exploiting the theoretically appealing features of the D algorithm in an investigation of 3- and 4-jet rates measured by the ALEPH collaboration at LEP I [53], the strong coupling was inferred in Ref. [134], where the R-matched NLO + NLLA calculations for 3- and 4-jet rates were used and certain soft logarithms were taken into account (K term). The resulting fits, for which only statistical errors of the data were considered and the statistical correlation between the data points

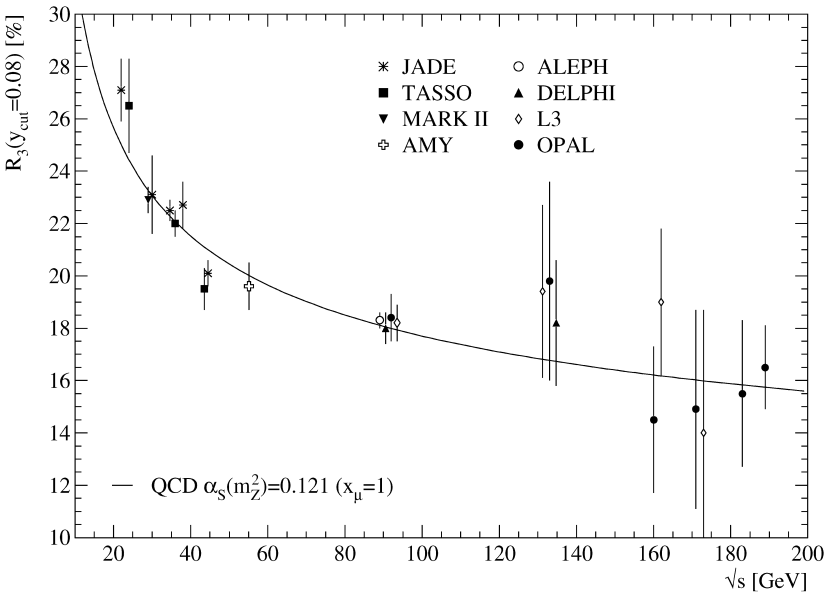

Fig. 16. The 3-jet rate (R_3) at $y_{\rm cut} = 0.08$ using the JADE jet finder, for values of $\sqrt{s}$ between 22 and 183 GeV. The $\mathcal{O}(\alpha_S^2)$ QCD prediction for $\alpha_S(m_Z^2) = 0.121$ and $x_\mu = 1$ is overlaid.

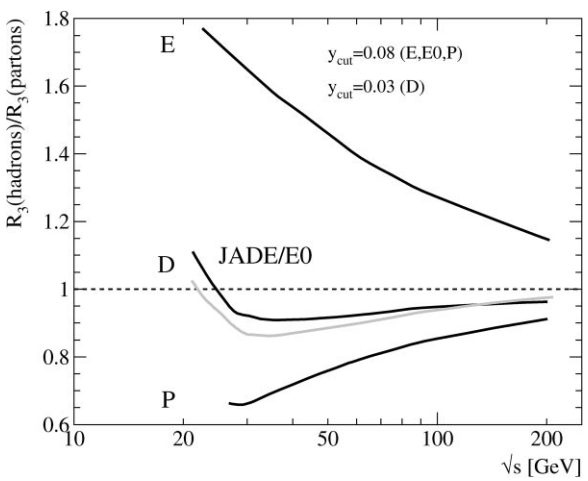

Fig. 17. Centre-of-mass energy dependence of the hadronization correction of the 3-jet rate for various jet algorithms. Figure adapted from Ref. [108].

was neglected, are presented in Fig. 18. In general the agreement between data and theoretical expectation gets better if more higher-order radiative corrections are included. Thus, a remarkably good description is achieved over a very large $y_{\rm cut}$ range and, in particular, in the low $y_{\rm cut}$ regime, when parts of subleading terms (K) are included. Combining both 3- and 4-jet rates one arrives at

$$\alpha_S(m_Z^2) = 0.1175 \pm 0.0018\,, \tag{72}$$

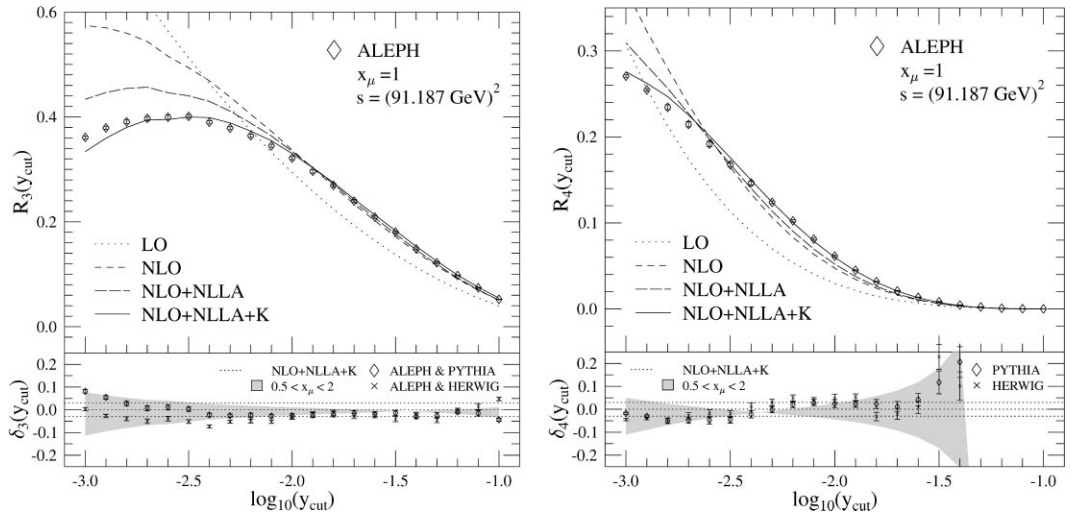

Fig. 18. Leading order (LO), next-to-leading order (NLO), R-matched NLO + NLLA (next-to-leading-logarithmic approximation), and QCD prediction with subleading soft logarithms included, NLO + NLLA + K, for 3- (left) and 4-jet rates (right) are compared to ALEPH data showing statistical errors only. The lower part shows the relative deviation of the measured data from the NLO + NLLA prediction, where the band is the scale uncertainty from varying x_μ between 0.5 and 2. Figures adapted from Ref. [134].

where the error is dominated by the scale choice, whereas experimental uncertainties are negligible. Recently an analytic expression for the 4-jet rate has been calculated in which all the leading and next-to-leading kinematic logarithms have been resummed [135].

The n-jet rates for adjacent $y_{\rm cut}$ values are strongly correlated, thus being favourable for studies at a single $y_{\rm cut}$ value only. Experimental investigations now widely consider the differential 2-jet rate $D_2(y)$ instead. It may be considered as the differential cross-section $D_2(y_3) = 1/\sigma_{\rm had}\, {\rm d}\sigma/{\rm d}y_3$ of y_3 which is the lowest value of y_{ij} in a 3-jet configuration. The perturbative prediction for D_2 is obtained from the derivative ${\rm d}R_2/{\rm d}y$ of the 2-jet rate R_2, calculated as $R_2 = 1 - R_3 - R_4$ assuming negligible contributions from $>$ 4-jet rates.

Fig. 19 shows some of the many measurements of the differential y_3 cross-section based on the DURHAM jet algorithm (references to the measurements next to the Z pole are listed in Ref. [9], measurements away from the Z mass can be found in Refs. [129,130,136–139]). The differential cross-section is shown for $-\ln y_3$ instead of y_3 thus stretching the low y_3 region. The figure reveals a change of the differential 2-jet rate $D_2(-\ln y_3)$ with the energy scale. The distributions are shifted towards higher values of $-\ln y_3$ as the centre-of-mass energy increases. This trend is a manifestation of the running of $\alpha_{\rm S}$, as it corresponds to a reduced amount of highly energetic and well separated 3-jet events, thus indicating a decrease of $\alpha_{\rm S}$.

Moreover, the figure shows results from the re-analysis of data measured at lower energies by experiments which already terminated long before the advent of the D algorithm. Several attempts have been undertaken [137–139] to re-analyse lower-energy data using the DURHAM algorithm, in order to accurately test the energy dependence of the strong coupling, to exploit the improved theoretical predictions for the D algorithm, and to exclude uncertainties due to different

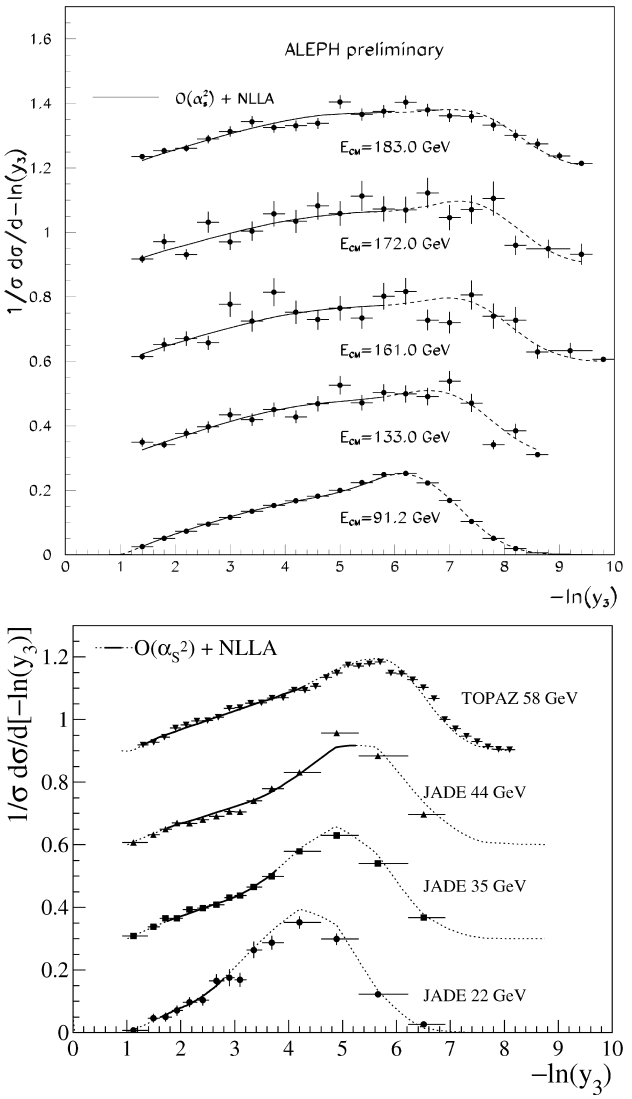

Fig. 19. Differential 2-jet rate versus $-\ln y_3$ obtained at centre-of-mass energies between 22 and 183 GeV using the DURHAM jet algorithm. The data, which are displaced vertically by multiples of 0.3, are corrected to hadron level. At each energy the result of a fit of the combined fixed second-order calculation ($\mathcal{O}(\alpha_S^2)$) and the next-to-leading logarithmic approximation (NLLA) to the distributions is overlaid. The range of data used in the fit is indicated by a solid line. The extrapolations are shown as dashed and dotted curves. The upper figure is taken from Ref. [136], the data of the lower figure are compiled from Refs. [138,139].

observables. In combination with measurements obtained at the high energies of LEP II a significant observation of the running of the strong coupling constant becomes possible.

4.1.2.3. Event shapes. In the spirit of the differential cross-section for y_3 in the preceding section, cross-sections of further observables commonly called event shapes can be used to survey the

hadronic final state. As in the case of the differential jet rate these observables assign to each event a single number whose value indicates the presence of highly energetic, well separated gluon radiation. Besides the *thrust* observable already introduced in Section 3.1.2 as a measure of parton configurations, many other variables were proposed (see for instance Refs. [111,123,140]).

In the following a few of the event shape observables will be briefly introduced. A particular weight is given to those which are frequently used in investigations of hadronic final states, and for which leading and next-to-leading logarithms were resummed to all orders (NLLA) in addition to the next-to-leading order (NLO) perturbation calculation. All event shape observables are to be calculated from the three-momenta $\boldsymbol{p}_i$ of the particles measured in the detector. Although most experiments have sophisticated detectors to identify particles, they are usually assumed to be either pions, if a charged particle is observed, or photons for neutral ones. The particles' energies E_i, when required in the following, are calculated under this assumption.

Thrust T is defined by the expression [141]

$$T = \max_{\boldsymbol{n}} \frac{\sum_i |\boldsymbol{p}_i \cdot \boldsymbol{n}|}{\sum_i |\boldsymbol{p}_i|}. \tag{73}$$

The thrust axis $\boldsymbol{n}_\mathrm{T}$ is the direction of the unit vector $\boldsymbol{n}$ which maximizes the ratio. Each event may be divided into two hemispheres using the thrust axis, such that particle i belongs to hemisphere H_1 (H_2) if $\boldsymbol{p}_i \cdot \boldsymbol{n}_\mathrm{T} > 0$ (< 0). The vector $\boldsymbol{n}_\mathrm{T}$ is one axis of an orthogonal coordinate system describing the event. A second axis is the thrust major axis which is found as an axis perpendicular to $\boldsymbol{n}_\mathrm{T}$, yielding the thrust major value T_maj, from the maximization in Eq. (73). The third axis is thrust minor, given by the vector product of thrust and thrust major axis, from which the thrust minor value T_min is obtained by calculating the ratio in Eq. (73).

Heavy jet mass M_H *or* $\rho \equiv M_\mathrm{H}^2/s$ is given by the larger value of the total invariant mass in each of the hemispheres H_k, $k = 1, 2$, defined by the thrust axis, normalized by the centre-of-mass energy $\sqrt{s}$, that is [111,142]

$$M_\mathrm{H} = \frac{1}{\sqrt{s}} \max_{k=1,2} \left(\sqrt{\left[\sum_{i \in H_k} E_i\right]^2 - \left[\sum_{i \in H_k} \boldsymbol{p}_i\right]^2} \right). \tag{74}$$

Correspondingly, the light jet mass, M_L, is the lighter of the two hemispheres, M_D is the difference and the total jet mass, M_T, the sum of the heavy and light jet masses.

Jet broadening B is determined for each hemisphere, according to

$$B_k = \frac{\sum_{i \in H_k} |\boldsymbol{p}_i \times \boldsymbol{n}_\mathrm{T}|}{2 \sum_i |\boldsymbol{p}_i|}, \tag{75}$$

from which the total, $B_\mathrm{T} = B_1 + B_2$, and the wide jet broadening observables, $B_W = \max(B_1, B_2)$, are derived [115].

C-parameter C is obtained from the three eigenvalues λ_1, λ_2, λ_3 of the linearized momentum tensor [32]

$$\theta^{\alpha\beta} = \sum_i \frac{p_i^\alpha \cdot p_i^\beta}{|\boldsymbol{p}_i|} \Big/ \sum_i |\boldsymbol{p}_i| \tag{76}$$

according to $C = 3(\lambda_1\lambda_2 + \lambda_2\lambda_3 + \lambda_3\lambda_1)$. It can also directly be obtained from the characteristic equation of the tensor, yielding the expression [12]

$$C = \frac{3}{2}\frac{\sum_{i,j}|\boldsymbol{p}_i||\boldsymbol{p}_j| - (\boldsymbol{p}_i \cdot \boldsymbol{p}_j)^2/(|\boldsymbol{p}_i||\boldsymbol{p}_j|)}{\sum_{i,j}(|\boldsymbol{p}_i||\boldsymbol{p}_j|)^2}\,. \tag{77}$$

All these event shapes except thrust acquire zero value in the extreme two jet region and adopt the maximum value for isotropic events. For consistency with the other event shapes $1 - T$ is usually considered rather than T.

As an example of event shapes, Fig. 20 presents some distributions of the C-parameter obtained from measurements at various centre-of-mass energies between 35 and 161 GeV [104,129,130,139]. A clear dependence of the differential cross-section on the centre-of-mass energy is visible. It can be considered as being due to a change of the coupling α_S. The curves overlaid on the distributions resulted from fits of NLLA and $\mathcal{O}(\alpha_S^2)$ (NLO) calculations combined using the $\ln R$ matching scheme.

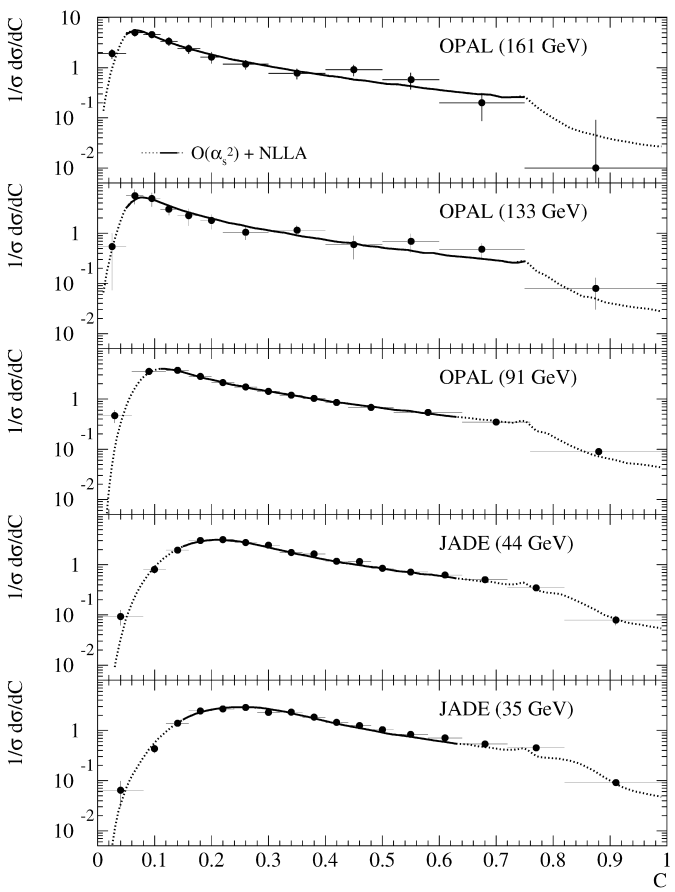

Fig. 20. Distributions of C-parameter as measured between 35 and 161 GeV. The fit results of $\ln R$-matched NLLA + $\mathcal{O}(\alpha_S^2)$ predictions are superimposed as dotted curves where the solid line indicates the fit range. Data are taken from Refs. [104,129,130,139].

Over the whole energy range an excellent description can be observed. Results of α_s fits to the C-parameter data of JADE at 35 and 44 GeV were published in Ref. [139], yielding

$$\alpha_s((35\,\mathrm{GeV})^2) = 0.1480 \pm 0.0017\ (\mathrm{exp.}) \pm 0.0097\ (\mathrm{had.}) \pm 0.0138\ (\mathrm{scale}),$$

$$\alpha_s((44\,\mathrm{GeV})^2) = 0.1470 \pm 0.0032\ (\mathrm{exp.}) \pm 0.0073\ (\mathrm{had.}) \pm 0.0133\ (\mathrm{scale}).$$

where the experimental errors (exp.) are the statistical and experimental systematic uncertainties quadratically combined and where the hadronization error (had.) summarizes all MC modelling uncertainties. The last error stems from the choice of the renormalization scale. As has been mentioned in the beginning of this section, the uncertainties coming from the choice of the scale must not be neglected when applying NLO calculations. To estimate this uncertainty the renormalization scale factor $x_\mu = \mu/\sqrt{s}$ is usually changed from its natural value, 1, to 0.5 and 2, respectively. The result for α_s at a varied scale, which is $x_\mu m_Z$ in this case, is evolved back to $\sqrt{s} = m_Z$ by solving Eq. (20) numerically. Any deviation of $\alpha_s(m_Z^2)$ obtained for $x_\mu \neq 1$ from the value obtained for $x_\mu = 1$ is attributed to the uncertainty due to the choice of the renormalization scale. It yields the dominating error contribution as can be seen from the result above, thus setting a theoretical limit on the precision of the α_s determination.

We performed similar fits to the OPAL data [104,129,130], which yielded χ^2/d.o.f. values of about 0.5 to 0.6 and

$$\alpha_s((91.2\,\mathrm{GeV})^2) = 0.1245 \pm 0.0013\ (\mathrm{exp.}) \pm 0.0062\ (\mathrm{had.}) \pm 0.0071\ (\mathrm{scl.}),$$

$$\alpha_s((133\,\mathrm{GeV})^2) = 0.1097 \pm 0.0099\ (\mathrm{exp.}) \pm 0.0034\ (\mathrm{had.}) \pm 0.0053\ (\mathrm{scl.}),$$

$$\alpha_s((161\,\mathrm{GeV})^2) = 0.1070 \pm 0.0060\ (\mathrm{exp.}) \pm 0.0067\ (\mathrm{had.}) \pm 0.0046\ (\mathrm{scl.}).$$

The experimental and scale uncertainties are defined as for the JADE result. The hadronization uncertainty has been estimated by varying several parameters of the PYTHIA generator and also by employing HERWIG and ARIADNE to correct for hadronization effects choosing the same parameter as described in Refs. [104,129,130].

Exploiting the data taken above the Z pole, the ALEPH collaboration performed a simultaneous analysis of the distributions of thrust, heavy jet mass, wide jet broadening, C-parameter and $-\ln y_3$ [136]. The data taken at the Z pole were excluded because they would have dominated the results owing to their large statistical weight. Although the statistical error is larger without the LEP I data, the systematic uncertainties were found to be essentially reduced because of a decreased impact of hadronization effects and the explicit enforcement of the energy scale dependence according to perturbative QCD.

In all these results the uncertainty due to the choice of the renormalization scale x_μ yields a large contribution to the total error. Consequently, missing higher-orders, whose effect on the value of the coupling are assessed by varying x_μ, are still important. The fitted value for α_s changes considerably for different choices of the scale. This is demonstrated for the C-parameter in Fig. 21. Plot (a) shows the strong dependence of the fitted $\alpha_s(m_Z^2)$ on the renormalization scale factor x_μ (solid curve) for the $\ln R$-matched fixed order and resummed next-to-leading logs. The χ^2/d.o.f. represented by the dotted curve has a flat minimum around $x_\mu = 1$. Juxtaposing this result to the scale dependence of α_s in (b), where only the fixed-order calculation was fitted, reveals that the

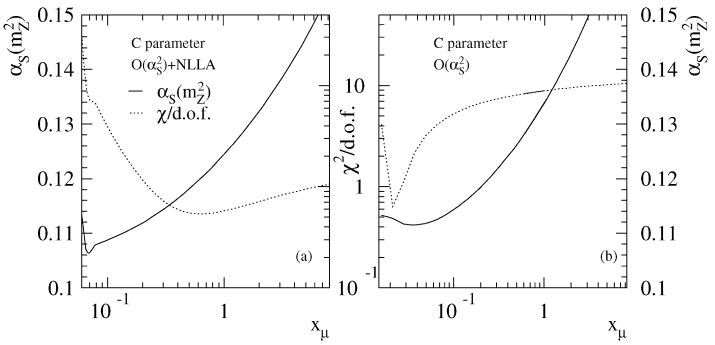

Fig. 21. Renormalization scale factor (x_μ) dependence of the α_S fits to C-parameter data as measured by the OPAL collaboration at the Z pole [104]. The solid curves show $\alpha_S(m_Z^2)$, the dotted curves show χ^2/d.o.f. Plot (a) is the result obtained from the $\ln R$-matched NLLA + $\mathcal{O}(\alpha_S^2)$ calculation, while in (b) only fixed-order calculations ($\mathcal{O}(\alpha_S^2)$) were used.

combination with the resummation results yields some improvement. A pronounced scale dependence is notable in (b) and, in particular, the χ^2/d.o.f. is much worse so that one finds a minimum at extremely low scales of about 0.02 close to the end of the region of stable fits. Although the improvement from the inclusion of resummed leading and next-to-leading logs is appreciable, the calculation of higher orders is desperately needed to reduce the renormalization scale dependence of the determined $\alpha_S(m_Z^2)$ value. Until then, given the rather small experimental errors, this scale uncertainty is a dominant contribution to the total error on α_S determinations from jet rates and event shapes.

Keeping in mind the large uncertainty from the scale choice, one finds evidence for the energy scale dependence of the strong coupling from a comparison of the results on $\alpha_S(s)$ not only for the C-parameter, but also for other event shapes. In general, the correspondence between the measured data and the perturbative calculations is very good when hadronization Monte Carlo models (MC) are invoked for the correction of hadronization effects.

4.1.2.4. Summary of α_S determinations from jet rates and event shapes. Although the variety of event shape observables is large, only a fraction of them has been investigated at LEP II energies, in particular those for which the resummation of large leading and next-to-leading logarithms is available. These are the differential 2-jet rate $D_2(y_3) = 1/\sigma\, \mathrm{d}\sigma/\mathrm{d}y_3$ obtained using the DURHAM jet finder, thrust T, heavy jet mass M_H, total and wide jet broadening B_T and B_W, and the C-parameter. Table 7 lists the averaged α_S values at several centre-of-mass energies ranging from 22 to 183 GeV. The average value and its error are calculated as weighted means of the individual measurements and their errors, respectively, using the total error of each single measurement to determine the weights. Assuming a large correlation between the individual errors, it yields a conservative estimate of the total error.

Using data from measurements at the Z pole, the L3 collaboration determined α_S at energy scales far below m_Z, down to 30 GeV [143]. They exploited photon bremsstrahlung off electron and positron before they annihilate (cf. Fig. 3), and also off the quark and antiquark. Photon radiation in the initial state obviously lowers the centre-of-mass energy that is available for the annihilation and, therefore, for gluon radiation. When a photon is radiated from a quark at high energy and at a large angle to the remaining quark–antiquark final state, it can also be assumed to reduce the

Table 7
Summary of α_S determinations based on matched fixed order and resummed perturbation calculations ($\mathcal{O}(\alpha_S^2)$ + NLLA). The values are averages of the measurements from the individual experiments (A: ALEPH, D: DELPHI, L: L3, O: OPAL, S: SLD, TPC: TPC/TWOGAMMA). The α_S determinations of these experiments were based on measurements of the following observables: differential 2-jet rate D_2 from the DURHAM jet finder, thrust T, heavy jet mass M_H, total and wide jet broadening B_T and B_W, and C-parameter. Data are compiled from Refs. [87,88,104,129–132,136–139,143–145]

$\sqrt{s}$(GeV)	Exp.	Observables	$\alpha_S(s)$	$\alpha_S(m_Z^2)$
22	JADE	D_2	$0.161^{+0.016}_{-0.011}$	$0.124^{+0.009}_{-0.006}$
29	TPC	D_2	0.160 ± 0.012	0.129 ± 0.008
35	JADE	D_2, T, m_H, B_T, B_W, C	$0.1448^{+0.0122}_{-0.0077}$	$0.1228^{+0.0086}_{-0.0055}$
44	JADE	D_2, T, M_H, B_T, B_W, C	$0.1394^{+0.0113}_{-0.0082}$	$0.1233^{+0.0087}_{-0.0064}$
58	TOPAZ	D_2	0.1390 ± 0.0080	0.1286 ± 0.0068
41.2	L	T, M_H, B_T, B_W	0.140 ± 0.013	0.122 ± 0.010
55.3			0.126 ± 0.012	0.117 ± 0.010
65.4			0.134 ± 0.011	0.127 ± 0.010
75.7			0.121 ± 0.011	0.118 ± 0.010
82.3			0.120 ± 0.011	0.118 ± 0.011
85.1			0.120 ± 0.011	0.115 ± 0.011
91.2	A, L, D, O, S	D_2, T, M_H, B_T, B_W	0.1211 ± 0.0068	0.1211 ± 0.0068
133	A, L, D, O	D_2, T, M_H, B_T, B_W, C	0.1132 ± 0.0075	0.1197 ± 0.0085
161	A, L, D, O	D_2, T, M_H, B_T, B_W, C	0.1070 ± 0.0069	0.1160 ± 0.0082
172	A, L, D, O	D_2, T, M_H, B_T, B_W, C	0.1012 ± 0.0070	0.1102 ± 0.0084
183	A, L, D, O	D_2, T, M_H, B_T, B_W, C	0.1084 ± 0.0051	0.1200 ± 0.0063
189	L, O	D_2, T, M_H, B_T, B_W, C	0.1076 ± 0.0051	0.1196 ± 0.0064
91.2	Weighted average			0.1212 ± 0.0079

centre-of-mass energy of this final state if the (time) scale involved is much less than the scale at which the parton shower develops from the quark–antiquark pair. This condition has to be guaranteed by the experimental selection cuts such that radiative events are characterized by a hadronic system recoiling against an isolated photon with energy E_γ and large transverse momentum $k_\perp$ with respect to quark and antiquark. The reduced centre-of-mass energy $\sqrt{s'}$ is given in terms of the nominal energy $\sqrt{s}$ by $s' = s - 2E_\gamma\sqrt{s}$. The coupling constant was determined at this scale from the hadronic system using event shape observables.

The averaged results of Table 7 are presented in Fig. 22. In addition to the total errors, which include the correlated uncertainties due to the hadronization correction and, in particular, the uncertainties from the choice of the scale, also the statistical and uncorrelated experimental uncertainties added in quadrature, are indicated in the figure. The data agree nicely with the QCD prediction for $\alpha_S(m_Z^2) = 0.122$. The same conclusion can be drawn from a direct comparison of the individual α_S results in Table 7 after being evolved to the m_Z scale.

The DELPHI collaboration determined $\alpha_S(m_Z^2)$ from 17 differential jet rate and event shape quantities [146]. The study investigated the dependence of the differential distributions on the polar angle of the thrust axis. Good consistency of the single α_S values from fits of the NLO predictions to the data was achieved when allowing both α_S and the renormalization scale factor

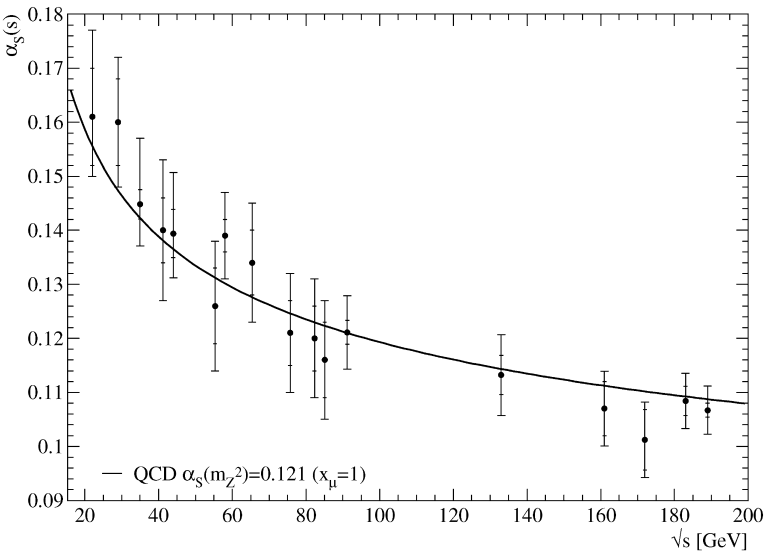

Fig. 22. Values of the strong coupling α_S obtained from jet rates and event shapes, their total errors (outer ticks), and the quadratically combined statistical and experimental systematic uncertainties (inner ticks). The results from several determinations, which considered the ln R-matched $\mathcal{O}(\alpha_S^2)$ + NLLA perturbation calculation for the differential 2-jet rate D_2 from the DURHAM jet finder, thrust, heavy jet mass, total and wide jet broadening, and C-parameter, at various centre-of-mass energies are shown. References for data are given in Table 7. Overlaid to the data is the QCD expectation at 4-loop precision using $\alpha_S(m_Z^2) = 0.121$.

x_μ to vary. This observation was also made in Refs. [104,147]. Fig. 23 is a compilation of the results of $\alpha_S(m_Z^2)$ obtained for (a) fixed $x_\mu = 1$ and (b) varying x_μ. The optimized renormalization scale factors range from $x_\mu \approx 0.057$ for thrust up to ≈ 2.66 for the GENEVA jet finder. To estimate the uncertainty due to the choice of the renormalization scale the x_μ factors were scaled by $1/\sqrt{2}$ and $\sqrt{2}$, respectively, and the fits were repeated with the scale fixed to these values. In part (b) of the figure, a weighted average, $\alpha_S(m_Z^2) = 0.1168 \pm 0.0026$, is quoted which is in good agreement with the other results although the error is smaller because of the smaller variation of x_μ and since it has been calculated using the "optimized correlation" method of Ref. [148] which takes into account an unknown correlation between the individual results. In brief, this method yields an average assuming a common correlation factor between the single measurements obtained from the requirement that χ^2/d.o.f. must be unity.

In conclusion, even not fully inclusive quantities yield an energy scale dependence in agreement with the QCD expectation. It has to be kept in mind, however, that the quoted errors are dominated by the uncertainty from the choice of the renormalization scale which would have limited any stringent conclusion if a deviation from the predicted energy dependence had been observed.

4.2. Quark mass effects

Most experimental investigations of the strong coupling constant which have been presented so far neglected effects due to finite quark masses since massless quarks were assumed in many theoretical calculations. In the case of the jet finders, where many final state particles are combined

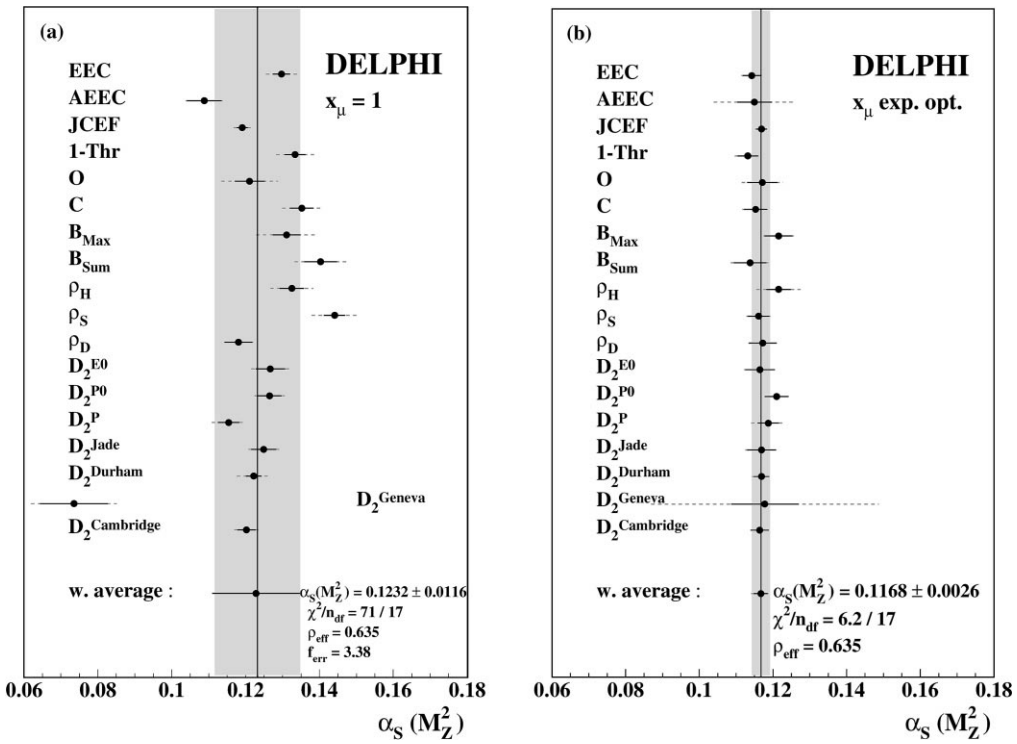

Fig. 23. Values of $\alpha_S(m_Z^2)$ obtained from fits of the NLO prediction of QCD for oriented event shapes using (a) fixed $x_\mu \equiv 1$ and (b) allowing x_μ to vary in the fit. The bars, which are the total errors from experimental, hadronization and scale uncertainty added in quadrature, are subdivided in (b) to indicate by the dashed lines the contribution due to the choice of the renormalization scale. Figures taken from Ref. [146].

into jets, one has to take special measures in the recombination to ensure that the jets remain massless (for instance, rescaling of energy or momentum of the jets). The impact of quark masses is known for a long time in leading order ($\mathcal{O}(\alpha_s)$) [149] for γ and Z exchange in e^+e^- annihilation. A partial calculation of second-order terms in Ref. [150] was lately extended to full next-to-leading order ($\mathcal{O}(\alpha_S^2)$) by three independent groups [151–153] yielding consistent predictions [154].

The effect of a finite quark mass is twofold. Besides an obvious reduction of the phase space available for gluon emission, QCD radiation is also reduced. This follows from the differential cross-section of Eq. (35). After being complemented by further terms which explicitly depend on the quark mass m_Q it reads in leading order [149]

$$\frac{1}{\sigma_0}\frac{\mathrm{d}^2\sigma}{\mathrm{d}x_Q\mathrm{d}x_{\bar{Q}}} = C_F\frac{\alpha_S}{2\pi}\left[\frac{x_Q^2 + x_{\bar{Q}}^2}{(1-x_Q)(1-x_{\bar{Q}})} - \frac{4m_Q^2}{s}\left(\frac{1}{1-x_Q} + \frac{1}{1-x_{\bar{Q}}}\right)\right.$$

$$\left. - \frac{2m_Q^2}{s}\left(\frac{1}{(1-x_Q)^2} + \frac{1}{(1-x_{\bar{Q}})^2}\right) - \frac{4m_Q^4}{s^2}\left(\frac{1}{1-x_Q} + \frac{1}{1-x_{\bar{Q}}}\right)^2\right], \qquad (78)$$

where x_i for $i = Q, \bar{Q}$, are the centre-of-mass energy fractions of the massive quark and antiquark, respectively. The reduction of QCD radiation is immediately apparent in this equation since all terms that depend on the mass are subtracted.

An important feature should be noted for the differential cross-section in Eq. (78). Collinear singularities do not affect the cross-section owing to the quark's finite mass. When recalling Eq. (36), it can be seen that the mass of a Q–G system is restricted by the relation $1 - x_Q = m_{QG}^2/s \geq m_Q^2/s$. Thus the limit $x_Q \to 1$, which is the collinear singularity, does not occur. The infrared singularity at $x_G \to 0$, however, is still present.

The cross-section in Eq. (78) reveals another remarkable feature if the gluon radiation is quite collinear with the heavy quark. In this region of the phase space close to the kinematical boundary, one finds a *dead cone* for radiation which is due to the helicity conservation in the radiation of a spin-1 gluon off a spin-$\frac{1}{2}$ massive quark. To derive an expression for the particular phase space region, one considers a gluon of fractional energy $x_G = 2 - x_Q - x_{\bar{Q}} \ll 1$ which is close in angle to the heavy quark, $\theta \approx 0$. This yields a simplification of Eq. (78) [12]

$$\frac{1}{\sigma_0}\frac{\mathrm{d}^2\sigma}{\mathrm{d}x_G \mathrm{d}\theta^2} \approx C_F \frac{\alpha_S}{\pi}\frac{1}{x_G}\frac{\theta^2}{(\theta^2 + 4m_Q^2/s)^2}\,. \tag{79}$$

Thus gluon radiation is suppressed if $\theta \lesssim 2m_Q/\sqrt{s}$. This is the dead cone the angular size of which grows with the quark mass.

In brief, according to QCD heavy quarks radiate fewer gluons than light quarks. Although the effect might be small at high energies, it has to be accounted for in precision determinations of the strong coupling constant. From the considerations above it is rather obvious that, in particular, the 3-jet rate is expected to be reduced for heavy quarks. In the energy range considered for this report the case of the bottom quark will be of special interest since it is the heaviest quark accessible at centre-of-mass energies between 10 and 190 GeV. Furthermore, at the Z pole all five quark flavours are produced at roughly the same frequency owing to their coupling to the Z (cf. Fig. 5(b)).

While the impact of the massive bottom quark is small for investigations that consider all quark flavours inclusively, it will play a major role in studies of the properties of individual quark flavours. QCD, however, is a field theory in which the coupling α_S is independent of the quark flavours. It therefore is a significant test of QCD to verify the independence of the strong interaction of the flavours involved, and also to test the calculated quark mass effects. The latter procedure may be inverted. A measurement of quark mass effects can be exploited to determine the quark masses assuming flavour independence of the coupling. At this point it has to be recalled from Section 2.2.2 that within the $\overline{\mathrm{MS}}$ renormalization scheme quark masses depend on the energy scale. Measuring different quark masses at different scales is therefore another stringent test of QCD and its renormalization.

4.2.1. Tagging the flavour of a quark

Testing the dependence of the strong interaction on the flavour of a quark requires the identification of the flavour from the hadronic remnants of quark, antiquark and gluons. In connection with the large data statistics and the high precision investigations in the bottom and charm sector at LEP I and SLC many sophisticated methods were established to tag these flavours

which became possible after the installation of high precision silicon vertex detectors (see, e.g. Ref. [155]).

For bottom quarks one uses the large decay multiplicity, the high mass, the semileptonic decays, and, in particular, the long lifetime[12] of B hadrons (for details see, e.g. [156]) which allow for an event-by-event classification.

Although charm quarks can be tagged by the decay vertex of a D meson [157] one usually reconstructs the decay of a charged $D^*(2010)^{\pm}$ meson into a D^0 and a $\pi^{\pm}$ where the D^0 is searched for in various decay channels [158] whose small branching ratios lead to marginal efficiencies only. Since charm mesons also occur in the decay chain of B hadrons one has to fight against bottom quarks spoiling the tagged charm events.

To enrich a primary flavour the leading particle effect [159,160] is used, that is, one assumes that the highest energy hadron is likely to contain the primary quark. Exploiting this effect even the light uds quarks can be tagged, for instance the strange quark by looking for K_S^0 or charged $K^{\pm}$ [161]. Contributions from other quark flavours, however, can only be removed by statistical methods. More efficiently and less biased by the demand for high energy particles, but without any distinction between primary u, d, and s quarks, these light quarks can be selected recalling the fact, that in such events no hadrons of long lifetime similar to bottom and charm hadrons can occur. Therefore, reversing the search for decay vertices yields a very pure light quark tag [156,158].

4.2.2. *Flavour independence of* QCD

All LEP and SLC collaborations performed tests of the flavour independence of the strong interaction at the Z pole employing various tagging methods to measure flavour dependent jet rates or event shapes [157,158,161–167]. In general, the studies are designed to determine the ratio of the coupling for a selected flavour f to the one obtained from the light (from all, or from the complementary, i.e. all but f) quark flavours, that is $\alpha_S^f/\alpha_S^{uds}$ ($\alpha_S^f/\alpha_S^{all}$ or $\alpha_S^f/\alpha_S^{compl}$, respectively). Such ratios have the advantage of reduced systematic uncertainties. For instance, the effects of the choice of the renormalization scale largely cancel in the ratio, thus becoming less significant than experimental systematics. Instead of this, mass effects and the uncertainty of the mass of the bottom quark contribute to the total error.

Fig. 24 shows results for the ratios $\alpha_S^b/\alpha_S^{uds}$ and $\alpha_S^c/\alpha_S^{uds}$ which were obtained from 3-jet rates of several jet finders and from various event shapes, respectively. Considering different flavours in numerator and denominator is advantageous in order to avoid correlations between them. Having included the mass effects, which are of the order of 5–7% for b quarks and 1% for c, the flavour dependent α_S ratios conform to unity for all 3-jet rates and event shapes considered, as expected for a flavour independent strong coupling.

Averaging the ratios in order to diminish the statistical and systematic fluctuations of the individual results, one arrives at the values listed in Table 8, which is a compilation of measurements of the LEP and SLC collaborations [157,158,162,164,166]. A weighted average of the determinations has been calculated deriving the weights from the total errors. For the calculation of the

[12] Unstable particles having lifetimes of $> 3 \times 10^{-10}$ s are usually regarded as stable owing to their tiny probability to decay within the detector.

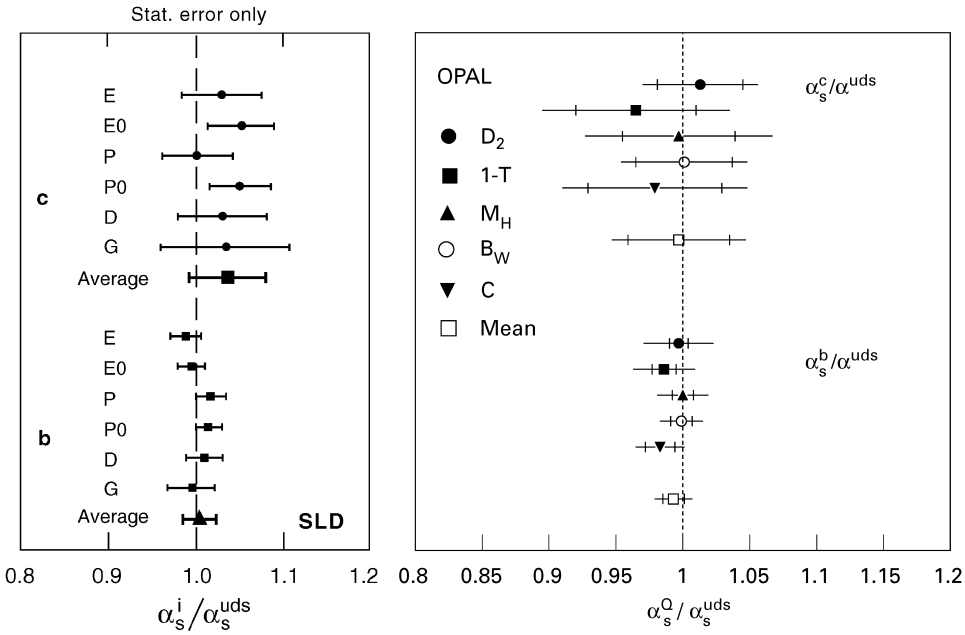

Fig. 24. Flavour dependent ratios of α_S for bottom and charm quarks to the light uds quarks, respectively. Shown are the results obtained from 3-jet rates measured with different jet algorithms [157], and from several event shapes [158]. All ratios were determined using NLO calculations with massive quarks [151,153].

total error of the average, the statistical uncertainties of the individual determinations are taken as uncorrelated. The systematic errors, which are considered as fully correlated, are averaged using the same weights as before. This prescription closely follows that of Ref. [104] which has already been outlined in Section 4.1.1.

From the averages of Table 8 one can conclude that the flavour independence of the strong interaction is proven at the level of the systematic errors of 1–4%. The perturbation calculation to next-to-leading order ($\mathcal{O}(\alpha_S^2)$) for massive quarks, however, is inseparably connected to it. Even at energies as high as at LEP I mass effects would imitate a flavour dependence at the level of several percent.

4.2.3. Running quark masses

Assuming the flavour independence of the strong interaction one can turn the tables and use the perturbation calculations for massive quarks to determine the masses of the quarks. This constitutes another important test of QCD since one expects quark masses in the $\overline{\text{MS}}$ renormalization scheme to depend on the energy scale (see Section 2.2.2).

In principle one would assume that quarks have a unique and constant mass value. Owing to confinement, however, quarks can only be observed inside hadrons. In order to assess the value of the mass one needs a theoretical prescription that is based on perturbation calculations. Among several mass definitions (for an overview see the notes on quark masses in Ref. [28]), two are widely used in these calculations: the *pole mass* M_{pole} and the $\overline{\text{MS}}$ mass $\bar{m}(\mu^2)$. The pole mass is related to the pole of the heavy quark propagator in perturbation theory. This mass is, in fact, independent of

Table 8
Compilation of ratios of α_S determined for bottom and charm quark events to the coupling determined for light uds quarks, respectively [157,158,162,164,166] (A: ALEPH, D: DELPHI, L: L3, O: OPAL, S: SLD3). The first error is statistical, the second comprises systematic and theoretical uncertainties added in quadrature. The ALEPH and L3 values are derived from the measured $\alpha_S^b/\alpha_S^{udsc}$ by assuming $\alpha_S = \sum_{f=uds,c,b} \gamma^f \alpha_S^f$, where $\gamma^f = B(e^+e^- \to \bar{f}f)$ is the standard model hadronic branching fraction for Z decays into flavour f. For the determination of the averages and the total errors see the text

Exp.	$\alpha_S^b/\alpha_S^{uds}$	$\alpha_S^c/\alpha_S^{uds}$	Observables	Theory
A	$1.002 \pm 0.009 \pm 0.022$		T, C, y_3(E0), y_3(D),	Partly massive NLO
D	$1.007 \pm 0.005 \pm 0.009$		R_3(E0)	Massive NLO
L	$1.07 \pm 0.05 \pm 0.06$		R_3(E0)	Partly massive NLO
O	$0.998 \pm 0.005 \pm 0.012$	$1.002 \pm 0.017 \pm 0.027$	D_2(D), T, M_H, B_T, B_W, C	Massive NLO
S	$1.004 \pm 0.005^{+0.032}_{-0.042}$	$1.036 \pm 0.043 \pm 0.047$	R_3(E), R_3(E0), R_3(P), R_3(P0), R_3(D), R_3(G)	Massive NLO
avg.	1.004 ± 0.013	1.009 ± 0.035		

the renormalization scheme [25] and, therefore, independent of the energy scale. However, the pole mass is defined only within the context of perturbation theory because, owing to confinement, the full quark propagator has no poles.

Perturbatively, however, both M_{pole} and $\bar{m}(\mu^2)$ are related in $\mathcal{O}(\alpha_S^3)$ [168]. In $\mathcal{O}(\alpha_S^2)$ the relation for M_{pole} is

$$M_{pole} = \bar{m}(\mu^2)\Bigg[1 + \frac{\alpha_S(\mu^2)}{\pi}\left(\frac{4}{3} - 2\pi\gamma_{m,0}\cdot\ell\right) + \frac{\alpha_S^2(\mu^2)}{\pi^2}\left(K - \frac{8\pi}{3}\gamma_{m,0} + \pi\left(\frac{2}{3}\gamma_{m,0} - \frac{4}{3}\beta_0 - \pi\gamma_{m,1}\right)\ell + \frac{\pi^2}{2}\gamma_{m,0}(\beta_0 + \gamma_{m,0})\ell^2\right) + \mathcal{O}(\alpha_S^3)\Bigg], \tag{80}$$

where $\beta_0 = (33 - 2n_f)/12\pi$, $\gamma_{m,0} = 1/\pi$, and $\gamma_{m,1} = (303 - 10n_f)/72\pi^2$ are defined in Eqs. (21) and (24), $K \approx 13.3$ (12.4) for charm (bottom) quarks [169], and $\ell = \ln(\bar{m}(\mu^2)/\mu)$. It must be pointed out that the convergence of the perturbative expansion for the expression of the $\overline{MS}$ mass via the pole mass is known to be worse [169] (see Ref. [23] for a review). This is mostly due to non-perturbative effects (NP) which are found to contribute an additional correction of [170]

$$\delta^{NP} = -\frac{2\pi}{3}\frac{\sqrt{\lambda^2}}{\bar{m}} \tag{81}$$

to the coefficient of the term linear in α_S, where λ is some regulator, acting like a small gluon mass, to account for the pole at very small energy scales (see Section 5.3).

Many estimates, in particular of the bottom quark mass from bottomonium and B hadron masses, were done (see compilation in Ref. [28]) which usually suffer large uncertainties due to the

small scales involved and due to non-perturbative effects. All values of the $\overline{\text{MS}}$ bottom quark mass range between 4.1 and 4.4 GeV. A combination of some of the estimates in Ref. [171] yielded $\bar{m}_c(\bar{m}_c^2) = (1.30 \pm 0.03)\,\text{GeV}$ and $\bar{m}_b(\bar{m}_b^2) = (4.34 \pm 0.05)\,\text{GeV}$. Next-to-next-to-leading order (NNLO) corrections were considered in estimating the bottom quark mass, yielding $\bar{m}_b(\bar{m}_b^2) = (4.25 \pm 0.09)\,\text{GeV}$ [172] and $\bar{m}_b(\bar{m}_b^2) = (4.19 \pm 0.06)\,\text{GeV}$ [173]. All these results are of the same magnitude. Given the errors assigned to the masses, however, some results are in contradiction. In the following, the estimate of the Particle Data Group in Ref. [28] will therefore be adopted, that is $\bar{m}_b(\bar{m}_b^2) = 4.1\text{–}4.4\,\text{GeV}$.

In order to determine the quark masses at energies far above the region of the quarkonia, one has to employ perturbative calculations which consider massive quarks. Only recently such calculations became available for the gluon radiation from heavy quarks in $\mathcal{O}(\alpha_S^2)$. The calculations consider both mass definitions, the $\overline{\text{MS}}$ mass $\bar{m}(\mu^2)$ [151,152] and the pole mass M_{pole} [153]. The consistency of these calculations was verified [154].

Using the large data statistics available from e^+e^- annihilation at the Z pole and, furthermore, highly efficient and very pure bottom quark tagging methods, the DELPHI [164,174] and SLD collaborations [156] investigated mass effects for bottom quarks. In Refs. [151,152] the ratio of the 3-jet rates for bottom and the light uds quarks, $R_3^{\text{bl}} = R_3^{\text{b}}/R_3^{\text{uds}}$, was proposed as being sensitive to the value of the b mass. Fig. 25 shows this ratio versus y_{cut} for the DURHAM and the CAMBRIDGE jet finders. Taking into account the large correlations between adjacent data points, a good agreement with the next-to-leading order (NLO) calculation for massive quarks is observed. From a fit of the theoretical expression to the 3-jet data of the DURHAM algorithm only, the DELPHI collaboration obtained a bottom quark mass at the Z scale of

$$\bar{m}_b(m_Z^2) = (2.67 \pm 0.25(\text{stat.}) \pm 0.34(\text{hadr.}) \pm 0.27(\text{theory}))\,\text{GeV}\,. \tag{82}$$

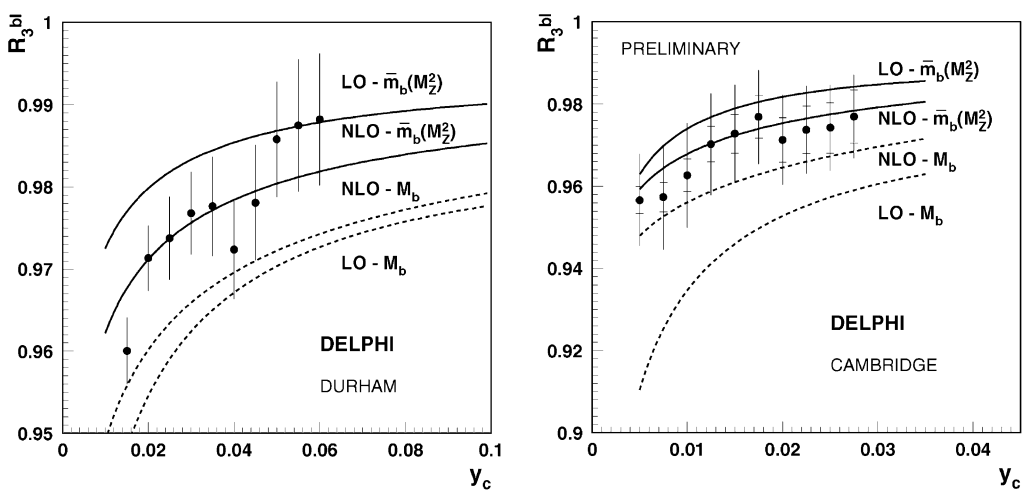

Fig. 25. The 3-jet rate ratio for bottom and light quarks is shown for the DURHAM and CAMBRIGDE jet algorithms [164,174]. The curves stem from leading (LO) and next-to-leading (NLO) calculations for the pole mass, M_b, or the $\overline{\text{MS}}$ mass at the Z scale. Plots are taken from Ref. [174].

The error on this result has contributions from statistics, the hadronization uncertainty (hadr.), which is dominated by the choice of the model (either STRING or CLUSTER), and from missing higher orders in the theoretical expression, which were assessed by varying the scale μ by a factor of two around m_Z, and by changing from the pole to $\overline{\text{MS}}$ running mass in the fitted expression.

Fixing y_{cut} at a value specific for the jet finder under consideration the dependence of the mass value on the jet algorithm has been investigated in Ref. [156]. The theoretical expectation for the same ratio for six different jet algorithms is shown versus m_b in Fig. 26, and the measured ratios with their statistical uncertainties are overlaid as gray bands. It is remarkable at first sight to find some ratios increasing with the bottom quark mass. This can be understood from the resolution variables y_{ij} of the jet finders. If they are defined as a mass, as it is the case for the E, E0, P, P0 schemes, a finite and large mass results in a shift of the 3-jet rate towards higher values of the resolution parameter y_{cut} since y_{ij} has to be at least as large as the quark mass. Since this is not the case for *massless* quarks, one may find, particularly at rather low values of y_{cut}, a higher 3-jet rate for bottom than for light quarks.

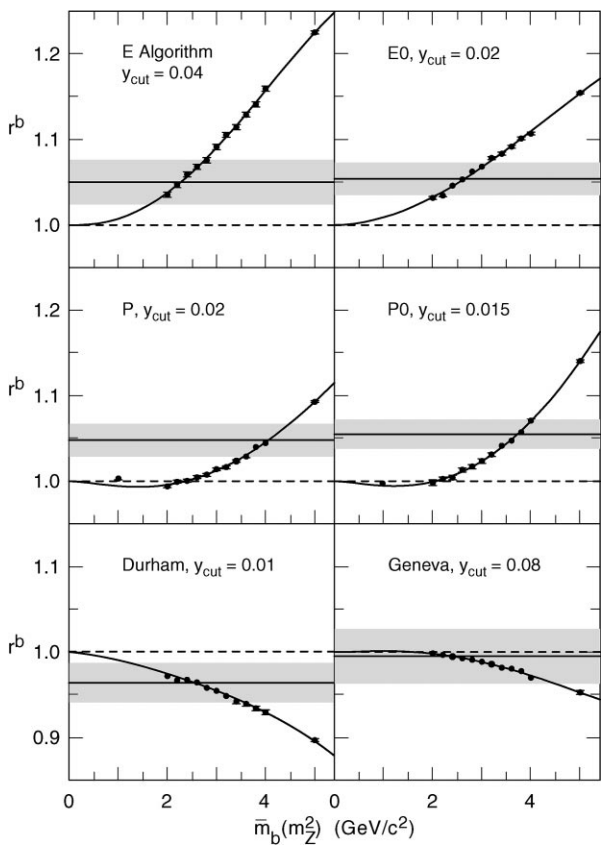

Fig. 26. At fixed y_{cut} the theoretically expected dependence of the 3-jet rate ratio, $r_b \equiv R_3^b/R_3^{uds}$, for bottom and light quarks on the bottom quark mass is shown for various jet finders as points with error bars and parameterized by a curve. The gray bands represent the experimentally measured values of the ratio and the respective statistical errors as obtained by the SLD collaboration. The figure is taken from [156].

Values for the mass were derived from the data by employing the theoretical expression and by combining the six results taking into account the correlations. This way an estimate of the $\overline{\text{MS}}$ bottom quark mass at the Z scale of

$$\bar{m}_b(m_Z^2) = (2.56 \pm 0.27(\text{stat.})^{+0.38}_{-1.47}(\text{syst.})^{+0.42}_{-0.42}(\text{theory}))\,\text{GeV} \tag{83}$$

was obtained in Ref. [156] where the systematic error includes the hadronization uncertainties. The theory error comprises hadronization uncertainties and an additional uncorrelated 2% uncertainty on each ratio $r_b \equiv R_3^b/R_3^{uds}$, which is attributed due to missing higher-orders.

Although these two determinations of the bottom quark mass at the Z scale agree within the significant errors, the calculation of an average requires care because of the large spread of the results for different jet finders and the significant but unknown correlations between the measurements. As already described in Section 4.2.2, a large correlation of systematic and theory errors is therefore assumed in the calculation of a weighted average of the two results. The weights are obtained from the symmetrized total errors. This yields

$$\bar{m}_b(m_Z^2) = (2.65 \pm 0.18(\text{stat.}) \pm 0.44(\text{syst.}) \pm 0.30(\text{theory}))\,\text{GeV}\,, \tag{84}$$

where the systematic error is dominated by hadronization uncertainties.

Fig. 27 compares the $\overline{\text{MS}}$ value of the bottom quark mass at the Z mass scale with that at the $\bar{m}_b$ scale. The solid curve in this figure is the QCD prediction for the scale dependence of the running mass, that is Eq. (26), where the bottom quark mass value of the particle data group PDG from Ref. [28] was used. The dashed and dotted bands indicate the uncertainties from the PDG bottom quark mass value and from a 0.006 error on $\alpha_S(m_Z^2)$.

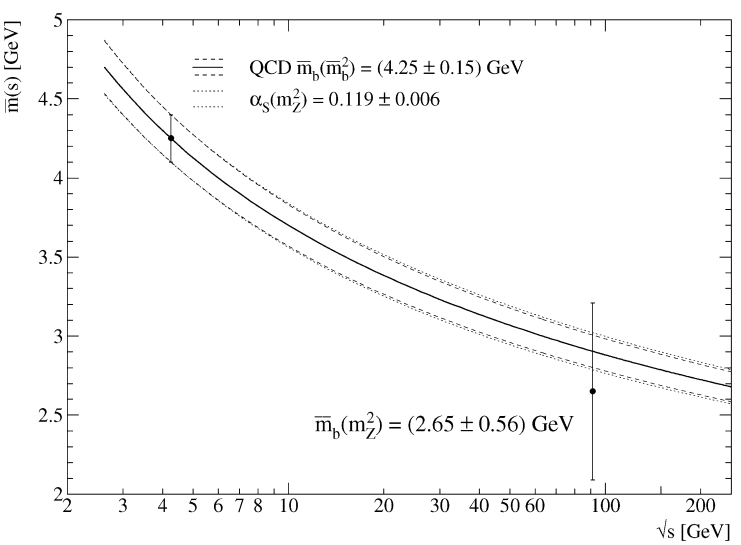

Fig. 27. Values of the $\overline{\text{MS}}$ bottom quark mass at the Z and the $\bar{m}_b$ mass scales are shown. Overlaid is the theoretically expected running of the mass assuming $\alpha_S(m_Z^2) = 0.119$. The dashed lines indicate the uncertainty due to the error on $\bar{m}_b(\bar{m}_b^2)$, the dotted lines represent the error band when an additional 0.006 uncertainty on $\alpha_S(m_Z^2)$ is included.

Although the uncertainty of the determined value for $\bar{m}_b(m_Z^2)$ is large, it supports the predicted scale dependence of the $\overline{\text{MS}}$ quark masses. This becomes more obvious from the difference between the masses at the two scales

$$\bar{m}_b(\bar{m}_b^2) - \bar{m}_b(m_Z^2) = (1.60 \pm 0.57)\,\text{GeV}, \tag{85}$$

which deviates from zero by about 2.8 standard deviations. Further investigations of the effects on $\bar{m}_b$ from different jet finders are clearly necessary. But nevertheless, the agreement of the current results with the expectation from the perturbative calculations in Fig. 27 is remarkable.

5. Tests of QCD treatments of hadronization

Most of the investigations of strong interactions that have been described in the previous section rely on phenomenological models in order to account for hadronization effects. Although the models provided a well-suited representation of the effects, they contributed an inherent and hardly reducible uncertainty to each determination of the strong coupling constant. Efforts to open the hadronization phenomena to a proper treatment in the framework of perturbative QCD theory are required to diminish the influences of the various models. Such approaches necessarily consider techniques that go beyond a simple perturbative expansion in powers of α_S.

Two such methods will be presented in this section, viz. the *modified leading logarithm approximation* (MLLA) in conjunction with the conjecture of *local parton–hadron duality* (LPHD), and the concept of renormalons which leads to *power corrections* to the perturbative calculations. As a start, light is shed on the perturbative picture of fragmentation functions and scaling violation.

5.1. Inclusive fragmentation function and scaling violation

5.1.1. Fragmentation function and evolution equation

Inclusive hadron production in $e^+e^- \to \gamma, Z \to hX$, where h is either a given hadron species or a sum over all charged hadrons, is governed by the strong interaction and, therefore, by the strength of the coupling. The differential cross-section of this process in the case of unpolarized e^+ and e^- beams receives contributions from the polarization states of the exchange vector bosons γ, Z, viz. transverse and longitudinal polarization, respectively. In addition, there is an asymmetric component due to the parity-violating interference. Each of these three contributes to the differential cross-section via its characteristic dependence on the polar angle θ between the direction of the incoming e^- and the outgoing hadron h, according to the relation [175]

$$\frac{d^2\sigma^h}{dx\,d\cos\theta} = \frac{3}{8}(1+\cos^2\theta)\frac{d\sigma_T^h}{dx} + \frac{3}{4}\sin^2\theta\frac{d\sigma_L^h}{dx} + \frac{3}{4}\cos\theta\frac{d\sigma_A^h}{dx}, \tag{86}$$

where $x \equiv x_E = 2E/Q$, E being the particle's energy, is the fractional energy of the hadron and $Q = \sqrt{s}$ is the centre-of-mass energy.

Recalling energy conservation, a sum rule for the inclusive cross-section summed over all outgoing hadrons h can be obtained

$$\frac{1}{2}\sum_h \int dx\,d\cos\theta\, x\frac{d^2\sigma^h}{dx\,d\cos\theta} = \sigma_{\text{had}} = \sigma_T + \sigma_L, \tag{87}$$

where

$$\sigma_P \equiv \frac{1}{2}\sum_h \int_0^1 \mathrm{d}x\, x\frac{\mathrm{d}\sigma_P^h}{\mathrm{d}x} \quad (P = T, L, A). \tag{88}$$

Thus the total inclusive cross-section is the sum of the transverse and the longitudinal cross-section. For unpolarized beams and high centre-of-mass energy, $\sqrt{s}$, the latter contribution is, depending on the fermion mass m_f, largely suppressed by a factor m_f^2/s due to the approximate helicity conservation at the γ^*/Z-$f\bar{f}$ vertex [176]. A significant longitudinal cross-section is generated by gluon radiation off quarks, rendering it proportional to α_S.

The three differential cross-sections $\mathrm{d}\sigma_P^h/\mathrm{d}x$, for $P = T$, L, A, can be expressed by perturbative QCD, based on the factorization property proven in Ref. [177], as a convolution [175]

$$\frac{\mathrm{d}\sigma_P^h(s)}{\mathrm{d}x}(\mathrm{e}^+\mathrm{e}^- \to hX) = \sum_{f=q,\bar{q},\mathrm{G}} \int_x^1 \frac{\mathrm{d}z}{z} C_{P,f}(z, \alpha_S(\mu_R^2), \mu_F^2/s) \cdot D_f^h(x/z, \mu_F^2), \tag{89}$$

of *coefficient functions* $C_{P,f}$, being the cross-section for the inclusive production of $f =$ quark q, antiquark $\bar{q}$, or gluon G in the given process, and of the *fragmentation functions*[13] $D_f^h(x, \mu_F^2)$, which represent the distributions of the energy fraction x of hadron h stemming from the fragmentation of parton f. The shape of the D_f^h functions has to be obtained from experimental measurements, because the production of a hadron is a non-perturbative process and the parton fragmentation functions are, therefore, not perturbatively calculable.

The coefficient functions $C_{P,f}$ are known up to corrections of the order α_S^2 [43,175,178]. In leading order the transverse coefficient is proportional to the Born level production cross-section of parton f, $C_{T,f} = \delta(1-x)\sigma_{0,f}(s)$. It is, for instance, zero for gluons. The longitudinal coefficient $C_{L,f}$ vanishes at this order. It solely receives corrections of the order α_S, thus allowing a determination of the coupling from a measurement of the longitudinal cross-section. The full coefficient functions up to $\mathcal{O}(\alpha_S)$ are too involved to be repeated here. They can be found in Ref. [175] for instance.

Although calculable, the coefficient functions $C_{P,f}$ contain collinear singularities whose renormalization renders both the coefficient and the fragmentation functions dependent on an arbitrary factorization scale μ_F which is analogous to the renormalization scale μ_R introduced in Section 2.2.3. However, physical cross-sections as in Eq. (89) must be independent of the μ_F scale if they are determined from an all-order perturbation calculation. This fact can be used to derive the scale dependence of the parton fragmentation functions D_f^h from the one of $C_{P,f}$ (see Refs. [12,175]). In the perturbative regime the scale dependence of D_f^h is given by the DGLAP[14] evolution

[13] Here, the meaning of the term fragmentation function is slightly different from that introduced in Section 3.2 in the context of hadronization models. The fragmentation function in such models determines the fraction $z = (E + p_\parallel)_{\mathrm{hadron}}/(E+p)_{\mathrm{parton}}$ of energy and momentum which is transferred from the parton to the hadron during hadronization. Experimentally one measures $x_E = 2E/\sqrt{s}$ or $x_p = 2p/\sqrt{s}$, that is the hadron's energy or momentum fraction of half of the centre-of-mass energy.

[14] Dokshitzer, Gribov, Lipatov, Altarelli and Parisi.

equation [42,179]

$$\frac{\partial D_i^h(x,s)}{\partial \ln s} = \sum_{j=q,\bar{q},G} \int_x^1 \frac{dz}{z} \frac{\alpha_S(\mu_R^2)}{2\pi} P_{ji}(z, \alpha_S(\mu_R^2)) D_j^h(x/z, s), \tag{90}$$

where $i = q$, $\bar{q}$, G and

$$P_{ji}(z, \alpha_S(\mu_R^2)) = P_{ji}^{(0)}(z) + \frac{\alpha_S(\mu_R^2)}{2\pi} P_{ji}^{(1)}(z) + \mathcal{O}(\alpha_S^2) \tag{91}$$

is the perturbative expansion of the Altarelli-Parisi splitting functions, whose leading order representation has already been introduced in Eq. (43) of Section 3.1.3. The full terms for $P_{ji}^{(1)}$ are lengthy and, therefore, not repeated here. They can be found for instance in Ref. [12].

The remarkable feature of the DGLAP evolution equation (90) is its dependence on α_S in the convolution integral. Due to this the scaling of the fragmentation function $D_f(x,s)$ with the energy scale $Q = \sqrt{s}$ is violated. A scale-independent x distribution is expected for instance in the independent fragmentation model. Historically it was this scaling violation which gave a first indication for the running nature of the strong coupling.

5.1.2. Determination of α_S from scaling violation

An experimental determination of α_S from the scaling violation was proposed in Ref. [180]. It suffers, however, from several complications. Firstly, in the comparison of fragmentation functions at very different energies care must be devoted to the details of the flavour composition. In e^+e^- annihilation the relative production rates of the various quark flavours change considerably from the very low energy region, which is dominated by photon exchange only, to the Z region, where the electroweak couplings dominate (see Section 3.1). Parton fragmentation functions may, in general, be different for different quark flavours, as can be seen from Eq. (89). Hence the fragmentation functions have to be measured separately for the different quark flavours. This is possible with sophisticated flavour tagging methods, some of which have already been described in Section 4.2.1. Employing these techniques the fragmentation functions shown in Fig. 28 were obtained separately for bottom, charm and light uds quarks [53,140,181–183]. Another method to extract flavour dependent fragmentation functions is based on the momentum spectrum of a single particle species. Conjectures on the production of the particle species from a flavour f have to be applied in order to reduce the number of unknown fragmentation functions. This approach will not be described in this report, but details can be found in Ref. [178] (see also Ref. [160] for a different approach).

A particular property of these flavour-dependent fragmentation functions should be noted for b quarks. Although bottom quarks have been shown to transfer a large fraction of their energy and momentum to the b-flavoured hadron (see Section 3.2), the differential cross-section for hadrons of high scaled momentum x_p is significantly less than for light quarks, u, d, s. This is due to the cascade decays of the heavy b-flavoured hadrons via charmed into light hadrons. About 5.5 charged hadrons are found on average in the decay of one b-hadron [184]. The available energy is thus distributed over many particles, the decay products are low in energy, and the fragmentation function of b quarks is softer than for u, d, and s. As the flavour composition changes with the centre-of-mass energy, this mimics a scaling violation which has to be taken into account in the determination of the strong coupling constant.

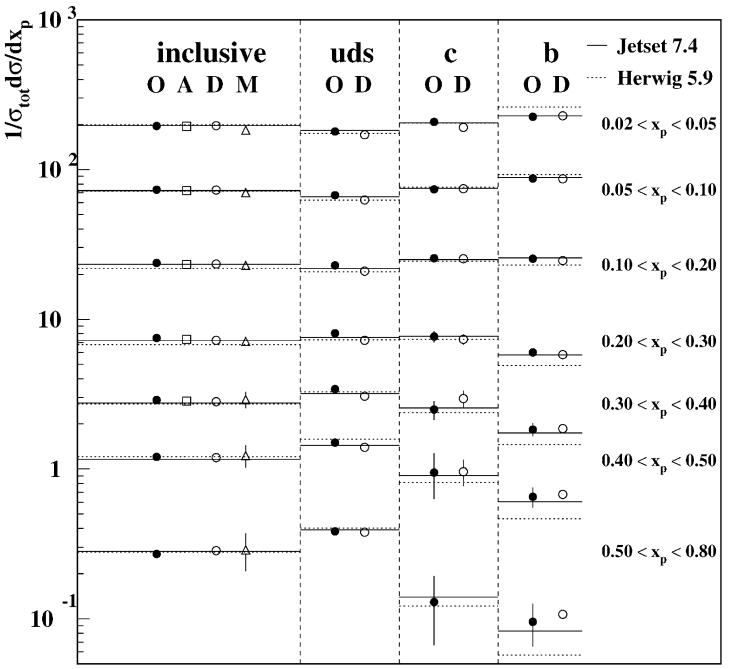

Fig. 28. Comparison of the inclusive and the flavour-dependent fragmentation functions obtained at $\sqrt{s} = m_Z$ by the ALEPH (A), DELPHI (D), OPAL (D), and MARK II (M) collaborations. Statistical and systematic uncertainties are included in the error bars. The solid and dotted horizontal lines indicate the JETSET and HERWIG predictions, respectively. Figure taken from Ref. [181].

A second complication in the determination of α_S from fragmentation functions is due to the gluon fragmentation function $D_G(x, s)$ which is part of the convolution integral in Eq. (90). This function cannot be measured directly in e^+e^- annihilation since gluons enter the hadronic final state only through their radiation off quarks, thus appearing always in conjunction with the quark fragmentation functions. One approach is to identify the gluon jet in a clear 3-jet final state by tagging both of the quark jets [185,186]. The results of this method are best at large x where the identification of the gluon jet and the assignment of particles to the gluon jet is less ambiguous. Another approach to infer the gluon fragmentation function makes use of the lowest-order properties of the longitudinal coefficient function C_L which, as has been mentioned above, is proportional to α_S while the transverse coefficient function for quarks is a δ-function. For this reason the longitudinal fragmentation function $F_L(x) = (1/\sigma_{had})(d\sigma_L/dx)$ can be regarded in leading order as being composed of the transverse and the gluon fragmentation functions [175]

$$F_L(x) = \frac{\alpha_S}{2\pi} C_F \int_x^1 \frac{dz}{z} \left[F_T(z) + 4\left(\frac{z}{x} - 1\right) D_G(z) \right] + \mathcal{O}(\alpha_S^2). \tag{92}$$

Fig. 29 shows gluon fragmentation functions as obtained by the ALEPH, DELPHI, and OPAL collaborations. DELPHI's result is based on identifying the gluon jet in 3-jet configurations (Y and *Mercedes* topologies exemplified in Fig. 30; an example of the latter is shown in Fig. 7). In such

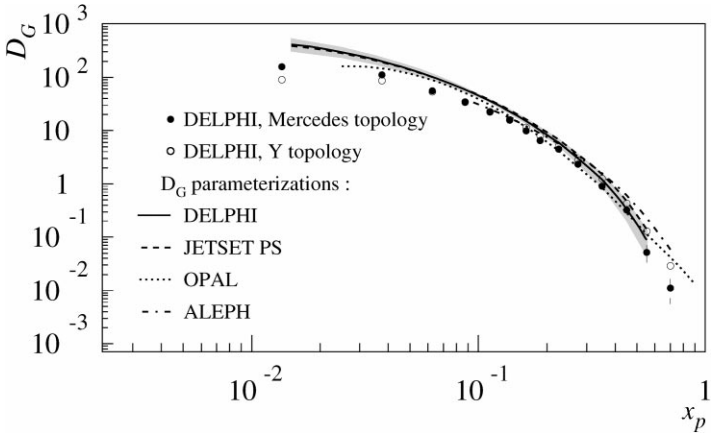

Fig. 29. Gluon fragmentation function D_G at $Q^2 = m_Z^2$ measured by ALEPH, DELPHI, and OPAL. The data points correspond to DELPHI's analysis of tagged gluon jets in very symmetric 3-jet events (*Y* or *Mercedes* topologies). The curves are from fits of the parameterization described in the text to the gluon fragmentation function derived from the measured longitudinal and transverse fragmentation functions. Figure taken from Ref. [186].

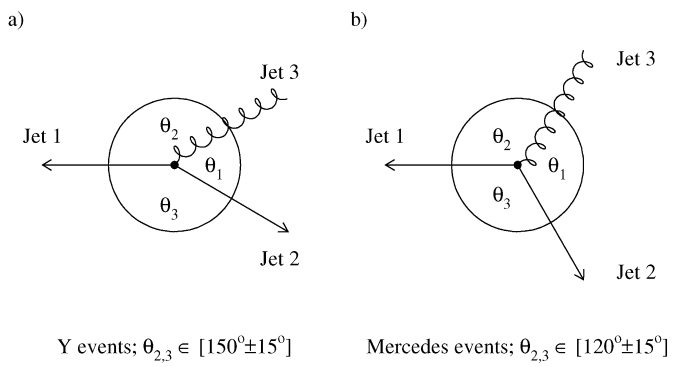

Fig. 30. *Y* and *Mercedes* shaped 3-jet topologies used to investigate the properties of gluon jets. Figure taken from Ref. [52].

a configuration the most energetic jet is very likely to originate from a quark. The second quark jet is tagged by finding a displaced decay vertex of a bottom-flavoured heavy hadron (see Fig. 31 and Section 4.2.1). The remaining lower energetic jet is assumed to stem from a gluon. Biases due to the specific properties of b jets are avoided by statistical decomposition of gluon and quark jet contributions for which identical 3-jet configurations without tagging are considered.

ALEPH and OPAL determined the gluon fragmentation function from the longitudinal and transverse fragmentation data by solving Eq. (92). The curves in Fig. 29 result from a purely phenomenological parameterization of the data [186–188]. Apart from some differences at very low x the agreement is good between the parameterized gluon fragmentation functions $D_G(x)$ at the Z scale.

In every determination of α_S from scaling violation the problem of hadronization effects must be considered which likewise affect the measured fragmentation functions and the event shapes.

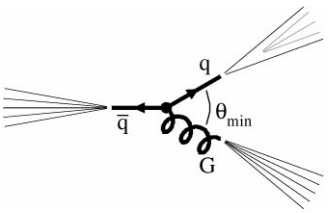

Fig. 31. Pictorial representation of the tagging of gluon jets by reconstruction of a displaced decay vertex from a bottom-flavoured heavy hadron.

On phenomenological and theoretical grounds such effects are expected to fall with reciprocal powers of the centre-of-mass energy $\sqrt{s}$ (see Section 3.2.4), thus leading to power suppressed corrections. Approaches to account for hadronization effects involve either a shift or a rescaling of the scaled momentum fraction x by terms proportional to $1/\sqrt{s}$ as is discussed in Refs. [175,188]. The method to obtain α_s employs purely phenomenological parameterizations of the fragmentation functions for b, c, uds quarks, and gluons at $\sqrt{s} = m_Z$ based on the formula

$$D_f(x) = N_f x^{a_f}(1-x)^{b_f} \exp(-c \ln^2 x), \tag{93}$$

where except for c, which is assumed to be flavour independent by MLLA, the normalization N_f, and the powers a_f and b_f depend on the flavour of the parton f. This function implies a strong correlation between the parameters N, a, b, and c such that no unique set of parameters may exist. The value of $\alpha_s(m_Z^2)$ can then be obtained from fits to the fragmentation function for the inclusive hadronic final state measured by many experiments over a wide range of centre-of-mass energies. The scale dependence is treated according to the evolution equation (90). Fig. 32 shows a compilation of some of the data available. The result of a fit is superimposed [188]. The scaling violation is immediately visible from the change of the slope with the energy scale, particularly at low values of x. The DELPHI and ALEPH collaborations performed such fits, taking into account the variation of the flavour composition, and found consistent values [188–190]

$$\text{ALEPH:} \quad \alpha_s(m_Z^2) = 0.126 \pm 0.007 \text{ (exp.)} \ \pm 0.006 \text{ (theory)} \tag{94}$$

$$\text{DELPHI:} \quad \alpha_s(m_Z^2) = 0.124^{+0.006}_{-0.007} \text{ (exp.)} \pm 0.009 \text{ (theory)} \tag{95}$$

$$\text{average:} \quad \alpha_s(m_Z^2) = 0.125 \pm 0.009 \tag{96}$$

which are also in good agreement with the values obtained from completely inclusive quantities, and from jet rates and event shapes. Theoretical uncertainties, which dominate the total error, were estimated by the collaborations by varying both the renormalization scale μ_R and the factorization scale μ_F in the range $0.5\sqrt{s}$ to $2\sqrt{s}$.

Until now the contributions of quarks and gluons have always been separated by the fit procedure. Exploiting the vast data statistics at LEP I and the high resolution vertex detectors of the experiments, jets can be classified as to whether they originate from a quark or a gluon using the method described above. The DELPHI collaboration [191] tagged quark and gluon jets in their LEP I data. The scale relevant for the gluon jet under scrutiny was taken to be the maximum allowed

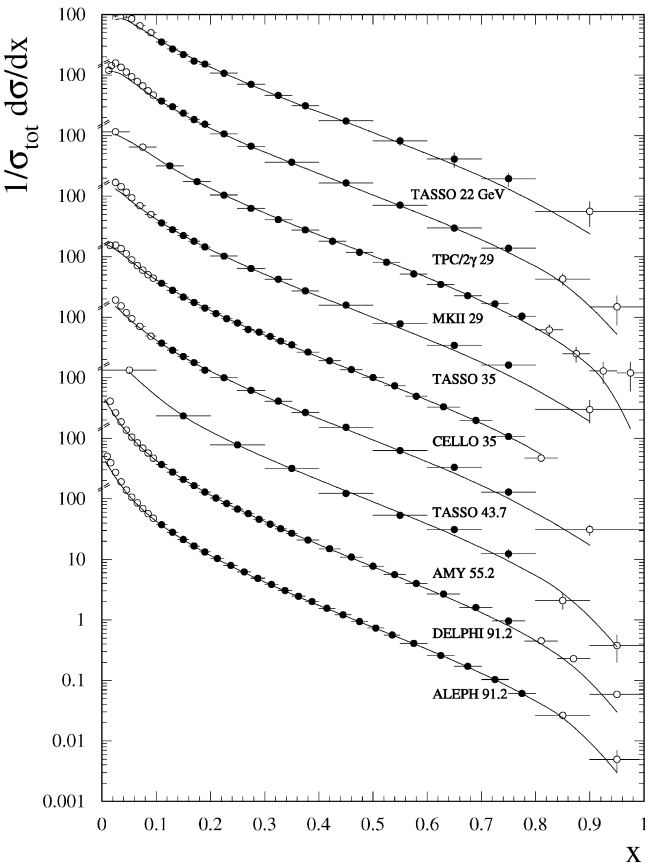

Fig. 32. Inclusive fragmentation functions measured by several experiments at various centre-of-mass energies are shown vertically displaced. The errors on data points include statistical and systematic uncertainties. The full points were used in a fit which is shown as a curve. Figure taken from Ref. [188].

transverse momentum in a jet, that is

$$\kappa = E_{\text{jet}} \sin\frac{\theta_{\min}}{2}, \tag{97}$$

where $\theta_{\min}$ is the angle of that jet to the closest jet. The resulting fragmentation functions for quarks and gluons are shown versus the hardness scale κ for fixed x_E intervals in Fig. 33. Parameterizing the fragmentation functions at $\kappa = 6.5\,\text{GeV}$ for x_E between 0.15 and 0.90 using Eq. (93) and going to other scales by means of the DGLAP evolution equations yields a good overall description of the data, except for very small values of x_E which were not considered in the parameterization of the functions. Scaling violation is again clearly visible from the large difference between quark and gluon fragmentation functions regarding the κ dependence and also from the slopes of the evolution.

Since the DGLAP evolution equation (90) relates the logarithmic derivative of the fragmentation function to the colour factors via the Altarelli-Parisi splitting functions, the DELPHI collaboration

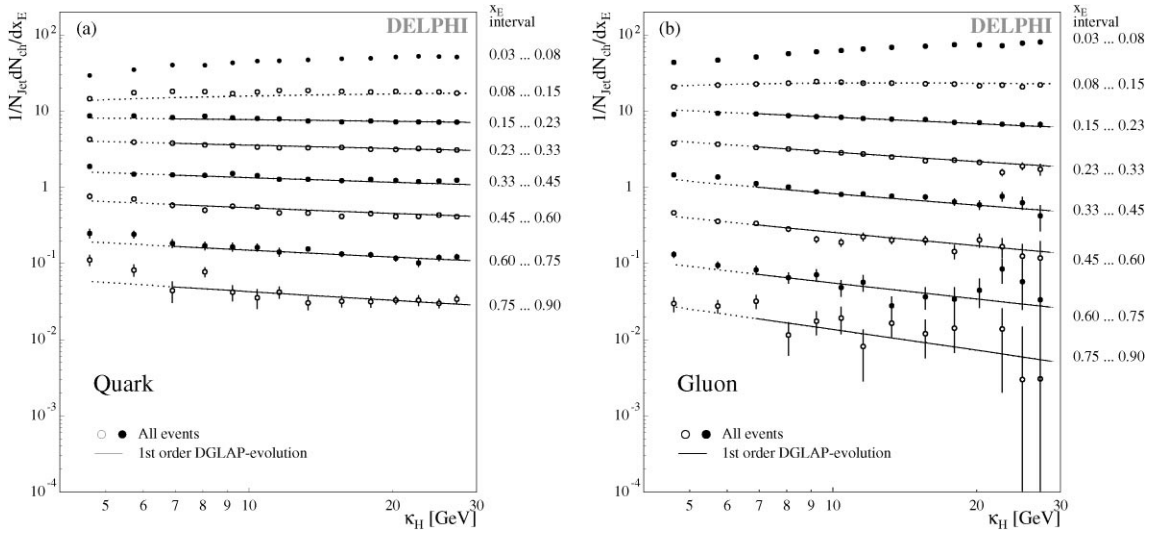

Fig. 33. Scale dependence of (a) the quark and (b) the gluon fragmentation function. The functions are parameterized at $\kappa = 5.5\,\text{GeV}$ for x_E between 0.15 and 0.90 using Eq. (93). The evolution to different scales as shown by the solid line is done using the DGLAP evolution equations. Figures adapted from Ref. [191].

performed a measurement of the ratio

$$\frac{C_A}{C_F} = 2.44 \pm 0.21\ (\text{stat.})$$

from a fit to the data in the range $8\,\text{GeV} \leq \kappa \leq 29\,\text{GeV}$. This ratio is in good agreement with the QCD expectation of 9/4. The fit also yielded $\alpha_S(m_Z^2) = 0.116^{+0.010}_{-0.008}$ to leading order consistent with the higher-order results presented above within the errors.

5.1.3. Longitudinal and transverse cross-sections

The sum rule in Eq. (87) yields a relation between the total, transverse, and longitudinal cross-sections. Recalling that the leading contributions to the longitudinal cross-section, σ_L, are of the order α_S, the coupling strength may be determined from a σ_L measurement. The cross-section can be obtained experimentally from the integrals of the longitudinal fragmentation function

$$\frac{1}{2}\int_0^1 \mathrm{d}x\, x F_L(x) \sim \frac{\sigma_L}{\sigma_{had}}, \tag{98}$$

where σ_{had} is the total hadronic cross-section defined in Eq. (50). Both the longitudinal and the transverse fragmentation functions are shown in Fig. 34. It may be noticed from the figure that F_L is significantly below F_T which is due to the additional suppression of the former by a factor of α_S/π. From the measured fragmentation functions, the value of the above cross-section ratio was determined by the OPAL and DELPHI collaborations to be [186,187]

$$\text{OPAL:} \qquad \frac{\sigma_L}{\sigma_{had}} = 0.057 \pm 0.005, \tag{99}$$

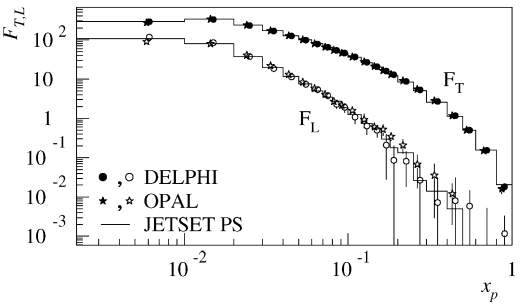

Fig. 34. Transverse and longitudinal fragmentation functions as measured by the OPAL and DELPHI collaborations at $\sqrt{s} = m_Z$. Figure taken from Ref. [190].

$$\text{DELPHI:} \quad \frac{\sigma_L}{\sigma_{had}} = 0.051 \pm 0.007, \tag{100}$$

$$\text{average:} \quad \frac{\sigma_L}{\sigma_{had}} = 0.055 \pm 0.006, \tag{101}$$

where a simple weighted average is formed from both individual values and their associated total errors which are dominated by systematic uncertainties.

Using the perturbative prediction of the cross-section ratio [192]

$$\frac{\sigma_L}{\sigma_{had}} \approx \frac{\alpha_S}{\pi} + \left(13.583 - \frac{11}{4}\ln\frac{s}{\mu_R^2} + \frac{n_f}{6}\left[\ln\frac{s}{\mu_R^2} - \frac{37}{6}\right]\right)\frac{\alpha_S^2}{\pi^2} \tag{102}$$

for $n_f = 5$ flavours one arrives at a value for the coupling strength at the Z mass of

$$\alpha_S^{(NLO)}(m_Z^2) = 0.128 \pm 0.011\ (\text{exp.}) \pm 0.009\ (\text{scale}), \tag{103}$$

which is in agreement with other α_S determinations from cross-sections and also with those from jet rates, event shapes and scaling violation. Corrections due to the production of heavy quarks at the Z scale were investigated in Ref. [193] and were found to be much smaller than the uncertainty due to the choice of the renormalization scale.

It must be noted, however, that the longitudinal cross-section is known to be affected by significant hadronization corrections, which were estimated under the assumptions of an infrared-regular effective behaviour of α_S and of an ultraviolet dominance of higher-twist matrix elements [74,194,195]. These theoretical considerations will be presented in more detail in Section 5.3. According to these estimates, the corrections, which are suppressed by reciprocal powers of the centre-of-mass energy $\sqrt{s}$, may be as large as $\delta(\sigma_L/\sigma_{had}) = 0.010 \pm 0.001$, leading to a corrected value for the coupling of

$$\alpha_S^{(NLO+POW)}(m_Z^2) = 0.118 \pm 0.014, \tag{104}$$

which is also in good agreement with the other α_S determinations mentioned before.

Besides the longitudinal and transverse cross-sections extracted from measurement of fragmentation functions in single hadron production, these cross-sections have also been investigated

for the polar angle of the thrust axis, for which NLO calculations are available. The thrust axis is a good representation of the primary quark direction which is not accessible directly. Despite the same naming these cross-sections are different from those measured from single hadron production. However, an expression completely analogous to that in Eq. (86) holds for θ denoting the polar angle of the thrust axis instead of the hadron. Here, σ_P, $P = T, L$, refer to the corresponding cross-sections, where the asymmetric term is absent since the definition of the thrust axis, Eq. (39), cannot distinguish the sense of the axis. The perturbative QCD prediction for the ratio of the longitudinal and the total hadronic cross-section is [196]

$$\frac{\sigma_L}{\sigma_{had}} = 2C_F\left(-3 - 8\ln\frac{2}{3}\right)\frac{\alpha_S}{2\pi}\left(1 + (l-2)\frac{\alpha_S}{2\pi}\right) + \mathcal{O}(\alpha_S^3), \tag{105}$$

where $l = 0.7 \pm 0.2$ governs the size of the next-to-leading term.

The OPAL collaboration has measured both the cross-section ratio σ_L/σ_{had} and the differential longitudinal cross-section $d\sigma_L/dT$ for thrust [197]. Fig. 35 shows the differential cross-section with the superimposed LO and NLO QCD expectation. A poor description of the distribution by the leading order prediction can be seen, indicating significant higher-order corrections. The next-to-leading order predictions were calculated in [197] using the program of Ref. [198]. Adding this contribution yields a much improved agreement although the statistical error on the calculation close to the kinematical boundary at $T = 1$ is still large.

The measurement of the cross-section ratio yielded, after correcting for detector and hadronization effects,

$$\frac{\sigma_L}{\sigma_{had}} = 0.0127 \pm 0.0016\ (\text{stat.}) \pm 0.0013\,(\text{syst.}).$$

This can be translated using Eq. (105) into

$$\alpha_S(m_Z^2) = 0.126 \pm 0.016\ (\text{stat.}) \pm 0.013\ (\text{syst.}) \pm 0.001\ (\text{theory}), \tag{106}$$

where the theory error is due to the uncertainty of the l parameter. Despite the large error, this value of $\alpha_S(m_Z^2)$ is consistent with the results from other determinations.

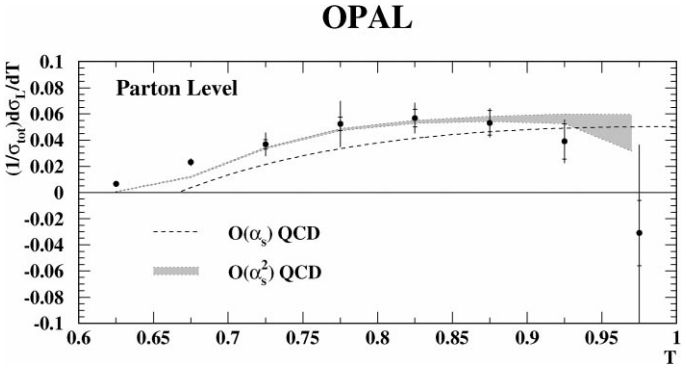

Fig. 35. The differential longitudinal cross-section is shown for thrust measured at $s = m_Z^2$ and corrected for detector and hadronization effects (parton level). The dashed curve is the leading-order prediction taking $\alpha_S(m_Z^2) = 0.119$. The shaded area represents the NLO prediction and its statistical error. Figure taken from Ref. [197].

5.2. QCD *at small x: MLLA and multiplicities*

Gluon radiation at large angle and high energy has a small probability. This can be seen from rewriting Eq. (35) to yield the differential spectrum of bremsstrahlung off a quark (see e.g. Ref. [41])

$$\mathrm{d}\omega^{q\to qG} = C_F \frac{\alpha_S(k_\perp^2)}{2\pi}\left[1+\left(1-\frac{k}{p}\right)^2\right]\frac{\mathrm{d}k}{k}\frac{\mathrm{d}k_\perp^2}{k_\perp^2}, \tag{107}$$

where p and k are the momenta of the quark and gluon, respectively, in the final state. The relevant scale for the coupling is set by $k_\perp$, the gluon transverse momentum with respect to the q direction. When $k_\perp \sim k \sim E$, corresponding to gluon emission at large angle and at high energy, $E = p$ for massless partons, one rediscovers multijet topologies with $\omega \sim \alpha_S/\pi \ll 1$, which have been discussed in the previous section.

The activity inside a jet is governed by quasi-collinear and soft partons which are characterized by $k_\perp \ll k \ll E$. Their emission probability, according to the differential spectrum in Eq. (107), is $\omega \sim \alpha_S \ln^2 E \sim 1$. In the formation of the parton shower, this "Double-Logarithmic" (DL) $q \to qG$ process has to be supplemented by the DL gluon radiation $G \to GG$ and the "Single-Logarithmic" (SL) gluon splitting $G \to q\bar{q}$ (see also Section 3.1.3). All these are not supposed to yield additional jets but to contribute to the jet initiated by the highly energetic parton. Furthermore, the contributions from such DL gluon radiation obey colour coherence which leads to a prominent effect: *angular ordering*. It means, in a classical picture, that for consecutive emissions of gluons the angle Θ between the emitter and the emitted gluon must decrease [41]. This effect can be explained by the transverse wavelength of the last emitted gluon which becomes too large to resolve the system formed by the emitter and the gluon emitted immediately before. Colour coherence and angular ordering entail a depletion of soft emission such that particles with intermediate energies are predominantly created in QCD cascades and, therefore, the particle spectrum has a *hump-backed* shape at small values of x.

It follows that quasi-collinear and soft partons determine the details of the fragmentation function at small values of the scaled energy x. From the evolution equation (90) in this regime much can be learnt about the dynamics of low energy partons, in particular gluons. A widely used method to solve the evolution equation for $D_i(x, Q^2)$ is that of the Mellin transformation, i.e. considering moments with respect to x

$$\tilde{D}_i(N, Q^2) = \int_0^1 \mathrm{d}x\, x^{N-1} D_i(x, Q^2). \tag{108}$$

In lowest order (leading-logarithmic approximation LLA) and using the explicit 1-loop expression for α_S the solution of Eq. (90) is of the form [12,199]

$$\begin{aligned}\tilde{D}_i(N, Q^2) &= \sum_{j=q,\bar{q},G} \tilde{D}_j(N, Q_0^2)\exp\left[\int_{Q_0}^{Q}\frac{\mathrm{d}q}{q}\,\gamma_{ji}(\alpha_S(q^2), N)\right] \\ &= \sum_{j=q,\bar{q},G} \tilde{D}_j(N, Q_0^2)\left(\frac{\alpha_S(Q_0^2)}{\alpha_S(Q^2)}\right)^{\gamma_{ji}(1/(2\beta_0),N)},\end{aligned} \tag{109}$$

where γ_{ji} is the Mellin transform of $\alpha_S/2\pi \cdot P_{ji}(z,\alpha_S)$, which are the Altarelli-Parisi splitting functions introduced in Eq. (91). This equation explicitly exhibits the scaling violation due to the scale dependence of the strong coupling. The power γ_{ji} is called *anomalous dimension*.

Including the known next-to-leading corrections [43] Eq. (109) is supplemented by a *coefficient function*, C, and becomes

$$\tilde{D}_i(N,Q^2) = \sum_{j=q,\bar{q},G} C(\alpha_S(Q^2),N)\tilde{D}_j(N,Q_0^2)\exp\left[\int_{Q_0}^{Q}\frac{dq}{q}\gamma_{ji}(\alpha_S(q^2),N)\right], \tag{110}$$

which, being of a similar form to Eq. (67), incorporates the exponentiation property of the elementary splitting processes. The coefficient function C describes multijet contributions to the evolution of the system, given by large angle and high-energy parton emission. Small angle emission and, therefore, the evolution of a jet is determined by the anomalous dimension.

Studying the fragmentation of quarks and gluons at small x involves the investigation of the first ($N=1$) moment of the anomalous dimension γ_{ji} and the coefficient function C. This region is dominated by the DL gluon radiation processes for which γ_{GG}, evaluated to $\mathcal{O}(\alpha_S^n)$, contains for $N \to 1$ an infrared singularity of the form $1/(N-1)^{2n-1}$. Resumming the series to all orders of α_S one arrives at the expression [12,199]

$$\gamma_{GG}(\alpha_S,N) \approx \frac{1}{4}\sqrt{(N-1)^2+24\frac{\alpha_S}{\pi}} - \frac{1}{4}(N-1) \overset{N\to 1}{\to} \sqrt{\frac{3\alpha_S}{2\pi}}, \tag{111}$$

which is in fact finite at $N=1$. With Eqs. (110) and (111) the characteristics of the small-x regime of fragmentation, which concerns most of the produced particles, thus becomes accessible to perturbative predictions and their experimental testing. For instance, inserting the Taylor expansion of Eq. (111) at $N-1$ into Eq. (109) and performing the integration one finds a Gaussian function of N. This yields, employing an inverse Mellin transformation, a Gaussian in the variable $\xi_p \equiv \ln(1/x_p)$ for the small-x fragmentation function (for details see [12])

$$xD(x,s) \sim \exp\left[-\frac{1}{2\sigma^2}(\xi_p - \langle\xi_p\rangle)^2\right]. \tag{112}$$

Two omissions have to be recalled at this stage. First, the calculation of the anomalous dimension considered so far uses DL terms only, hence it is a double-logarithmic approximation (DLA) which also disregards energy conservation. It yielded $\gamma_{GG} \sim \sqrt{\alpha_S}$. In the parton shower cascade, however, the SL terms from $G \to q\bar{q}$ contribute as well. The corrections due to these should be of the order of $\Delta\gamma \sim \alpha_S$. One has to account for such next-to-leading terms, since they will cause essential energy-dependent factors appearing in front of the exponential in Eq. (110). The approach of Refs. [41,64,200] adopted the shower picture, implying a dependence of the structure of the elementary parton decays (see Eq. (43)) on just the nearest *forefathers* of a considered parton. This yields an analytic prediction for the small-x fragmentation functions known as the *modified leading logarithmic approximation* (MLLA) which obeys energy conservation. In Ref. [201] the next-to-leading corrections to the LLA prediction, which will be referred to as NLLA, were used to calculate higher moment corrections (*skewness* and *kurtosis*, see Ref. [199]) to the Gaussian in Eq. (112) of the small-x fragmentation function. Predictions of both approaches will be confronted with experimental data in the following section.

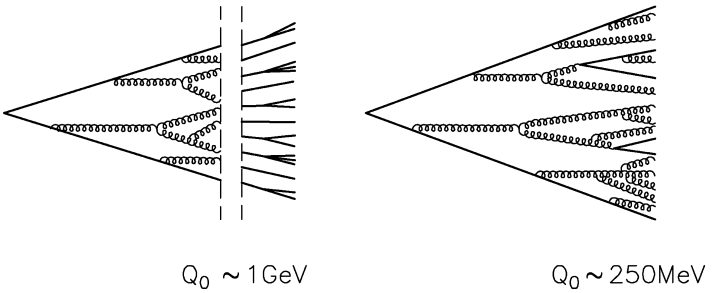

Fig. 36. In standard hadronization models (left) the parton shower, being terminated at some virtuality scale cut-off Q_0, is followed by a hadronization step. The MLLA plus LPHD concept assumes the hadronization phase to be represented on average by the parton cascade evolved down to Q_0 close to the QCD scale Λ. Figure taken from Ref. [202].

Secondly, all the calculations quoted refer to partons and are, thus, not directly applicable to observables measured from the hadronic final state. Although phenomenological hadronization models have been shown in the previous section to be quite successful, a simple and fair assumption is that the hadronic spectra are directly related to and, in fact, are proportional to the partonic ones if the conversion from partons to hadrons occurs at a virtuality scale of the order of the hadron masses. This is depicted in Fig. 36. Thus, the formation of hadrons is independent of the primary hard process and its energy scale. This concept is known as the hypothesis of *Local parton hadron duality* (LPHD) [64] which originates from the *preconfinement* properties of QCD cascades [63]. It means, broadly speaking, that the long-range effects between partons in phase space are of secondary importance in the process of the blanching of coloured partons to form hadrons from them. Although intriguing, LPHD has a conceptual problem describing the production of massive hadrons such as baryons in the QCD jets [203]. It also assumes the spectrum of hadrons, whether they originate from decays of other hadrons or directly from the partons, to be reproduced by the calculated spectrum of the parton shower. Thus, finding LPHD not to describe experimental data may open the view on the details of hadronization physics.

5.2.1. Small-x fragmentation function

The spectra of the hadron's energy fraction x were measured by many experiments covering a vast energy range. In order to focus on the small-x region of the fragmentation function one usually considers the variable $\xi_p \equiv \ln(1/x_p)$ where x_p is the momentum, rather than the energy fraction of a particle. Fig. 37 shows $(1/N)(\mathrm{d}n/\mathrm{d}\xi_p)$, the differential distribution of the ξ_p variable for charged particles at centre-of-mass energies between 14 and 183 GeV [130,204–206]. Shown as curves are the NLLA and MLLA calculations and the dependence of the *hump-backed* shape of these spectra on the energy scale. The scale, which also controls the average multiplicity $\langle n_h(Y)\rangle$ as will be detailed below, is given by the variable $Y \approx \ln(E_{\mathrm{beam}}/Q_0) = \ln(\sqrt{s}/2Q_0)$, where the parton shower cut-off Q_0 equals Λ_{eff} in the limiting spectrum. Both calculations, NLLA and MLLA, consequently have only one free parameter, Λ_{eff}, which is connected to the running of the strong coupling constant. Since the leading and next-to-leading terms in the MLLA and NLLA calculations are scheme independent, the parameter Λ_{eff} can be related to $\Lambda_{\overline{\mathrm{MS}}}$ only once the calculation has been done in the $\overline{\mathrm{MS}}$ renormalization scheme. In Fig. 37(a) Λ_{eff} was obtained from a fit of the distorted Gaussian to the data, whereas in Fig. 37(b), in order to be able to present the MLLA

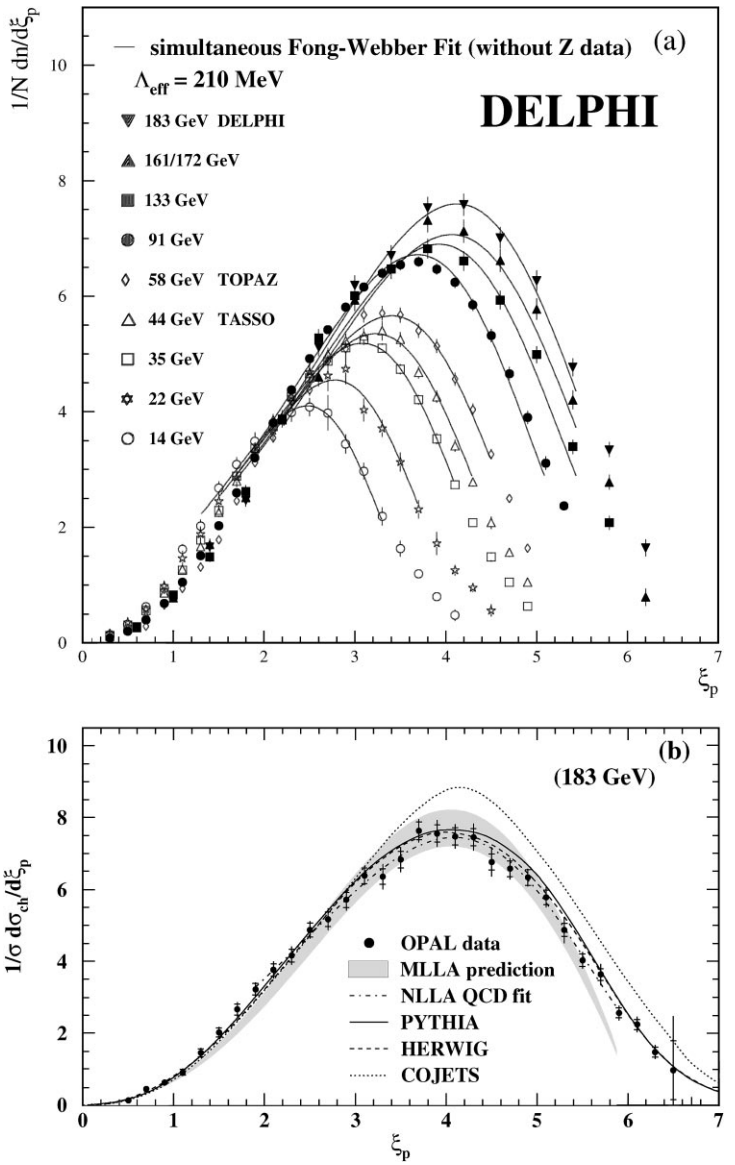

Fig. 37. Differential distribution of $\xi_p \equiv \ln(1/x_p)$ for charged particles. In plot (a) Gaussian curves including skewness and kurtosis, which correspond to the NLLA calculation of Ref. [201] of the limiting shape, have been simultaneously fitted to the distributions, excluding the 91 GeV data. Plot (b) shows a comparison of the fitted distorted Gaussian (NLLA) together with the MLLA prediction of Ref. [41], which is a pure prediction with all parameters taken from a fit of the data at 91 GeV. The predictions of three MC hadronization models are also shown. Figures are taken from Refs. [130,206].

prediction of the *hump-backed* distribution, the respective value was taken from the fit of the ξ_p distribution at 91 GeV in Ref. [207].

Although MLLA yields an analytic expression for the shape of the distribution it is not well-suited for numerical evaluation. In the limit of very high energies, however, the shape of the spectrum

becomes insensitive to the cut-off of very low energy gluon radiation. For this reason, one usually considers the limiting spectrum, i.e. $Q_0 = \Lambda_{\rm eff}$, for which a more convenient, but still involved expression was derived, for instance in Ref. [41]. At asymptotically high energies the distribution of partons is expected to be Gaussian in ξ_p (see Eq. (112) above). One can then represent the shape even more conveniently by a distorted Gaussian [41,201]

$$\bar{D}(\xi_p, Y) \equiv x_p \bar{D}(x_p, Y) \approx \frac{\langle n_h(Y)\rangle}{\sigma\sqrt{2\pi}} \exp\left[\frac{1}{8}K - \frac{1}{2}S\delta - \frac{1}{4}(2+K)\delta^2 + \frac{1}{6}S\delta^3 + \frac{1}{24}K\delta^4\right] \quad (113)$$

with $\delta = (\xi_p - \langle\xi_p\rangle)/\sigma$. The perturbative predictions for mean $\langle\xi_p\rangle$, width σ, skewness S, and kurtosis K of this Gaussian for gluon initiated jets are[15]

$$\begin{aligned}
&\text{mean:} && \langle\xi_p\rangle = \frac{1}{2}Y\left(1 + \frac{\rho}{24}\sqrt{\frac{12}{\pi\beta_0 Y}}\right) + \mathcal{O}(Y^0),\\
&\text{width:} && \sigma \equiv \langle(\xi_p - \langle\xi_p\rangle)^2\rangle,\\
&\text{skewness:} && S \equiv \frac{\langle(\xi_p - \langle\xi_p\rangle)^3\rangle}{\sigma^3},\\
&\text{kurtosis:} && K \equiv \frac{\langle(\xi_p - \langle\xi_p\rangle)^4\rangle}{\sigma^4} - 3,
\end{aligned} \quad (114)$$

where ρ is defined as $\rho \equiv 11 + 2n_f/27$ and β_0 has already been given in Eq. (21). Some additional corrections need to be applied to account for jets initiated by quarks. These are known to leading order for all four parameters P of Eq. (114), and are of the order $\Delta P/P \sim \mathcal{O}(0.1)(1 + n_f/27)/Y$ [201].

Both perturbative calculations, MLLA and NLLA, yield good descriptions of the *hump-backed* shape of the small-x fragmentation function data over a large energy range. This becomes even more convincing when plotting the energy dependence of the peak position of the ξ_p spectra, ξ_0, as is done in Fig. 38 using the data from Refs. [87,88,129–131,204,206–214]. In the MLLA framework the energy scale dependence of the peak position is predicted to be

$$\xi_0 \equiv \ln(1/x_{\max}) = Y\left(\frac{1}{2} + \rho\sqrt{\frac{\alpha_S(Y)}{96\pi}} - \rho^2\frac{\alpha_S(Y)}{96\pi} + \mathcal{O}(\alpha_S^{3/2})\right). \quad (115)$$

Fitting the single free parameter $\Lambda_{\rm eff}$ to the data yields a very satisfactory description. Without coherence in gluon radiation a decrease at very small x would be of purely kinematic origin due to the finite particle masses, $x \sim \sqrt{s}/m$. Thus the dependence of the peak position on the energy scale would be expected to be $\xi_0 \sim Y$, which is twice the value including coherent radiation and not in accordance with the data as can be seen in Fig. 38. Even though the effective Λ may not be related to $\Lambda_{\overline{\rm MS}}$ it is nevertheless instructive to find $\alpha_S(m_z^2) \approx 0.118$ assuming the crude but plausible approximation $\Lambda_{\overline{\rm MS}} \sim \Lambda_{\rm eff}$.

[15] Explicit expressions can be found, e.g. in Ref. [201].

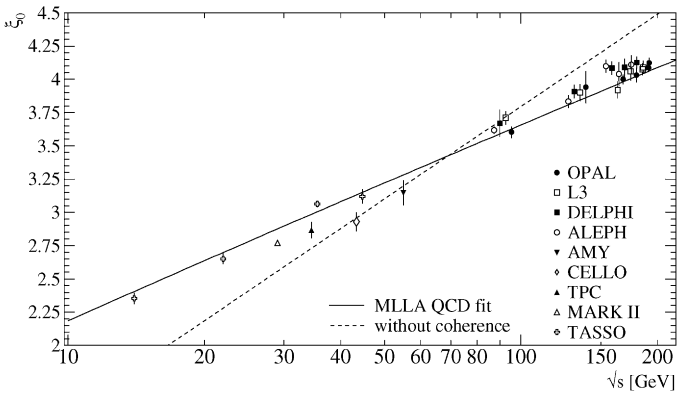

Fig. 38. Evolution of the peak position, ξ_0, of the ξ_p distribution with the centre-of-mass energy $\sqrt{s}$. The MLLA QCD prediction [41] (solid) and the expectation without gluon coherence (dashed) were fitted to the data.

A further test of the MLLA calculation was conducted by the DELPHI collaboration [206] in order to examine the prediction $\xi_0 - \langle\xi_p\rangle \approx \rho/32 \approx 0.351$. The ξ_p distributions shown in Fig. 37(a) were re-fitted around the peak region considering $\langle\xi_p\rangle$ as an additional free parameter since determining it from the whole spectrum would ignore the fact that the distorted Gaussian is only valid close to the maximum. Averaging the results on $\xi_0 - \langle\xi_p\rangle$ obtained from the data measured between 14 and 183 GeV, the DELPHI collaboration arrived at 0.35 ± 0.14 which agrees with the MLLA expectation.

The success of the MLLA plus LPHD approach was continued in an attempt to extend the perturbative predictions to the soft momentum domain [215–218]. Exploiting the representation of the analytic results for the spectrum $D(\xi, Y)$ in moments in ξ [219], an analysis over a large centre-of-mass energy range available in e^+e^- annihilation was performed. The investigation of moments has a number of advantages over the analysis of the spectrum itself owing to simplified theoretical calculations. In Refs. [215–218] the invariant hadronic density $E(dn/d^3p)$ was studied in the limit of vanishing absolute hadron momentum p and compared with the prediction

$$\frac{dn}{d^3p} = 2K_h \frac{C_F}{C_A} \frac{D_G(\xi, Y)}{4\pi N_c E(E^2 - Q_0^2)}, \tag{116}$$

where $Y = \ln(E_{\text{beam}}/Q_0)$, $E = \sqrt{p^2 + Q_0^2}$ is the particle's energy and K_h is a normalization parameter. The factor of 2 accounts for adding both hemispheres of an $e^+e^- \to q\bar{q}$ annihilation event. The function $D_G(\xi, Y)$ is the inclusive energy distribution of soft gluons originating from a primary gluon for which an approximate solution of the MLLA evolution equation was derived in Refs. [216,217]. The appropriate leading order colour factor ratio C_F/C_A is introduced to translate this result to the case of a primary quark. Fig. 39 shows the momentum dependence of dn/d^3p for several centre-of-mass energies between 3 and 133 GeV in comparison with the extended MLLA prediction, Eq. (116), using $K_h = 0.45$ and $Q_0 = 270$ MeV. Besides the overall good agreement a marginal excursion can be seen for the very high energy data at very small momenta of the order

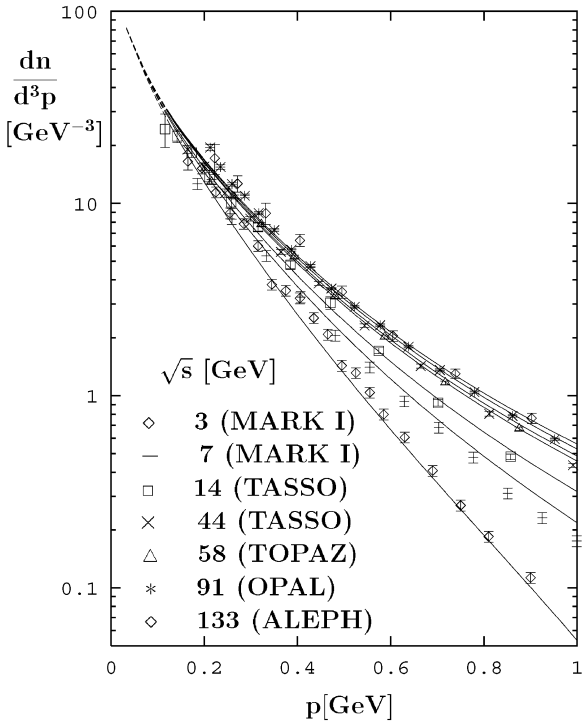

Fig. 39. Charged particle distribution $\mathrm{d}n/\mathrm{d}^3p$ versus particle momentum p at several centre-of-mass energies [204,205,207,212,222]. The data are compared with the extended MLLA calculations which are detailed in the text. The figure is taken from Ref. [217].

of 200 MeV which remains at even higher centre-of-mass energies (see Ref. [206]). In general, however, a remarkable agreement of the extended MLLA prediction [215–218] with the data can be observed and in particular the data in the figure approach a common limit for $p \to 0$ as expected.

Several further investigations of the *analytical perturbative approach* (APA ≡ QCD + LPHD) have been conducted. An overview can be found in Refs. [220,221].

5.2.2. Mean charged particle and mean jet multiplicities

Perturbative calculations of the fragmentation function $D(x,s)$ are primarily applicable in the neighbourhood of the maximum of the hump-backed ξ spectrum. Nevertheless, further quantities can be derived and confronted with experimental data. In the first place these are the Mellin moments of the fragmentation function in ξ or x

$$M(N,s) = \int_0^1 \mathrm{d}x\, x^{N-1} D(x,s). \tag{117}$$

For instance, the $N = 1$ moment, being just the integral of the fragmentation function, corresponds to the mean parton multiplicity $M(1,s) \equiv \langle N_p(s) \rangle$. Both the MLLA and the NLLA calculations arrive

at the same prediction for this multiplicity (see for instance Refs. [41,223]). In Refs. [224,225][16] the next-to-next-to-leading logarithmic approximation (NNLLA) and in Ref. [226] even the next-to-next-to-next-to-leading logarithmic approximation (3NLLA) was calculated for the mean parton multiplicity in jets initiated by a gluon. Rewriting the formula to explicitly show the dependence of the parton multiplicity on α_S one obtains

$$\langle N_p^G(Q^2)\rangle \sim \alpha_S^b(Q^2)\exp\left[\frac{c}{4\pi\beta_0\sqrt{\alpha_S(Q^2)}}\left(1+6a_2\frac{\alpha_S(Q^2)}{\pi}\right)\right][1+\mathcal{O}(\alpha_S^{3/2})] \tag{118}$$

where β_0 is defined in Eq. (21) and[17]

$$\begin{aligned} b &= \frac{1}{4}+\frac{10}{27}\frac{n_f}{4\pi\beta_0} \\ c &= \sqrt{96\pi} \\ a_2 &\approx -0.502+0.0421n_f-0.00036n_f^2\,. \end{aligned} \tag{119}$$

5.2.2.1. Gluon to quark multiplicity ratio. Since the parton cascade in an e^+e^- annihilation event is initiated by quarks rather than gluons, the above formulae have to be modified to account for the different colour factors of quarks and gluons which leads to a lower showering activity for quark jets compared with gluon jets. A naïve estimate can be derived from the colour factors C_F and C_A since these determine the probability to radiate a gluon off a quark or a gluon, respectively (see Eqs. (13) and (14)). The ratio of multiplicities of gluon, $\langle N_G\rangle$, and quark jets, $\langle N_F\rangle$, is thus expected to be asymptotically $r = C_A/C_F = 9/4$ [227]. Including higher-order corrections and explicitly exhibiting the dependence on α_S, this ratio becomes

$$\frac{\langle N_G\rangle}{\langle N_F\rangle} \equiv r(Q^2) = \frac{C_A}{C_F}\left(1-r_1\sqrt{\frac{6\alpha_S(Q^2)}{\pi}}-r_2\frac{6\alpha_S(Q^2)}{\pi}+\mathcal{O}(\alpha_S^{3/2})\right) \tag{120}$$

where the coefficients are (see [225] for exact expressions)

$$r_1 = \frac{1}{6}+\frac{1}{162}n_f, \quad r_2 \approx 0.292+0.0457n_f-0.00041n_f^2\,. \tag{121}$$

It should be noted that the above coefficients were derived by means of generating functions and Taylor series in such a way that energy conservation is respected in three-parton vertices [224]. The respective values of r_1 and r_2 given in Refs. [228,229] are therefore slightly different.

The multiplicity ratio was measured by the experiments at LEP I. The measurements applied the general technique of identifying the gluon jet by vertex tagging of the lower energetic bottom quark jet in very symmetric, *Y*-shaped 3-jet events and deriving multiplicities of pure gluon and quark jets by means of statistical decomposition using an identical sample of untagged symmetric 3-jet events

[16] There is a minor misprint in Eqs. (23) and (24) of Ref. [225]: the exponent of y should read $-a_1/2B$ instead of $a_1/2B$.
[17] The analytic expression for a_2 can be found in Ref. [225].

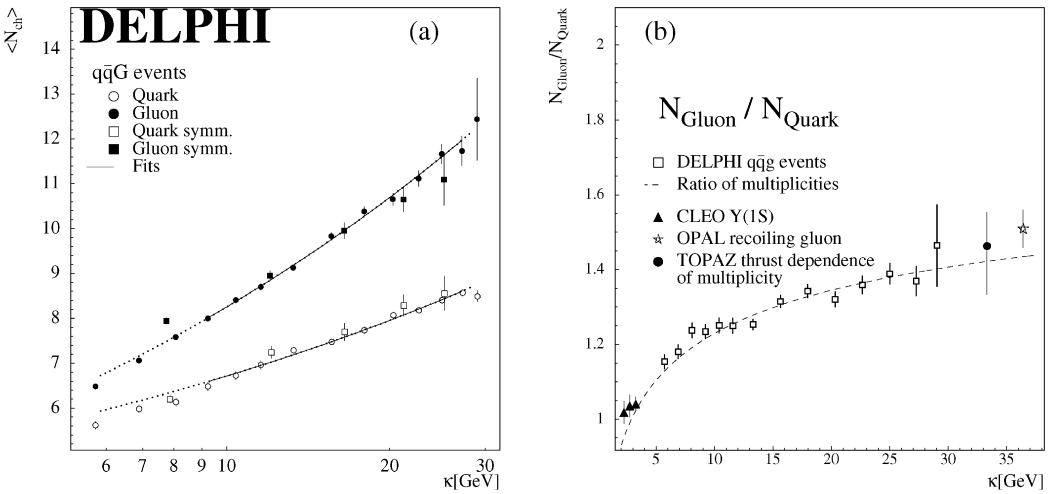

Fig. 40. (a) The scale dependence of the mean charged multiplicity in quark and gluon jets is shown. Part (b) presents the ratio of the multiplicities. The curves are results of fits of the perturbative expression for the mean multiplicity allowing for a constant offset. Figures adapted from Ref. [233].

from light quarks (cf. Section 5.1.2). All such investigations yielded a ratio $r(m_z^2)$ of about 1.25 with a total error of less than 3% [52,185,230,231].

Extending the study by including asymmetric 3-jet configurations, where one jet is less energetic than the others, the DELPHI collaboration [232] determined the energy scale dependence of the particle multiplicity in quark and gluon jets and of the ratio $r(s)$. The relevant scale, κ, of the jet was taken to be the transverse momentum of the jet with respect to the closest jet according to Eq. (97). Fig. 40(a) shows the average multiplicities found in quark and gluon jets, respectively, and Fig. 40(b) the ratio of these multiplicities. The data were fitted using the NLL approximation of the expressions in Eq. (118) and (120). In addition, a constant offset was allowed which was determined to be approximately 2.6 for the quark and zero for the gluon multiplicities. The multiplicity ratio grows with an increasing scale κ, seemingly approaching some asymptotic value, but still staying significantly below the expectation of ≈ 1.7 from Eq. (120).

The determinations of r discussed up to now are all based on the reconstruction of jets from the hadronic final state. The jets from highly energetic partons need not be well separated due to the collinear singularity. Thus the measurements might be biased by the use of a jet finder. An investigation of the TOPAZ collaboration [234] avoids such biases using an approach which is based on the thrust observable rather than jets. They measured the multiplicity as a function of the thrust of an event and extrapolated to a thrust value of 2/3 which corresponds to the three-fold symmetric *Mercedes* topology of $q\bar{q}$G events. The mean charged multiplicity of gluon jets follows by subtracting the $q\bar{q}$ contribution from the extrapolated multiplicity, $\langle N\rangle_{T=2/3}$. For the subtraction one can use $q\bar{q}$ events at the appropriate energy scale of $\sqrt{s'} = \sqrt{s/3}$ (cf. Eq. (36)), that is the mass of the $q\bar{q}$ system recoiling against the gluon G. The ratio r can then be calculated by

$$r(s/3) = \frac{\langle N\rangle_{T=2/3} - \langle N\rangle_{q\bar{q}}}{\frac{1}{2}\langle N\rangle_{q\bar{q}}}. \tag{122}$$

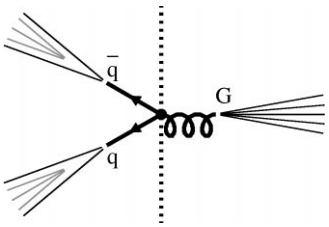

Fig. 41. Topology of 3-jet events in which two quark jets are tagged by a secondary decay vertex in one hemisphere. The opposite hemisphere is considered as an inclusive gluon jet.

The TOPAZ collaboration calculated $\langle N\rangle_{q\bar{q}}$ at $\sqrt{s/3} = 57.8\,\mathrm{GeV}/\sqrt{3}$ using the next-to-leading-logarithmic approximation of Eq. (118) which was fitted to mean charged multiplicity data measured from 12 up to 91 GeV. Inserting their extrapolated value for $\langle N\rangle_{T=2/3}$, they finally obtained $r((57.8\,\mathrm{GeV})^2/3) = 1.46^{+0.09}_{-0.13}$ [234]. This value is less than 1.7 which is expected from Eq. (120), but it agrees well with the scale dependence of the multiplicity ratio shown in Fig. 40(b).

One has to be aware, however, that the calculation assumes a pair of either gluon or quark jets to emerge from a colour singlet point source whereas the gluon jets considered in the experimental investigations are radiated off a quark and have to be reconstructed by employing some jet algorithm. In Ref. [235] a measurement was proposed yielding inclusive gluon jets that are similar to those used for analytic calculations. To this end, 3-jet events are selected, in which the identified quark and antiquark jets appear in the same hemisphere. This situation is depicted in Fig. 41. All particles in the hemisphere opposite to the two tagged quark jets are inclusively considered as belonging to the gluon jet without application of a jet algorithm. Although gluon jets defined by this prescription still do not precisely match the jets considered in the theory calculations, they were found in Refs. [235,236] to be essentially identical to gluon jets in GG events from a colour singlet point source generated using a QCD Monte Carlo event generator. The OPAL collaboration performed a study in which inclusive gluon jets, after accounting for the different mean jet energies, were compared with 2-jet events of light quarks [237,238]. Fig. 42 shows the multiplicity distributions for the inclusive gluon and light quark jets, respectively. The ratio of the mean multiplicities yields

$$r(m_Z^2/4) = 1.471 \pm 0.024\ (\mathrm{stat.}) \pm 0.043\ (\mathrm{syst.})\,. \tag{123}$$

This result is also shown in Fig. 40 to be consistent with the overall scale dependence of the multiplicity ratio. Although this value is still below the expectation from Eq. (120) the agreement is better.

The $r(s)$ ratio was calculated analytically in Ref. [239] by exact numerical integration of the complete MLLA evolution equations for parton multiplicities, derived from Eq. (90), with full account of energy conservation and the correct threshold behaviour, i.e. the mean parton multiplicity in a single jet approaches 1 for $\sqrt{s} \to 0$. In particular, this calculation refers to the multiplicity in the full hemisphere of a gluon jet emerging from a colour singlet state, and thus does not immediately apply to the symmetric Y-shaped 3-jet events [239]. Choosing the parton shower cut-off[18] to be

[18] Ref. [239] quotes the results for r at the scale m_Z^2, but the energy scale of the experimental measurement is $\approx m_Z^2/4$. The Q_0 value quoted in the reference is, therefore, scaled by one-half here.

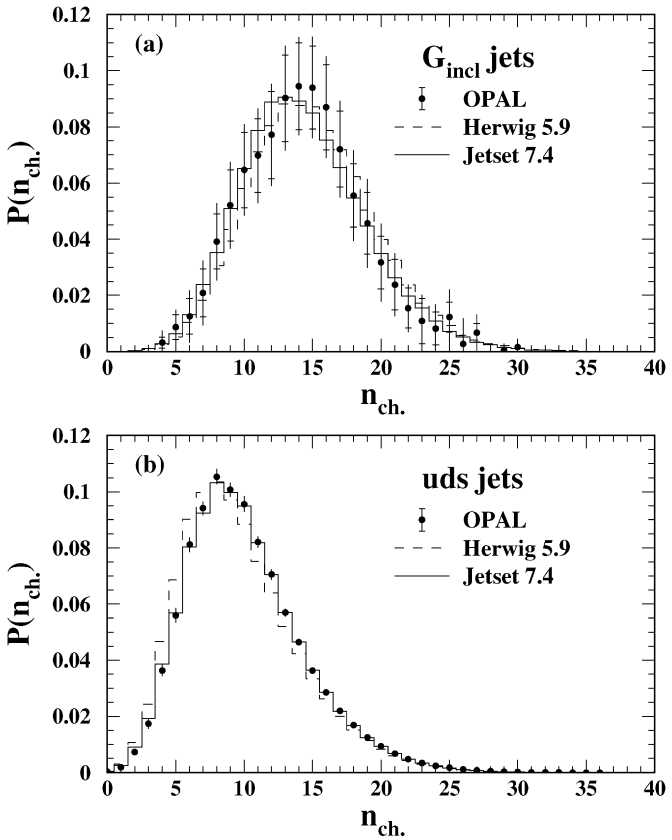

Fig. 42. Corrected charged multiplicity distributions for (a) inclusive gluon and (b) light quark jets are shown with statistical (horizontal ticks) and total uncertainties. For comparison, the expectations from two phenomenological hadronization models, JETSET and HERWIG, implementing string and cluster fragmentation, respectively, are superimposed. Figures taken from Ref. [238].

$Q_0 \approx 250\,\mathrm{MeV}$, for which the mean particle multiplicities are well described as will be discussed below, the numerical integration yielded $r(m_Z^2/4) \approx 1.56$. A similar calculation was done in the context of the colour dipole cascade model in Ref. [240]. It employed the ARIADNE Monte Carlo generator [61] to fix the unknown parameters of the calculation, thus yielding $r \approx 1.5$ consistent with the experimental measurement.

In addition, the DELPHI collaboration [232] determined the colour factor ratio C_A/C_F from the multiplicities in quark and gluon jets, using multiplicity data from e^+e^- events at comparable scales obtained from previous measurements and also from events with hard photon radiation. Their result,

$$\frac{C_A}{C_F} = 2.266 \pm 0.053\ (\mathrm{stat.}) \pm 0.055\ (\mathrm{syst.}) \pm 0.096\ (\mathrm{theory})\,,$$

is, within the statistical, systematic and theoretical uncertainties, in good agreement with the QCD expectation of 9/4. It is also more precise than the corresponding determinations using 4-jet final states, that will be presented in Section 6.3.1.

5.2.2.2. Mean charged particle multiplicity. From the combination of Eq. (118) with the multiplicity ratio for quark and gluon jets (120) and by relating parton and hadron multiplicities by a factor K_h according to the LPHD hypothesis, the mean multiplicity in $e^+e^- \to$ hadrons can be derived. A low-energy constraint has to be considered in addition. In the limit of vanishing centre-of-mass energy the parton multiplicity should approach some non-zero value. This is most obvious for massive quarks for which the minimum parton multiplicity must be two since at a centre-of-mass energy of twice the quark mass there will be no phase space left for the quark–antiquark pair to radiate gluons [241]. The approximate expression for the mean hadron multiplicity, therefore, reads [239,241]

$$\langle N(s)\rangle \approx 2K_h \frac{\langle N_p^G(s/4)\rangle}{r(s/4)} + c(s)\,, \tag{124}$$

where the factor 2 takes into account that both quark and antiquark will initiate a jet. It should be noted that for both the r ratio and the parton multiplicity the appropriate energy scale is $s/4$, i.e. that for a single jet. Moreover, at very high centre-of-mass energies the ratio, $r(s)$, of gluon and quark multiplicities should approach the asymptotic value of $C_A/C_F = 9/4$. The additive term $c(s)$, therefore, needs to vanish at asymptotic energies which could be achieved by a power suppressed behaviour like $c(s) \sim \text{const.}/\langle N_p^G(s/4)\rangle$ or $c(s) \sim \text{const.}/\sqrt{s}$.

The upper plot of Fig. 43 shows the mean multiplicity of charged hadrons [53,87,88,129,130, 132,182,187,212,214,242–244] measured in e^+e^- annihilation at centre-of-mass energies from about 10 up to 190 GeV. The predicted energy scale dependence of the mean multiplicity is superimposed on the data. The strong coupling constant is chosen to be $\alpha_S(m_Z^2) = 0.119$ and the two non-calculable parameters of Eq. (124) are adjusted appropriately. The description of the data by the NNLLA formula over this large energy range is satisfactory.

The fact that the mean multiplicity exhibits a larger scaling violation than any other moment of the fragmentation function could render it one of the best quantities to determine $\Lambda_{\overline{\text{MS}}}$, the QCD parameter determining the scale dependence of the coupling α_S. It would, however, require a calculation of Eq. (124) in the $\overline{\text{MS}}$ renormalization scheme [199,201].

5.2.2.3. Moments of the multiplicity distribution. From a theoretical point of view, higher moments of the multiplicity distribution shown in Fig. 42, such as skewness and kurtosis, are more favourable since these scale with the mean multiplicity such that non-calculable factors like K_h cancel. One example of such moments is the second binomial moment R_2 for which a NLLA prediction was obtained in Refs. [199,228]

$$R_2 \equiv \frac{\langle N(N-1)\rangle}{\langle N\rangle^2} = \frac{11}{8}\left[1 - \left(\frac{5}{2} - \frac{20n_f}{891}\right)\sqrt{\frac{\alpha_S}{6\pi}} + \mathcal{O}(\alpha_S)\right]. \tag{125}$$

Some of the experiments also quoted values for R_2, but in most cases only the average multiplicity $\langle N\rangle$ and the ratio, $\langle N\rangle/D$ of the mean to the dispersion $D = \sqrt{\langle N^2\rangle - \langle N\rangle^2}$, i.e. the width of the multiplicity distribution, are given. It is possible, however, to calculate R_2 from these two numbers according to $R_2 = 1 + (D/\langle N\rangle)^2 - 1/\langle N\rangle$. This was done in Ref. [9] for the measurements at and below the Z pole. In the lower part of Fig. 43 the data compiled in this reference, complemented by the values available or calculable from Refs. [87,88,129,130,132,212,244], are shown. It can be seen

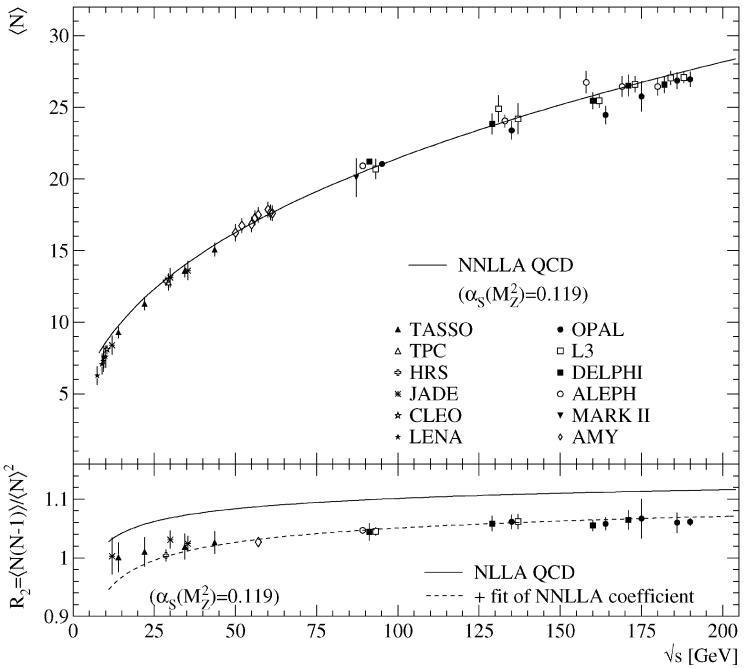

Fig. 43. In the upper plot, the mean multiplicity of charged particles measured in e^+e^- annihiliation by various experiments is shown. The measurements include contributions from K^0_S and Λ decays. Overlaid is the NNLLA prediction using $\alpha_S(m_Z^2) = 0.119$. The lower plot shows the second binomial moment R_2 of the multiplicity distribution. Superimposed as a solid line is the NLLA prediction for this moment. The dashed line shows the result when fitting for the unknown NNLLA coefficient of the prediction. In both cases, the indicated errors comprise statistical and systematic errors added in quadrature. The data are compiled from Refs. [53,87,88,129,130,132,182,187,212,214,242–244].

from the figure that the NLLA prediction using $\alpha_S(m_Z^2) = 0.119$ overestimates the R_2 moment. Adding to Eq. (125) a term $C_{\mathrm{NNLLA}}\alpha_S/6\pi$, a satisfactory description of the data with a χ^2/d.o.f. = 13.9/20 is obtained with the fitted value $C_{\mathrm{NNLLA}} = -0.537 \pm 0.021$, where the error is due to the experimental uncertainties only. The fitted NNLLA coefficient is about 20% of the NLLA one in Eq. (125) which is approximately -2.38 for $n_f = 5$. Calculated at the Z scale the value of the NNLLA correction to Eq. (125) is only about 3.4×10^{-3}.

The MLLA predictions for even higher moments of the multiplicity distribution show perfect agreement with the measurements. Exploiting the multiplicity distributions measured from the inclusive gluon hemisphere, as described above and shown in Fig. 42, the OPAL collaboration [238] determined the cumulant factorial moments K_i. In terms of the normalized factorial moments F_i of rank i,

$$F_i \equiv \frac{\langle N(N-1)\cdots(N-i+1)\rangle}{\langle N\rangle^i} \tag{126}$$

these are defined as

$$K_i \equiv F_i - \sum_{m=1}^{i-1} \frac{(i-1)!}{m!(i-1-m)!} K_{i-m} F_m \,. \tag{127}$$

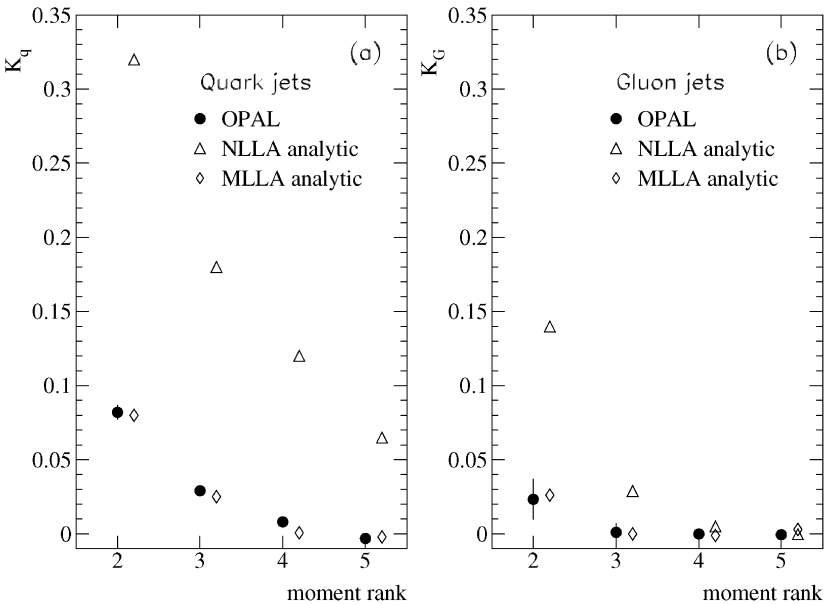

Fig. 44. Cumulant factorial moments K_i of rank $i = 2$–5 are shown as determined by the OPAL collaboration [238] separately for (a) quark and (b) gluon jets. Overlaid are the results of NLLA [245] and MLLA [246] calculations.

Thus, R_2 is identical with K_2. The K_i moments have several advantages over the F_i moments because the former are more sensitive to the effects of higher-order QCD, largely independent of each other, and directly related to dispersion D, skewness S and kurtosis K (see [238]). Fig. 44 shows the measured cumulant factorial moments K_i of rank $i = 2$–5 separately for quark and gluon jets. The results of the NLLA [245] calculations and of the exact numerical solution of the MLLA DGLAP equation [246] are superimposed. In general, there is a remarkable qualitative and even quantitative agreement with the OPAL results for both gluon and quark jets, in particular for the exact numerical MLLA calculations.

5.2.2.4. Mean jet multiplicities. The MLLA calculations give a detailed insight into the low-x phenomena inside the jets, but they are also able to describe average hadron and jet multiplicities simultaneously over a wide range of centre-of-mass energies as is shown in Ref. [239]. In order to obtain predictions in the region of large values of the jet resolution parameter y_{cut} (cf. Section 4.1.2), i.e. for large angle 3-jet events, the lowest order contribution $N_q^{(1)}$ of the evolution equation is replaced by the explicit result for $e^+e^- \to 3$ partons in $\mathcal{O}(\alpha_S)$. The full contribution $N^{3\text{-jet}}$ follows from numerical integration of Eq. (35) as in Eq. (38), but replacing the δ function by the step function $\Theta(y_3 - y_{\mathrm{cut}})$ which depends on y_3, the value of the jet resolution parameter at the flip from 3 to 2 jets. In Ref. [239] this value is given for the DURHAM jet finder in terms of the fractional energies of quark, antiquark and gluon by $y_3 = \min(x_{\bar{q}}/x_G, x_G/x_{\bar{q}})(1 - x_q)$. The $\mathcal{O}(\alpha_S)$ corrected prediction is then applicable to both hadron multiplicities, choosing $y_c \equiv (Q_0/Q)^2$, and jet multiplicities, i.e. $y_c \equiv (Q_c/Q)^2$, and reads [239]

$$N_{\mathrm{corr}}^{e^+e^-}(y_c) = 2N_q(y_c) - 2N_q^{(1)}(y_c) + N^{3\text{-jet}}(y_c), \tag{128}$$

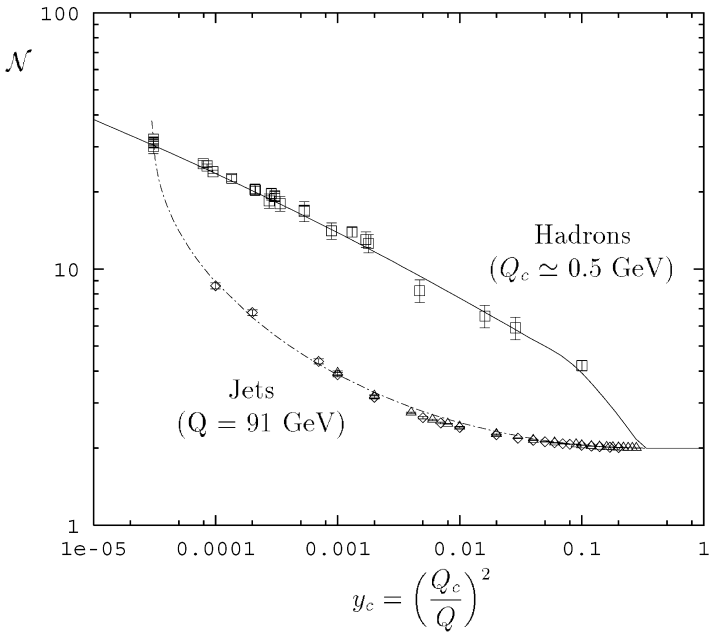

Fig. 45. The mean jet multiplicity at 91 GeV versus $y_c \equiv y_{\text{cut}}$ for the DURHAM jet finder, and the mean charged particle multiplicity, the latter scaled by 3/2 to account for the unmeasured contribution from neutral particles, in the range of $Q = 1.6$ to 91 GeV, versus $y_c = (Q_0/Q)^2$ for $Q_0 \approx 500$ MeV are shown. Overlaid is the expectation from the exact solution of the evolution equation, using the same QCD parameter Λ_{eff}. Figure taken from Ref. [239].

where N_q is obtained from the numerical solution of the evolution equation, Q_0 is the usual cut-off scale of the parton cascade adjusted to the typical mass of the hadrons produced, and $Q_c = \sqrt{sy_{\text{cut}}}$.

Fig. 45 shows mean jet multiplicities obtained with the DURHAM jet algorithm at $\sqrt{s} = 91$ GeV. The jet multiplicity is used to fix the QCD parameter Λ_{eff} which controls the scale dependence of the coupling α_S. Moreover, the mean charged particle multiplicities are shown, as measured at centre-of-mass energies from 1.6 to 91 GeV. These are scaled by 3/2 to account for the contributions from neutral particles. Using the value of Λ_{eff} from the jet multiplicities, the values of the parton shower cut-off Q_0 and the overall normalization factor K_h which relate parton and hadron multiplicities in Eq. (128) are adjusted to the data. A remarkably good description of the data is achieved for $Q_0 \approx 500$ MeV and $K_h \approx 1$.

5.2.3. *Summary of* QCD *at small-x*

Processes taking place at small values of the fractional energy x are, in general, not expected to be accessible to perturbative QCD calculations. This small-x regime should be governed by the physics of confinement. It turns out, however, that perturbative QCD works down to scales as low as about 1 GeV. Moreover, when energy scales of a few hundred MeV are considered and the conjecture of local parton-hadron duality (LPHD) is invoked, perturbative calculations can even describe inclusive distributions of energy and multiplicity of hadrons originating from a hard process.

Despite the support found for the hypothesis of LPHD adapted to the modified leading-logarithmic approximation (MLLA) some questions still have to be addressed. Due to their larger colour charge and the gluon self-interaction, gluons play the dominant role in the development of the parton cascade, but the hadrons observed in the detector are built up of quarks and antiquarks. Although LPHD performs rather successfully it cannot explain the formation of hadrons from quarks and gluons emerging from the parton cascade. What the experimental verification of LPHD can tell us is that hadronization and, hence, confinement is likely to take place at very small energy scales as low as the mass of the lightest mesons despite the fact that many of these mesons arise from the decay of heavier hadrons.

5.3. Power corrections

Precision measurements of the strong coupling constant α_S from hadronic event shapes require a solid understanding of hadronization effects. During the past years the approach of trying to deduce as much information as possible about hadronization from perturbation theory has been intensively pursued [66–68,70,72–74,76,194,195,247,248]. When trying, however, to extend the standard perturbation expansion in powers of the strong coupling, one realizes that in high orders the coefficients of the power series start to grow factorially and, hence, the series does not converge (see for instance Refs. [73,249,250]). At low scales, which one has to deal with in the context of hadronization, this is connected to the *infrared renormalon* divergence (see, e.g. Refs. [251,252]) that arises in the calculation of a propagating gluon with many successive insertions of virtual quark–antiquark loops as is depicted in Fig. 46. Thus, any perturbative treatment of hadronization effects has to somehow account for the renormalon divergence. By perturbative factorization it is possible to separate effects which are characterized by large energy scales from those of small scales up to inverse powers of the energy scale. This corresponds to the result, already obtained from the simple tube model described in Section 3.2.4, that hadronization effects induce corrections which are suppressed by reciprocal powers of the hard interaction energy scale $Q \equiv \sqrt{s}$. In general, one expects for a perturbatively calculable (PT) observable, which is safe against collinear and infrared gluon radiation (see Section 3.1.2), deviations of the type [249]

$$\frac{\mathrm{d}\sigma^{\mathrm{NP}}}{\sigma} \sim \frac{\ln^q Q}{Q^p} \tag{129}$$

owing to non-perturbative (NP) effects from the physics of confinement. What can be inferred from perturbation calculations are the powers p and q.

In principle, one may regard hadronization as being governed by soft gluons as is suggested by the success of LPHD and MLLA. The contribution from these gluons is given by the size of the strong

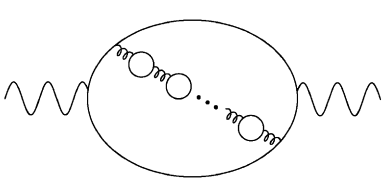

Fig. 46. Graph related to an infrared renormalon. Figure taken from Ref. [247].

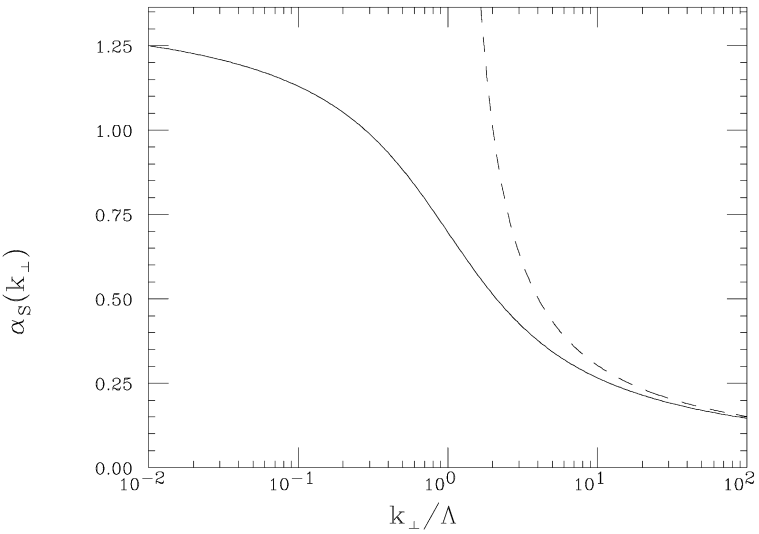

Fig. 47. Strong coupling at low energy scales: The scale dependence of the perturbative expression for α_s which has a pole at $k_\perp^2 = \Lambda^2$ is shown by the dashed line. The solid line represents a possible infrared-finite behaviour of the strong coupling at low scales. Figure adapted from Ref. [250].

coupling at a low energy scale, which is usually the transverse momentum $k_\perp$ of the soft gluon with respect to the radiating parton. At such a low energy scale the strong coupling is supposed to be large. From the explicit perturbative expression, Eq. (22), one may read off that a pole is encountered when the energy scale approaches the QCD parameter Λ. It is known as the Landau pole [24]. The divergence of the coupling α_s close to $k_\perp^2 = \Lambda^2$ is shown by the dashed line in Fig. 47. On general grounds, the coupling is expected to be free of poles for $k_\perp^2 > 0$ if it is related to physical observables. Several explicit models were proposed which modify the scale dependence of the coupling to cancel the Landau pole by the inclusion of non-perturbative contributions at low $k_\perp^2$ [253–255].

Instead of detailing these approaches in the following, a method yielding analyticity of the coupling will be briefly introduced. It has been applied successfully to predict non-perturbative corrections to event shape observables (for further details see Ref. [71]). Its basic concept, in order to remove the Landau pole, is to introduce a gluon mass, which is not a physical mass,[19] but is related to the virtual states of the gluon consisting of various parton configurations, like $q\bar{q}$, GG, etc. These virtual states, appearing when renormalizing the gluon field, can be represented by a *virtual mass m* via the dispersion relation

$$\alpha_s(Q^2) = \int_0^\infty \frac{Q^2\,\mathrm{d}m^2}{(m^2+Q^2)^2}\alpha_{\mathrm{eff}}(m^2), \tag{130}$$

[19] A gluon mass would spoil the renormalizability of the theory.

where $\alpha_{\rm eff}$ is an effective coupling constant whose definition is inspired by equivalent relations of an Abelian theory like, for instance, QED. It should be regarded as a continuation of the physical perturbative coupling, α_S, into the non-perturbative domain.

Calculations based on the dispersion relation usually split the coupling constant into a perturbative (PT) and a non-perturbative part (NP), formally,

$$\alpha_S(k_\perp^2) = \alpha_S^{\rm PT}(k_\perp^2) + \alpha_S^{\rm NP}(k_\perp^2). \tag{131}$$

When substituting $\alpha_S(k_\perp^2)$ according to this relation in the calculation of an observable, the PT part is connected to a perturbative expansion in powers of $\alpha_S(Q^2)$. The NP contribution is related to the non-perturbative component of the effective coupling, $\delta\alpha_{\rm eff}$, which is to be calculated from $\alpha_{\rm eff}$ using the dispersion relation Eq. (130). It is supposed to vanish in the regime of large momentum transfer such that for some arbitrary finite value μ_I one has $\alpha_S^{\rm NP}(k_\perp^2) \approx 0$ for $k_\perp^2 > \mu_I^2$. Hence, integrals of the type

$$\int_0^\infty \frac{{\rm d}k_\perp^2}{k_\perp^2}\alpha_S^{\rm NP}(k_\perp^2)(k_\perp)^p \approx \int_0^{\mu_I} \frac{{\rm d}k_\perp^2}{k_\perp^2}\alpha_S^{\rm NP}(k_\perp^2)(k_\perp)^p$$

are convergent and will determine the $1/Q^p$ suppressed non-perturbative contribution to collinear and infrared safe observables. For instance, the $p = 1$ correction obtained for the mean values of most event shapes is [71,249]

$$\begin{aligned}\langle \mathscr{F} \rangle^{\rm NP} &= \frac{a_{\mathscr{F}}}{Q}\frac{C_F}{2\pi}\int_0^\infty \frac{{\rm d}m^2}{m^2}\sqrt{m}\,\delta\alpha_{\rm eff}(m^2)\\ &= \frac{a_{\mathscr{F}}}{Q}\frac{2C_F}{\pi^2}\int_0^\infty {\rm d}k_\perp\,\alpha_S^{\rm NP}(k_\perp^2)\\ &= \frac{a_{\mathscr{F}}}{Q}\frac{2C_F}{\pi^2}\int_0^{\mu_I} {\rm d}k_\perp\,\alpha_S^{\rm NP}(k_\perp^2) + \mathcal{O}\left(\frac{\mu_I}{Q}\alpha_S^{\rm NP}\right),\end{aligned} \tag{132}$$

where $a_{\mathscr{F}}$ is a calculable number depending on the observable. If $\alpha_S^{\rm NP}$ from Eq. (131) is used for substitution, one can express the NP coupling by α_S and $\alpha_S^{\rm PT}$, according to

$$\int_0^{\mu_I} {\rm d}k_\perp\,\alpha_S^{\rm NP}(k_\perp^2) = \int_0^{\mu_I} {\rm d}k_\perp\,\alpha_S(k_\perp^2) - \int_0^{\mu_I} {\rm d}k_\perp\,\alpha_S^{\rm PT}(k_\perp^2). \tag{133}$$

The integral over α_S quantifies the strength of the strong interaction in the region $k_\perp^2 < \mu_I^2$. Its value is not perturbatively calculable at such low scales. One, therefore, introduces a non-perturbative quantity

$$\alpha_{p-1}(\mu_I) \equiv \frac{p}{\mu_I^p}\int_0^{\mu_I} {\rm d}k_\perp\,\alpha_S(k_\perp^2)k_\perp^{p-1}, \tag{134}$$

which, in general, depends on the power p of the non-perturbative correction. An important property of the difference in Eq. (133) should be noted. Both, α_S and $\alpha_S^{\rm PT}$ have the same factorial divergence in high orders which cancel in the difference such that the term on the left-hand side has, in fact, no renormalon embedded.

Table 9
Coefficients of the perturbative prediction [32,115,198,256] and the coefficients of the power correction of various event shapes [72,73]. In the case of the jet broadenings B_T and B_W the leading power correction is enhanced by additional factors [249,257], see text. The coefficient a_{y_3} for the DURHAM 3-jet flip parameter y_3 is unknown, but the leading power correction is logarithmically enhanced [71]

Observable $\mathscr{F}$	$A_{\mathscr{F}}$	$B_{\mathscr{F}}$	$a_{\mathscr{F}}$	p	enhanced $1/Q^p$
$\langle 1-T\rangle$	2.103	44.99	2	1	—
$\langle C\rangle$	8.638	146.8	3π	1	—
$\langle M_H^2/s\rangle$	2.103	23.24	1	1	—
$\langle B_T\rangle$	4.066	64.24	1	1	$\mathcal{O}(1/\sqrt{\alpha_S})$
$\langle B_W\rangle$	4.066	−9.53	1/2	1	$\mathcal{O}(1/\sqrt{\alpha_S})$
$\langle y_3\rangle$	0.895	12.68		2	$\ln Q$

Performing the expansion of α_S^{PT} in terms of $\alpha_S(Q^2)$, one obtains from Eq. (132) the prediction for the power corrected mean of an event shape observable $\mathscr{F}$

$$\langle\mathscr{F}\rangle = \langle\mathscr{F}\rangle^{PT} + \langle\mathscr{F}\rangle^{NP} = \left[A_{\mathscr{F}}\left(\frac{\alpha_S}{2\pi}\right) + (B_{\mathscr{F}} - 2A_{\mathscr{F}})\left(\frac{\alpha_S}{2\pi}\right)^2\right] + a_{\mathscr{F}}\mathscr{P}, \tag{135}$$

where $A_{\mathscr{F}}$, $B_{\mathscr{F}}$ and $a_{\mathscr{F}}$ are observable-dependent constants. The term in square brackets is the general perturbative expression up to second order in α_S for the mean of an observable. The coefficients $A_{\mathscr{F}}$ and $B_{\mathscr{F}}$ can be derived from the $\mathcal{O}(\alpha_S^2)$ perturbative calculations [32,115,198,256]. It should be noted that the term $-2A_{\mathscr{F}}$ accounts for the QCD corrections of the total hadronic cross-section as shown in Eq. (50) of Section 4.1.1. The $a_{\mathscr{F}}$ coefficient of the power correction $\mathscr{P}$ was determined in Refs. [72,73]. The numerical values of these coefficients are shown in Table 9.

With the exception of the DURHAM 3-jet flip parameter y_3 and the jet broadening measures, which will be discussed below, the NP parameter $\mathscr{P}$ in Eq. (135) is given for the shapes as [74,249]

$$\mathscr{P} = \frac{4C_F\mathscr{M}}{\pi^2}\frac{\mu_I}{Q}\left\{\alpha_0(\mu_I) - \left[\alpha_S(\mu_R^2) + 2\beta_0\alpha_S^2(\mu_R^2)\left(\ln\frac{\mu_R}{\mu_I} + 1 + \frac{K}{4\pi\beta_0}\right) + \cdots\right]\right\}, \tag{136}$$

where the factor

$$K \equiv C_A\left(\frac{67}{18} - \frac{\pi^2}{6}\right) - \frac{5}{9}n_f \tag{137}$$

is due to the choice of the $\overline{\text{MS}}$ scheme. The expression in square brackets of Eq. (136) stems from the expansion of the α_S^{PT} integral up to second order in α_S at some renormalization scale μ_R. In addition, there appears the *Milan* factor $\mathscr{M}$. From a two-loop analysis of the $1/Q$ correction in Refs. [72,73], its value is determined as[20] $\mathscr{M} \approx 1 + (2.437C_A - 0.052n_f)/(4\pi\beta_0) \approx 1.79$, for[21] $n_f = 3$. Large

[20] See: Note added at the end of this paper.

[21] A value of 3 flavours is natural for the parton cascading considered here since the gluon splitting into pairs of heavy quark flavours is strongly suppressed.

contributions from the next loop correction are expected such that a 20% uncertainty in the value cannot be excluded [249].

Universality of the power correction is an important issue since the concept of a finite coupling at small scales, Eq. (134), should be independent of the type of event shape observable. The coefficient $a_{\mathscr{F}}$ contains the whole dependence on the observable $\mathscr{F}$. In the above mentioned two-loop analysis the Milan factor is found to be universal for the event shapes considered in the following. Moreover, this analysis resolved the intrinsic ambiguity as to how the effects of finite masses should be included in the definition of the event shape observables. The origin of this ambiguity is the inclusive treatment of gluon decays, where the actual contribution of final-state partons is replaced by that of a massive parent gluon. The analysis also takes into account that event shapes are not completely inclusive observables.

In addition to the mean values of event shape observables, it was shown in Refs. [66,67,247] that differential distributions of the observables can also be described by power corrections using the same NP parameter $a_{\mathscr{F}}\mathscr{P}$ as in Eq. (135). In the region of small values of the observable $\mathscr{F}$, but still large compared with the ratio of the QCD parameter Λ to Q, i.e. $\mathscr{P} \gg \Lambda/Q$, the power correction shifts the perturbative spectrum,

$$\frac{\mathrm{d}\sigma}{\mathrm{d}\mathscr{F}}(\mathscr{F}) = \frac{\mathrm{d}\sigma^{\mathrm{PT}}}{\mathrm{d}\mathscr{F}} \quad (\mathscr{F} - \Delta_{\mathscr{F}}), \tag{138}$$

where the shift of the argument is

$$\Delta_{\mathscr{F}} \equiv a_{\mathscr{F}}\mathscr{P}. \tag{139}$$

An extension for $\mathscr{F} \to 0$ is possible but an additional phenomenological shape function has to be introduced [258]. The perturbative expression for the differential cross-section in Eq. (138) corresponds to the matched resummed NLLA and $\mathcal{O}(\alpha_S^2)$ calculations,[22] introduced in Section 4.1.2.

The non-perturbative prediction [73] for jet broadening had to be modified because its comparison with experiment yielded results for the non-perturbative parameter α_0 which did not support the conjecture of universality when compared with those obtained for thrust and C-parameter [259]. In brief, a shift as in Eqs. (138) and (139) was found to be insufficient to describe the data without an additional squeeze of the differential distribution. The squeeze is due to the interdependence of the perturbative and non-perturbative treatment. After being appropriately modified in Refs. [249,257], the non-perturbative contributions to be added to the PT term $\langle B\rangle^{\mathrm{PT}}$ for the mean values of the respective jet broadening observable are up to terms of $\mathcal{O}(\sqrt{\alpha_S})$

$$\begin{aligned}
\langle B_{\mathrm{T}}\rangle^{\mathrm{NP}} &\approx a_{B_{\mathrm{T}}}\mathscr{P}\left(\frac{\pi}{2\sqrt{C_F\bar{\alpha}_S[1 + K\bar{\alpha}_S/(2\pi)]}} + \frac{3}{4} - \frac{2\pi\beta_0}{3C_F} + \eta_0\right)\\
\langle B_{\mathrm{W}}\rangle^{\mathrm{NP}} &\approx a_{B_{\mathrm{W}}}\mathscr{P}\left(\frac{\pi}{2\sqrt{2C_F\bar{\alpha}_S[1 + K\bar{\alpha}_S/(2\pi)]}} + \frac{3}{4} - \frac{\pi\beta_0}{3C_F} + \eta_0\right),
\end{aligned} \tag{140}$$

[22] Although in Refs. [73,120] the resummed perturbative expression was considered, the inclusion of the fixed-order calculations does not significantly affect the shift. Therefore, for instance in Ref. [66], the ln R matched calculations were used. In fact, the power corrections are useful only in the regime where $\mathscr{F}$ is small, but still larger than $\mathscr{P}$. It is this regime where the resummed calculations are more appropriate to represent the data.

where $\bar{\alpha}_S$ is to be evaluated at the scale $\bar{Q} = Qe^{-3/4}$, K is already given in Eq. (137), and $\eta_0 \approx -0.6137$ is a constant.

The shift that has to be applied to the argument of the perturbative expression for the differential broadening distributions is rather complicated and will, therefore, not be repeated here. It can be found in Ref. [257]. For most applications the following approximations of the shifts Δ_B can be used if the study is constrained to the region of $B > 0.05$ and energy scales greater than about 35 GeV

$$\Delta_W(B_W) \approx a_{B_W} \mathscr{P}\left(\ln\frac{1}{B_W} + \eta_0\right)$$

$$\Delta_T(B_T) \approx a_{B_T} \mathscr{P}\left(\ln\frac{1}{B_T} + \eta_0 + \left\{\frac{\pi}{2\sqrt{C_F\bar{\alpha}_S[1 + K\bar{\alpha}_S/(2\pi)]}} + \frac{3}{4} - \frac{2\pi\beta_0}{3C_F} + \eta_0\right\}\right). \quad (141)$$

The more involved formula for the shift in the B_T case, although its first part is the same as that of B_W, includes an additional contribution from the hemisphere where no significant perturbative gluon contribution is present. It is given by the term in braces and is identical with the correction to the mean value. In general, the $\ln(1/B)$ enhancement of the shift leads to the squeezing of the differential distribution.

5.3.1. Application of power corrections to mean values

A huge collection of data on mean values of event shape observables covering a vast range of centre-of-mass energies is available [88,104,129–132,140,143,145,204,208,210–212,260–266], in particular for thrust and jet mass. Although the C-parameter has been known for a long time, measurements of this observable at energies below the Z pole became available only recently as is the case for the jet broadening and the DURHAM jet finder which were proposed too late for the experiments prior to LEP [139]. All such measurements constitute a broad basis for scrutinizing the theoretical concept of power suppressed corrections to the mean values of event shape observables. Such investigations have been done rather extensively [74,131,136,139,145,212,257,267–270].

Considering the most prominent observables which were already used in the previous section, viz. thrust, heavy jet mass, C-parameter, total and wide jet broadening, and the $3 \to 2$-jet flip parameter y_3 obtained from the DURHAM jet finder, one finds a dependence on the centre-of-mass energy as is shown in Fig. 48. The solid line shows the result of fits with $\alpha_S(m_Z^2)$ and α_0 as the only free parameters. A very remarkable agreement of the theoretical prediction with the data is observed. From the difference between the dashed line which shows the perturbative contribution and the solid curve, one can infer the size of the power suppressed contribution.

Since for the jet flip parameter y_3 the structure of the leading power corrections is only known to include $(\ln Q)/Q^2$ and $1/Q^2$ terms [71], but the corresponding coefficients are not yet calculated, several variations, $1/Q^2$, $(\ln Q)/Q^2$, $1/Q$, $(\ln Q)/Q$ and omitting power correction terms, were tried in Refs. [259,268], introducing an unknown coefficient a_{y_3} as an additional fit parameter. In general, none of these corrections is favoured by the χ^2/d.o.f. of the fits. When using $1/Q$-type corrections the fits yielded tiny values for a_{y_3} of less than 10^{-2} and values of $\alpha_S(m_Z^2)$ which exceed the world average by many standard deviations. Although fits employing $1/Q^2$-type corrections yielded $\alpha_S(m_Z^2) \approx 0.125$, the coefficients a_{y_3}, which came out as about -0.2 to -0.5, have very large errors rendering them compatible with zero. In conclusion, there are still insufficient data on $\langle y_3 \rangle$ to

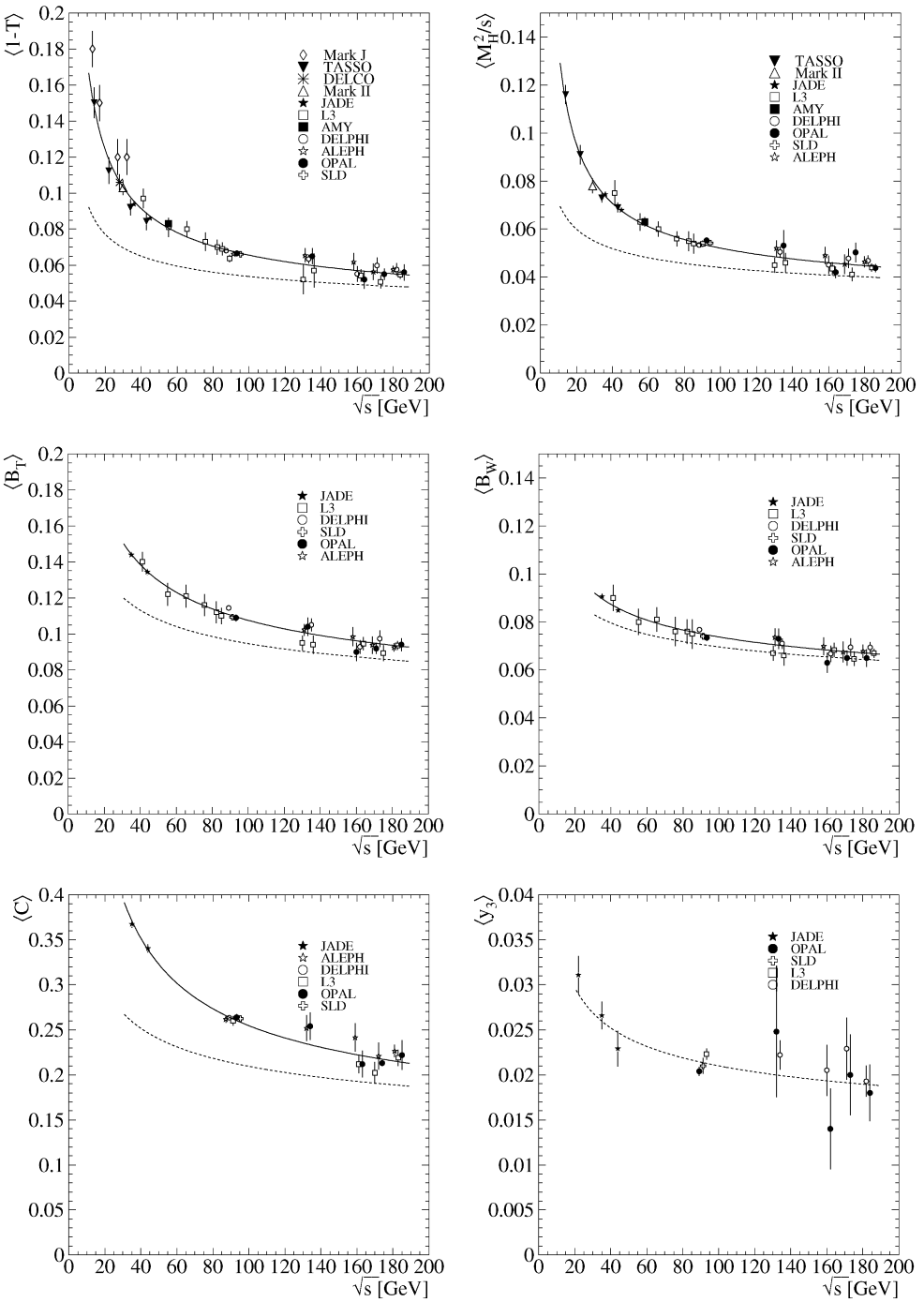

Fig. 48. The energy dependence of the mean values of thrust $\langle 1-T\rangle$, heavy jet mass $\langle M_H^2/s\rangle$, total $\langle B_T\rangle$ and wide jet broadening $\langle B_W\rangle$, C-parameter $\langle C\rangle$, and of the $3\to 2$-jet flip parameter $\langle y_3\rangle$ is shown [88,104,129–132, 139,140,143,145,204,208,210–212,260–266,271]. The solid curve is the result of the fit using perturbative calculations plus power corrections, while the dashed line indicates the contribution from the perturbative prediction only.

determine the details of the power correction for this observable. Recalling, however, that the expected leading correction is $(\ln Q)/Q^2$, a very large coefficient would be needed for a significant power correction to $\langle y_3 \rangle$. The fact that the coefficient is found to be small justifies the neglect of any power correction to the mean of the DURHAM $3 \to 2$-jet flip parameter, yielding a very stable fit with χ^2/d.o.f. of almost unity.

The individual fit results for each of the six observables considered here are summarized in Table 10. It shows the dependence of the fit values on the choice of the renormalization scale, μ_R, varied between 0.5 and 2, and on the arbitrary matching scale, μ_I, varied between 1 and 3 GeV, which enters the definition of the parameter α_0 in Eq. (134) and which marks the boundary between the non-perturbative and the perturbative regime. The dependence on unknown higher-order corrections of the Milan factor is also included. These are of the order α_S/π, where the coupling strength is to be evaluated at some small scale resulting in an estimated uncertainty of about 20%

Table 10
Fitted values of (a) $\alpha_S(m_Z^2)$ and (b) α_0 derived for $\mu_I = 2$ GeV and $x_\mu = 1$ using the $\mathcal{O}(\alpha_S^2)$ calculations and two-loop power corrections, including the Milan factor and the modified predictions for the jet broadening variables [72,73,249,257]. Statistical and systematic uncertainties are also given. Signs indicate the direction in which $\alpha_S(m_Z^2)$ and α_0 change with respect to the standard analysis. The renormalization and infrared scale uncertainties are added asymmetrically to the errors of $\alpha_S(m_Z^2)$. α_0 has error contributions from the choice of the renormalization scale and the Milan factor only

(a)	$\langle 1-T \rangle$	$\langle M_H^2/s \rangle$	$\langle B_T \rangle$	$\langle B_W \rangle$	$\langle C \rangle$	$\langle y_3 \rangle$	Average
$\alpha_S(m_Z^2)$	**0.1198**	**0.1141**	**0.1183**	**0.1190**	**0.1176**	**0.1215**	**0.1181**
Q range (GeV)	13–183	14–183	35–183	35–183	35–183	22–183	
χ^2/d.o.f.	52.2/39	22.0/33	22.1/25	18.8/26	18.8/16	13.6/13	
exp.	$\pm$ 0.0013	$\pm$ 0.0010	$\pm$ 0.0016	$\pm$ 0.0020	$\pm$ 0.0013	$\pm$ 0.0014	$\pm$ 0.0016
$x_\mu = 0.5$	− 0.0049	− 0.0026	− 0.0038	+ 0.0017	− 0.0043	− 0.0040	− 0.0028
$x_\mu = 2.0$	+ 0.0061	+ 0.0037	+ 0.0048	+ 0.0003	+ 0.0053	+ 0.0054	+ 0.0029
$\mathcal{M}$ − 20%	+ 0.0011	+ 0.0013	+ 0.0008	+ 0.0005	+ 0.0009	—	+ 0.0008
$\mathcal{M}$ + 20%	− 0.0011	− 0.0001	− 0.0007	− 0.0005	− 0.0009	—	− 0.0005
$\mu_I = 1$ GeV	+ 0.0025	+ 0.0013	+ 0.0017	+ 0.0011	+ 0.0020	—	+ 0.0014
$\mu_I = 3$ GeV	− 0.0019	− 0.0011	− 0.0014	− 0.0009	− 0.0016	—	− 0.0012
Total error	+ 0.0068	+ 0.0043	+ 0.0054	+ 0.0029	+ 0.0058	+ 0.0056	+ 0.0037
	− 0.0055	− 0.0030	− 0.0044	− 0.0022	− 0.0049	− 0.0042	− 0.0035

(b)	$\langle 1-T \rangle$	$\langle M_H^2/s \rangle$	$\langle B_T \rangle$	$\langle B_W \rangle$	$\langle C \rangle$	$\langle y_3 \rangle$	Average
α_0	**0.509**	**0.614**	**0.442**	**0.392**	**0.451**	—	**0.473**
exp.	$\pm$ 0.012	$\pm$ 0.018	$\pm$ 0.015	$\pm$ 0.028	$\pm$ 0.010	—	$\pm$ 0.014
$x_\mu = 0.5$	+ 0.003	+ 0.011	+ 0.020	+ 0.109	+ 0.005	—	+ 0.018
$x_\mu = 2.0$	− 0.002	− 0.005	− 0.014	− 0.042	− 0.003	—	− 0.009
$\mathcal{M}$ − 20%	+ 0.058	+ 0.084	+ 0.046	+ 0.032	+ 0.050	—	+ 0.053
$\mathcal{M}$ + 20%	− 0.040	− 0.064	− 0.031	− 0.022	− 0.034	—	− 0.037
Total error	+ 0.059	+ 0.087	+ 0.052	+ 0.117	+ 0.051	—	+ 0.058
	− 0.042	− 0.067	− 0.037	− 0.055	− 0.036		− 0.041

for $\mathscr{M}$, according to Refs. [73,249]. All fits obtained χ^2/d.o.f. close to unity. A large anticorrelation of over 90% is observed in all fits. The individual results agree well within the correlated errors. To form a weighted average of the $\alpha_S(m_Z^2)$ results, taking into account the correlations, the procedure of Ref. [104] which has already been detailed in Section 4.1.1 is applied again. The average $\alpha_S(m_Z^2)$ is in very good agreement with other α_S determinations, quoted in this article, and also with the world average $\alpha_S(m_Z^2) = 0.119 \pm 0.004$ [272].

Similarly, a fair agreement is found between the values of the non-perturbative parameter α_0, which is regarded as universal parameter in the theory calculations. Although the value from B_W is a little low, and that from M_H^2/s somewhat high, all values agree within about 20%. In the table the result of averaging these values is shown using the same procedure as for the strong coupling. The quoted error is determined from the combined experimental, renormalization scale, and Milan factor uncertainties only. It therefore does not consider the much larger spread of the individual α_0 values. This could be accounted for by quadratically adding the r.m.s. of the five single results, which is 0.076, to the quoted error. These results, in general, support the dispersion method to calculate power suppressed contributions to mean values of event shape observables. The conjecture of universality of the power correction, which was argued for in Refs. [66–68,70–73,195,247–249,257], is roughly confirmed by the data.

Moreover, there is also remarkable agreement of the measured values of α_0 with the value obtained from explicitly calculating the integral in Eq. (134) using an 'analytically-improved' running coupling (see for instance Ref. [254]). The improvement concerns the cancellation of the Landau pole by adding to the explicit formula of α_S a 'counter term' of the form $\Lambda^2/(\Lambda^2 - Q^2)$ depending only on the QCD parameter Λ and the energy scale Q. No additional parameters are required. After adjusting Λ to reproduce the value of the strong coupling constant measured at the τ mass scale, the integration in Eq. (134) yielded the prediction $\alpha_0(2\,\mathrm{GeV}) \approx 0.46$ [254] in good agreement with the measured value.

General properties of power suppressed corrections to mean values of event shapes were studied in Refs. [131,145,267], allowing also for different integer and half-integer powers of the reciprocal energy scale Q. In particular, the power parameter p of a c/Q^p correction term was found in the case of the thrust variable to be $p = 0.92 \pm 0.19$ from a simultaneous fit of p, α_S and the constant c that determines the size of the non-perturbative correction [267]. No indication of higher-order power corrections was observed for thrust given the present precision of the data.

In Ref. [131] the DELPHI collaboration investigated power corrections to different observables shown in Fig. 49. Among them were the 3-jet rates, R_3, at fixed values of $y_{cut} = 0.08$ and 0.04 for the JADE and DURHAM algorithms, respectively. Allowing for corrections of the order $1/Q$ and $1/Q^2$ satisfactory fits were obtained for both quantities as shown in plot (a) of the figure. While for the JADE case a significant negative $1/Q$ correction is found, the DURHAM data yielded a $1/Q$ contribution consistent with zero within the errors. This agrees with the expectation mentioned above that the leading correction in the DURHAM case is of the order $(\ln Q)/Q^2$.

Observables are expected to lack significant $1/Q$ corrections if the regions dominated by 2-jet events are excluded from the mean value. Such truncated mean values are shown in Fig. 49(b) for thrust ($T < 0.8$), heavy jet mass ($M_H^2/s > 0.1$) and the energy–energy correlation EEC (see Ref. [140], $|\cos\psi| < 0.5$). Fixing the value of α_S in order to obtain satisfactory fits, the power correction to the heavy jet mass was found to be predominantly of order $1/Q^2$ as predicted [70], while both thrust and EEC require considerable $1/Q$ corrections.

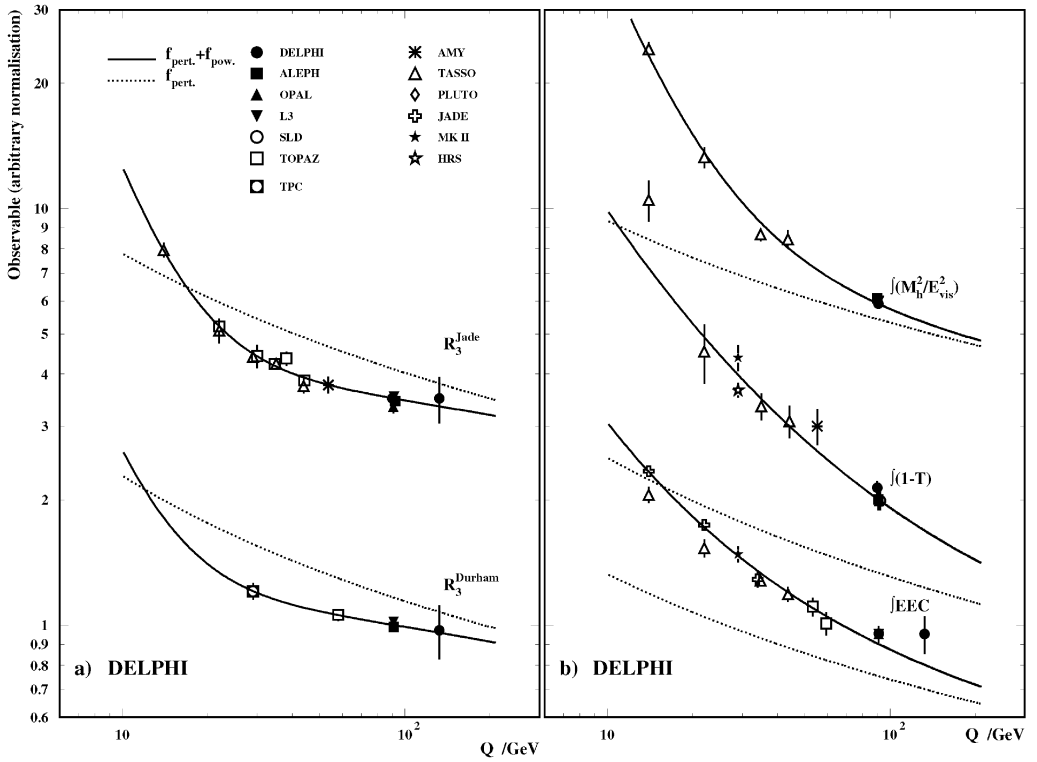

Fig. 49. (a) Energy dependence of the 3-jet rates, R_3, from the JADE and the DURHAM jet finders, and (b) of the truncated mean values of thrust (< 0.8), heavy jet mass (> 0.1), and energy–energy correlation EEC, ($|\cos\psi| < 0.5$). Results of fits of the perturbative calculations plus terms proportional to $1/Q$ and $1/Q^2$, considering the coefficients and α_S as parameters of the fits, are overlaid as solid curves. The bare perturbative contribution is represented by the dotted lines. Figure taken from Ref. [131].

Even higher moments of the event shape distributions have been invoked to determine the coupling strength. The non-perturbative contribution to the nth moment of an event shape distribution is found to be of the order $1/Q^n$, which leads one to expect a significant suppression of non-perturbative effects here. In fact, if one considers both the perturbative and non-perturbative contribution to the nth moment of an event shape, one finds the leading power correction to be of the order $\alpha_S A/Q$, i.e. suppressed by an additional factor of $\alpha_S(Q^2)$ only [249]. Considering combinations of such moments, one may indeed construct observables in which the leading power corrections cancel. For instance such a cancellation was shown in Ref. [273] for the *thrust variance*

$$\sigma_{1-T}^2 = \langle(1-T)^2\rangle - \langle 1-T\rangle^2 \approx 0.030\alpha_S + 0.037\alpha_S^2 . \tag{142}$$

It has not yet been experimentally investigated. The measurement of the thrust variance will be difficult because its size is tiny. Systematic uncertainties may, therefore, eventually render the measurement impossible if they are not well under control.

The situation is more promising for the C-parameter whose variance should not have any leading power correction. The perturbative prediction is

$$\sigma_C^2 = \langle C^2 \rangle - \langle C \rangle^2 \approx 0.387\alpha_s + 0.0435\alpha_s^2, \tag{143}$$

which has a quite small second-order contribution. This prediction was derived from the results of a numerical integration of the full second-order matrix element for the moments of many event shape observables [274] using the program of Ref. [198]. Calculating the C-parameter variance from the high precision LEP I and SLC data [140,262,265] only and estimating the uncertainties using error propagation yields

$$\text{DELPHI: } \langle C^2 \rangle - \langle C \rangle^2 = 0.0331 \pm 0.0025 \text{ (stat.)} \pm 0.0106 \text{ (syst.)},$$

$$\text{L3: } \langle C^2 \rangle - \langle C \rangle^2 = 0.0359 \pm 0.0016 \text{ (stat.)} \pm 0.0145 \text{ (syst.)},$$

$$\text{SLD: } \langle C^2 \rangle - \langle C \rangle^2 = 0.0340 \pm 0.0046 \text{ (stat.)} \pm 0.0084 \text{ (syst.)},$$

$$\text{average: } \langle C^2 \rangle - \langle C \rangle^2 = 0.0341 \pm 0.0013 \text{ (stat.)} \pm 0.0104 \text{ (syst.)},$$

where the weighted average and its systematic uncertainty are calculated using the total errors for the weights while the statistical error is assumed to be uncorrelated. Using the weighted average and solving Eq. (143) for $\alpha_s(m_Z^2)$ one obtains

$$\alpha_s(m_Z^2) = 0.087 \pm 0.003 \text{ (stat.)} \pm 0.026 \text{ (syst.)} \pm 0.007 \text{ (scale.)},$$

where the uncertainty due to the choice of the scale is estimated by changing x_μ from unity to 0.5 and 2. Although the total error is large, the central value is rather small compared with other determinations possibly indicating larger contributions from missing higher-order terms in α_s or from power corrections.

5.3.2. Power corrections to differential distributions

The investigation of power corrections to differential distributions of event shape observables has only just begun. A few such studies have been done up to now [136,257,259,267] which are based on the general concept presented in Ref. [66], extended to next-to-leading order accuracy and other event shape observables in Refs. [72,73]. The next-to-leading order treatment of the power corrections changed the shape dependent coefficients $a_{\mathcal{F}}$ and, finally, yielded the values shown in Table 9.

Fig. 50 shows results of the application of the power corrections to differential distributions of the thrust and the C-parameter observables. A good description of the distributions is found by applying the predicted shift to the matched fixed order and resummed calculation. Only at very small centre-of-mass energies is the agreement between data and expectation moderate. Since neither the perturbative nor the non-perturbative calculations applied in the fit accounts for finite quark masses, one may expect mass effects to modify the distributions in the proximity of the bottom quark production threshold.

The numerical values of $\alpha_s(m_Z^2)$ and α_0 are summarized in Table 11. It has to be recalled that the fit parameters $\alpha_s(m_Z^2)$ and α_0 are strongly anti-correlated (60–84%), as is illustrated in Fig. 51. The results shown were obtained by the ALEPH collaboration considering only data from the ALEPH experiment. Therefore, a detailed treatment of the correlation between the data at different energies

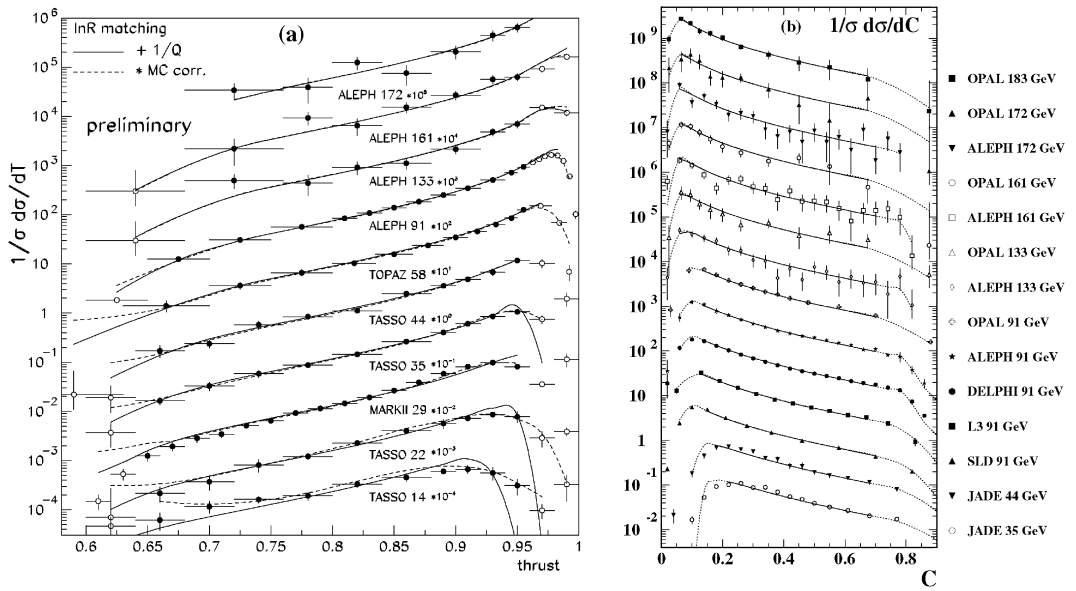

Fig. 50. (a) Thrust and (b) C-parameter distributions, measured at different centre-of-mass energies $\sqrt{s} \equiv Q$ and corrected for detector effects, are shown vertically displaced. Overlaid as a solid curve is the result of a fit of each of the observables simultaneously for all energies using matched $\mathcal{O}(\alpha_s^2)$ and resummed NLLA calculations complemented by power corrections. The dashed line in (a) shows the result of a corresponding fit applying corrections from the JETSET Monte Carlo. The dotted line in (b) is the extrapolated fit result. Figures taken from Refs. [259,267].

was possible. The figure shows the results obtained from both the differential thrust and C-parameter distributions. The impact of each systematic variation is indicated. Combining the values of Refs. [136,259] yields

$$\alpha_s(m_Z^2) = 0.1150 \pm 0.0036\,,$$

$$\alpha_0(2\,\mathrm{GeV}) = 0.464 \pm 0.067\,. \tag{144}$$

These values are in good agreement with the world average of $\alpha_s = 0.119 \pm 0.004$ [272] and with the average values obtained from the fits to the mean values of the event shapes, respectively.

Table 11 also lists the results obtained from similar fits to the differential heavy jet mass and total jet broadening distributions, respectively. Further results on the broadening observables are available [136] but not listed because they were obtained using the older prediction for the power correction which neglected the interplay between perturbative and non-perturbative contributions (see Ref. [249]). Fig. 52 shows the result of the fit to the total jet broadening based on the new prediction at two distinct centre-of-mass energies. Numerical results of this fit are also listed in Table 11.

Considering the results of the fits to the differential distributions of single event shape observables, shown in Table 11, one finds the overall concept of power corrections to be confirmed. The results on α_s are all compatible with the world average, even though some of them tend to be small. For the non-perturbative parameter α_0 it has to be noted that the values agree very well with the

Table 11
Fitted values of $\alpha_s(m_Z^2)$ and α_0 for $x_\mu = 1$ using the ln R-matched $\mathcal{O}(\alpha_s^2)$ and resummed NLLA calculations completed with the 2-loop power corrections, including the Milan factor and the modification of the prediction for the jet broadening variables [72,73,249,257] to describe the differential distributions. The errors correspond to the total uncertainties except for the values marked with an asterisk (*) where only the fit uncertainty is given in the references

		$(1/\sigma)(\mathrm{d}\sigma/\mathrm{d}(1-T))$				
Ref.	$\sqrt{s}$ range	$\alpha_s(m_Z^2)$		$\alpha_0(2\ \mathrm{GeV})$		χ^2/d.o.f.
[136]	91–183	0.1185	± 0.0064	0.449	± 0.082	140/42
[259]	35–183	0.1156	$^{+0.0066}_{-0.0049}$	0.469	$^{+0.077}_{-0.060}$	284/277

		$(1/\sigma)(\mathrm{d}\sigma/\mathrm{d}C)$				
Ref.	$\sqrt{s}$ range	$\alpha_s(m_Z^2)$		$\alpha_0(2\ \mathrm{GeV})$		χ^2/d.o.f.
[136]	91–183	0.1145	± 0.0043	0.443	± 0.060	30/36
[259]	35–183	0.1137	$^{+0.0058}_{-0.0044}$	0.437	$^{+0.081}_{-0.049}$	163/170

		$(1/\sigma)(\mathrm{d}\sigma/\mathrm{d}M_H)$				
Ref.	$\sqrt{s}$ range	$\alpha_s(m_Z^2)$		$\alpha_0(2\ \mathrm{GeV})$		χ^2/d.o.f.
[136]	91–183	0.1157	± 0.0039	0.437	± 0.003*	2.1

		$(1/\sigma)(\mathrm{d}\sigma/\mathrm{d}B_T)$				
Ref.	$\sqrt{s}$ range	$\alpha_s(m_Z^2)$		$\alpha_0(2\ \mathrm{GeV})$		χ^2/d.o.f.
[257]	35–183	0.1140	± 0.0007*	0.514	± 0.007*	61/57
[259]	35–183	0.1125	$^{+0.0082}_{-0.0061}$	0.562	$^{+0.099}_{-0.071}$	161/171

results obtained from fits to the mean values of event shape observables in the previous section. This gives further support for the conjecture of α_0 being a universal non-perturbative parameter.

5.3.3. Summary of power corrections

In general, a remarkable ability of power corrections to describe non-perturbative hadronization effects is found. This holds for the mean values as well as for the differential distributions. Moreover, the power corrections are also applicable to other processes besides e^+e^- annihilation. In the analysis of deep inelastic scattering of positrons off protons at the HERA collider at DESY, for instance, power corrections were also found to be a good description of non-perturbative

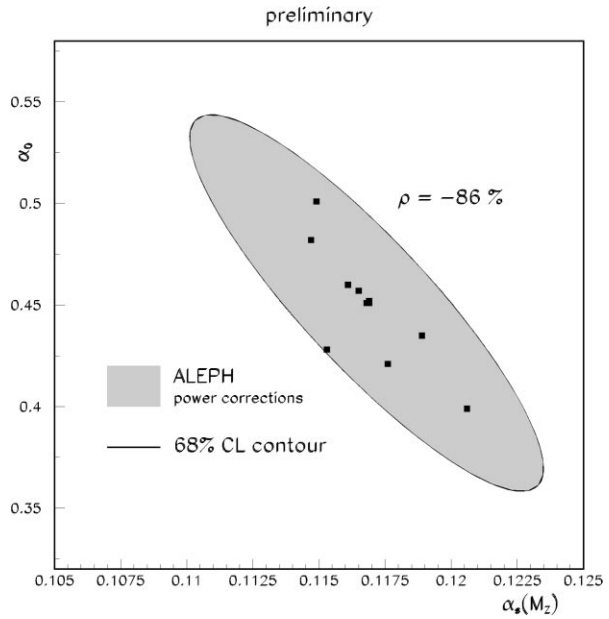

Fig. 51. The correlation contour of $\alpha_S(m_Z^2)$ and α_0 obtained from combined fits to thrust and C-parameter distributions is shown at the 68% confidence level. For its calculation statistical and systematic errors were considered. The points indicate the individual results from systematic variations of the analysis. Figure taken from Ref. [136].

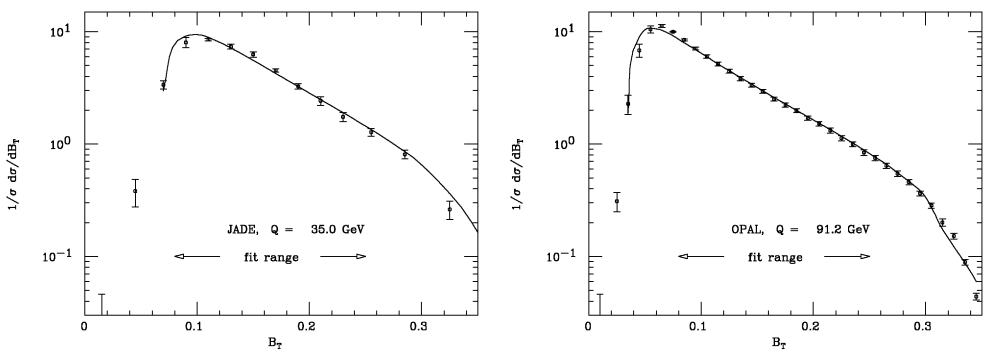

Fig. 52. Total jet broadening distributions at 35 and 91 GeV are shown. The curves are from fits of the ln R-matched perturbative calculations and the modified prediction for the power correction to the differential B_T distribution. The data sets considered for the fit ranged from 35 to 183 GeV in centre-of-mass energy. Figures taken from Ref. [257].

contributions to the mean values of event shapes (see summary in Refs. [83,275,276]), yielding results consistent with those presented in the previous sections (see Fig. 53).

Although the success of power corrections might be surprising, their ability to describe non-perturbative effects could have been expected from the successes of the hypothesis of local parton–hadron duality (LPHD). In this respect, it is another indication that the strong interaction physics at very low energy scales is governed by soft gluons. As for the LPHD approach, power corrections cannot resolve the process of hadronization, but it increases the confidence that one

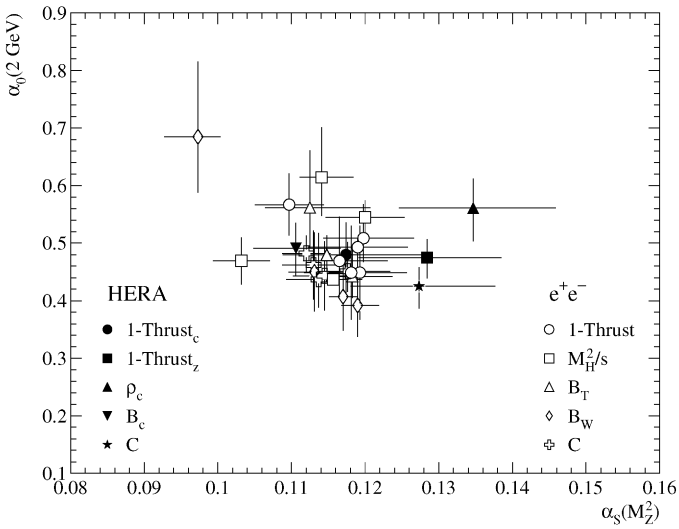

Fig. 53. Compilation of various results on $\alpha_S(m_Z^2)$ shown versus the corresponding $\alpha_0(2\ \mathrm{GeV})$. The values have been obtained from e^+e^- annihilation using different event shape observables and also from deep inelastic scattering of positrons off protons [136,139,259,277].

may consider quarks and gluons for a perturbative treatment even at very small energy scales, close to the stage of confinement [249,275].

6. Studies related to the running of α_S

The results presented in the previous sections clearly show that the coupling strength of the strong interaction is dependent on the energy scale. Although the precision of the tests has improved considerably owing to improved and extended calculations and owing to new experiments at high energy colliders, details of the running are still unclear. Some aspects of possible deviations from and extensions to the standard $SU(3)$ QCD structure will be briefly addressed in this section. As a starting point, however, the exclusive validity of QCD will be assumed, thus allowing conclusions to be drawn concerning unknown higher-order corrections.

6.1. Higher-order corrections from energy dependence

Higher-order corrections are a major source contributing to the overall uncertainty of every determination of the strong coupling constant α_S, in particular from quantities that are not completely inclusive as was shown in Section 4. The effort of calculating the next-to-next-to-leading order corrections (NNLO) to such observables like jet rates and event shapes has just started (see Refs. [35,37]) and will very likely require many years until completion. And, in view of the renormalons as being connected with the factorial divergence of the coefficients of a high-order Taylor expansion as discussed in Section 5.3, one might even argue that the next order of the series will not yield improved predictions.

Other approaches might achieve useful results earlier, although they may be affected by intrinsic uncertainties. One such approach is related to the *Padé approximants* $[L/M]$ (see Ref. [278] for an introduction) which expresses a Taylor series $S(x)$ up to x^N by the ratio of an Lth and an Mth order polynomial. These two polynomials are chosen such that $L + M = N$ and that $S(x) = [L/M]$ modulo terms of the order x^{N+1}. In detail this means that

$$S(x) = c_0 + c_1 x + c_2 x^2 + \cdots + c_N x^N + \mathcal{O}(x^{N+1}) \tag{145}$$

is expressed by

$$\begin{aligned}[L/M] &\equiv \frac{a_0 + a_1 x + \cdots + a_L x^L}{1 + b_1 x + \cdots + b_M x^M} + \mathcal{O}(x^{N+1}) \\ &= c_0 + c_1 x + c_2 x^2 + \cdots + c_N x^N + \tilde{c}_{N+1} x^{N+1} + \cdots . \end{aligned} \tag{146}$$

The Padé approximant is formally a valid representation of $S(x)$ at a given finite order in x. Moreover, the Padé approximants possess useful properties which are absent in the simple Taylor series of $S(x)$. For instance, the coefficient $\tilde{c}_{N+1}$ of the Taylor expansion of $[L/M]$, which is usually called *Padé Approximant Prediction* (PAP), can provide a good estimate of the c_{N+1} coefficient of the Taylor series of $S(x)$. The relative deviation of the estimate from c_{N+1} decreases exponentially with N [278].

It seems obvious to apply the PAP to second-order perturbation series which are available for most observables. In Refs. [278,279] this was done for the 4-loop coefficient, β_3, of the β-function in Eq. (21), among other quantities. Once the exact result became available, it was realized that the quartic gluon vertices, which start to contribute at this order, were not predicted by simple PAP. A modification was required to retrieve the exact β_3 coefficient with better than 1% accuracy. This indicates a basic deficiency of the approach due to its purely mathematical nature. Anyhow, it should be recalled, that no further gluon vertices are expected to contribute beyond that order, and, hence, PAP might indeed yield satisfactory results.

Padé approximant predictions were also employed for the determination of α_S. In Ref. [280] the hadronic branching ratio of the τ lepton, R_τ, was investigated (see Section 4.1.1), to attempt to estimate the next term of the slow converging perturbative series in Eq. (59) from PAP. The inclusion of the Padé approximant term lowered the value of $\alpha_S^2(m_\tau^2)$ by about 10% [280].

In Ref. [281] the α_S determination from hadronic event shape observables was studied using the *Padé approximant predictions*. In total 15 observables were considered to determine the $\mathcal{O}(\alpha_S^3)$ term from the exact $\mathcal{O}(\alpha_S^2)$ prediction. The extended series was then fitted to SLD data to determine $\alpha_S(m_Z^2)$, finding for a fixed renormalization scale factor $x_\mu \equiv 1$ a reduced scatter of the individual results about their common mean value. A similar study by the DELPHI collaboration [146] using 17 observables yielded $\alpha_S(m_Z^2) = 0.1168 \pm 0.0054$ where the error includes statistical and systematic uncertainties as well as uncertainties due to the scale choice. Although these results look promising, they can only be verified upon completion of the full $\mathcal{O}(\alpha_S^3)$ perturbative QCD calculation.

A completely distinct approach exploits the wealth of data available at very different centre-of-mass energies [270]. It makes use of the fact that the basic structure of the perturbative expression for an event shape observable like thrust, appropriately normalized, is known to be

$$R(Q) = \frac{\alpha_S}{\pi} + r_1 \frac{\alpha_S^2}{\pi^2} + r_2 \frac{\alpha_S^3}{\pi^3} + \cdots + \frac{\lambda}{Q}\left(1 + \lambda_1 \frac{\alpha_S}{\pi} + \cdots\right), \tag{147}$$

which includes simplified power corrections that have already been introduced in Section 5.3.[23]

Using the large range of energies available, one can avoid the renormalization scale uncertainty entirely by taking the derivative of $R(Q)$ with respect to $\ln Q$, which can be written as [270]

$$\frac{\mathrm{d}R}{\mathrm{d}\ln Q} = -2\pi R^2(\beta_0 + \pi\beta_1 R + \beta_0\rho_2 R^2 + \cdots) + K_0 R^{-\beta_1/(2\beta_0)} \mathrm{e}^{-1/(2\pi\beta_0 R)} \cdot (1 + K_1 R + \cdots)$$

$$\equiv -2\pi\beta_0\rho(R) \tag{148}$$

where

$$\rho_2 = r_2 + \frac{\pi^2\beta_2}{\beta_0} - \frac{\pi\beta_1}{\beta_0} r_1 - r_1^2 .$$

Here, β_0, β_1 and β_2 are the coefficients from the renormalization group equation (21), ρ_2 depends on the NNLO coefficient r_2, which is unknown, and K_0, in combination with $\Lambda_{\overline{\mathrm{MS}}}$, is directly connected with λ.

One may fit Eq. (148) to the observables $R(Q)$ and $\mathrm{d}R/\mathrm{d}\ln Q$, both of which can be determined from the data, in order to determine the unknowns, r_2 and K_0. In fact, in Ref. [270] Eq. (148) was integrated exploiting asymptotic freedom, that is $R(Q) \to 0$ as $Q \to \infty$, leaving, in principle, $\Lambda_{\overline{\mathrm{MS}}}$ as the constant of integration. Fig. 54 shows the results of three (ρ_2, λ, $\Lambda_{\overline{\mathrm{MS}}}$) and one parameter ($\Lambda_{\overline{\mathrm{MS}}}$) fits to the mean value of the thrust observable over a large range of centre-of-mass energies from 14 to 172 GeV. When fitting with ρ_2 and λ fixed to zero, $\Lambda_{\overline{\mathrm{MS}}} = 266$ MeV with $\chi^2/\mathrm{d.o.f.} = 82/32$ was found in Ref. [270] for 5 flavours. For the three parameter fit, however, the minimum was reached with $\chi^2/\mathrm{d.o.f.} = 40/30$ for $\Lambda_{\overline{\mathrm{MS}}} = 245^{+20}_{-17}$ MeV, $\rho_2 = -16 \mp 11$, and $\lambda = 0.27^{+0.12}_{-0.10}$ GeV. This corresponds to $\alpha_s(m_Z^2) = 0.1194 \pm 0.0014$ when using the 2-loop relation between $\Lambda_{\overline{\mathrm{MS}}}$ and α_s. The value of ρ_2 yields $r_2 = 89 \pm 11$ which comes out rather large compared with $r_1 \approx 9.7$, due to the contribution $r_1^2 + cr_1$ in Eq. (148). Moreover, the value of λ is rather small compared with the results obtained in Section 5.3, which would suggest a value of about 1 GeV. This difference is due to the third-order contribution, ρ_2, which is determined from the fit, and the neglect of higher-order terms when transforming K_0 into a value of λ [285]. Since ρ_2 absorbs a significant fraction of the power corrections, there is a strong anticorrelation between ρ_2 and λ, which is the reason for the large relative fit errors for ρ_2 and λ.

In general, exploiting the known structure of the unknown next order of a perturbative series together with the available data over a vast energy region is a promising approach to constrain the value of the higher-order coefficients until the completion of the exact calculation. The approach should be applicable also to other observables, and maybe even to differential distributions. This method's very appealing feature is that the large uncertainties due to the choice of the renormalization scale, which are usually attributed to unknown higher-order corrections, no longer appear. In fact, a part of these higher-order corrections is calculable and resummable to all orders

[23] The value of $r_1 = (B_T - 2A_T)/(2A_T) \approx 9.7$ can be determined from Table 9.

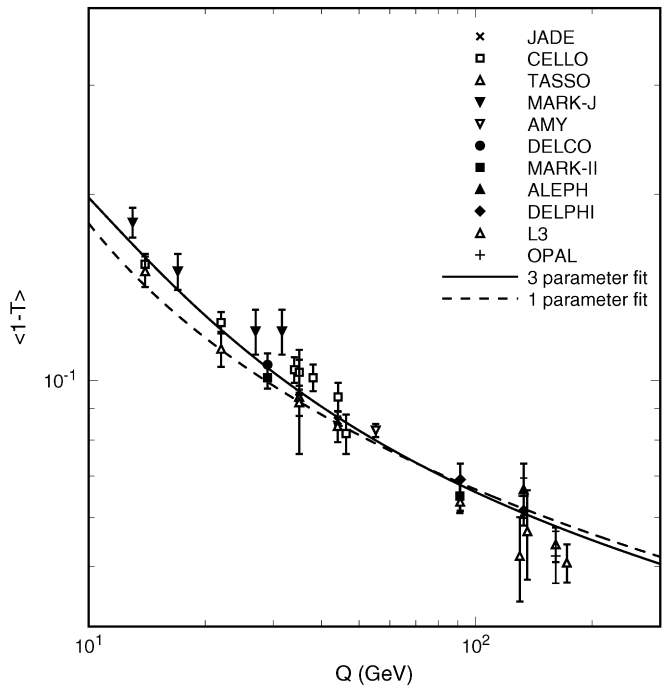

Fig. 54. The energy dependence of the data on $\langle 1 - T \rangle$ [129–132,139,143,145,204,208,210,212,260,262–264,266,282–284] is shown. Overlaid are the fit results for a three parameter fit (see text) using $\Lambda_{\overline{\rm MS}}$, ρ_2, and λ as parameters (solid line), and for a one parameter fit with $\rho_2 = 0$ and $\lambda = 0$ fixed (dashed). Figure taken from Ref. [270].

[286]. Once the resummation is done, this approach may lead to an improved precision for α_S determinations.

6.2. Power corrections to the running

The data on α_S and the respective uncertainties shown in Figs. 15 and 22 in Sections 4.1.1 and 4.1.2, respectively, agree reasonably well with the expectation of QCD. Deviations from this expectation, however, cannot yet be ruled out. In fact, the Landau pole [24], appearing at low scales, induces $1/Q^2$ corrections at large Q^2 [287]. Such corrections are also found from the investigation of the ultraviolet (UV) renormalons, which dominate the perturbation expansions in $\alpha_S(Q^2)$ at large orders n, because of factorially divergent coefficients with alternating signs, in contrast to the infrared (IR) renormalon discussed in Section 5.3, where the coefficients have the same sign.

The emergence of $1/Q^2$ contributions can easily be seen when one tries to remove the Landau pole of the coupling, as has been done by various approaches, to render the coupling finite at low scales. For instance, in Ref. [254], a scale-dependent term is added to the explicit representation of α_S in order to cancel the pole, viz.

$$\tilde{\alpha}_S(Q^2) = \frac{1}{\beta_0 \ln(Q^2/\Lambda^2)} + \frac{\Lambda^2}{\beta_0(\Lambda^2 - Q^2)}. \tag{149}$$

This 'analytically-improved' coupling $\tilde{\alpha}_S$ no longer has a pole at $Q^2 = \Lambda^2$ and remains finite for all values of Q^2. Admittedly, it introduces a $1/Q^2$ contribution at large scales, $Q^2 \gg \Lambda^2$, which has to be cancelled in quantities that are proportional to $\alpha_S(Q^2)$ to leading order but are not expected to have $1/Q^2$ corrections, like the total cross-section in e^+e^- annihilation [71,253]. To overcome this potential problem, one could further extend the expression in Eq. (149) by adding $\Lambda^2/(\beta_0 Q^2)$, which would remove the $1/Q^2$ contribution at large Q^2 at the expense of bringing in a new pole, which, however, is now at the limit of the physical regime, i.e. at $Q^2 = 0$. Moreover, with this extension the improved coupling differs from the standard formula only by $1/Q^4$ terms.

With the large quantity of available α_S determinations over a vast energy range in hand, one could test the possibility of $1/Q^2$ and $1/Q^4$ contributions. Fig. 55 presents the data shown in Figs. 15 and 22. The 2-loop part of the explicit expression for α_S (Eq. (22)) is complemented by adding either c_2/Q^2 or c_4/Q^4 and then, for illustrative purposes, fitting to the α_S data using experimental errors only. Both fits yield a value of $\alpha_S(m_Z^2) = 0.122$ with a $\chi^2/\text{d.o.f.} = 25/22$. The values of the coefficient for the additional term are $c_2 = -0.66 \pm 0.60$ and $c_4 = -0.18 \pm 0.19$, respectively. Even though the sign of the c parameters is just what is expected for the improved coupling, no indication of such contributions is seen from these data. The same observation has also been made for $1/Q^p$ corrections for other integer powers in the range of 0–7.

One has to be aware, however, that the α_S values used in the fit were determined assuming neither $1/Q^2$ nor $1/Q^4$ contributions. Thus, any influence of these could already have been absorbed into the value of α_S. A new determination of each α_S value, allowing for $1/Q^2$ or $1/Q^4$ corrections, would be required to find the full contribution from such terms. Moreover, the α_S value determined from the hadronic τ lepton decays is of particular importance for the values of the c_2 and c_4 parameters. If this α_S value comes out a little low (high) compared with the determinations at high energies, the two parameters will have negative (positive) signs. Recalling the importance of

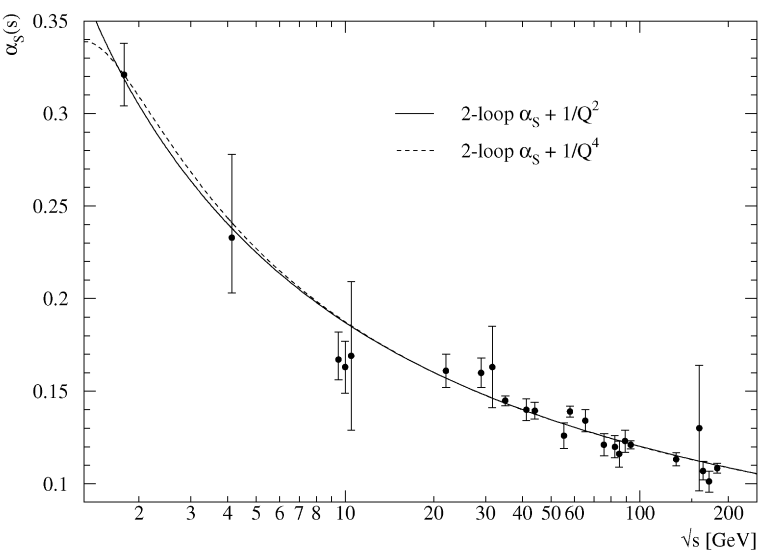

Fig. 55. Combined results on α_S from Figs. 15 and 22 are shown. The curves show the results of fits of the explicit 2-loop expression for α_S supplemented by either a $1/Q^2$ (solid) or a $1/Q^4$ (dashed) term. Only experimental errors are shown and were considered in the fit.

non-perturbative corrections in the determination of α_s from the τ (see Section 4.1.1), no conclusions should be drawn about $1/Q^2$ or $1/Q^4$ corrections from the sign of the c_2, c_4 parameters. In fact, the fit is done for illustrative purposes only, indicating that, although the data look rather imprecise, there is no freedom to modify the running of the coupling by additional terms like $1/Q^p$ for any integer power $p \geq 0$.

6.3. Additional coloured objects

In addition to gluons and quarks which are known to be coloured particles in the standard QCD theory, other coloured particles which participate in the strong interaction may exist. Two examples of candidate particles are: the gluino [288], which will be discussed in the following, and coloured Higgs particles [289]. Even though these particles might be heavy, they could contribute to loop corrections and, hence, affect the energy scale dependence of the strong coupling constant. The contribution of such particles would, in general, alter the number of active flavours, n_f, and also the coefficients of the β-function in Eq. (21). They might also introduce new and, therefore, anomalous strong couplings.

6.3.1. Light gluinos

A particle whose existence is conjectured is the gluino, the supersymmetric spin-$\frac{1}{2}$ partner of the gluon (for an introduction to supersymmetry (SUSY) see Ref. [28] and references therein and for the gluino see Ref. [288]). If it is sufficiently light, its appearance will increase the number of active flavours in lowest non-trivial order by up to 3 [270,290]. A high gluino mass will suppress its contribution to the loops by a kinematic factor such that the number of active flavours is raised by an amount less than 3, and which is not constrained to be an integer.

In general, all cross-sections for strong interaction processes depend on the QCD colour factors C_A, C_F, and $n_f T_F$. It is possible to infer the number of active flavours n_f from the measured values of such cross-sections. For this purpose the dependence of the perturbative expansion on n_f has to be made explicit for each cross-section. In Ref. [290] such an investigation was performed using, in addition to the 4-jet events which will be discussed below, the energy dependence of the 3-jet rate and the thrust distribution, and the R ratios. The result is $n_f = 6.3 \pm 1.1$, where the error is dominated by systematic uncertainties.

With the bulk of LEP I data being available now, a more significant study has become possible using 4-jet events. The number of active flavours appears in the determination of the ratios C_A/C_F and T_F/C_F from these events using 4-jet angular distributions which are sensitive to the colour factors [291]. Various angles were proposed [292] motivated by the notion of an intermediate gluon splitting into a pair of partons. Due to the spin structure at this vertex a quark–antiquark pair obeys a different distribution than a gluon–gluon pair. Moreover, the coupling differs due to the colour factors involved (see Eqs. (12) and (14) of Section 2.1). This is the origin of the colour factor sensitivity of angular distributions when associating the 4 jets with the 2 partons from the splitting of the intermediate gluon plus quark and antiquark from the primary hard process.

An overview of measurements of the QCD colour factors at LEP can be found in Ref. [293]. Fig. 56 shows a contour plot of the colour factor ratios obtained from angular distributions using LEP I data. Despite the large statistics available, most of the measurements were statistically limited. The combination of these results with those from jet rates and event shape observables, whose

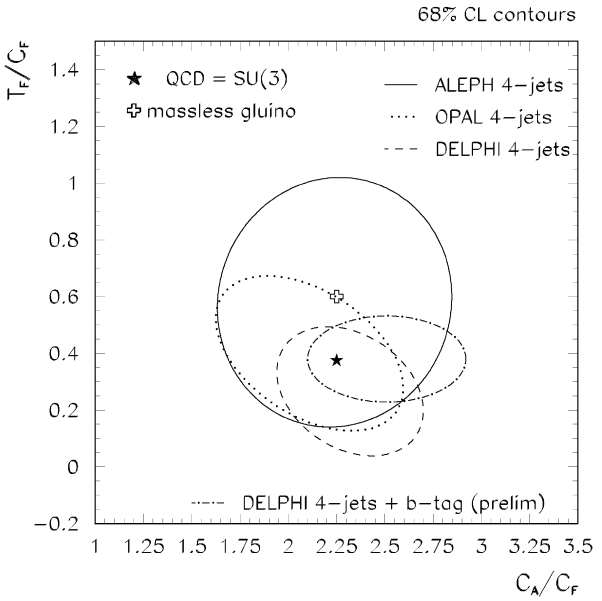

Fig. 56. Colour factor measurements based on 4-jet event angular distributions. The open plus sign shows the increased value of $T_F'/C_F = 3/5$ due to the contribution of a massless gluino, without which it is $T_F/C_F = 3/8$. Figure taken from Ref. [293].

second order coefficient of the perturbative prediction depends on the two colour factor ratios, might improve the precision. The ALEPH collaboration performed a simultaneous determination of $\alpha_S(m_Z^2)$, C_A/C_F, and $n_f T_F/C_F$ from the differential DURHAM 2-jet rate and the 4-jet angular distributions [294]. Accounting for mass effects, the colour factor ratios were determined to be

$$\frac{C_A}{C_F} = 2.20 \pm 0.09\ (\text{stat.}) \pm 0.13\ (\text{syst.}),$$

$$\frac{T_F}{C_F} = 0.29 \pm 0.05\ (\text{stat.}) \pm 0.06\ (\text{syst.}),$$

in agreement with the expectations of $C_A/C_F = 9/4$ and $T_F/C_F = 3/8$ for the $SU(3)$ group structure of QCD (see Section 2.1). One may now assume these to be the correct colour factors to determine $\alpha_S(m_Z^2) = 0.1162 \pm 0.0042$ and the number of active flavours $n_f = 4.2 \pm 1.2$, where the errors are statistical and systematic uncertainties added in quadrature [294]. The upper limit on an excess of the number of active flavours is thus $\Delta n_f < 1.9$ at a confidence level of 95%.

Besides these measurements further investigations were done studying the running of α_S from the R ratio and the hadronic cross-section at different scales [295]. None of these found evidence for contributions from a light gluino (see also Ref. [7]).

6.3.2. Anomalous coupling

New physics beyond the standard model may contribute to the strong interaction if the new particles involved are carriers of colour charge. Deviations of experimentally measured

cross-sections from the QCD predictions are to be expected. These may, however, be small if the new particles are heavy.

Without assuming a particular model for the extension of the standard model, the standard model Lagrangian was supplemented in Ref. [296] by non-standard operators of (energy) dimension six. Besides new couplings for left-handed quarks, these operators give rise to new qqG and qqGG vertices involving right-handed quarks and the Higgs field doublet. Recalling the experimental evidence for the flavour independence of the strong coupling presented in Section 4.2.2, the new couplings are assumed to be universal with respect to the quark flavour. The strength of the new anomalous couplings is expressed by a constant $A_{q\mathrm{G}\phi}$ and by a scale Λ_{an} which characterizes the new physics. Fig. 57 shows the net effect of the new anomalous coupling on some event shape distributions compared with the standard QCD expectation. A prominent difference in the shape of the distributions due to the anomalous couplings can be noted.

By fitting the anomalous plus standard distributions to the data with Λ_{QCD} and the renormalization scale fixed, the relative contributions of the anomalous parts were obtained. From these, bounds on the strength of the anomalous coupling and its characteristic scale were derived in Ref. [296] for each of the four shape distributions, yielding results of the order $A_{q\mathrm{G}\phi}/\Lambda_{\mathrm{an}}^2 < 14$ through $16\,\mathrm{TeV}^{-2}$ at the 95% confidence limit. If the unknown coupling strength $A_{q\mathrm{G}\phi}$ is chosen to

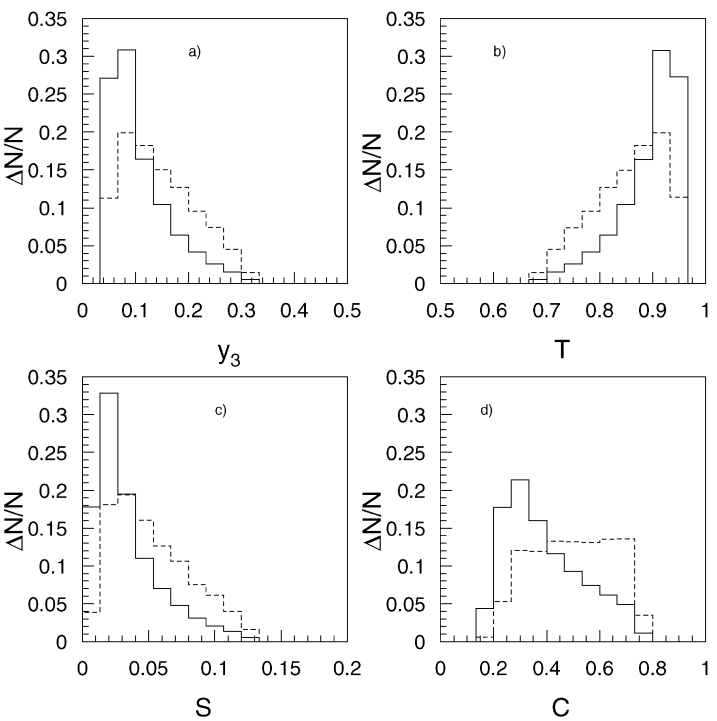

Fig. 57. (a) Relative production of 3-jet events and differential distributions of (b) thrust, (c) spherocity, and (d) C-parameter are shown. The solid line corresponds to the standard QCD prediction. The contribution from the anomalous couplings described in the text is shown by the dashed line. The spherocity is defined as $S = (4/\pi)^2 \min_{\vec{n}}(\sum_i |\boldsymbol{p}_i \times \boldsymbol{n}|/\sum_i |\boldsymbol{p}_i|)^2$ [297]. Figures taken from Ref. [296].

be of the order of unity, the scale of new physics associated with the anomalous coupling is above 270 GeV at least, and hence beyond the direct reach of LEP II.

A comparable study considering the gluon energy was done by the SLD collaboration [298]. The gluons were identified by tagging both bottom quark jets in a 3-jet configuration by the reconstruction of a displaced decay vertex. The distribution of the gluon energy is potentially sensitive to an anomalous chromomagnetic moment of the bottom quark, but no evidence was found from the comparison of the distribution with perturbative QCD predictions [298].

Nevertheless, both results demonstrate the sensitivity of the qqG vertex to anomalous couplings due to new physics effects.

6.4. α_s determinations from other hard processes

The value of the strong coupling constant α_s can also be determined from hard processes other than e^+e^- annihilation. It is beyond the scope of this report to present all such determinations in detail. A compact description of the theoretical predictions used in these determinations can be found in Ref. [12], experimental details in the references to be mentioned in the following.

Refs. [108,272,299] contain compilations of the most recent determinations of α_s from various hard processes. Table 12, which is an excerpt of the results given in Refs. [12,108,272,299] for the processes other than e^+e^- annihilation, complements the results from e^+e^- annihilation listed in Table 4 of Section 4.1.1 and Table 7 of Section 4.1.2. In brief, α_s was obtained using:

- Deep inelastic scattering (DIS) of either leptons (e or μ) or neutrinos off nucleons from which the structure functions (polarized in the case of a polarized lepton beam) of proton, neutron, or deuteron were measured. The value of the strong coupling was extracted either directly from the

Table 12
Listing of α_s determinations from processes other than e^+e^- annihilation. Excerpt from Refs. [12,108,272,299]. (DIS = deep inelastic scattering, Bj-SR = Bjorken sum rule, GLS-SR = Gross–Llewellyn–Smith sum rule, LGT = lattice gauge theory.)

Process	Ref.	Q (GeV)	$\alpha_s(Q^2)$	$\alpha_s(m_Z^2)$	Theory
DIS [pol. strct. fctn.]	[300]	0.7–8		$0.120^{+0.010}_{-0.008}$	NLO
DIS [Bj-SR]	[301]	1.58	$0.375^{+0.062}_{-0.081}$	$0.121^{+0.005}_{-0.009}$	NNLO
DIS [GLS-SR]	[302]	1.73	$0.295^{+0.092}_{-0.073}$	$0.114^{+0.010}_{-0.012}$	NNLO
DIS [ν; F_2, F_3]	[303]	5.0	0.215 ± 0.016	0.119 ± 0.005	NLO
DIS [μ; F_2]	[304]	7.1	0.280 ± 0.014	0.113 ± 0.005	NLO
DIS [HERA; F_2]	[305]	2–10		0.120 ± 0.010	NLO
DIS [HERA; jets]	[306]	10–100		0.118 ± 0.009	NLO
DIS [HERA; ev.shps.]	[307]	7–100		$0.118^{+0.007}_{-0.006}$	NLO
$Q\bar{Q}$ states	[308]	0.7-8		$0.120^{+0.010}_{-0.008}$	LGT
$p\bar{p} \to b\bar{b}X$	[309]	20	$0.145^{+0.018}_{-0.019}$	0.113 ± 0.011	NLO
$p\bar{p}, pp \to \gamma X$	[310]	24.2	$0.137^{+0.017}_{-0.014}$	$0.111^{+0.012}_{-0.008}$	NLO
$\sigma(p\bar{p} \to W$ jets)	[311]	30–500		0.121 ± 0.009	NLO

structure functions, F_2, F_3, or g_1 for polarized beams, or by exploiting higher-order corrections to the Bjorken or Gross–Llewellyn–Smith sum rules for the structure functions. At sufficiently high momentum transfer $q^2 = -Q^2$, available at the HERA electron–proton collider, α_S was also extracted from jet rates and mean values of event shapes including power corrections as presented in Section 5.3.

- Lattice gauge theory (LGT) calculations which, roughly speaking, discretize the four-dimensional space–time into hypercubes. The quark fields reside on the corners of the cubes, the gauge fields (gluons) are associated with the cubes' edges. One can explicitly calculate the action on such a lattice since the finite lattice spacing serves as an ultraviolet cut-off and, therefore, regulates the short distance divergence of the QCD Lagrangian (renormalization on the lattice, cf. Section 2.2). To obtain the value of the strong coupling constant from the lattice one usually calculates the Υ or charmonium spectrum and uses the true mass splitting from experimental measurements to set the scale for α_S.
- Hadron–hadron scattering by comparing heavy quark, direct photon and 2-jet cross-sections with next-to-leading order predictions.

A more elaborate presentation of each topic can be found in Ref. [12].

The agreement of these results with the value of α_S obtained from the investigation of e^+e^- annihilation is remarkable. The values of the coupling at the Z mass scale all cluster closely around a value of approximately 0.119. Taking into account the unknown correlation between the individual results by the "optimized correlation" method of Ref. [148], a common average of all available data on $\alpha_S(m_Z^2)$ was calculated, yielding [272]

$$\alpha_S(m_Z^2) = 0.119 \pm 0.004 ,$$

where the overall correlation varies between about 50% and 80% depending on the subset of data chosen for the average. This average perfectly agrees with the value presented in this report.

6.5. A glance at asymptotic freedom

Utilizing all results on $\alpha_S(Q^2)$ determined from e^+e^- annihilation as well as other hard processes at different scales Q^2 one obtains the behaviour depicted in Fig. 58. All individual values agree very well with the expectation of QCD over a vast energy range covering more than two orders of magnitude. The expectation of QCD shown in the figure is the exact solution of the 4-loop renormalization group equation (21) using the world average of $\alpha_S(m_Z^2) = 0.119 \pm 0.004$. These data are presented differently in part (b) of the figure, in order to make the property of asymptotic freedom visible.

Fig. 58(b) shows, in addition, how the running of the strong coupling constant changes when the threshold to SUSY particle production, which is assumed for this plot to be at 1 TeV, is passed. A clear excursion from the straight path to asymptotic freedom can be seen which is due to new supersymmetric particles carrying colour charge and, therefore, participating in the strong interaction. Supersymmetry changes the β-function of Eq. (21) and, consequently, the energy dependence of the coupling constant α_S. Moreover the running of the quark masses is also affected, see for instance Ref. [312]. The corresponding modifications of the 2-loop coefficients of the β-function were taken from Ref. [313]. At the 2-loop level of the perturbation theory, one also has to consider

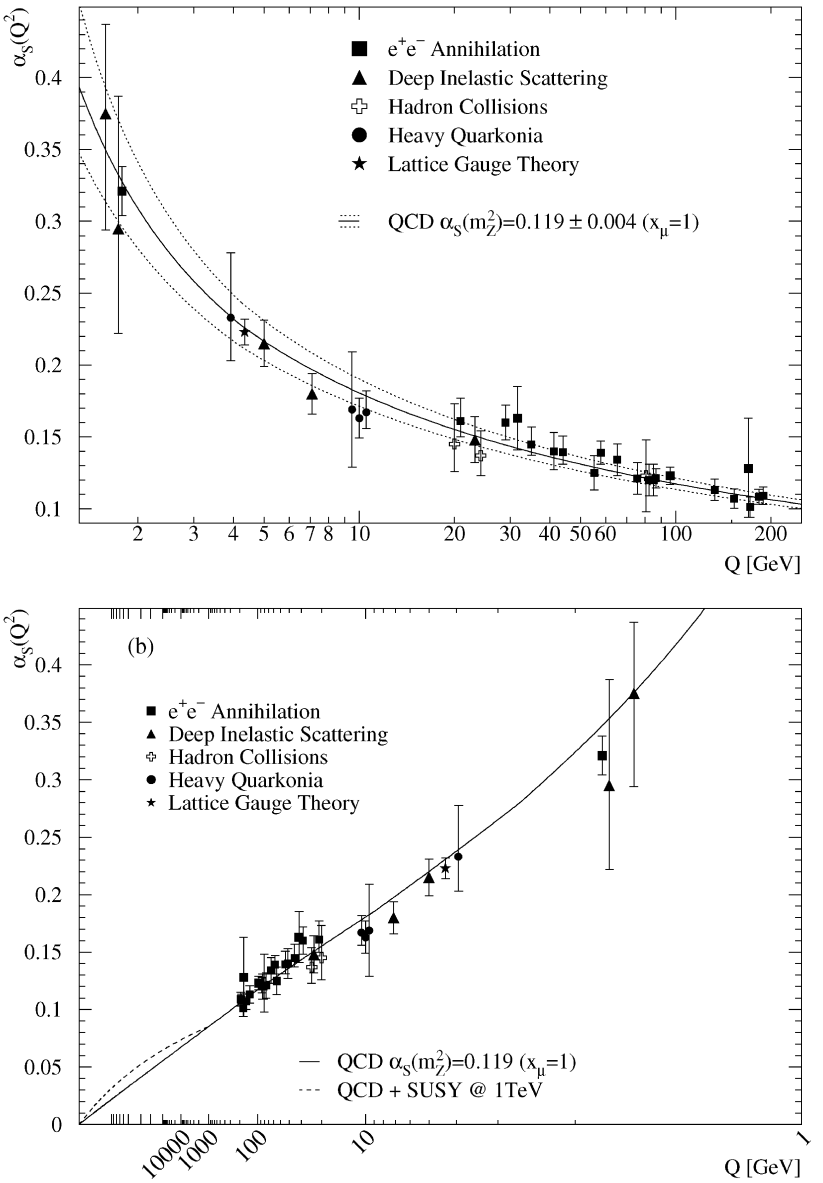

Fig. 58. (a) Summary of $\alpha_S(Q^2)$. The QCD expectation for the energy scale dependence is shown using the world average value $\alpha_S(m_Z^2) = 0.119 \pm 0.004$ [272]. (b) shows the same data with the abscissa chosen as to emphasize the property of asymptotic freedom. The dashed curve shows how the onset of supersymmetry at an assumed threshold of 1 TeV would change the energy dependence of the strong coupling.

the connection of the running of the strong coupling constant with that of the electromagnetic and weak coupling constants. The dashed curve in Fig. 58(b) is, in fact, the result of a numerical solution of a coupled system of three differential equations of the same type as Eq. (21) (see Ref. [313] for further details).

The small size of the excursion indicates that a very precise determination of α_s is required to notice the impact of SUSY. It is therefore more likely that SUSY particles will be discovered by a dedicated search rather than by an excursion in the running of α_s. Nevertheless, the figure demonstrates in principle the sensitivity of the strong interaction to new physics processes. Thus any significant deviation of the strong coupling from the prediction could be evidence of yet unknown physics.

7. Summary and outlook

Electron–positron annihilation experiments have reached a high level of sophistication in testing the predictions of QCD. This became possible only with the employment of colliders providing highly intense particle beams at very high energies. Below, at, and above the Z resonance an incredible amount of data statistics on annihilation into quark–antiquark pairs could be accumulated. By the juxtaposition of the results of the precise measurements with the predictions of perturbative QCD, the theory could be shown to be well-suited to describe the properties of the strong interaction.

In this report QCD theory was first of all investigated using processes involving large energy scales. The property of asymptotic freedom, meaning that the strong coupling constant α_s diminishes as the energy scale goes towards infinity, renders perturbative QCD predictions particularly reliable in these regions. The calculations were used to determine the strong coupling constant from (i) *completely inclusive* quantities as the hadronic cross-section and hadronic branching fractions of the τ lepton and Υ mesons, and also (ii) from *inclusive* quantities as the production rate of n-jet final states and event shape observables which inclusively measure the distribution of the detected particles. Since QCD only operates on quarks and gluons, but experiments observe and measure hadrons, photons, and leptons, completely inclusive observables have a significant advantage over inclusive quantities due to their insensitivity to the details of the final state. Precise determinations of the strong coupling constant are therefore possible from completely inclusive quantities, in particular, if next-to-next-to-leading order calculations are available. This is the case for the ratio R of the hadronic over the leptonic cross-section and for the hadronic τ decays. However, the precision of these results is limited for the R ratio through its weak dependence on α_s contributing only a small higher-order correction, and for the τ decays by unknown higher-order terms which are important because of the large size of the coupling at such a low energy scale.

Inclusive quantities as jet rates and event shapes are directly proportional to the coupling, thus promising an excellent sensitivity to the size of α_s. To perform any QCD test with them, however, one needs to consider the effects from the transition of quarks and gluons into hadrons, that is, of hadronization. As the relevant energy scale at this stage is too low and the size of the coupling constant is too large, perturbation theory cannot be employed to describe this transition. The better sensitivity is traded for a considerable uncertainty coming from the necessity to use phenomenological models to account for hadronization effects. Perturbation calculations are available up to next-to-leading order only, but the large leading and next-to-leading logarithms could be resummed to all orders. Joining fixed order and resummed calculations allowed an extension of the range that can be used for the determination of α_s from a fit to the data significantly towards the 2-jet regime. The 2-jet region comprises the bulk of data characterized by

hadronic final states where gluon emission at large angle and high energy is suppressed. Although improved, the contribution to the total error on α_S due to the arbitrariness of the choice of the renormalization scale in next-to-leading order is still large.

A missing ingredient of the perturbation theory calculation of inclusive quantities has finally been added, viz. the exact treatment of finite quark masses in jet rates and event shapes. Although mass effects may be expected to be small at high energy scales, their impact on flavour-dependent quantities has long been known. The high data statistics in conjunction with high resolution vertex detectors yielded very precise tests of the flavour dependence of the strong interaction. Deviations as large as 5% from the expected flavour independence of the strong coupling can now be fully explained by the effects of heavy bottom and charm quarks. Reversing the assumptions, a determination of the scale dependence of the bottom quark mass has become possible. It is found to be of the expected size of approximately 3 GeV at the Z pole, although the measurement is affected by large hadronization and renormalization scale uncertainties.

Several approaches may be pursued to bypass, at least partly, the ignorance about hadronization, while still accounting for the details of the hadronic final state. The scaling violation, which yielded the first evidence for the energy dependence of the strong coupling in deep inelastic scattering, has been studied in inclusive fragmentation functions. In addition to the strong coupling, which was also obtained from the longitudinal cross-section, flavour-dependent fragmentation functions for quarks and gluons were determined.

Stepping down the energy scale and looking inside the jets, the combination of the modified leading-logarithmic approximation with the hypothesis of local parton–hadron duality is found to provide an excellent description of details connected with hadronization. The successful application of perturbative QCD in this framework at scales as low as a few hundred MeV leads to the conclusion that hadronization and confinement of coloured partons into colour-neutral objects takes place at a scale which is of the order of the mass of the lightest mesons.

A completely new approach to advance into the non-perturbative domain of hadronization and confinement using the tools of perturbation theory is pursued by the investigation of power suppressed corrections to event shape observables. Although expected on general grounds from phenomenological hadronization models as well as from renormalons, their quantitative calculation became possible only with the assumption of a finite coupling strength even at very small scales. The prediction could successfully be applied in the determination of α_S from both the mean values and the differential distributions of event shape observables.

Finally, the high precision of all the various determinations of α_S allowed further investigations on the explicit energy dependence of the strong coupling. The known structure of the next order of the perturbation theory was used to determine its unknown expansion coefficient from fits to the data exploiting the energy dependence of α_S. Moreover, since no excursions from the QCD expectation of energy dependence of the coupling constant were found, there is no evidence for either additional power suppressed contributions to the running of the coupling or additional coloured objects.

After all the detailed investigations one might consider QCD as *the* theory of the strong interaction whose single unknown parameter is the strength of the coupling, α_S. Its size can be obtained from joining the individual results from very many different analyses of hadronic final states in e^+e^- annihilation presented in this report and summarized in Table 13. The error of the α_S result from cross-sections and branching ratios is dominated by statistical uncertainties. It has,

Table 13
Summary and weighted average of $\alpha_s(m_Z^2)$ determinations presented in this article

Quantity	$\alpha_s(m_Z^2)$
Cross-sections, branching ratios	0.1195 ± 0.0025
Jet rates, event shapes	0.1212 ± 0.0079
Scaling violation	0.125 ± 0.009
Longitudinal cross-section	0.118 ± 0.014
Power corrections to mean values	$0.1181^{+0.0037}_{-0.0035}$
Power corrections to differential shapes	0.1150 ± 0.0036
Weighted average	0.1189 ± 0.0025

therefore, been regarded as uncorrelated with the other α_s determinations which have been averaged taking correlations due to theory uncertainties conservatively into account. Then the weighted average of all results yields a total relative error of about 2% and is in perfect agreement with the world average [272] which includes also α_s determinations from other hard scattering processes.

Recalling that new physics might slightly alter the running of the coupling, and because of the importance of knowing the precise value of the strong coupling, and also in view of future experiments at new e^+e^- colliders (see Ref. [314]), the options to further improve on the precision need to be reviewed. Four major sources of error can be identified, viz. (i) data statistics, (ii) finite detector resolution and acceptance, (iii) hadronization, and (iv) the choice of the renormalization scale. Most of these can easily be reduced by improving experimental aspects of the determination:

(i) data statistics, by improving the efficiency of the event selection and by increasing the specific luminosity of the collider, and by combining the data of many experiments,
(ii) detector effects, by better corrections or optimized detector designs,
(iii) hadronization effects, by an ultimate tuning of the parameters of the phenomenological hadronization models using the vast amount of LEP I data statistics; by using higher centre-of-mass energies since the size of the corrections decreases like $\ln(\sqrt{s})/\sqrt{s}$ in the worst case; or by using power corrections, thus avoiding the effects completely.

The uncertainty due to (iv) the arbitrariness of the choice of the renormalization scale can be solely reduced by a complete third-order calculation of jet rates and event shapes. The very first steps towards the completion of the calculation are complete. New computational tools for numerical integration of matrix elements might accelerate the pace of the progress [198,315]. And even the energy dependence of the strong interaction can be invoked to gain estimates of the size of the third-order terms.

Moreover, further experimental tests can be performed at existing colliders using the hadronic final state of $\gamma\gamma$ collisions. In particular the high centre-of-mass energy and huge luminosity at LEP II populates the region of $\gamma\gamma$ events with high momentum transfer $q^2 \equiv -Q^2$, eventually allowing to study jet rates and event shapes over a significant range of Q^2 up to $40\,000\,\mathrm{GeV}^2$.

Beyond the necessity to improve the precision on α_S, there are still more open questions to be answered by QCD experiments. Besides topics like top quark physics, many questions concern the issue of hadronization and confinement such as the existence of di-meson, di-baryon states, glue balls, quark–gluon plasma, just to mention a few. More generally, a proof of confinement from the basic QCD Lagrangian would, besides asymptotic freedom, be another major supporting pillar of QCD as *the* theory of the strong interaction.

Note added

A re-evaluation of the *Milan* factor in Ref. [316] revealed an omission in the original derivation of $\mathscr{M}$ in Refs. [72,73]. The corrected formula is $\mathscr{M} \approx 1 + (1.575C_A - 0.104n_f)/(4\pi\beta_0) \approx 1.49$ [317] (cf. Section 5.3). Since this correction became available only after the investigations discussed in Sections 5.3.1 and 5.3.2 were completed, all results presented in these sections were obtained assuming $\mathscr{M} = 1.79$.

The reduced size of $\mathscr{M}$ leads to increased values of α_0 but has a negligible effect on the value obtained for $\alpha_S(m_Z^2)$. First investigations of power corrections to the mean values of the event shape observables presented in Section 5.3.1 (cf. Table 10) showed that α_0 is increased by about 9%. The value of $\alpha_s(m_Z^2)$ is found to be marginally enlarged by 0.6%. In general, the correction of the Milan factor does not affect the observation that the non-perturbative parameter α_0 has a universal character at the level of 20%.

Acknowledgements

Many people were involved in the preparation of this manuscript, whether for giving the opportunity, for encouraging, teaching, discussing, helping, providing data, providing information, proof-reading, or many more -ings. In particular, I would like to thank:

- S. Bethke for giving me the opportunity to write this report and also for his continuous support and encouragement;
- A. Brandenburg for several discussions about the determination of running quark masses using his second-order calculations;
- Yu. Dokshitzer for providing me information about the modified power corrections for jet broadening observables;
- Yu. Dokshitzer and B.R. Webber for answering my questions concerning power corrections;
- T. Kawamoto for helping me to use the ZFITTER program;
- E.W.N. Glover for providing additional information about his determination of higher-order corrections from the energy dependence of the mean thrust;
- W. Bernreuther for interesting discussions about QCD and quark mass effects in QCD;
- S. Kluth for providing the results from the numerical integration of the ERT matrix elements for several observables;
- P.A. Movilla Fernández for compiling differential event shape data from the Durham reaction database and from publications;
- J. Letts, D.R. Ward, P. Pfeifenschneider, and M. Tönnesmann for proof-reading this manuscript.

References

[1] S. Myers, E. Picasso, Contemp. Phys. 31 (1990) 387.
[2] J.M. Paterson, in: W.S. Newman (Ed.), 11th International Conference on High-Energy Accelerators, Birkhauser, Geneva, July 7–11, 1980; P. Oddone, Phys. Scr. 23 (1981) 601.
[3] PETRA Storage Ring Group: D. Degèle et al., DESY M-83-20; PETRA Storage Ring Group: D. Degèle et al., in: F.T. Cole, R. Donaldson (Eds.), 12th International Conference on High-Energy Accelerators, Fermilab, August 11–16, 1983.
[4] The LEP collaborations: ALEPH, DELPHI, L3, and OPAL, CERN-PPE/99-15.
[5] G. Quast, Prog. Part. Nucl. Phys. 43 (1999) 87.
[6] P. Renton, Electroweak Interactions, Cambridge University Press, Cambridge, 1990.
[7] M.G. Green, S.L. Lloyd, P.N. Ratoff, D.R. Ward, Electron Positron Physics at the Z, Institute of Physics Publishing, IOP, Bristol, 1998.
[8] T. Hebbeker, Phys. Rep. 217 (1992) 69.
[9] M. Schmelling, Phys. Scr. 51 (1995) 683.
[10] A. Boehrer, Phys. Rep. 291 (1997) 107.
[11] I.G. Knowles, G.D. Lafferty, J. Phys. G 23 (1997) 731.
[12] R.K. Ellis, W.J. Stirling, B.R. Webber, QCD and Collider Physics, Cambridge University Press, Cambridge, 1996.
[13] F. Halzen, A.D. Martin, Quarks & Leptons, Wiley, New York, 1984.
[14] G. Altarelli, Phys. Rep. 81 (1982) 1.
[15] J. Collins, Renormalization, Cambridge University Press, Cambridge, 1984.
[16] G. 't Hooft, Nucl. Phys. B 33 (1971) 173.
[17] G. 't Hooft, M. Veltman, Nucl. Phys. B 44 (1972) 189; C.G. Bollini, J.J. Giambiagi, Phys. Lett. 40B (1972) 599.
[18] G. 't Hooft, Nucl. Phys. B 61 (1973) 455.
[19] W.A. Bardeen, A.J. Buras, D.W. Duke, T. Muta, Phys. Rev. D 18 (1978) 3998.
[20] S. Weinberg, Phys. Rev. D 8 (1973) 3497.
[21] D.J. Gross, F. Wilczek, Phys. Rev. Lett. 30 (1973) 1343; H.D. Politzer, Phys. Rev. Lett. 30 (1973) 1346; W.E. Caswell, Phys. Rev. Lett. 33 (1974) 244; D.R.T. Jones, Nucl. Phys. B 75 (1974) 531; E.S. Egorian, O.V. Tarasov, Theor. Mat. Fiz. 41 (1979) 26; O.V. Tarasov, A.A. Vladimirov, A.Yu. Zharkov, Phys. Lett. B 93 (1980) 429; S.A. Larin, J.A.M. Vermaseren, Phys. Lett. B 303 (1993) 334.
[22] T. van Ritbergen, J.A.M. Vermaseren, S.A. Larin, Phys. Lett. B 400 (1997) 379.
[23] K.G. Chetyrkin, B.A. Kniehl, M. Steinhauser, Phys. Rev. Lett. 79 (1997) 2184.
[24] L.D. Landau, I.Ya. Pomeranchuk, On point interactions in quantum electrodynamics, Dokl. Acad. Nauk Ser. Fiz. 102 (1955) 489; L.D. Landau, in: W. Pauli (Ed.), Niels Bohr and the Development of Physics, Pergamon Press, London, 1955.
[25] R. Tarrach, Nucl. Phys. B 183 (1981) 384.
[26] O. Nachtmann, W. Wetzel, Nucl. Phys. B 187 (1981) 333; S.A. Larin, Phys. Lett. B 303 (1993) 113; K.G. Chetyrkin, Phys. Lett. B 404 (1997) 161.
[27] J.A.M. Vermaseren, S.A. Larin, T. van Ritbergen, Phys. Lett. B 405 (1997) 327.
[28] C. Caso et al., Review of particle properties, Eur. Phys. J. C 3 (1998) 1.
[29] G. Rodrigo, A. Pich, A. Santamaria, Phys. Lett. B 424 (1998) 367, hep-ph/9707474.
[30] D. Bardin et al., CERN-TH.6443/92; D. Bardin et al., Phys. Lett. B 255 (1991) 290; D. Bardin et al., Nucl. Phys. B 351 (1991) 1; D. Bardin et al., Z. Phys. C 44 (1989) 493, We use ZFITTER version 5.0 with default parameters, except BOXD = 1, CONV = 1, INTF = 0, FINR = 0, and with the following input parameters: $m_Z = 91.1863\,\text{GeV}$, $m_{\text{top}} = 175.6\,\text{GeV}$, $m_{\text{Higgs}} = 300\,\text{GeV}$, $\alpha_{\text{em}}(m_Z) = 1/128.896$, $\alpha_S(m_Z) = 0.118$.
[31] J. Ellis, M.K. Gaillard, G.G. Ross, Nucl. Phys. B 111 (1976) 253, Erratum: ibid. 516.
[32] R.K. Ellis, D.A. Ross, A.E. Terrano, Nucl. Phys. B 178 (1981) 421.
[33] K. Fabricius, G. Kramer, G. Schierholz, I. Schmitt, Z. Phys. C 11 (1982) 315; J.A.M. Vermaseren, K.J.F. Gaemers, S.J. Olsham, Nucl. Phys. B 187 (1981) 301.

[34] A. Ali, J.G. Körner, G. Kramer, J. Willrodt, Nucl. Phys. B 168 (1980) 409; A. Ali, E. Pietarinen, G. Kramer, J. Willrodt, Phys. Lett. B 93 (1980) 155; K.J.F. Gaemers, J.A.M. Vermaseren, Z. Phys. C 7 (1980) 81; D. Daenckaert, P. De Causmaecker, R. Gastmanns, W. Troost, T.T. Wu, Phys. Lett. B 114 (1982) 203; B.A. Kniehl, J.H. Kühn, Phys. Lett. B 224 (1989) 229.
[35] L. Dixon, A. Signer, Phys. Rev. D 56 (1997) 4031, hep-ph/9806285; E.W.N. Glover, D.J. Miller, Phys. Lett. B 396 (1997) 257, hep-ph/9609474; J.M. Campbell, E.W.N. Glover, D.J. Miller, Phys. Lett. B 409 (1997) 503, hep-ph/9706297; J.M. Campbell, M.A. Cullen, E.W.N. Glover, DTP-98-58, hep-ph/9809429; Z. Nagy, Z. Tróscányi, Phys. Rev. Lett. 79 (1997) 3604, hep-ph/9707309; Z. Nagy, Z. Tróscányi, Phys. Rev. D 59 (1999) 014020, hep-ph/9806317; S. Weinzierl, D.A. Kosower, Phys. Rev. D 59 (1999) 094018, hep-ph/9901227.
[36] K. Hagiwara, D. Zeppenfeld, Nucl. Phys. B 313 (1989) 560; N.K. Falck, W.T. Giele, G. Kramer, Phys. Lett. B 220 (1989) 299; N.K. Falck, D. Graudenz, G. Kramer, Nucl. Phys. B 328 (1989) 317; F.A. Berends, W.T. Giele, H. Kuijf, Nucl. Phys. B 321 (1989) 39.
[37] S. Moretti, Phys. Lett. B 420 (1998) 367, hep-ph/9711518; S. Moretti, Nucl. Phys. B 544 (1998) 289, hep-ph/9808430.
[38] A. Bassetto, M. Ciafaloni, G. Marchesini, Phys. Rep. 100 (1983) 201.
[39] B.R. Webber, Ann. Rev. Nucl. Part. Sci. 36 (1986) 253.
[40] L.A. Gribov, E.M. Levin, M.G. Ryskin, Phys. Rep. 100 (1983) 1.
[41] Yu.L. Dokshitzer, V.A. Khoze, A.H. Mueller, S.I. Troyan, Basics of Perturbative QCD, Edition Frontières, Gif-sur-Yvette, 1991.
[42] G. Altarelli, G. Parisi, Nucl. Phys. B 126 (1977) 298.
[43] G. Curci, W. Furmanski, R. Petronzio, Nucl. Phys. B 175 (1980) 27; W. Furmanski, R. Petronzio, Phys. Lett. B 97 (1980) 437; E.F. Floratos, R. Lacaze, C. Kounnas, Nucl. Phys. B 192 (1981) 417.
[44] E.G. Floratos, D.A. Ross, C.T. Sachrajda, Nucl. Phys. B 129 (1977) 66, Errata: ibid. B 139 (1978) 545; ibid. B 152 (1979) 493; A. Gonzalez-Arroyo, C. Lopez, F.J. Yndurain, Nucl. Phys. B 153 (1979) 161.
[45] T. Sjöstrand, Int. J. Mod. Phys. A 3 (1988) 751.
[46] QCD Working Group: T. Sjöstrand (conv.) et al., in: G. Altarelli, R. Kleiss, C. Verzegnassi (Eds.), Z Physics at LEP 1, CERN Yellow Report, Vol. 89-08, v.3, 1989, p. 143.
[47] R.D. Field, R.P. Feynman, Nucl. Phys. B 136 (1978) 1.
[48] Ya.I. Azimov, Yu.L. Dokshitzer, V.A. Khoze, S.I. Troyan, Phys. Lett. B 165 (1985) 147; Yu.L. Dokshitzer, V.A. Khoze, S.I. Troyan, A.H. Mueller, Rev. Mod. Phys. 60 (1988) 373.
[49] JADE collaboration: W. Bartel et al., Phys. Lett. B 101 (1981) 129.
[50] L3 collaboration: M. Acciarri et al., Phys. Lett. B 345 (1995) 74.
[51] OPAL collaboration: R. Akers et al., Z. Phys. C 68 (1995) 531.
[52] DELPHI collaboration: P. Abreu et al., Z. Phys. C 70 (1996) 179.
[53] ALEPH collaboration: E. Barate et al., Phys. Rep. 294 (1998) 1.
[54] R. Odorico, Comput. Phys. Comm. 72 (1992) 238.
[55] C. Peterson, D. Schlatter, I. Schmitt, P. Zerwas, Phys. Rev. D 27 (1983) 105.
[56] OPAL collaboration: G. Alexander et al., Z. Phys. C 69 (1996) 543.
[57] X. Artru, G. Mennessier, Nucl. Phys. B 70 (1974) 93.
[58] B. Andersson, G. Gustafson, G. Ingelmann, T. Sjöstrand, Phys. Rep. 97 (1983) 31.
[59] B. Andersson, G. Gustafson, Z. Phys. C 3 (1980) 223.
[60] T. Sjöstrand, Comput. Phys. Comm. 82 (1994) 74.
[61] L. Lönnblad, Comput. Phys. Comm. 71 (1992) 15.
[62] G. Marchesini, B.R. Webber, M.H. Seymour, G. Abbiendi, L. Stanco, I.G. Knowles, Comput. Phys. Comm. 67 (1992) 465.
[63] D. Amati, G. Veneziano, Phys. Lett. B 83 (1979) 87; G. Marchesini, L. Trentadue, G. Veneziano, Nucl. Phys. B 181 (1981) 335.
[64] Yu.L. Dokshitzer, S.I. Troyan, in: Proceedings of the XIX Winter School of the LNPI, Vol. 1, Leningrad, 1984, p. 144; Ya.I. Azimov, Yu.L. Dokshitzer, V.A. Khoze, S.I. Troyan, Z. Phys. C 27 (1985) 65.
[65] B.R. Webber, Phys. Lett. B 339 (1994) 148, hep-ph/9408222.
[66] Yu.L. Dokshitzer, B.R. Webber, Phys. Lett. B 404 (1997) 321, hep-ph/9704298.

[67] G.P. Korchemsky, G. Sterman, Nucl. Phys. B 437 (1995) 415, hep-ph/9411211; G.P. Korchemsky, G. Sterman, in: J. Trhatan Thanh Vân (Ed.), QCD and High Energy Hadronic Interactions, 30th Rencontres de Moriond, Editions Frontières, Gif-sur-Yvette, 1995, p. 383. hep-ph/9505391.
[68] R. Akhoury, V. Zakharov, Nucl. Phys. B 357 (1995) 646, hep-ph/9504248; R. Akhoury, V. Zakharov, Nucl. Phys. B 465 (1996) 295, hep-ph/9507253.
[69] M. Beneke, V.M. Braun, Nucl. Phys. B 454 (1995) 253, hep-ph/9506452.
[70] P. Nason, M.H. Seymour, Nucl. Phys. B 454 (1995) 291, hep-ph/9506317.
[71] Yu.L. Dokshitzer, G. Marchesini, B.R. Webber, Nucl. Phys. B 469 (1996) 93, hep-ph/9512336.
[72] Yu.L. Dokshitzer, A. Lucenti, G. Marchesini, G.P. Salam, Nucl. Phys. B 511 (1998) 396, hep-ph/9707532.
[73] Yu.L. Dokshitzer, A. Lucenti, G. Marchesini, G.P. Salam, J. High Energy Phys. 05 (1998) 003, hep-ph/9802381.
[74] Yu.L. Dokshitzer, B.R. Webber, Phys. Lett. B 352 (1995) 451, hep-ph/9504219.
[75] R.P. Feynman, Photon Hadron Interactions, Benjamin, New York, 1972.
[76] B.R. Webber, in: M.P. Locher (Ed.), Summer school on hadronic aspects of collider physics, Villingen, 1994, p. 49. hep-ph/9411384.
[77] OPAL collaboration: P. Acton et al., Z. Phys. C 59 (1993) 1.
[78] A. Höcker, V. Kartvelishvili, Nucl. Instrum Methods A 372 (1996) 469; G. d'Agostini, Nucl. Instr. and Methods A 362 (1995) 487; V. Blobel, Unfolding methods in high-energy physics experiments, CERN School of Computing; R.K. Bock, W. Krischer, The Data Analysis Brief Book. Springer, Heidelberg, 1998.
[79] S.G. Gorishny, A.L. Kataev, S.A. Larin, Phys. Lett. 259B (1991) 144; L.R. Surguladze, M.A. Samuel, Phys. Rev. Lett. 66 (1991) 560; Erratum: ibid. 2416.
[80] T. Hebbeker, M. Martinez, G. Passarino, G. Quast, Phys. Lett. B 331 (1994) 165.
[81] R. Partridge, Heavy quark production and decay: t, b, and onia, in: A. Astbury, D. Axen, J. Robinson (Eds.), Proceedings of the 29th International Conference on High-Energy Physics, ICHEP 98, World Scientific, Singapore, 1998, p. 107.
[82] E. Tournefier, Extraction of α_S and constraint on the Higgs mass from electroweak fits at the Z resonance, LAL 98-67, hep-ex/9810042, talk at the 10th International Seminar Quarks '98, Suzdal, Russia, May 18–24, 1998.
[83] S. Catani, Proceedings of the XVIII International Symposium on Lepton-Photon Interactions, LP 97, Hamburg, July, 1997, p. 149. hep-ph/9712442.
[84] ALEPH collaboration: Preliminary results on standard model processes in $e^+ e^-$ collisions at 189 GeV, contributed paper to ICHEP98 #908 (1998); ALEPH collaboration: R. Barate et al., Eur. Phys. J. C 12 (2000) 183.
[85] DELPHI collaboration: P. Abreu et al., Eur. Phys. J. C 11 (1999) 383; DELPHI collaboration: Results on Fermion-Pair production at LEP energies up to 183 GeV, contributed paper to ICHEP98 #441 (1998); DELPHI collaboration: Results on Fermion-Pair production at LEP running near 189 GeV, contributed paper to ICHEP98 #643 (1998).
[86] L3 collaboration: M. Acciarri et al., Phys. Lett. B 370 (1996) 195; L3 collaboration: M. Acciarri et al., Phys. Lett. B 407 (1997) 361; L3 collaboration: Preliminary L3 results on Fermion-Pair production in 1997, contributed paper to ICHEP98 #510 (1998).
[87] L3 collaboration: Preliminary cross section measurements from the L3 experiment at $\sqrt{s} = 189$ GeV, contributed paper to ICHEP98 #484 (1998).
[88] L3 collaboration: M. Acciarri et al., Phys. Lett. B 444 (1998) 569.
[89] OPAL collaboration: K. Ackerstaff et al., Eur. Phys. J. C 2 (1998) 441; OPAL collaboration: G. Abbiendi, Eur. Phys. J. C 6 (1999) 1; OPAL collaboration: G. Abbiendi et al., CERN-EP/99-097, Eur. Phys. J. C 13 (2000) 553.
[90] JADE collaboration: W. Bartel et al., Phys. Lett. B 160 (1985) 337; JADE collaboration: W. Bartel et al., Phys. Lett. B 129 (1983) 145; TASSO collaboration: M. Althoff et al., Phys. Lett. B 138 (1984) 441; CELLO collaboration: H.J. Behrend et al., Phys. Lett. B 183 (1987) 400; MARK J collaboration: B. Adeva et al., Phys. Rev. Lett. 50 (1983) 799; MARK J collaboration: B. Adeva et al., Phys. Rev. D 34 (1986) 681; MAC collaboration: E. Fernandez et al., Phys. Rev. D 31 (1985) 1537; VENUS collaboration: H. Voshida et al., Phys. Lett. B 198 (1987) 570; TOPAZ collaboration: I. Adachi et al., Phys. Rev. Lett. 60 (1988) 97; AMY collaboration: T. Mori et al., Phys. Lett. B 218 (1989) 499.
[91] G. d'Agostini, W. de Boer, G. Grindhammer, Phys. Lett. B 229 (1989) 160; R. Marshall, Z. Phys. C 43 (1989) 595.
[92] PLUTO collaboration: L. Criegee et al., Phys. Rep. 83 (1981) 151; DASPII collaboration: H. Albrecht et al., Phys. Lett. 116B (1982) 383; DESY-HAMBURG-HEIDELBERG-MUNICH collaboration: P. Bock et al., Z. Phys. C 6 (1980) 125;

LENA collaboration: B. Niczporuk et al., Z. Phys. C 15 (1982) 299; CUSB collaboration: E. Rice et al., Phys. Rev. Lett. 48 (1982) 906; CLEO collaboration: R. Giles et al., Phys. Rev. D 29 (1984) 1285; CRYSTAL BALL collaboration: Z. Jakubowski et al., Z. Phys. C 40 (1988) 49; ARGUS collaboration: H. Albrecht et al., Z. Phys. C 54 (1991) 13; MD-1 collaboration: A.E. Blinov et al., Z. Phys. C 70 (1996) 31.
[93] CLEO collaboration: R. Ammar et al., Phys. Rev. D 57 (1998) 1350.
[94] K.G. Chetyrkin, J.H. Kühn, Phys. Lett. B 308 (1993) 127; K.G. Chetyrkin, J.H. Kühn, Phys. Lett. B 356 (1995) 356; hep-ph/9409444; K.G. Chetyrkin, J.H. Kühn, T. Teubner, Phys. Rev. D 56 (1997) 3011, hep-ph/9609411.
[95] BES collaboration: J.Z. Bai et al., Phys. Rev. Lett. 84 (2000) 594, hep-ex/9908046.
[96] E. Braaten, S. Narison, A. Pich, Nucl. Phys. B 373 (1992) 581.
[97] F. Le Diberder, A. Pich, Phys. Lett. B 289 (1992) 165.
[98] E. Braaten, C.S. Li, Phys. Rev. D 42 (1990) 3888.
[99] M.A. Shifman, A.I. Vainshtein, V.I. Zakharov, Nucl. Phys. B 147 (1979) 385; S. Narison, A. Pich, Phys. Lett. B 211 (1988) 183.
[100] M. Neubert, Nucl. Phys. B 463 (1996) 511.
[101] ALEPH collaboration: D. Buskulic et al., Phys. Lett. B 307 (1993) 209; ALEPH collaboration: R. Barate et al., Eur. Phys. J. C 4 (1998) 409.
[102] OPAL collaboration: K. Ackerstaff et al., Eur. Phys. J. C 7 (1999) 571.
[103] CLEO collaboration: T. Coan et al., Phys. Lett. B 356 (1995) 580.
[104] OPAL collaboration: P.D. Acton et al., Z. Phys. C 55 (1992) 1.
[105] S. Narison, Phys. Lett. B 341 (1994) 73.
[106] B.P. Mackenzie, G.P. Lepage, Phys. Rev. Lett. 47 (1981) 1244; B.P. Mackenzie, G.P. Lepage, in: Perturbative QCD, D.W. Duke, J.F. Owens (Eds.), AIP, Tallahassee, 1981, p. 176; S.J. Brodsky, G.P. Lepage, P. Mackenzie, Phys. Rev. D 28 (1983) 228.
[107] M. Kobel, in: J. Trân Thanh Vân (Ed.), Perturbative QCD and Hadronic Interactions, 27th Rencontres de Moriond, Editions Frontières, Gif-sur-Yvette, 1992, p. 145.
[108] S. Bethke, Nucl. Phys. Proc. Suppl. 54A (1997) 314, hep-ex/9609014.
[109] CLEO collaboration: B. Nemati et al., Phys. Rev. D 55 (1997) 5273, hep-ex/96011020.
[110] M. Jamin, A. Pich, Nucl. Phys. B 507 (1997) 334, hep-ph/9702276.
[111] Z. Kunszt, P. Nason, G. Marchesini, B.R. Webber, in: G. Altarelli, R. Kleiss, C. Verzegnassi (Eds.), Z Physics at LEP 1, Vol. 89-08, v.1, 1989, p. 373.
[112] S. Catani, L. Trentadue, G. Turnock, B.R. Webber, Nucl. Phys. B 407 (1993) 3.
[113] S. Catani, L. Trentadue, G. Turnock, B.R. Webber, Phys. Lett. B 263 (1991) 491.
[114] S. Catani, G. Turnock, B.R. Webber, Phys. Lett. B 272 (1991) 368.
[115] S. Catani, G. Turnock, B.R. Webber, Phys. Lett. B 295 (1992) 269.
[116] Yu.L. Dokshitzer, A. Lucenti, G. Marchesini, G.P. Salam, J. High Energy Phys. 01 (1998) 011, hep-ph/9801324.
[117] G. Turnock, Cambridge Preprint Cavendish-HEP-92/3; J.C. Collins, D.E. Soper, Nucl. Phys. B 193 (1981) 381; J.C. Collins, D.E. Soper, Nucl. Phys. B 197 (1982) 446, Erratum: ibid. B 213 (1983) 545; J.C. Collins, D.E. Soper, Nucl. Phys. B 284 (1987) 253; J. Kodaira, L. Trentadue, Phys. Lett. B 112 (1982) 66; R. Fiore, A. Quartarolo, L. Trentadue, Phys. Lett. B 294 (1992) 431.
[118] S. Catani, Yu.L. Dokshitzer, M. Olsson, G. Turnock, B.R. Webber, Phys. Lett. B 269 (1991) 432.
[119] G. Dissertori, M. Schmelling, Phys. Lett. B 361 (1995) 167.
[120] S. Catani, B.R. Webber, Phys. Lett. B 427 (1998) 377, hep-ph/9801350.
[121] S. Catani, Yu.L. Dokshitzer, F. Fiorani, B.R. Webber, Nucl. Phys. B 377 (1992) 445.
[122] JADE and OPAL collaborations: P. Pfeifenschneider et al., QCD analyses and determinations of α_S in $e^+ e^-$ Annihilations at Energies between 35, 189 GeV, CERN-EP/99-175, Eur. Phys. J. C, in press.
[123] S.L. Wu, Phys. Rep. 107 (1984) 59.
[124] JADE collaboration: W. Bartel et al., Z. Phys. C 33 (1986) 23; JADE collaboration: S. Bethke et al., Phys. Lett. B 213 (1988) 235.
[125] S. Bethke, Z. Kunszt, D.E. Soper, W.J. Stirling, Nucl. Phys. B 370 (1992) 310, Erratum: ibid. B 523 (1998) 681; S. Moretti, L. Lönnblad, T. Sjöstrand, Phys. Rev. D 58 (1998) 094006, hep-ph/9804294.
[126] Yu.L. Dokshitzer, G.D. Leder, S. Moretti, B.R. Webber, J. High Energy Phys. 08 (1997) 001, hep-ph/9707323.

[127] S. Bentvelsen, I. Meyer, Eur. Phys. J. C 4 (1998) 623, hep-ph/9803322.
[128] S. Bethke, J. Phys. G 17 (1991) 1455.
[129] OPAL collaboration: G. Alexander et al., Z. Phys. C 72 (1996) 191, variation of tuned PYTHIA parameters to estimate hadronization uncertainties: $b = 0.52 \pm 0.04$, $\sigma_q = 0.40 \pm 0.03$, $Q_0 = 1.9 \pm 0.5$, only u, d, s, c quarks considered for the correction.; OPAL collaboration: K. Ackerstaff et al., Z. Phys. C 75 (1997) 193.
[130] OPAL collaboration: G. Abbiendi et al., CERN-EP/99-178, Eur. Phys. J. C, submitted for publication.
[131] DELPHI collaboration: P. Abreu et al., Z. Phys. C 73 (1997) 229.
[132] L3 collaboration: M. Acciarri et al., Phys. Lett. B 371 (1996) 137; L3 collaboration: M. Acciarri et al., Phys. Lett. B 404 (1997) 390.
[133] N. Brown, W.J. Stirling, Phys. Lett. B 252 (1990) 657.
[134] Z. Nagy, Z. Tróscányi, Nucl. Phys. B (Proc. Suppl.) 74 (1999) 44, hep-ph/9808364.
[135] S.J. Burby, DTP/99/12, hep-ph/9902305.
[136] ALEPH collaboration: Measurements of α_S with e^+e^- annihilation data from 91 to 183 GeV, contributed paper to ICHEP98 #940 (1998).
[137] TPC/TWO-GAMMA collaboration: D.A. Bauer et al., Measurement of α_S in e^+ e^- annihilation at $E_{cm} = 29$ GeV, contributed paper to ICHEP94 GLS0254 (1994), SLAC-PUB-6518.
[138] TOPAZ collaboration: Y. Ohnishi et al., Phys. Lett. B 313 (1993) 475; TOPAZ collaboration: M. Aoki et al., Updated measurement of strong coupling constant α_S at $\sqrt{s} = 58$ GeV and evidence for its running nature, contributed paper to ICHEP94 GLS0944 (1994).
[139] P.A. Movilla Fernández, O. Biebel, S. Bethke, S. Kluth, P. Pfeifenschneider, the JADE collaboration, Eur. Phys. J. C 1 (1998) 461, hep-ex/9708034; O. Biebel, P.A. Movilla Fernández, S. Bethke, the JADE collaboration, Phys. Lett. B 459 (1999) 326, hep-ex/9903006. and hep-ex/9807007.
[140] DELPHI collaboration: P. Abreu et al., Z. Phys. C 73 (1996) 11.
[141] S. Brandt et al., Phys. Lett. B 12 (1964) 57; E. Fahri, Phys. Rev. Lett. 39 (1977) 1587.
[142] T. Chandramohan, L. Clavelli, Nucl. Phys. B 184 (1981) 365; L. Clavelli, D. Wyler, Phys. Lett. B 103 (1981) 383.
[143] L3 collaboration: M. Acciarri et al., Phys. Lett. B 411 (1997) 339.
[144] ALEPH collaboration: D. Decamp et al., Phys. Lett. B 284 (1992) 163; DELPHI collaboration: P. Abreu et al., Z. Phys. C 59 (1993) 21; L3 collaboration: S. Banerjee, S. Müller, Determination of α_S from hadronic event shapes measured on the Z resonance, L3 Internal Note 1441 (1993) available on request; SLD collaboration: K. Abe et al., Phys. Rev. Lett. 71 (1993) 2528.
[145] DELPHI collaboration: α_S from DELPHI Measurements at LEP 2, contributed paper to ICHEP98 #137 (1998); DELPHI collaboration: QCD Results from the DELPHI measurements at 161 GeV and 172 GeV, contributed paper to HEP97 #544 (1997).
[146] DELPHI collaboration: P. Abreu et al., CERN-EP/99-133, hep-ex/0002026, Eur. Phys. J. C 14 (2000) 557.
[147] S. Bethke, Z. Phys. C 43 (1989) 331; OPAL collaboration: M.Z. Akrawy et al., Phys. Lett. B 235 (1990) 389; DELPHI collaboration: P. Abreu et al., Z. Phys. C 54 (1992) 55.
[148] M. Schmelling, Phys. Scr. 51 (1995) 676.
[149] B.L. Ioffe, Phys. Lett. 78B (1978) 277; E. Laermann, P.M. Zerwas, Phys. Lett. 89B (1980) 225; Erratum: ibid. 91B (1980) 487; J. Jersák, E. Laermann, P.M. Zerwas, Phys. Rev. D 25 (1982) 1218, Erratum: ibid. D 36 (1987) 310; R.G. Rizzo, Phys. Rev. D 22 (1980) 2213; H.P. Nilles, Phys. Rev. Lett. 45 (1980) 319. M. Bilenky, G. Rodrigo, A. Santamaria, Nucl. Phys. B 439 (1995) 505.
[150] A. Ballestrero, E. Maina, S. Moretti, Phys. Lett. B 294 (1992) 425; A. Ballestrero, E. Maina, S. Moretti, Nucl. Phys. B 415 (1994) 265.
[151] W. Bernreuther, A. Brandenburg, P. Uwer, Phys. Rev. Lett. 79 (1997) 189, hep-ph/9703305; A. Brandenburg, P. Uwer, Nucl. Phys. B 515 (1998) 279; A. Brandenburg, W. Bernreuther, P. Uwer, Nucl. Phys. B (Proc. Suppl.) 64 (1998) 387, hep-ph/9709282.
[152] G. Rodrigo, A. Santamaria, M. Bilenky, Phys. Rev. Lett. 79 (1997) 193, hep-ph/9703358; G. Rodrigo, Nucl. Phys. Proc. Suppl. 54A (1997) 60, hep-ph/9609213; G. Rodrigo, A. Santamaria, M. Bilenky, Nucl. Phys. B (Proc. Suppl.) 64 (1998) 380, hep-ph/9709313; G. Rodrigo, Quark mass effects in QCD jets, Ph.D. Thesis, Departament de Física Teòrica Unversitat de València, October, 1996. hep-ph/9703359.

[153] P. Nason, C. Oleari, Nucl. Phys. B 521 (1998) 237, hep-ph/9709360; C. Oleari, Next-to-leading-order corrections to the production of heavy-flavour jets in e^+e^- collisions, Ph.D. Thesis, Dipartimento di Fisica Università degli Studi di Milano, 1997. hep-ph/9802431.
[154] A. Brandenburg, private communication.
[155] A.S. Schwarz, Phys. Rep. 238 (1994) 1.
[156] SLD collaboration: P.N. Burrows et al., Heavy quark mass effects and improved tests of the flavour independence of strong interactions, in: A. Astbury, D. Axen, J. Robinson (Eds.), Proceedings of the XXXIX International Conference on High Energy Physics, World Scientific, Vancouver, July 23–39, 1999, p. 728. hep-ph/9808017; A. Brandenburg, P.N. Burrows, D. Muller, N. Oishi, P. Uwer, Phys. Lett. B 468 (1999) 168, hep-ph/9905495.
[157] SLD collaboration: K. Abe et al., Phys. Rev. D 59 (1999) 012002, hep-ex/9805023.
[158] OPAL collaboration: G. Abbiendi et al., Test of the flavour independence of α_S using next-to-leading order calculations for heavy quarks, Eur. Phys. J. C 11 (1999) 643, CERN-EP/99-045, hep-ex/9904013.
[159] SLD collaboration: K. Abe et al., Phys. Rev. Lett. 78 (1997) 3442, hep-ex/9702009 Erratum: ibid. 79 (1997) 959; J. Schwiening, in: J. Trân Thanh Vân (Ed.), QCD and High-Energy Hadronic Interactions, 32nd Rencontres de Moriond, Editions Frontières, Gif-sur-Yvette, 1997, p. 293. hep-ph/9705454.
[160] J. Letts, P. Mättig, Z. Phys. C 73 (1997) 217.
[161] OPAL collaboration: R. Akers et al., Z. Phys. C 60 (1993) 397.
[162] L3 collaboration: B. Adeva et al., Phys. Lett. B 271 (1991) 461.
[163] DELPHI collaboration: P. Abreu et al., Phys. Lett. B 307 (1993) 221.
[164] DELPHI collaboration: P. Abreu et al., Phys. Lett. B 418 (1998) 430.
[165] OPAL collaboration: M.Z. Akrawy et al., Z. Phys. C 65 (1995) 31.
[166] ALEPH collaboration: D. Buskulic et al., Phys. Lett. B 335 (1995) 381.
[167] SLD collaboration: K. Abe et al., Phys. Rev. D 53 (1996) 2271.
[168] K.G. Chetyrkin, M. Steinhauser, DESY-99-174, hep-ph/9911434; K. Melnikov, T. van Ritbergen, SLAC-PUB-8321, hep-ph/9912391.
[169] N. Gray, D.J. Broadhurst, W. Grafe, K. Schilcher, Z. Phys. C 48 (1990) 673.
[170] V.M. Braun, in: J. Trân Thanh Vân (Ed.), QCD and High Energy Hadronic Interactions, 30th Rencontres de Moriond, Editions Frontières, Gif-sur-Yvette, 1995, p. 271. hep-ph/9505371.
[171] H. Fusaoka Y. Koide, Phys. Rev. D 57 (1998) 3986, hep-ph/9706211.
[172] A.H. Hoang, Phys. Rev. D 59 (1999) 014039, hep-ph/9803454.
[173] M. Jamin, A. Pich, Nucl. Phys. (Proc. Suppl.) 74 (1999) 300, hep-ph/9810259.
[174] DELPHI collaboration: New determination of the b-quark mass using improved jet clustering algorithms, contributed paper to ICHEP98 #152 (1998).
[175] P. Nason, B.R. Webber, Nucl. Phys. B 421 (1995) 473; B. Mele, in: B.F.L. Ward (Ed.), Tennessee International Symposium on Radiative Corrections: Status and Outlook, World Scientific, Gatlinburg, 27 June–1 July, 1994, p. 519.
[176] A_{FB} Working Group: M. Böhm, W. Hollik (conv.), et al., in: G. Altarelli, R. Kleiss, C. Verzegnassi (Eds.), Z Physics at LEP 1, CERN Yellow Report, Vol. 89-08, v. 1, 1989, p. 203.
[177] J.C. Collins, D.E. Soper, Ann. Rev. Nucl. Part. Sci. 37 (1987) 383; J.C. Collins, D.E. Soper, G. Sterman, in: A.H. Mueller (Ed.), Perturbative Quantum Chromodynamics, World Scientific, Singapore, 1989, p. 1.
[178] J. Binnewies, B.A. Kniehl, G. Kramer, Z. Phys. C 65 (1995) 471, hep-ph/9407347; J. Binnewies, B.A. Kniehl, G. Kramer, Phys. Rev. D 52 (1996) 4947, hep-ph/9503207; J. Binnewies, B.A. Kniehl, G. Kramer, Phys. Rev. D 53 (1996) 3573, hep-ph/9506437; J. Binnewies, Fragmentation functions in next-to-leading order QCD, Ph.D. Thesis, II, Institut für Theoretische Physik, Universität Hamburg, 1997. hep-ph/9707269.
[179] V.N. Gribov, L.N. Lipatov, Sov. J. Nucl. Phys. 15 (1972) 438; Yu.L. Dokshitzer, Sov. Phys. JETP 46 (1977) 641.
[180] B.R. Webber, J. Phys. G 17 (1991) 1579.
[181] OPAL collaboration: K. Ackerstaff et al., Eur. Phys. J. C 7 (1999) 369, hep-ex/9807004.
[182] MARK II collaboration: G.S. Abrams et al., Phys. Rev. Lett. 64 (1990) 1334.
[183] ALEPH collaboration: R. Barate et al., CERN-EP/98-16, Eur. Phys. J. C, submitted for publication.
[184] OPAL collaboration: R. Akers et al., Z. Phys. C 61 (1994) 209.
[185] OPAL collaboration: P.D. Acton et al., Z. Phys. C 58 (1993) 387.

[186] DELPHI collaboration: P. Abreu et al., Eur. Phys. J. C 6 (1999) 19.
[187] OPAL collaboration: R. Akers et al., Z. Phys. C 86 (1995) 203.
[188] ALEPH collaboration: D. Buskulic et al., Phys. Lett. B 357 (1995) 487, Erratum: ibid. B 364 (1995) 247.
[189] DELPHI collaboration: P. Abreu et al., Phys. Lett. B 398 (1997) 194.
[190] DELPHI collaboration: P. Abreu et al., Phys. Lett. B 311 (1993) 408.
[191] DELPHI collaboration: P. Abreu et al., CERN-EP/99-144, Eur. Phys. J. C 13 (2000) 573.
[192] R.J. Rijken, W.L. van Neerven, Phys. Lett. B 386 (1996) 422, hep-ph/9604436; W.L. van Neerven, in: Results and Perspectives in Particle Physics, 11th Rencontre de Physique de la Vallée D'Aoste, La Thuile, 2–8 March, 1997. hep-ph/9705343; W.L. van Neerven, Acta Phys. Pol. B 29 (1998) 2573, hep-ph/9805464.
[193] V. Ravindran, W.L. van Neerven, Phys. Lett. B 445 (1998) 206, hep-ph/9810258.
[194] M. Dasgupta, B.R. Webber, Nucl. Phys. B 484 (1997) 247, hep-ph/9608394; P. Nason, B.R. Webber, Nucl. Phys. B 395 (1997) 355, hep-ph/9612353.
[195] M. Beneke, V.M. Braun, L. Magnea, Nucl. Phys. B 497 (1997) 297, hep-ph/9701309; M. Beneke, V.M. Braun, L. Magnea, Nucl. Phys. Proc. Suppl. 54A (1997) 183, hep-ph/9609266.
[196] B. Lampe, Phys. Lett. B 301 (1993) 435.
[197] OPAL collaboration: G. Abbiendi et al., Phys. Lett. B 440 (1998) 393.
[198] S. Catani, M.H. Seymour, Phys. Lett. B 378 (1996) 287, hep-ph/9602277, The program EVENT2 of the authors was used to determine the perturbative coefficients by integrating the ERT $\mathcal{O}(\alpha_s^2)$ matrix elements [32]; S. Catani, M.H. Seymour, Nucl. Phys. B 485 (1997) 291, hep-ph/9605323, Erratum: ibid. B 510 (1997) 503.
[199] B.R. Webber, J. Phys. G 17 (1991) 1493.
[200] A.H. Mueller, Nucl. Phys. B 213 (1983) 85, Erratum: ibid. B 241 (1994) 141.
[201] C.P. Fong, B.R. Webber, Nucl. Phys. B 355 (1991) 54; C.P. Fong, B.R. Webber, Phys. Lett. B 241 (1990) 255; C.P. Fong, B.R. Webber, Phys. Lett. B 229 (1989) 289.
[202] W. Ochs, in: B. Kniehl, G. Kramer, A. Wagner (Eds.), New Trends in HERA Physics, World Scientific, Rinberg Castle, Tregernsee, May 25–30, 1998. hep-ph/9709248.
[203] F.E. Close, Yu.L. Dokshitzer, V.N. Gribov, V.A. Khoze, M.G. Ryskin, Phys. Lett. B 319 (1993) 291.
[204] TASSO collaboration: W. Braunschweig et al., Z. Phys. C 47 (1990) 187.
[205] TOPAZ collaboration: R. Itoh et al., Phys. Lett. B 345 (1995) 335.
[206] DELPHI collaboration: P. Abreu et al., Phys. Lett. B 459 (1999) 397.
[207] OPAL collaboration: M.Z. Akrawy et al., Phys. Lett. B 247 (1990) 617.
[208] MARK II collaboration: A. Petersen et al., Phys. Rev. D 37 (1988) 1.
[209] TPC/TWO-GAMMA collaboration: H. Aihara et al., Charged Hadron production in e^+e^- annihilation at $\sqrt{s} = 29\,\mathrm{GeV}$, LBL 23737.
[210] AMY collaboration: Y.K. Li et al., Phys. Rev. D 41 (1990) 2675.
[211] ALEPH collaboration: D. Buskulic et al., Z. Phys. C 55 (1992) 209.
[212] ALEPH collaboration: D. Buskulic et al., Z. Phys. C 73 (1997) 409; ALEPH collaboration: QCD studies with e^+e^- annihilation data from 130 to 183 GeV, contributed paper to ICHEP98, #945 (1998).
[213] DELPHI collaboration: P. Abreu et al., Phys. Lett. B 275 (1992) 231.
[214] L3 collaboration: B. Adeva et al., Phys. Lett. B 259 (1991) 199.
[215] S. Lupia, W. Ochs, Phys. Lett. B 365 (1996) 339: S. Lupia, W. Ochs, Eur. Phys. J. C 2 (1998) 307.
[216] V.A. Khoze, S. Lupia, W. Ochs, Phys. Lett. B 394 (1997) 179, hep-ph/9610204; S. Lupia, Nucl. Phys. Proc. Suppl. 54A (1997) 55; W. Ochs. Acta Phys. Pol. B 27 (1996) 3505.
[217] V.A. Khoze, S. Lupia, W. Ochs, in: R.C. Hwa, W. Kittel, W.J. Metzger, D.J. Schotanus (Eds.), Proceedings of Correlations and Fluctuations, Seventh International Workshop on Multiparticle Production, World Scientific, Nijmegen, June 30–July 6, 1996, hep-ph/9610348.
[218] V.A. Khoze, S. Lupia, W. Ochs, Eur. Phys. J. C 5 (1998) 77, hep-ph/9711392.
[219] Yu.L. Dokshitzer, V.A. Khoze, S.I. Troyan, Int. J. Mod. Phys. A 7 (1992) 1875.
[220] V.A. Khoze, W. Ochs, Int. J. Mod. Phys. A 12 (1997) 2949.
[221] N. Varelas, in: S. Bianco, A. Calcaterra, P. de Simone, F.L. Fabbri (Eds.), Proceedings of 18th International Physics in Collision, Frascati Physics Series 11, INFN, Frascati, June 17–19, 1998, p. 107. hep-ex/9809019.
[222] MARK I colloboration: J.L. Siegrist et al., Phys. Rev. D 26 (1982) 969.

[223] B.R. Webber, Phys. Lett. 143B (1984) 501.
[224] I.M. Dremin, JETP. Lett. 68 (1998) 559, hep-ph/9808481.
[225] I.M. Dremin, V.A. Nechitailo, Mod. Phys. Lett. A 9 (1994) 1471, hep-ex/9406002.
[226] I.M. Dremin, J.W. Gary, Phys. Lett. B 459 (1999) 341, hep-ph/9905477 A. Capella, I.M. Dremin, J.W. Gary, V.A. Nechitailo, J. Trân Thanh Vân, Evolution of average multiplicities of quark and gluon jets, FIAN-TD-22-99, hep-ph/9910226.
[227] S.J. Brodsky, J.G. Gunion, Phys. Rev. Lett. 37 (1976) 402; K. Konishi, A. Ukawa, G. Veneziano, Phys. Lett. B 78 (1978) 243.
[228] E.D. Malaza, B.R. Webber, Phys. Lett. B 149 (1984) 501; E.D. Malaza, B.R. Webber, Nucl. Phys. B 267 (1986) 702.
[229] J.B. Gaffney, A.H. Mueller, Nucl. Phys. B 250 (1985) 109.
[230] OPAL collaboration: R. Akers et al., Z. Phys. C 63 (1993) 197; OPAL colloboration: R. Akers et al., Z. Phys. C 68 (1994) 179.
[231] ALEPH collaboration: D. Buskulic et al., Phys. Lett. B 384 (1996) 353.
[232] DELPHI colloboration: P. Abreu et al., Phys. Lett. B 449 (1999) 383, hep-ex/9903073.
[233] K. Hamacher, in: A. Astbury, D. Axen, J. Robinson (Eds.), Proceedings of the XXXIX International Conference on High Energy Physics, World Scientific, Vancouver, July 23–29, 1999, p. 677. hep-ex/9809018.
[234] TOPAZ collaboration: K. Nakabayashi et al., Phys. Lett. B 413 (1997) 447.
[235] J.W. Gary, Phys. Rev. D 49 (1994) 4503.
[236] J.W. Gary, UCRHEP-E-181, hep-ex/9701005.
[237] OPAL collaboration: G. Alexander et al., Phys. Lett. B 388 (1996) 659; OPAL collaboration: G. Abbiendi et al., Eur. Phys. J. C 11 (1999) 217, hep-ex/9903027.
[238] OPAL collaboration, K. Ackerstaf et al., Eur. Phys. J. C 1 (1998) 479.
[239] S. Lupia, W. Ochs, Phys. Lett. B 418 (1998) 214, hep-ph/9707393.
[240] P. Edén, G. Gustafson, J. High Energy Phys. 09 (1998) 015, hep-ph/9805228.
[241] A.V. Kisselev, V.A. Petrov, O.P. Yushchenko, Z. Phys. C 41 (1988) 521.
[242] LENA collaboration: B. Niczporuk et al., Z. Phys. C 9 (1981) 1; CELO collaboration: M.S. Alam et al., Phys. Rev. Lett. 49 (1982) 357; JADE collaboration: W. Bartel et al., Z. Phys. C 20 (1983) 187; HRS collaboration: M. Derrick et al., Phys. Rev. D 34 (1986) 3304; TPC/TWO-GAMMA collaboration: H. Aihara et al., Phys. Lett. 134B (1987) 299; AMY collaboration: H.W. Zheng et al., Phys. Rev. D 42 (1990) 737.
[243] DELPHI collaboration: P. Abreu et al., Eur. Phys. J. C 6 (1999) 19.
[244] DELPHI collaboration: P. Abreu et al., Phys. Lett. B 372 (1996) 172; DELPHI collaboration: P. Abreu et al., Phys. Lett. B 416 (1998) 233.
[245] I.M. Dremin, V.A. Nechitailo, M. Biyajima, N. Suzuki, Phys. Lett. B 403 (1997) 149, hep-ex/9704318.
[246] S. Lupia, Phys. Lett. B 439 (1998) 150, hep-ph/9806493.
[247] A.V. Manohar, M.B. Wise, Phys. Lett. B 344 (1995) 407, hep-ph/9406392.
[248] G.P. Korchemsky, G. Oderda, G. Sterman, in: J. Repond, D. Krakauer (Eds.), Deep Inelastic Scattering and QCD, DIS 97, aip, Woodbury, New York, 1997, p. 988. hep-ph/9708346.
[249] Yu.L. Dokshitzer, in: A. Astbury, D. Axen, J. Robinson (Eds.), Proceedings of the XXXIX International Conference on High Energy Physics, World Scientific, Vancouver, July 23–29, 1999, p. 305. hep-ph/9812252.
[250] B.R. Webber, in: J.F. Laporte, Y. Sirois (Eds.), Workshop on Deep Inelastic Scattering and QCD, DIS 95, Ecole Polytechnique, Paris, 1995, p. 115. hep-ph/9510283.
[251] V.I. Zakharov, Nucl. Phys. B 385 (1992) 452.
[252] M. Beneke, Phys. Rep. 317 (1999) 1, hep-ph/9807443.
[253] B.R. Webber, J. High Energy Phys. 10 (1998) 012, hep-ph/9805484; Yu.L. Dokshitzer, V.A. Khoze, S.I. Troyan, Phys. Rev. D 53 (1996) 89, hep-ph/9506425.
[254] D.V. Shirkov, I.L. Solovtsov. JINR Rapid Comm. 2 [76] (1996) 5, hep-ph/9604363; D.V. Shirkov, I.L. Solovtsov, Phys. Rev. Lett. 79 (1997) 1209, hep-ph/9704333; D.V. Shirkov, Nucl. Phys. B (Proc. Suppl.) 64 (1998) 106, hep-ph/9708480.
[255] G. Grunberg, Phys. Lett. B 372 (1996) 121; A.I. Alekseev, B.A. Arbusov, Mod. Phys. Lett. A 13 (1998) 1747, hep-ex/9704228; D. Ebert, I.L. Solovtsov, O.P. Solovtsova, Nonperturbative expansion in QCD and e^+e^- annihilation into hadrons at low energies, DESY 96-075; K.A. Milton, O.P. Solovtsova, Phys. Rev. D 57 (1998) 5402, hep-ph/9710316; K.A. Milton, I.L. Solovtsov, O.P. Solovtsova, Analytic perturbative apporach to QCD,

OKHEP-98-06, hep-ph/9808457, Proceedings of the XXIX International Conference on High Energy Physics, Vancouver, July 23–29, 1998, to appear; D. Atkinson, J.C.R. Bloch, Phys. Rev. D 58 (1998) 094036, hep-ph/9712459; J.M. Namyslowksi, Nonperturbative QCD, IFT/10/94 Warsaw University.
[256] G. Altarelli, R. Kleiss, C. Verzegnassi (Eds.), Z Physics at LEP 1, CERN Yellow Report.
[257] Yu.L. Dokshitzer, G. Marchesini, G.P. Salam, Eur. Phys. J. direct C 3 (1999) 1, hep-ph/9812487; Yu.L. Dokshitzer, private communication.
[258] G.P. Korchemsky, Shape functions and power corrections to the event shapes, LPTHE-ORSAY-98-44, hep-ph/9806537, Proceedings of the 33rd Rencontres de Moriond, Les Arcs, March 21–28 1998, to appear.
[259] P.A. Movilla Fernández, Nucl. Phys. B (Proc. Suppl.) 74 (1999) 384, hep-ex/9808005; P.A. Movilla Fernández, O. Biebel, S. Bethke, Tests of power corrections to event shape distributions in e^+e^- annihilation, PITHA 99/21, hep-ex/9906033.
[260] DELCO collaboration: M. Sakuda et al., Phys. Lett. 152B (1985) 399.
[261] HRS collaboration: D. Bender et al., Phys. Rev. D 31 (1985) 1.
[262] L3 collaboration: B. Adeva et al., Z. Phys. C 55 (1992) 39.
[263] MARK J collaboration: D.P. Barber et al., Phys. Rev. Lett. 43 (1979) 901.
[264] MARK J collaboration: D.P. Barber et al., Phys. Lett. 85 B (1979) 463.
[265] SLD collaboration: K. Abe et al., Phys. Rev. D 51 (1995) 962.
[266] TASSO collaboration: W. Braunschweig et al., Z. Phys. C 41 (1988) 359.
[267] ALEPH collaboration: Power law corrections to hadronic event shape variables in e^+e^- annihilation, contributed paper to HEP97 and Lepton-Photon 97 #610, LP258 (1997).
[268] O. Biebel, Nucl. Phys. B (Proc. Suppl.) 64 (1998) 22, hep-ex/9708036.
[269] D. Wicke, Nucl. Phys. B (Proc. Suppl.) 64 (1998) 27, hep-ph/9708467; D. Wicke, Power corrections at LEP, hep-ph/9805392, Proceedings of the 33rd Rencontres de Moriond, Les Arcs, March 14–21, 1998, to appear; J.C. Thompson, hep-ex/9812004.
[270] J.M. Campbell, E.W.N. Glover, C.J. Maxwell, Phys. Rev. Lett. 81 (1998) 1568, hep-ph/9803254.
[271] D.E. Hutchcroft, Quantum Chromodynamics with the OPAL detector at LEP. Ph.D. Thesis, Trinity College, University of Cambridge, 1997, RAL-TH-1998-007.
[272] S. Bethke, in: J. Sola (Ed.), Proceedings of the Fourth International Symposium on Radiative Corrections, World Scientific, Barcelona, September 8–12, 1999, p. 243. hep-ex/9812026.
[273] B.R. Webber, Nucl. Phys. Proc. Suppl. 71 (1998) 66, hep-ph/9712236.
[274] S. Kluth, private communication.
[275] Yu.L. Dokshitzer, in: D. Lellouch, G. Mikenberg, E. Rabinovici (Eds.), International Europhysics Conference on High Energy Physics, Springer, Berlin, 1999, p. 47. hep-ph/9801372.
[276] M.L. Mangano, in: Proceedings of the International Europhysics Conference on High Energy Physics, HEP 99, Tampere, July, 1999, hep-ph/9911256.
[277] DELPHI collaboration: QCD Results from the Measurement of Event Shape Distributions between 41 GeV and 189 GeV, contributed paper to HEP99 #1_144 (1999); L3 collaboration: QCD studies and determination of α_s in e^+e^- collisions, contributed paper to HEP99 #1_279 (1999); H1 collaboration: Event shapes and power corrections in ep DIS, contributed paper to HEP99 #1_157k (1999).
[278] M. Karliner, Acta Phys. Pol. B 29 (1998) 1505, hep-ph/9804381.
[279] V. Elias, T.G. Steele, F. Chishtie, R. Migneron, K. Sprague, Phys. Rev. D 58 (1998) 116007, hep-ph/9806324.
[280] T.G. Steele, V. Elias, Mod. Phys. Lett. A 13 (1998) 3151, hep-ph/9902217.
[281] P.N. Burrows, T. Abraha, M. Samuel, E. Steinfelds, H. Masuda, Phys. Lett. B 392 (1997) 223, hep-ph/9609513.
[282] CELLO collaboration: H. Behrend et al., Z. Phys. C 44 (1988) 63.
[283] MARK II collaboration: G.S. Abrams et al., Phys. Rev. Lett. 63 (1989) 1558.
[284] OPAL collaboration: M.Z. Akrawy et al., Z. Phys. C 47 (1990) 505.
[285] E.W.N. Glover, private communication.
[286] C.J. Maxwell, Complete renormalization group improvement of QCD perturbation theory, DTP-98-54, hep-ph/9809270.

[287] R. Akhoury, V. Zakharov, Renormalons and $1/Q^2$ Corrections, in: G. Eigen, P. Osland, B. Stugu (Eds.), Proceedings of the Fifth International Conference on Physics Beyond the Standard Model, AIP, 1997, p. 274. hep-ph/9705318; R. Akhoury, V. Zakharov, Nucl. Phys. B (Proc. Suppl.) 64 (1998) 350, hep-ph/9510257.
[288] F. Cuypers, Phys. Rev. D 49 (1994) 3075, hep-ph/9310327; R. Muñoz-Tapia, W.J. Stirling, Phys. Rev. D 49 (1994) 3763, hep-ph/9309246; G.R. Farrar, Phys. Rev. D 51 (1994) 3904, hep-ph/9407401.
[289] W.-Y.P. Hwang, Phys. Rev. D 32 (1985) 824; G. Dvali, Phys. Lett. B 372 (1986) 113, hep-ph/9511237; J. Hisano, T. Moroi, K. Tobe, T. Yanagida, Mod. Phys. Lett. A 10 (1995) 2267, hep-ph/9411298; K.H. Cho, S.K. Han, J.K. Kim, Phys. Rev. D 29 (1984) 46; S. Lakshmibala, G. Rajasekaran, S.D. Rindani, Phys. Lett. B 105 (1981) 477; G. Rajasekaran, S.D. Rindani, Phys. Lett. B 99 (1981) 361.
[290] T. Hebbeker, Z. Phys. C 60 (1993) 63.
[291] S. Bethke, A. Richter, P.M. Zerwas, Z. Phys. C 49 (1991) 59.
[292] M. Bengtsson, P.M. Zerwas, Phys. Lett. B 208 (1988) 306; M. Bengtsson, Z. Phys. C 42 (1989) 75; J.G. Körner, G. Schierholz, J. Willrodt, Nucl. Phys. B 185 (1981) 365; O. Nachtmann, A. Reiter, Z. Phys. C 16 (1982) 45.
[293] G. Dissertori, Nucl. Phys. B (Proc. Suppl.) 65 (1998) 43, hep-ex/9705016.
[294] ALEPH collaboration: R. Barate et al., Z. Phys. C 76 (1997) 1.
[295] F. Csikor, Z. Fodor, in: D. Lellouch, G. Mikenberg, E. Rabinovici (Eds.), International Europhysics Conference on High Energy Physics, Springer, Berlin, 1999, p. 883. hep-ph/9712269; F. Csikor, Z. Fodor, Phys. Rev. Lett. 78 (1997) 4335, hep-ph/9611320; M. Schmelling, R.St. Denis, Phys. Lett. B 329 (1994) 393.
[296] A. Belyaev, F. de Campos, S.F. Novaes, R. Rosenfeld, Phys. Lett. B 447 (1999) 331, hep-ph/9811374.
[297] H. Georgi, M. Machacek, Phys. Rev. Lett. 39 (1977) 1237.
[298] SLD collaboration: K. Abe et al., Phys. Rev. D 60 (1999) 092002, hep-ex/9903004.
[299] S. Bethke, Nucl. Phys. B (Proc. Suppl.) 64 (1998) 54, hep-ex/9710030.
[300] G. Altarelli, R.D. Ball, S. Forte, G. Ridolfi, Nucl. Phys. B 496 (1997) 337, hep-ph/9701289.
[301] J. Ellis, M. Karliner, Phys. Lett. B 341 (1995) 397, hep-ph/9407287.
[302] CCFR collaboration: J.H. Kim et al., Phys. Rev. Lett. 81 (1998) 3595, hep-ex/9808015.
[303] CCFR collaboration: W.G. Seligman, Phys. Rev. Lett. 79 (1997) 1213.
[304] M. Virchaux, A. Milsztajn, Phys. Lett. B 274 (1992) 221.
[305] R.D. Ball, S. Forte, Phys. Lett. B 358 (1995) 365, hep-ph/9506233.
[306] H1 collaboration: C. Adloff et al., Eur. Phys. J. C 5 (1998) 625, hep-ex/9806028; H1 collaboration: C. Adloff et al., Eur. Phys. J. C 6 (1999) 575, hep-ex/9807019; ZEUS collaboration: M. Derrick et al., Phys. Lett. B 363 (1995) 201, hep-ex/9510001.
[307] H1 collaboration: C. Adloff et al., Phys. Lett. B 406 (1997) 256, hep-ex/9706002.
[308] C.T.H. Davies, K. Hornbostel, G.P. Lepage, A. Lidsey, J. Shigemitso, J. Sloan, Phys. Lett. B 345 (1995) 42, hep-ph/9408328.
[309] UA1 collaboration: C. Albajar et al., Phys. Lett. B 369 (1996) 46.
[310] UA6 collaboration: C. Ballocchi et al., Phys. Lett. B 317 (1993) 250.
[311] W.T. Giele, E.W.N. Glover, J. Yu, Phys. Rev. D 53 (1996) 120, hep-ph/9506442.
[312] M.K. Parida, B. Purkayastha, IC/99/10, hep-ph/9902374.
[313] U. Amaldi, W. de Boer, H. Füstenau, Phys. Lett. B 260 (1991) 447.
[314] P.N. Burrows, L. Dixon, A.X. El-Khadra, J.W. Gary, W. Giele, D.A. Harris, S. Ritz, B.A. Schumm, Prospects for the precision measurement of α_S, SLAC-PUB-7371, hep-ex/9612012; K. Hagiwara, D. Haidt, Eur. Phys. J. C 2 (1998) 95, hep-ph/9706331.
[315] D.E. Soper, in: J. Sola (Ed.), Proceedings of the Fourth International Symposium on Radiative Corrections, World Scientific, Barcelona, September 8–12, 1999, p. 305. hep-ph/9812324.
[316] M. Dasgupta, L. Magnea, G.E. Smye, Bicocca-FT-99-34, hep-ph/9911316.
[317] Yu.L. Dokshitzer, hep-ph/9911316, Proceedings of the conference Frontiers of Matter, Blois, June 1999, to appear.